

SECTION III
RESULTS &
DISCUSSION

5. RESULTS & DISCUSSION

5.1. Characterization of Physical Mixtures & Matrix Tablets

5.1.1. DRUG-EXCIPIENT INTERACTION STUDIES

The choice of the polymeric excipient is of obvious importance to get the desired release profile. To this aim, a compatible drug-excipient combination is necessary. DSC thermograms indicated the qualitative composition of the drug formulations and verified the identity of each of the components by their thermal properties. In addition, the DSC is also carried out to understand the solid-state interaction in tablets (Fassihi and Parker, 1986). Hence, the possibility of drug-excipient interaction was investigated by differential scanning calorimetry (DSC). The DSC thermograms of pure drug, individual excipients, drug-excipient physical mixture (proportion same as the tablet composition) were recorded. To evaluate the internal structure modifications after compression of physical mixtures into tablet, tablet powder was also included in the study. The thermogram of glipizide and nateglinide showed an endothermic peak corresponding to the melting of the drug at 213.96°C and 139.11°C, respectively indicated the crystalline anhydrous state of both the drugs. There was no peak (other than degradation exotherm at 330°C) observed for the non-crystalline HPMC, while for the semi-crystalline microcrystalline cellulose, a minor broad peak at 90°C and a small endothermic peak at 326.7°C was seen. Carbopol 931P showed a small moisture peak at 68.32°C and main broad endothermic peak at 271.5°C, which was typical of amorphous hydrated substances. Similar findings have been reported by other researchers also (Gomez-Carracedo et al., 2004). EC 7 FP Premium display a large exothermic peaks at 190°C and 383°C which resulted from the oxidative degradation of the polymer. Guyot and Sabcegez-Lafyebte have observed similar results in their studies (Guyot and Fawaz, 1998; Sanchez-Lafuente et al., 2002). Eudragit L 100 had a broad endothermic peak at 220.7°C corresponding to the glass transition of the polymer. Xanthan gum, a polysaccharide resulted in minor thermal transition at 286.2°C. The probable reason may be due to thermal scission of the carboxylate groups and evolution of CO₂ from the corresponding carbohydrate backbone (Zohuriaan and Shokrolahi, 2004). Starch 1500 gave two endothermic peaks, one at about 70-80°C due to gelation in the presence of moisture and the other at 265°C (Ferraria et al., 1997; Kapusniak and Siemion, 2007) corresponded to the

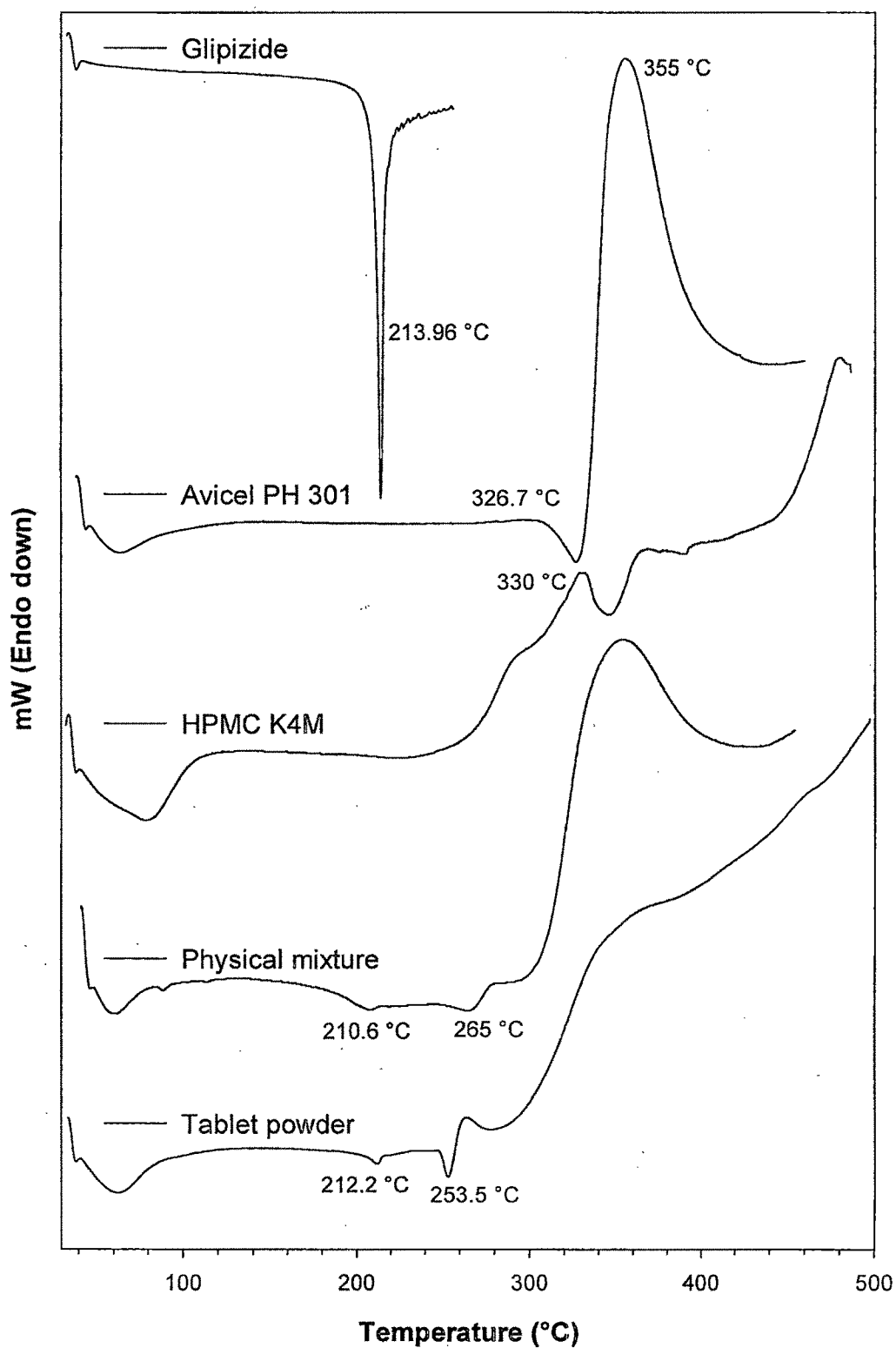


Figure .1. DSC thermograms of drug, individual excipient, physical mixture, and tablet powder for M-3 (HPMC K4M:MCC PH301 at 25:75) formulation.

thermal decomposition. Sodium alginate showed degradation exotherm at 251.2°C whereas carrageenan resulted in exothermic peak at 261.3°C and

degradation peak at 344°C. The thermogram of the cationic chitosan polymer exhibited an endothermic peak at about 94°C that has been attributed to the evaporation of absorbed water. The exothermic baseline deviation started after 250°C indicated the onset of chitosan degradation (Khalid et al., 2002). Two endothermic peaks at 97°C and 102°C were observed for magnesium stearate. In fact, glipizide or nateglinide crystallinity peaks were evident in the physical mixtures of all combination batches without any shift in the endotherms indicated the compatibility of both the drugs with all the polymers used in the study. The DSC curves for excipients, physical mixture, and tablet powder for M-3 formulation has been shown in Figure 5.1. Physical mixture showed simple superposition of their separated component DSC curves. According to the DSC findings of the matrix tablet powders, no major thermal event corresponding to chemical interaction was observed. Similar observations were obtained with all other optimized matrix tablets of glipizide and nateglinide, hence were not shown. The negligible shift of the individual components in the tablet powder may be as a consequence of mechanical treatment of the sample during compression, owing to the more intimate contact between the components, as well as the finer dispersion of the drug into the amorphous matrix of the polymer without suffering any chemical interaction or degradation process. Hence, it indicated the absence of any drug-excipient interaction or complex occurred during the manufacturing of all matrix studied. All these confirmed the suitability of all excipients with both the drugs to prepare controlled-release inert matrices.

5.1.2. CHARACTERIZATION OF PHYSICAL MIXTURE

Before tableting, the powder mixture was checked for its ability to flow and compress so that the tablets of desired characteristic can be obtained. The compressibility index is a measure of the propensity of a powder to consolidate. According to the literature data (Wells and Aulton, 1988; Wells, 1997), powders with a compressibility index (I_c) between 5 to 18% are suitable for producing tablets, and those with a Hausner ratio (R_H) below 1.25, and angle of repose (θ) between 20° to 42° are of good flowability (lower angle of repose indicate better flow). All studied powder blends, except few cases, were free flowing and suitable for compression as demonstrated by the values of I_c between 5.82 to 17.11, R_H in the range of 0.87-1.25, and angle of repose within 26.8° to 39.2°. These are important characteristics for a potential direct compression mixtures (Steendam and Lerk, 1998). For few systems, both I_c and R_H were beyond the range, thus not suitable for compression into tablets, and discussed in relevant subsequence sections.

5.1.3. CHARACTERIZATION OF MATRIX TABLETS

The results indicated that all the tablets prepared in this study meet the USP 29 requirements for weight variation tolerance (USP 29 - NF 24, 2006). Drug content of all tablet formulations were found in the range of 98.0 to 102.0%. The thicknesses, diameters, and hardness variation of the individual tablet batches were within ± 3 SD. Tablets of the same batch showed consistent dissolution behavior with small standard deviations in the subsequent dissolution studies.

5.2. Analytical Method development

5.2.1. ESTIMATION OF GLIPIZIDE (SPECTROSCOPIC METHOD)

For the spectroscopic method, a standard curve was plotted in phosphate buffer pH 6.8 at 276 nm and regression equation was calculated as $y=0.0166x+0.0093$, in which x is the concentration ($\mu\text{g ml}^{-1}$), and y is the absorbance. The method was found linear within the analytical range of 1–50 $\mu\text{g ml}^{-1}$ with regression coefficient r^2 of 0.9997.

5.2.2. ESTIMATION OF NATEGLINIDE (SPECTROSCOPIC METHOD)

Spectroscopic estimation of nateglinide was carried out in phosphate buffer pH 6.8 at 210 nm and regression equation was found to be $y=0.0326x-0.0087$, where x is the concentration ($\mu\text{g ml}^{-1}$), and y is the absorbance. The method was linear over an analytical range of 1–50 $\mu\text{g ml}^{-1}$ with regression co-efficient r^2 of 0.9991.

5.2.3. ESTIMATION OF GLIPIZIDE (HPLC METHOD)

A sensitive, fast and novel chromatographic method for the determination of glipizide in rabbit plasma was optimized and validated.

5.2.3.1. Optimization of Chromatographic Conditions

5.2.3.1.1. Effect of Mobile Phase pH

The pH was varied (2, 3, and 4) to achieve the satisfactory separation and quantitation, at fixed mobile phase composition (ACN:PBS; 70:30 v/v) and flow rate of 1 ml/min. Figure 5.2 shows the observed chromatographic responses as a

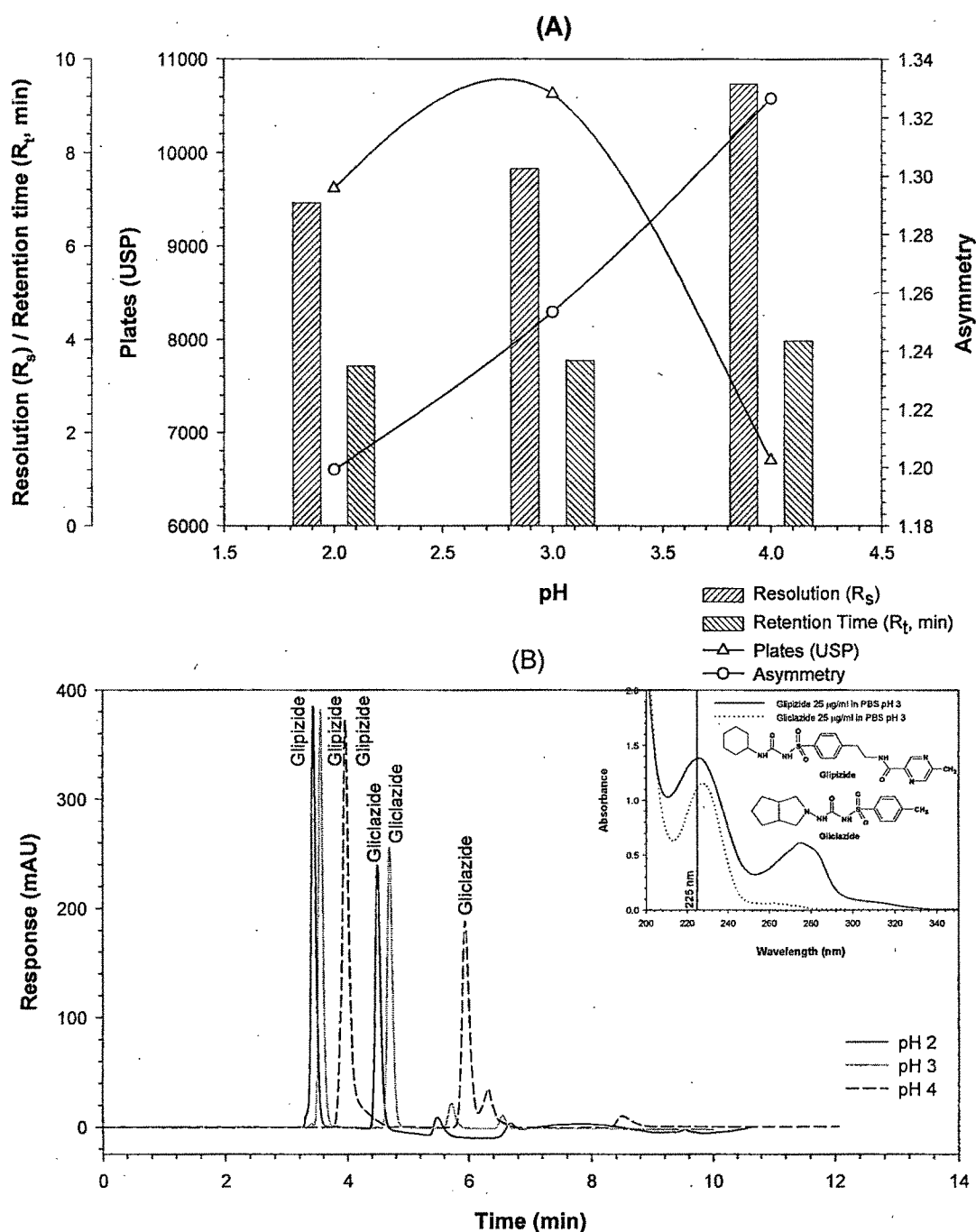


Figure .2. Effect of mobile phase pH (2, 3, 4) on (A) resolution, retention time, theoretical plates, and asymmetry; and on (B) chromatograms at mobile phase composition of 70:30 (ACN:PBS; v/v) and flow rate of 1.0 ml/min. Insert graph shows UV spectra of glipizide and gliclazide.

function of pH. It is obvious from the figure that as pH of the mobile phase increases; retention time increases and thereby results in similar pattern for resolution between glipizide and IS also. Similarly, as pH increases, the peak tailing increases thus increase in the asymmetry values of the peaks were

Table 1. Effect of mobile phase pH, composition, and flow rate on various chromatographic parameters for glipizide estimation.

Sr. No.	Variable	Value	Unretained Peak (t_0 , min)	Retention Time (R_t , min)	Width (W , min)	Width at 5% ($W_{5\%}$, min)	Width at 10% ($W_{10\%}$, min)	Width at 50% ($W_{50\%}$, min)	Capacity Factor (k')	Separation Factor (α)	HETP (h)
1	Mobile phase	2	0.9140	3.4285	0.1398	0.1967	0.1627	0.0817	2.7511	1.4245	0.0260
	(mobile phase) pH	3	0.9490	3.5487	0.1377	0.1838	0.1568	0.0808	2.7394	1.4422	0.0235
		4	0.9538	3.9608	0.1535	0.2073	0.1724	0.1117	3.1527	1.6592	0.0373
		60:40	0.9928	3.9993	0.1767	0.2413	0.2033	0.1027	3.0283	1.6860	0.0305
2	mobile phase	70:30	0.9490	3.5487	0.1377	0.1838	0.1568	0.0808	2.7394	1.4422	0.0235
	Composition (v/v)	80:20	1.0443	4.8193	0.1875	0.2487	0.2122	0.1097	3.6148	1.7469	0.0237
3	flow rate	0.8	1.0690	4.5933	0.1798	0.2475	0.2085	0.1050	3.2969	1.4863	0.0240
	(ml/min)	1	0.9490	3.5487	0.1377	0.1838	0.1568	0.0808	2.7394	1.4422	0.0235
		1.2	0.9165	3.0692	0.1268	0.1752	0.1470	0.0740	2.3488	1.5371	0.0267

observed. However, the number of theoretical plates reached its maximum level at pH 3 (as compared to pH of 2 and 4). Other important chromatographic parameters such as peak width, capacity factor, separation factor and HETP at different pH are enumerated in Table 5.1. Based on the importance of the different performance parameters of the method, pH 3 was found to be optimum and further optimization was carried out at this pH.

The dissociation constant (pK_a) of glipizide is ~ 5.9 . According to this value, degree of ionization increases with increase in pH. The retention time for glipizide could have decreased with using octadecylsilane (ODS, C_{18}) column because of the less interaction between drug and C_{18} under ionized condition with increase in pH. However, the mobile phase contained 70% ACN which does not have much affinity for the ionized hydrophilic drug species and elutes them later. This could be the probable reason for the delay of retention time for glipizide with increase in pH. The same can be the reason for increasing the asymmetry value with increase in pH value also. The IS (gliclazide, $pK_a \sim 5.98$) has the same reason for delay in retention time. Thus delay in retention time of both glipizide and IS, results in better resolution (due to increased distance between the adjacent peaks). The plate number is expected to be increased with increase in retention time because it is directly proportional to the same. However, plate number is also inversely proportional function of peak width (may be due to asymmetry/tailing). Thus the maximum plate number at pH 3 is indicative of optimum balance between retention time and asymmetry value.

5.2.3.1.2. Effect of Mobile Phase Composition

To study the effect of mobile phase composition on the chromatographic responses, the ACN:PBS ratio was varied from 60:40, 70:30, to 80:20 v/v at the pH of 3 and flow rate of 1 ml/min. As shown in Figure 5.3, the retention time was minimum at 70:30 v/v mobile phase composition, a one of the favorable criterion for the rapid and cost effective method. Even with the least retention time, the highest theoretical plates (>10000) and enough resolution (>7) and good peak shape was achieved. Values of other chromatographic parameters at different mobile phase composition are depicted in Table 5.1 for comparative study.

Generally, increasing the organic solvent concentration in the mobile phase induces a decrease in the distance between the solute molecule and the terminal carbon atoms (C_{18}) in the ODS ligand, and it results in lower retention time (Ban and Kiyokatsu, 2001). Similar findings were observed in the present study up to 70:30 v/v composition, but further increase in ACN content resulted in increased retention time. This may be explained by following. The elution power of mobile phase decreased at 60:40 v/v because relative amount of ACN decreased and

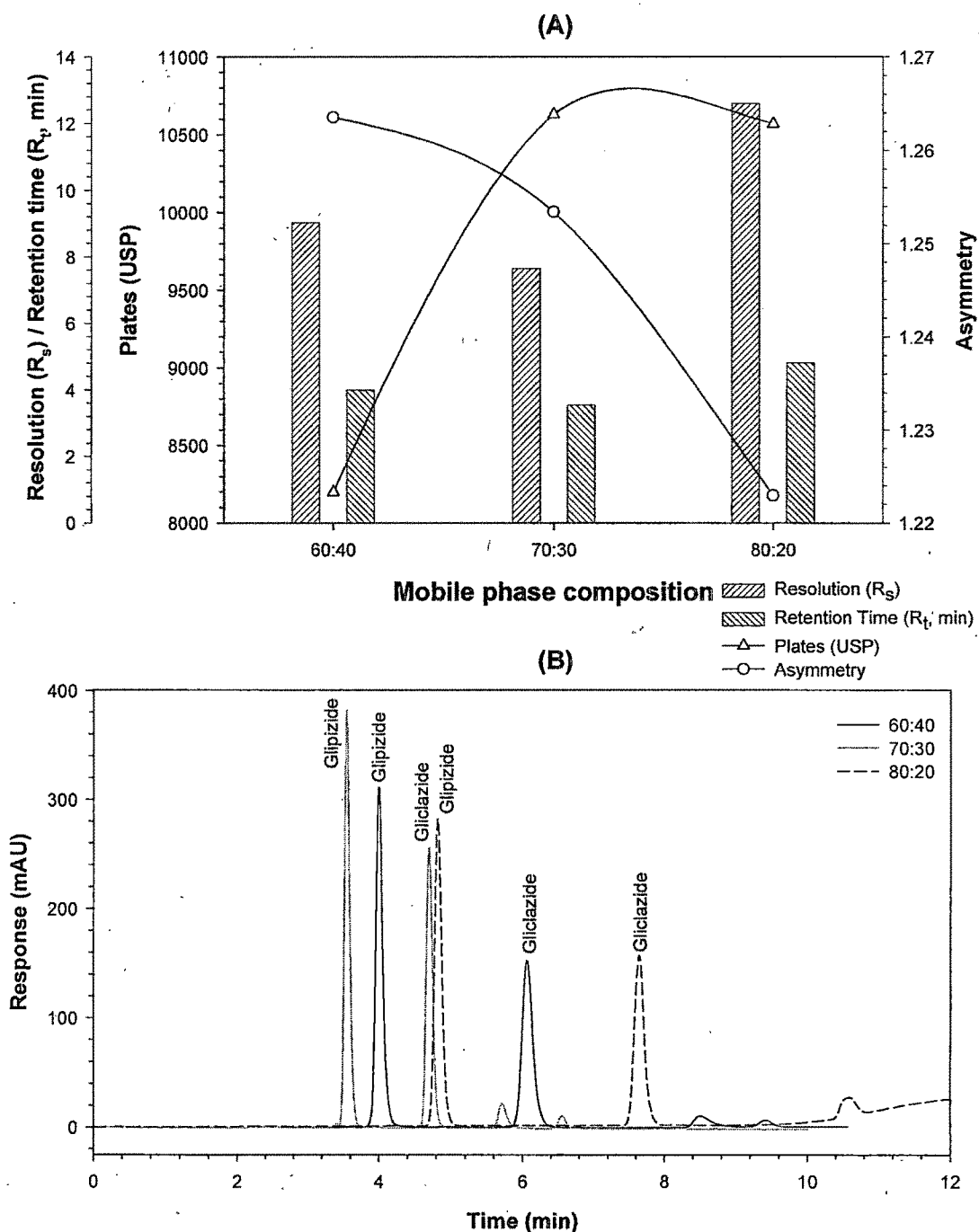


Figure 3. Effect of mobile phase composition (ACN:PBS, 60:40, 70:30, 80:20) on (A) resolution, retention time, theoretical plates, and asymmetry; and on (B) chromatograms at pH 3 and flow rate of 1.0 ml/min.

glipizide was eluted at higher retention time. In contrast to this at 80:20 v/v composition, the relative concentration of PBS decreased significantly and there was no sufficient buffer capacity to keep the fraction of drug in ionized form. Thus there was tremendous increase of unionized species which will strongly interact with stationary phase and result in delayed retention time with broad peak.

However, at 70:30 v/v composition, proper balance was attained between these two situations and resulted in least retention time. The continuous decrease in asymmetry value with decrease in PBS content of mobile phase composition can be explained by progressively decrease in ionized species (which is directly proportional to PBS content). The presence of only unionized species gives symmetric peak compare to a combination of ionized and unionized species. The peak width at 60:40 and 80:20 were more due to asymmetry and strong interaction of unionized species with stationary phase (as explained above), respectively. Thus, the plate number at 70:30 composition of ACN:PBS was maximum.

5.2.3.1.3. Effect of Mobile Phase flow rate

From Figure 5.4(A and B), it can be observed that theoretical plates were highest at flow rate of 1 ml/min. The asymmetry and retention time decreased as the flow rate increased. The values of capacity factor, and separation factor (Table 5.1) also indicate optimum flow rate of 1 ml/min.

At flow rate of 1.2 ml/min, due to higher mobile phase flux, the solute is eluted faster without proper partition and resulted in asymmetric broad peak. Whereas the flow rate of 0.8 ml/min gives solute sufficient time to partition with stationary phase and result in most symmetric peak but with delayed retention time. Thus, at flow rate of 1.0 ml/min, there was an optimum balance between retention time and peak width and resulted in maximum plate number.

5.2.3.2. Proposed Chromatographic Method

Looking at the different chromatographic parameters during the method development, the finally recommended mobile phase consisted of ACN:PBS of 70:30 v/v adjusted to pH 3. The best resolution and sensitivity of the method was obtained at 225 nm and at flow rate of 1 ml/min. Typical chromatogram at the optimized condition gave sharp and symmetric peak with retention time of 3.5 and 4.7 min for glipizide and IS, respectively. Thus, within very short time the system became ready for the next sample injection without the need for additional wash time.

5.2.3.3. Validation of the Proposed Method

5.2.3.3.1. Calibration Curve (Linearity)

Nine calibration standards prepared by spiking the blank plasma with glipizide and IS were chromatographed at the optimized condition. When the peak area

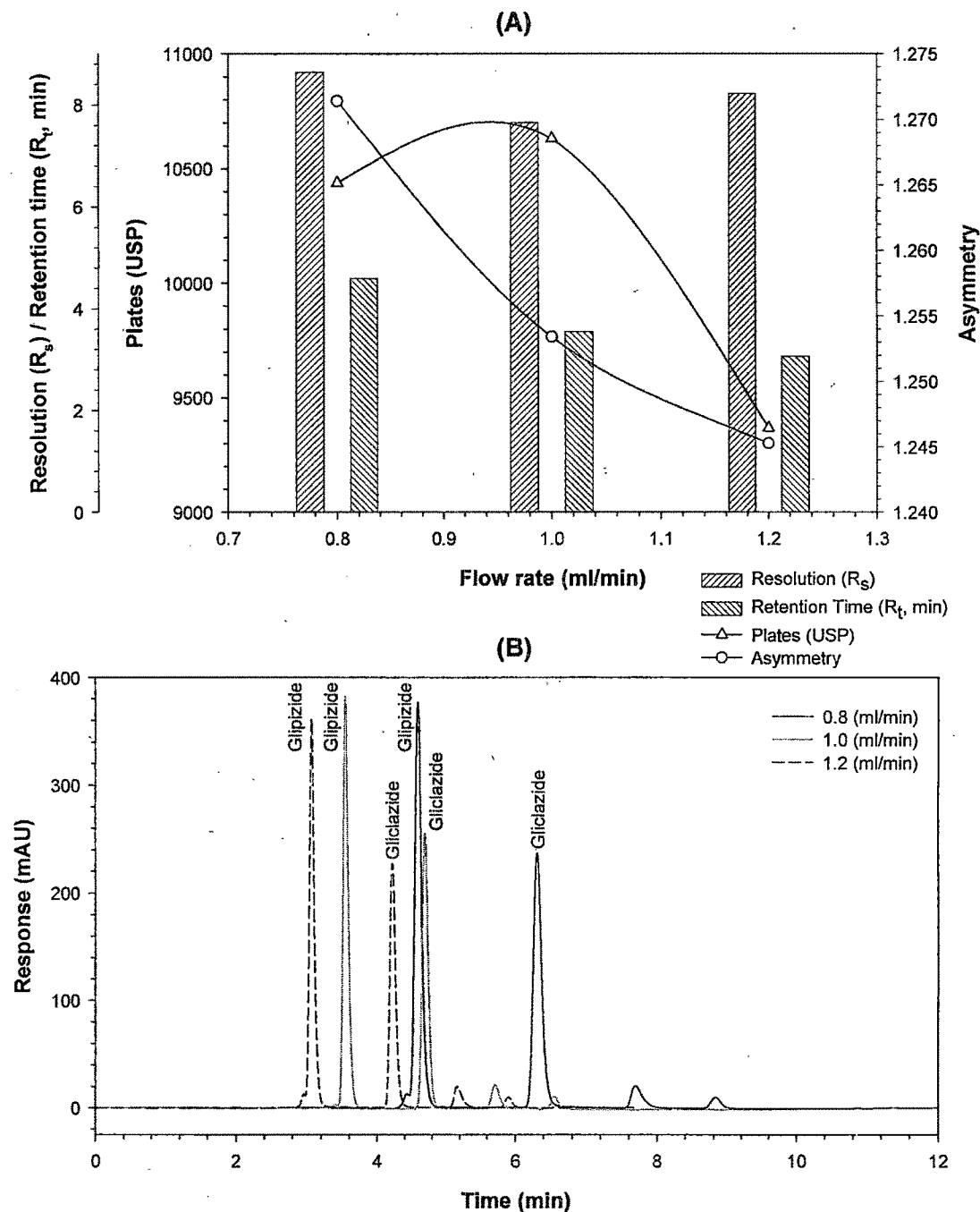


Figure .4. Effect of mobile phase flow rate (0.8, 1.0, 1.2 ml/min) on (A) resolution, retention time, theoretical plates, and asymmetry; and on (B) chromatograms at mobile phase composition of 70:30 (ACN:PBS) and pH 3.

ratios of glipizide to IS were plotted against the respective glipizide concentrations, an excellent linearity was achieved with correlation coefficients of 0.9944 over an analytical range of 10 to 2500 ng/ml. The linear regression equation was calculated by the least squares method using Microsoft Excel® program and summarized in Table 5.2.

The variance of response variable $S_{y,x}^2$, was calculated to be 49.73, indicates low variability between the estimated and calculated values. This further confirms negligible scattering of the experimental data points around the line of regression and good sensitivity of the proposed method. The variance of slope (S_b^2) and intercept (S_a^2) were obtained as 8.25 and 10.37, respectively. The calculated t -value for slope and intercept were reported in Table 5.2 and were less than tabulated t -values. This shows that the intercept is not significantly different from zero, indicating no interference in the estimations. Further the slope and intercept were within the confidence interval.

Table .2. Spectral and statistical data for determination of glipizide by proposed HPLC method.

Parameters	Value
Absorption maxima, λ_{\max} (nm)	225
Linearity range (ng ml ⁻¹)	10 – 2500
Coefficient of determination (r^2)	0.9944
Correlation coefficient (r)	0.9972
Regression equation (Y^a)	$Y=59.8925 x + 3.4306$
Slope (b)	59.8925
t_{cal}^b	0.7519
Confidence interval ^c	53.1141 to 66.6709
Intercept (a)	3.4306
t_{cal}^b	1.0654
Confidence interval ^c	-4.1687 to 11.0299
Limit of Detection, LoD (ng ml ⁻¹)	2.6409
Limit of Quantitation, LoQ (ng ml ⁻¹)	8.8030

^a $Y=a+bx$, where x is the concentration ($\mu\text{g/ml}$).

^b $t_{tab} = 2.36$ for 95% two sided confidence interval for 7 degrees of freedom.

^c Confidence interval was calculated at 95% two sided t value for 7 degrees of freedom.

5.2.3.3.2. Accuracy and Precision

Accuracy data in the present study ranged from 99.12 to 100.03% (Table 5.3) indicates that there was no interference from endogenous plasma components. Inter-day as well as intra-day replicates of glipizide, gave an SD below 10.74 (should be less than 15 according to CDER guidance for Bio-analytical Method Validation (US FDA CDER Guidance for the Industry, 2001)), revealed that the

proposed method is highly precise. Accuracy of the method was evaluated by using t -test at four different concentration levels within an analytical range. The t_{tab} value for significance at 5% level at 5 degrees of freedom is 2.57 (for intra-day) and that for 2 degrees of freedom is 4.30. The t_{cal} values obtained at each concentration level is shown in Table 5.3 and are well below t_{tab} values. Thus no significant difference was observed between the amounts of drug added and recovered. Overall, the data summarized in Table 5.3, enables the conclusion that an excellent accuracy and high precision was obtained.

Table .3. Summary of inter-day (n=3) and intra-day (n=6) precision and accuracy of the method in rabbit plasma

Nominal concentration (ng/ml)	Mean Concentration found ^a (ng/ml)	SD	Precision (RSD, %)	Mean Accuracy ^b (%)	t_{cal} ^c	Confidence interval (CI)
Inter-day (n=3) ($t_{tab} = 4.30$ for $n-1 = 2$)						
10	10.00	0.20	1.99	100.03	0.03	10±0.29
500	496.74	5.86	1.18	99.35	0.96	500±8.70
1000	993.96	8.04	0.81	99.40	1.29	1000±11.93
2500	2498.55	4.44	0.18	99.94	0.56	2500±6.59
Intra-day (n=6) ($t_{tab} = 2.57$ for $n-1 = 5$)						
10	10.02	0.15	1.54	100.18	0.29	10±0.16
500	495.62	6.11	1.23	99.12	1.74	500±6.41
1000	994.47	6.87	0.69	99.45	1.96	1000±7.20
2500	2491.45	10.74	0.43	99.66	1.94	2500±11.27

^a Average of three and six determinations at three concentration levels for inter-day and intra-day respectively.

^b All the mean accuracies were calculated against their nominal concentrations.

^c $t_{cal} = \frac{|100 - R| \sqrt{n}}{RSD}$, where t_{cal} is the calculated t value, n is the number of replicates, and R is mean accuracy. Tabulated t (t_{tab}) value for 95% two sided confidence interval for 5 and 2 degree of freedom were 2.57 and 4.30, respectively.

5.2.3.3.3. Sensitivity

The LoD and LoQ were found to be 2.64 and 8.80 ng/ml, respectively. When this method is applied to plasma samples, its sensitivity was found to be adequate for pharmacokinetic studies.

5.2.3.3.4. Selectivity

Any potential interference (overlapping peaks) due to plasma endogenous components were within 1.5 – 3.0 min only (Figure 5.5), later on there was no significant interference from blank plasma that affected the response of glipizide and IS.

5.2.3.3.5. Stability

Sample solution injected over a period of 1 month did not suffer any appreciable changes in assay value and meet the criterion mentioned above. Hence, the samples were stable during one month when stored at – 20°C until analysis.

5.2.3.3.6. Extraction efficiency

Extraction efficiency represents the effectiveness of the extraction step and the accuracy of the proposed method. As shown in Table 5.4, extraction efficiency of glipizide from rabbit plasma samples was satisfactorily ranged from 97.34 to 98.73%, which confirm no interference effects due to plasma components throughout the range studied. Recovery of IS was consistent with the accuracy of 98.69% and RSD of 1.77% ($n = 6$).

Table 5.4. Extraction efficiency of GPZ from rabbit plasma at various concentrations.

Theoretical concentration (ng/ml)	Concentration found ^a (ng/ml)	Extraction efficiency (%)	RSD
50	49.075	98.15	1.99
500	486.7	97.34	1.52
1000	987.3	98.73	1.21
2000	1951.2	97.56	0.97

^a Average of six determinations.

5.2.3.4. Pharmacokinetic Analysis of Glipizide from Rabbits

After glipizide oral solution administration, the drug plasma concentrations were monitored for 24 h and shown in Figure 5.6. However, glipizide plasma profile following oral solution after 12 h was below LoQ and hence the same for 16, 20, and 24 h were extrapolated using $A \cdot e^{-k \cdot t}$, where A is the intercept of the terminal elimination regression line of the $\ln(\text{concentration})$ vs. time profile. The mean glipizide pharmacokinetic parameters for oral solution are summarized in Table 5.5. The results were calculated by non-compartmental analysis. The rapid

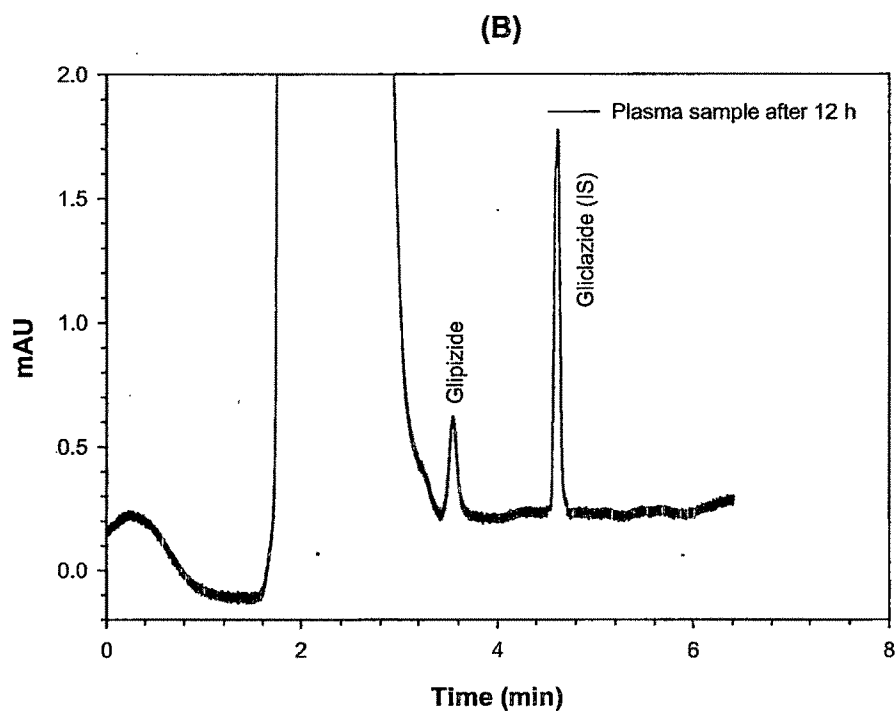
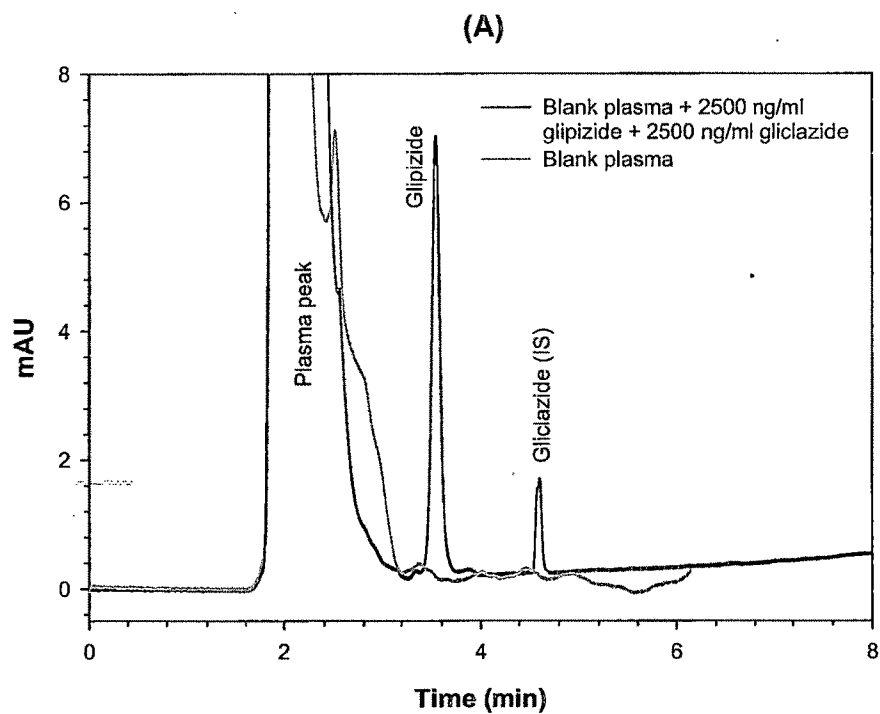
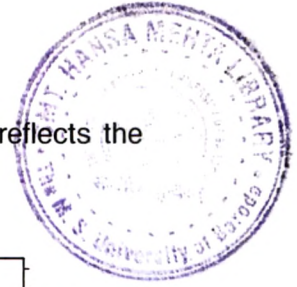


Figure 5.5. (A) Representative chromatograms of blank plasma and the same spiked with 2500 ng/ml of both glipizide and gliclazide (IS). (B) Plasma sample taken from a rabbit 12 h after a 1.87 mg oral dose of glipizide (quantitated to be 138.39 ng/ml) spiked with 2500 ng/ml IS.



decrease in glipizide concentration after oral solution administration reflects the fast disposition and elimination of the drug.

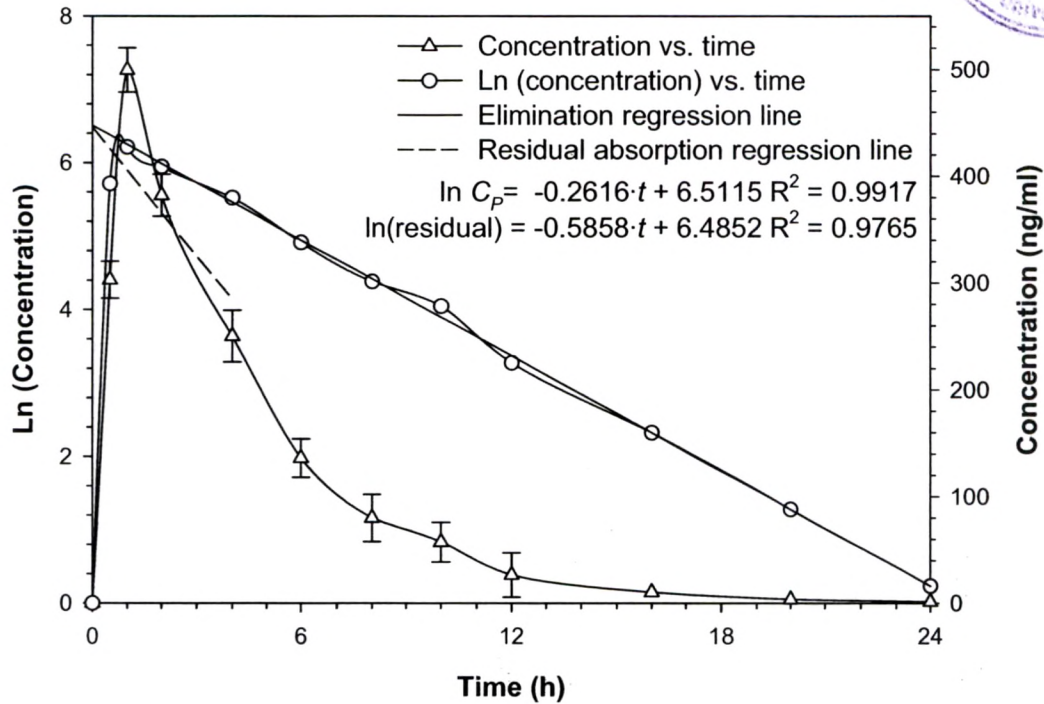


Figure 5.6. Mean plasma glipizide concentration vs. time profile after administration of single dose of oral solution.

Table 5.5. Pharmacokinetic parameters of glipizide after administration of single dose of oral solution.

Sr. No.	Pharmacokinetic parameters	Observed value
1	Absorption rate constant, k_a (h^{-1})	0.59
2	Elimination rate constant, k_{el} (h^{-1})	0.26
3	Time required for maximum plasma concentration, T_{\max} (h)	1.0
4	Maximum plasma concentration, C_{\max} (ng/ml)	499.41
5	Plasma half life, $T_{1/2}$ (h)	2.65
6	Area under curve at 12 hours, $AUC_{(0 \rightarrow 12)}$ (ng·h/ml)	2282.68
7	Area under curve from 12 hours to ∞ , $AUC_{(12 \rightarrow \infty)}$ (ng·h/ml)	4.83
8	Area under curve at infinite time, $AUC_{(0 \rightarrow \infty)}$ (ng·h/ml)	2287.51
9	Area under momentum curve at 12 h, $AUMC_{(0 \rightarrow 12)}$ (ng·h ² /ml)	9608.28
10	Volume of distribution, V_d (lit)	3.45
11	Mean residence time, MRT (h)	4.21
12	Total clearance rate, TCR (l/h)	1.31
13	Clearance, Cl ($\text{ml} \cdot \text{h}^{-1}$)	0.82

5.2.4. ESTIMATION OF NATEGLINIDE (HPLC METHOD)

Rapid, sensitive and novel HPLC method for determination of nateglinide in rabbit plasma was optimized and validated.

5.2.4.1. Optimization of Chromatographic Conditions

5.2.4.1.1. Effect of Mobile Phase pH

With the aim of the optimization of mobile phase pH (2, 3, and 4), the remaining two factors were kept constant i.e. mobile phase composition (ACN: PBS; 70:30 v/v) and flow rate of 1 ml/min. Observed chromatographic responses were plotted against respective pH. As shown in the Figure 5.7 (A), retention time increases with the increase in pH while asymmetry decreases. The number of theoretical plates as well as resolution between nateglinide and IS was maximum at pH 3. Moreover, the changes in peak width, capacity factor, separation factor and HETP are enumerated in Table 5.6. Looking at the importance of the different chromatographic parameters, pH 3 was found to be optimum. Figure 5.7 (B) shows the chromatograms at different pH and mobile phase composition of 70:30 (ACN:PBS; v/v) and flow rate of 1.0 ml/min.

The dissociation constant (pK_a) of nateglinide is ~ 3.1 at (21-24°C). According to this value, $\sim 90\%$, $\sim 50\%$, and $\sim 10\%$ of the drug will be unionized at pH 2, 3, and 4 respectively. As the pH increased, the retention time for nateglinide could have decreased with using octadecylsilane (ODS, C_{18}) column because of the less interaction between drug and C_{18} under ionized condition with increase in pH. However, the mobile phase contained 70% ACN which does not have much affinity for the ionized hydrophilic drug species. This could be the probable reason for the delay of retention time for nateglinide with increase in pH. The asymmetry value decreases with increase in pH. At lower pH the nateglinide will be carried out faster with mobile phase, however due to higher unionized species, the drug has a tendency to stick/partition with stationary phase too. This result in tailing and hence increase in asymmetry value at lower pH. At higher pH value, the ionized hydrophilic species are not much portioned with stationary phase and hence gives symmetric peak. The resolution was poor at pH 4 using gliclazide as an IS, but was highest at pH 3. Similarly, the plate number (highest for higher retention time and smallest peak width) was highest at pH 3. Thus, the best chromatographic separation was achieved at pH 3, and hence was considered to be optimum.

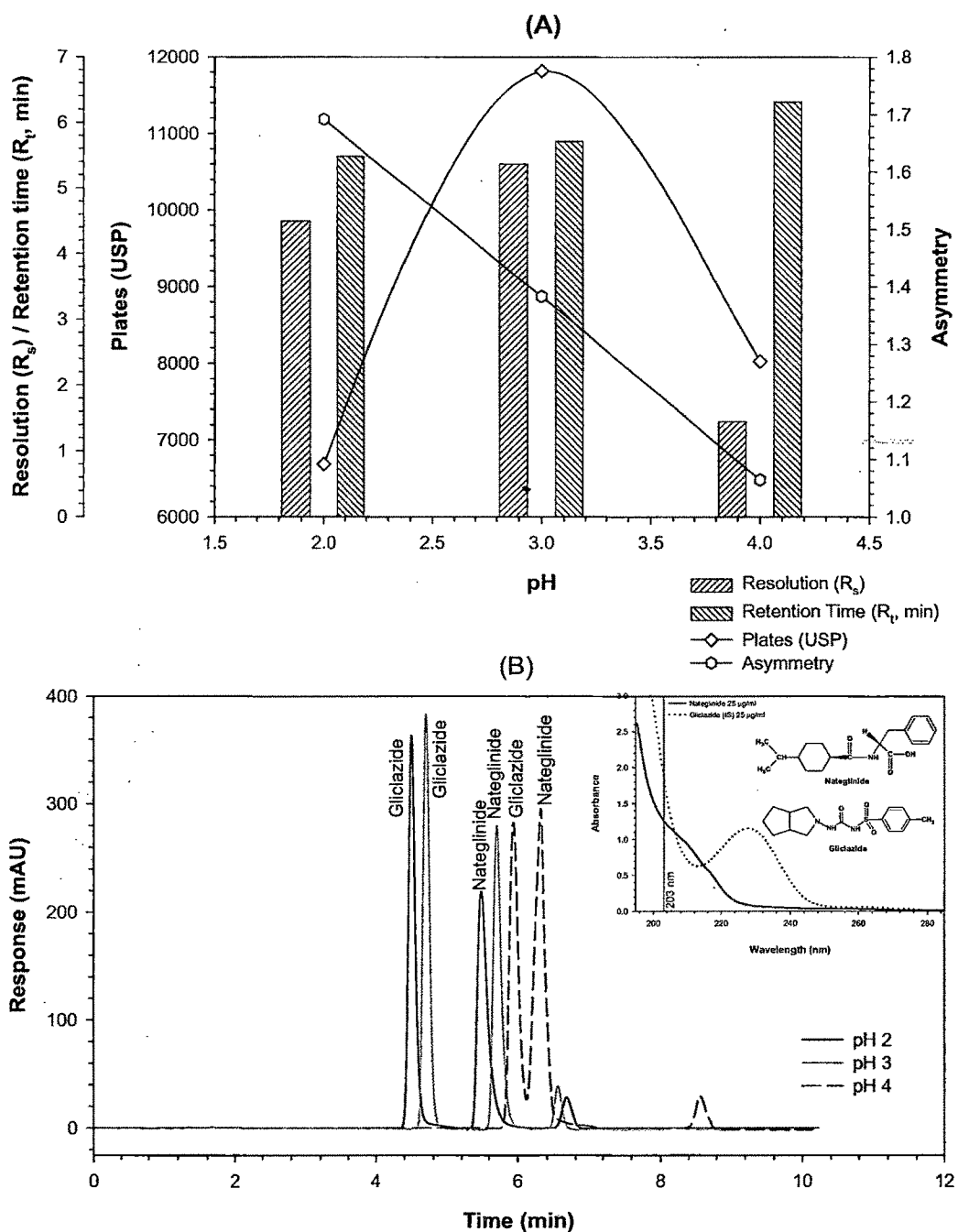


Figure 5.7. Effect of mobile phase pH (2, 3, 4) on (A) resolution, retention time, theoretical plates, and asymmetry; and on (B) chromatograms at mobile phase composition of 70:30 (ACN:PBS; v/v) and flow rate of 1.0 ml/min.

Table 5.6. Effect of mobile phase pH, composition, and flow rate on various chromatographic parameters for nateglinide estimation.

Sr. No.	Variable	Value	Unretained Peak (t_0 , min)	Retention Time (R_t , min)	Width (W, min)	Width at 5% ($W_{5\%}$, min)	Width at 10% ($W_{10\%}$, min)	Width at 50% ($W_{50\%}$, min)	Capacity Factor (k')	Separation Factor (α)	HETP (h)
1	Mobile phase pH	2	0.9140	5.4858	0.2683	0.3857	0.3228	0.1565	5.0020	0.7834	0.0374
		3	0.9490	5.7110	0.2102	0.2877	0.2427	0.1227	5.0179	0.7874	0.0212
		4	0.9538	6.3130	0.2818	0.3894	0.3237	0.1562	5.6188	0.9308	0.0311
		MP	60:40	0.9928	8.4978	0.4573	0.6847	0.5642	0.2637	7.5595	0.6754
2	Composition (v/v)	70:30	0.9490	5.7110	0.2102	0.2877	0.2427	0.1227	5.0179	0.7874	0.0212
		80:20	1.0443	10.5257	0.3635	0.4378	0.3797	0.2123	9.0789	0.6954	0.0186
3	Flow rate (ml/min)	0.8	1.0690	7.6972	0.2868	0.4133	0.3460	0.1678	6.2003	0.7901	0.0217
		1	0.9490	5.7110	0.2102	0.2877	0.2427	0.1227	5.0179	0.7874	0.0212
		1.2	0.9165	5.1685	0.2053	0.2985	0.2480	0.1202	4.6394	0.7781	0.0247

5.2.4.1.2. Effect of Mobile Phase Composition

The effect of mobile phase composition (i.e. ratio of ACN:PBS was studied at 60:40, 70:30, and 80:20 v/v levels) at pH 3 and the flow rate of 1 ml/min is shown in Figure 5.8. Minimum retention times of nateglinide and IS were obtained at 70:30 v/v level, which makes the method rapid, a one of the most desirable criteria. Though retention time was shorter, satisfactory resolution and asymmetry values were achieved. An adequate theoretical plates (~ 12000) is indicative of a good column performance. As can be seen from Figure 5.8, the asymmetry was >1.5 at 80:20 v/v and still higher at 60:40 v/v which indicates tailing of the peaks, but was < 1.4 at 70:30 v/v. Other chromatographic parameters at different composition of mobile phase are listed in Table 5.6.

Generally, increasing the organic solvent concentration in the mobile phase induces a decrease in the distance between the solute molecule and the terminal carbon atoms (C₁₈) in the ODS ligand, and it results in lower retention time (Ban and Kiyokatsu, 2001). Similar findings were observed in the present study up to 70:30 v/v composition, but further increase in ACN content resulted in increased retention time. This may be explained by following. The elution power of mobile phase decreased at 60:40 v/v because relative amount of ACN decreased and nateglinide was eluted at higher retention time. In contrast to this at 80:20 v/v composition, the drug affinity to stationary phase increased due to relatively lower buffer content in mobile phase and resulted in delayed elution. However, at 70:30 v/v composition, proper balance was attained between these two situations and resulted in least retention time. The least asymmetry at 70:30 compared to other two compositions can be explained on the same basis. Plate number increased with increase in ACN composition in mobile phase. However, the asymmetry value at 80:20 v/v was higher than that of at 70:30 v/v. These suggest that the increased plates at 80:20 v/v was due to higher retention time value (even though it had greater peak width due to tailing). Further, acceptable resolution (> 2) was achieved at 70:30 v/v composition and so was considered to be optimum.

5.2.4.1.3. Effect of Mobile Phase Flow Rate

From Figure 5.9(A and B), it can be observed that theoretical plates were highest at flow rate of 1 ml/min with asymmetry of less than 1.5. The change in flow rate had no significant effect on resolution while retention time decreased as the flow rate increased. The values of capacity factor, and separation factor (Table 5.6) also indicate optimum flow rate of 1 ml/min.

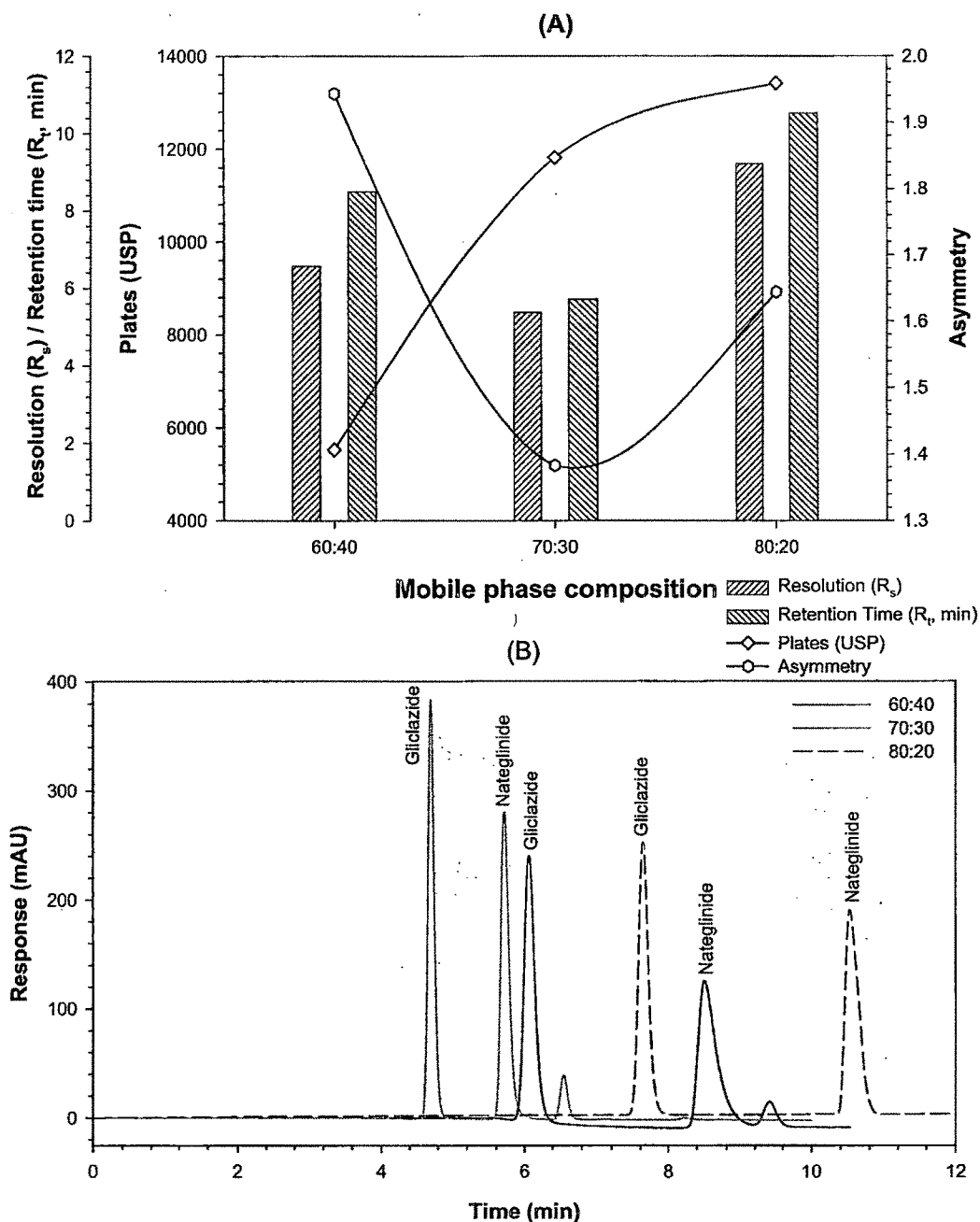


Figure 5.8. Effect of mobile phase composition (ACN:PBS, 60:40, 70:30, 80:20) on (A) resolution, retention time, theoretical plates, and asymmetry; and on (B) chromatograms at pH 3 and flow rate of 1.0 ml/min.

5.2.4.2. Proposed Chromatographic Method

Looking at the different chromatographic parameters during the method development, the finally recommended mobile phase consisted of ACN: 10 mM PBS of 70:30 v/v adjusted to pH 3. The best resolution and sensitivity of the

method was obtained at 203 nm and mobile phase flow rate of 1 ml/min. Typical chromatogram at the optimized condition gave sharp and symmetric peak with retention time of 4.7 and 5.7 min for IS and nateglinide, respectively. Thus within very short time the system became ready for the next sample injection without the need for additional wash time.

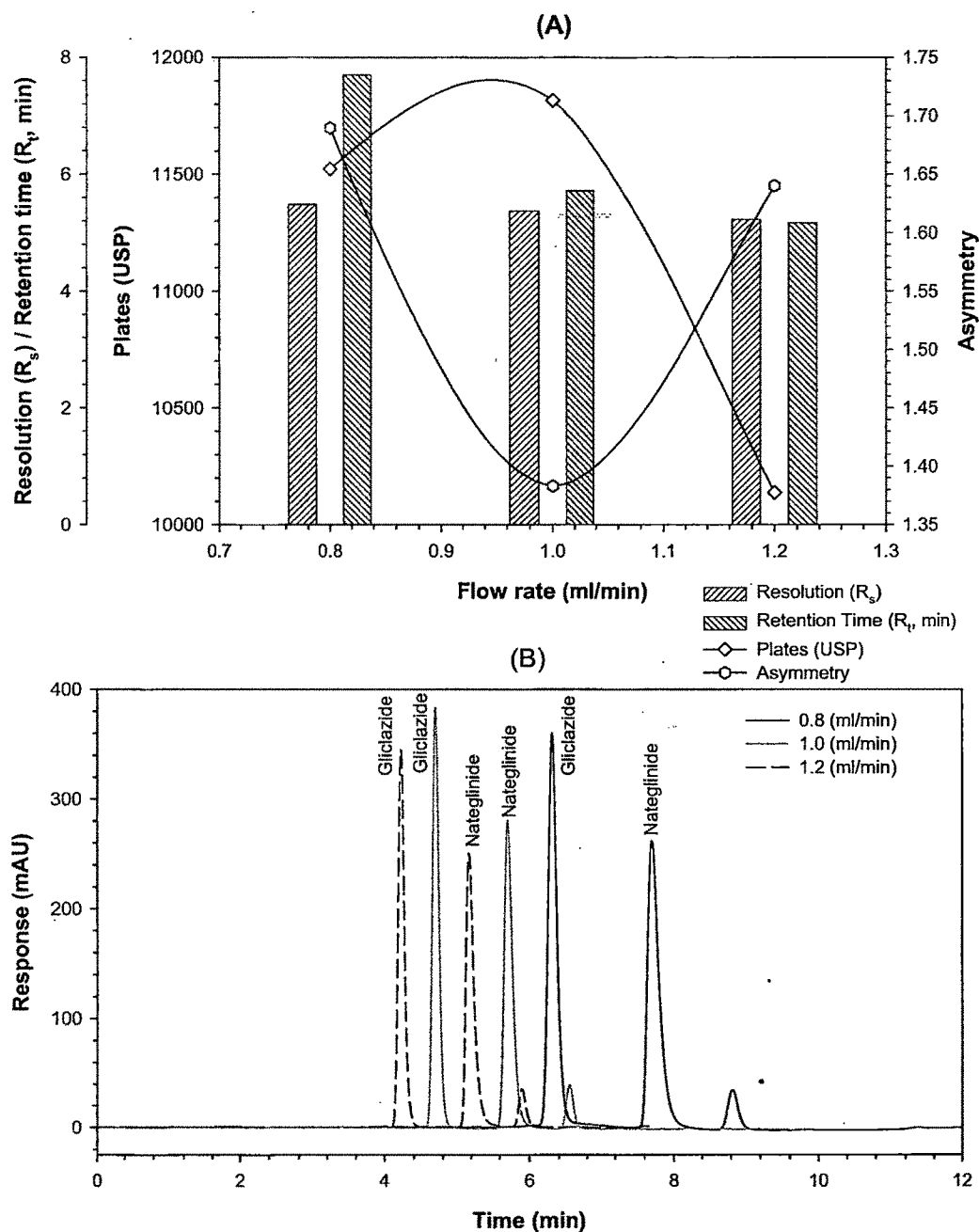


Figure 5.9. Effect of mobile phase flow rate (0.8, 1.0, 1.2 ml/min) on (A) resolution, retention time, theoretical plates, and asymmetry; and on (B) chromatograms at mobile phase composition of 70:30 (ACN:PBS) and pH 3.

5.2.4.3. Validation of the Proposed Method

5.2.4.3.1. Calibration Curve (Linearity)

Calibration curve (peak area ratio of nateglinide to IS versus nateglinide concentration) in plasma was constructed by spiking six different concentrations of nateglinide and fixed concentration of IS. The chromatographic responses were found to be linear over an analytical range of 10 to 2500 ng/ml and found to be quite satisfactory and reproducible with time. The linear regression equation was calculated by the least squares method using Microsoft Excel® program and summarized in Table 5.7. The correlation coefficient equals 0.9984, indicating a strong linear relationship between the variables.

Table 5.7. Spectral and statistical data for determination of nateglinide by proposed HPLC method.

Parameters	Value
Absorption maxima, λ_{\max} (nm)	203
Linearity range (ng ml ⁻¹)	10 – 2500
Coefficient of determination (r^2)	0.9969
Correlation coefficient (r)	0.9984
Regression equation (Y^a)	$Y=0.4186 + 3.9768 \cdot x$
Slope (b)	3.9768
t_{cal}^b	0.3799
Confidence interval ^c	2.4007 to 5.5529
Intercept (a)	0.4186
t_{cal}^b	0.6310
Confidence interval ^c	-1.2864 to 2.1236
Limit of Detection, LoD (ng ml ⁻¹)	2.91
Limit of Quantitation, LoQ (ng ml ⁻¹)	9.70

^a $Y=a+bx$, where x is the concentration ($\mu\text{g/ml}$).

^b $t_{\text{tab}} = 2.57$ for 95% two sided confidence interval for 5 degrees of freedom.

^c Confidence interval was calculated at 95% two sided t value for 5 degrees of freedom.

The variance of response variable $S_{y,x}^2$ calculated was 1.9634, indicates low variability between the estimated and calculated values. This further confirms negligible scattering of the experimental data points around the line of regression and good sensitivity of the proposed method. The variance of slope (S_b^2) and intercept (S_a^2) were obtained as 0.3761 and 0.4401, respectively. The calculated t -value for slope and intercept were reported in Table 5.7 and were less than tabulated t -values. This shows that the intercept is not significantly different from

zero, indicating no interference in the estimations. Further the slope and intercept were within the confidence interval.

5.2.4.3.2. Accuracy and Precision

Accuracy data in the present study ranged from 98.59 to 99.76% (Table 5.8) indicates that there was no interference from endogenous plasma components. Inter-day as well as intra-day replicates of nateglinide, gave an SD below 11.79 (should be less than 15 according to CDER guidance for Bio-analytical Method Validation (US FDA CDER Guidance for the Industry, 2001)), revealed that the proposed method is highly precise. Accuracy of the method was evaluated by using *t*-test at four concentration levels including the lowest quantifiable level. The *t*-values obtained for 10, 500, 1000, and 2500 ng/ml were 0.66, 2.17, 1.39, and 0.96 for inter-day whereas 0.74, 1.17, 1.64, and 1.22 for intra-day, respectively. The *t*-value required for significance at 5% level at 5 degrees of freedom is 2.57, and the obtained values were well below this value. Thus no significant difference was observed between the amounts of drug added and recovered. Overall, the data summarized in Table 5.8, enables the conclusion that an excellent accuracy and high precision was obtained.

Table 5.8. Summary of inter-day (n=3) and intra-day (n=6) precision and accuracy of the method in rabbit plasma.

Nominal concentration (ng/ml)	Mean Concentration found ^a (ng/ml)	SD	Precision (RSD, %)	Mean Accuracy ^b (%)	<i>t</i> _{cal} ^c	Confidence interval (CI)
Inter-day (n=3)						
10	9.95	0.13	1.31	99.50	0.66	10±0.19
500	492.93	5.57	1.13	98.59	2.17	500±8.26
1000	993.23	8.40	0.85	99.32	1.39	1000±12.47
2500	2493.68	11.38	0.46	99.75	0.96	2500±16.88
Intra-day (n=6)						
10	9.96	0.13	1.32	99.60	0.74	10±0.14
500	497.19	5.85	1.18	99.44	1.17	500±6.13
1000	995.21	7.12	0.72	99.52	1.64	1000±7.47
2500	2494.11	11.79	0.47	99.76	1.22	2500±12.37

^a Average of three and six determinations at three concentration levels for inter-day and intra-day respectively.

^b All the mean accuracies were calculated against their nominal concentrations.

^c $t_{cal} = \frac{|100 - R| \sqrt{n}}{RSD}$, where *t*_{cal} is the calculated *t* value, *n* is the number of replicates, and *R* is mean accuracy. Tabulated *t* value for 95% two sided confidence interval for 5 degree of freedom was (*t*_{tab}) 2.57.

5.2.4.3.3. Sensitivity

The LoD and LoQ were found to be 2.91 and 9.70 ng/ml, respectively. When this method is applied to plasma samples, its sensitivity was found to be adequate for pharmacokinetic studies.

5.2.4.3.4. Specificity

Any potential interference (overlapping peaks) due to plasma endogenous components were within 2-4 min only (Figure 5.10), later on there was no significant interference from blank plasma that affected the response of nateglinide and IS.

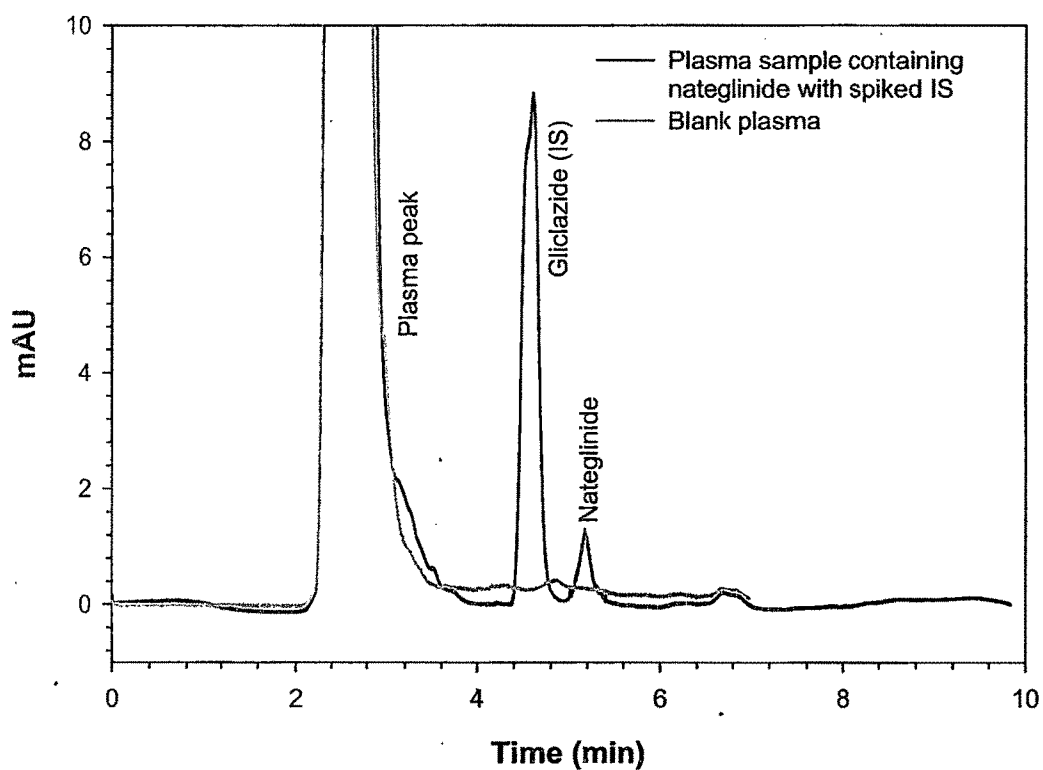


Figure 5.10. Representative chromatograms of blank plasma and clinical plasma sample taken from a rabbit 30 min after a 15mg oral dose of NTG (quantitated to be 26.42 ng/ml) spiked with IS.

5.2.4.3.5. Stability

Sample solution injected over a period of 1 month did not suffer any appreciable changes in assay value and meet the criterion mentioned above. Hence, the samples were stable during one month.

5.2.4.3.6. Extraction Efficiency

Extraction efficiency was performed to verify the effectiveness of the extraction step and the accuracy of the proposed method. As shown in Table 5.9, extraction efficiency of nateglinide from rabbit plasma samples was satisfactorily ranged from 97.86 to 98.62%, which confirm no interference effects due to plasma components. Recovery of IS was found to be 98.42% (% RSD = 1.47).

Table 5.9. Extraction efficiency of NTG from rabbit plasma at various concentrations.

Theoretical concentration (ng/ml)	Concentration found ^a (ng/ml)	Extraction efficiency (%)	RSD
50	48.93	97.86	2.05
1000	986.20	98.62	1.81
2000	1962.80	98.14	1.76

^a Average of six determinations.

5.2.4.3.7. System Suitability

System suitability tests, an integral part of a chromatographic analysis is used to verify that the resolution and reproducibility of the chromatographic system are adequate for the analysis (Meyyanathan et al., 2004). A system suitability test according to USP was performed on the chromatograms obtained from standard and test solutions to check different above mentioned parameters and the results obtained from six replicate injections of the standard solution are summarized in the Table 5.10.

Table 5.10. System suitability parameters.

Sr. No.	Parameters	Nateglinide ^a	Gliclazide (IS) ^a
1	Retention time, R _t (min)	5.70	4.68
2	Area (mAU·s)	10.680	11.023
4	Capacity Factor (<i>k'</i>)	5.0246	3.9210
5	Separation Factor (α)	0.7804	-
6	Theoretical plates (USP)	13259	13353
7	HETP (<i>h</i>)	0.0018	0.0019
8	Resolution (R _s)	5.3816	-
9	Asymmetry (A _s)	1.3721	1.1988
10	RSD (%)	1.43	1.38

^a Average of six determination.

5.2.4.4. Pharmacokinetic Analysis of Nateglinide from Rabbits

The developed method was applied to quantify nateglinide concentration in pharmacokinetic study carried out on rabbits. HPLC chromatogram of rabbit plasma is shown in Figure 5.10, which shows typical chromatograms of blank rabbit plasma and nateglinide in plasma after 30 min of drug administration. Representative mean plasma concentrations versus time profiles following a single oral administration of nateglinide to three rabbits are presented in Figure 5.11, it shows the natural log concentration versus time plot along with trendline for absorption and elimination rate constants. Various other pharmacokinetic parameters have been summarized in Table 5.11. The T_{max} and $T_{1/2}$ of nateglinide in the present study was similar, although the intake doses were different from those reported in literature (Freedom of Information, US FDA CDER, 2000).

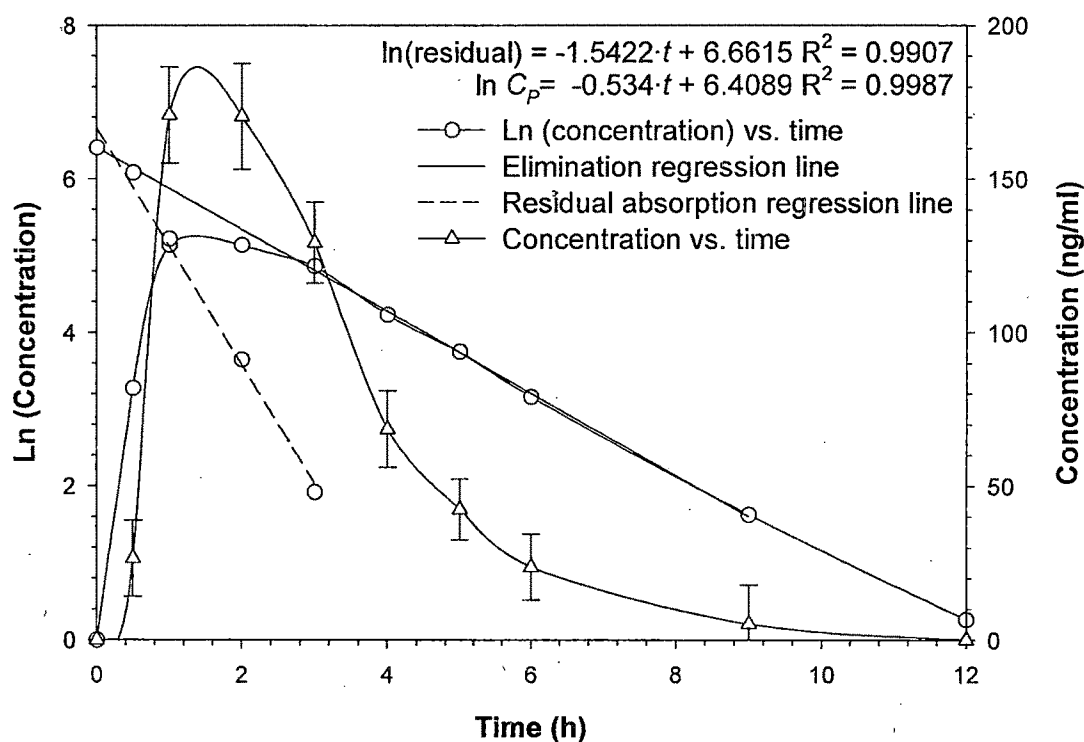


Figure 5.11. Representative mean plasma concentrations versus time profile following a single oral administration of nateglinide (15 mg) to three rabbits. Natural log plasma concentrations versus time profile for determination of k_a and k_{el} were also shown.

Table 5.11. Pharmacokinetic parameters of nateglinide after administration of single oral dose.

Sr. No.	Pharmacokinetic parameters	Observed value
1	Absorption rate constant, k_a (h^{-1})	1.54
2	Elimination rate constant, k_{el} (h^{-1})	0.53
3	Time required for maximum plasma concentration, T_{max} (h)	1.38
4	Maximum plasma concentration, C_{max} (ng/ml)	183.5
5	Plasma half life, $T_{1/2}$ (h)	1.30
6	Area under curve at 12 hours, $AUC_{(0 \rightarrow 12)}$ (ng·h/ml)	616.29
7	Area under curve from 12 hours to ∞ , $AUC_{(12 \rightarrow \infty)}$ (ng·h/ml)	2.43
8	Area under curve at infinite time, $AUC_{(0 \rightarrow \infty)}$ (ng·h/ml)	618.72
9	Area under momentum curve at 12 h, $AUMC_{(0 \rightarrow 12)}$ (ng·h ² /ml)	1793.81
10	Volume of distribution, V_d (lit)	40
11	Mean residence time, MRT (h)	2.91
12	Total clearance rate, TCR (l/h)	0.02

5.3. References

- BAN, K. and KIYOKATSU, J., **2001**. Molecular-Dynamics Simulation for Liquid Chromatographic Interactions: Effect of Mobile Phase Composition. *Anal. Sci.* 17, 113-117.
- FASSIHI, A. R. and PARKER, M. S., **1986**. Controlled drug release from a compressed heterogeneous polymeric matrix: kinetics of release. *Drug Dev. Ind. Pharm.* 12, 1649-1661.
- FERRARIA, F., ROSSIA, S., MARTINIB, A., MUGGETTIB, L., DE PONTIB, R. and CAMELLAA, C., **1997**. Technological induction of mucoadhesive properties on waxy starches by grinding. *European Journal of Pharmaceutical Sciences* 5, 277-285.
- Freedom of Information, US FDA CDER, **2000**. http://www.fda.gov/cder/foi/nda/2000/21-204_Stsrlix.htm, http://...../21-204_Stsrlix_pharmr_P1.pdf, http://...../21-204_Stsrlix_pharmr_P2.pdf. US Department of Health, Food and Drug Administration, Centre for Drug Evaluation and Research (CDER), Last accessed on July 13, 2006.
- GOMEZ-CARRACEDO, A., ALVAREZ-LORENZO, C., GOMEZ-AMOZA, J. L. and CONCHEIRO, A., **2004**. Glass transitions and viscoelastic properties of Carbopol and Noveon compacts. *Int. J. Pharm.* 274, 233-243.
- GUYOT, M. and FAWAZ, F., **1998**. Nifedipine loaded-polymeric microspheres: preparation and physical characteristics. *Int. J. Pharm.* 175, 61-74.
- KAPUSNIAK, J. and SIEMION, P., **2007**. Thermal reactions of starch with long-chain unsaturated fatty acids. Part 2. Linoleic acid. *Journal of Food Engineering* 78, 323-332.
- KHALID, M. N., AGNELY, F., YAGOU, N., GROSSIORD, J. L. and COUARRAZE, G., **2002**. Warer state characterization, swelling behavior, thermal and mechanical

- properties of chitosan based networks. *European Journal of Pharmaceutical sciences* 15, 425-432.
- MEYYANATHAN, S. N., RAMASARMA, G. V. S. and SURESH, B., **2004**. Analysis of simvastatin in pharmaceutical preparations by high performance thin layer chromatography. *ARS Pharma*. 45 (2), 121-129.
- SANCHEZ-LAFUENTE, C., RABASCO, A. M., ALVAREZ-FUENTES, J. and FERNANDEZ-AREVALO, M., **2002**. Eudragit® RS-PM and Ethocel® 100 Premium: influence over the behavior of didanosine inert matrix system. *II Farmaco* 57, 649-656.
- STEENDAM, R. and LERK, C. F., **1998**. Poly(DL-lactic acid) as a direct compression excipient in controlled release tablets Part I. Compaction behaviour and release characteristics of poly(DL-lactic acid) matrix tablets. *Int. J. Pharm.* 175, 33-46.
- US FDA CDER Guidance for the Industry, **2001**. Bioanalytical Method Validation (<http://www.fda.gov/cder/guidance/4252fnl.pdf>), US Department of Health, Food and Drug Administration, Centre for Drug Evaluation and Research (CDER), Rockville, MD.
- USP 29 - NF 24, **2006**. U. S. Pharmacopeial Convention, Rockville, MD.
- WELLS, J. I., **1997**. Tablet testing. in: SWARBRICK, J. and BOYLAN, J. C. (Eds.), *Encyclopaedia of Pharmaceutical Technology*, Vol. 141, Marcel Dekker, New York, pp. 401-418.
- WELLS, J. I. and AULTON, M. E., **1988**. Preformulation. in: AULTON, M. E. (Ed.) *Pharmaceutics: The Science of Dosage Form Design*, Churchill Livingstone, Edinburgh, pp. 223-253.
- ZOHURIAAN, M. J. and SHOKROLAHI, F., **2004**. Thermal studies on natural and modified gums. *Polymer Testing* 23, 575-579.

6. GLIPIZIDE MATRICES

Formulation compositions affect drug release rates from prepared matrices by polymer-excipients interactions, drug-polymer interaction, as well as modulating matrix swelling and erosion rates as water penetrates the matrix. Thus, to understand the functional contribution of each pharmaceutical excipient to the different polymer based matrices, dissolution studies were performed and the results are discussed below. For all glipizide matrices, theoretical content of glipizide, silicon dioxide and magnesium stearate per tablet was 10, 1, and 2 mg, respectively.

6.1. HPMC-MCC-Starch Matrices

Hydroxypropylmethylcellulose (HPMC) is propylene glycol ether of methylcellulose. In oral products, HPMC is primarily used as a tablet binder, in film-coating, and as a matrix for use in extended-release tablet formulations (Hogan, 1989; Shah et al., 1989; Wilson and Cuff, 1989; Dahl et al., 1990). Microcrystalline cellulose (MCC) is partially depolymerized cellulose in a porous particles form prepared by treating α -cellulose with mineral acids. MCC is widely used in pharmaceuticals, primarily as a binder/diluent in oral tablet and capsule formulations where it is used in both wet-granulation and direct-compression processes (Enézian, 1972; Lerk and Bolhuis, 1973; Lerk et al., 1974; Lamberson and Raynor, 1976; Lerk et al., 1979; Chilamkurti et al., 1982). 'In vitro' release profile for matrices prepared with different grades of HPMC, MCC and starch 1500 or lactose at different polymer levels and compression force are shown graphically in Figure 6.1 to Figure 6.7.

6.1.1. IN VITRO DISSOLUTION & RELEASE KINETIC STUDIES

To achieve controlled release through the use of a water-soluble polymer such as HPMC, the polymer must quickly hydrate on the outer tablet skin to form a gelatinous layer. A rapid formation of a gelatinous layer is critical to prevent wetting of the interior and disintegration of the tablet core. Once the original protective gel layer is formed, it controls the penetration of additional water into the tablet. As the outer gel layer fully hydrates and dissolves, a new inner layer must replace it and be cohesive and continuous enough to retard the influx of water and control drug diffusion. Although gel strength is controlled by polymer viscosity and concentration, polymer chemistry also plays a significant role. The

Table 6.1. An overview of the comparative characteristics of different drug release kinetic models, best fit model, MDT₅₀ and MDT₈₀ for batches M-1 to M-35.

Batch No	Release model										Best fit model	MDT ₅₀	MDT ₈₀	
	Zero-order	First-order	Higuchi matrix	Korsmeyer-Peppas	Hixson-Crowell	Zero-order	First-order	Higuchi matrix	Korsmeyer-Peppas	Hixson-Crowell				
	K_0	t_0	K_1	r_1	K_H	r_H	n	K_k	f_k	K_s	f_s			
M-1	16.25	0.84	-	-	38.84	0.99	0.55	36.76	0.99	-0.13	0.98	Matrix	0.60	1.43
M-2	15.88	0.96	-	-	34.21	0.97	0.69	26.21	0.99	-0.12	0.90	Peppas	1.00	2.22
M-3	9.36	0.99	-	-	26.37	0.97	0.84	13.58	1.00	-0.06	0.92	Peppas	2.09	3.73
M-4	8.18	0.99	-0.16	0.98	22.84	0.95	1.01	8.35	1.00	-0.04	1.00	Peppas	2.75	4.52
M-5	6.59	1.00	-0.11	0.98	18.22	0.93	1.02	6.44	1.00	-0.03	0.99	Peppas	3.78	6.05
M-6	5.82	0.99	-0.09	0.99	16.13	0.93	1.04	5.50	1.00	-0.02	0.99	Peppas	4.26	-
M-7	12.60	0.99	-	-	30.39	0.95	0.89	15.81	1.00	-0.09	0.94	Peppas	1.71	2.95
M-8	8.08	1.00	-0.18	0.90	22.33	0.93	1.05	7.35	1.00	-0.04	0.96	Zero order	3.07	4.90
M-9	7.11	1.00	-0.12	0.98	19.62	0.93	1.16	5.13	0.99	-0.03	0.99	Zero order	3.50	5.56
M-10	5.94	0.99	-0.09	0.97	16.18	0.90	1.28	3.28	0.99	-0.03	0.98	Peppas	4.61	-
M-11	4.41	0.99	-0.06	0.98	11.94	0.89	1.32	2.16	1.00	-0.02	0.98	Peppas	5.99	-
M-12	15.53	1.00	-	-	32.40	0.93	0.94	16.84	1.00	-0.12	0.91	Peppas	1.61	2.50
M-13	7.11	1.00	-0.12	0.97	19.46	0.91	1.28	4.05	1.00	-0.03	0.98	Peppas	3.85	5.71
M-14	3.67	0.97	-0.05	0.94	9.72	0.84	1.57	1.00	1.00	-0.01	0.95	Peppas	7.24	-
M-15	9.75	1.00	-	-	25.92	0.94	1.28	6.37	0.97	-0.07	0.86	Zero order	2.32	3.85
M-16	7.81	1.00	-0.15	0.97	21.58	0.93	1.21	5.24	1.00	-0.04	0.99	Peppas	3.15	5.03
M-17	4.06	1.00	-0.05	0.99	11.12	0.91	1.10	3.15	0.99	-0.02	0.99	Zero order	6.26	-

Batch No	Release model														Best fit model	MDT ₅₀	MDT ₈₀
	Zero-order		First-order		Higuchi matrix		Korsmeyer-Peppas		Hixson-Crowell		Hixson-Crowell		Hixson-Crowell				
	K_0	t_0	K_1	t_1	K_H	t_H	n	K_k	t_k	K_s	t_s	K_s	t_s	K_s			
M-18	14.98	0.99	-	-	30.62	0.89	2.04	3.68	0.97	-0.12	0.87	0.87	0.87	0.87	0.87	1.86	2.76
M-19	13.71	1.00	-	-	30.25	0.90	1.63	5.36	0.99	-0.11	0.87	0.87	0.87	0.87	0.87	1.99	2.98
M-20	14.64	0.99	-	-	29.92	0.89	1.62	6.12	0.99	-0.11	0.84	0.84	0.84	0.84	0.84	1.90	2.77
M-21	12.47	0.99	-	-	30.20	0.95	1.20	10.20	0.95	-0.09	0.90	0.90	0.90	0.90	0.90	1.52	2.76
M-22	5.60	0.99	-0.08	0.99	15.45	0.93	1.79	1.36	0.95	-0.02	0.99	0.99	0.99	0.99	Hix.Crow.	4.35	-
M-23	11.32	1.00	-	-	26.71	0.92	1.71	4.01	0.91	-0.08	0.87	0.87	0.87	0.87	0.87	2.32	3.59
M-24	10.12	0.82	-0.27	0.97	29.73	0.99	0.44	33.19	0.99	-0.06	0.98	0.98	0.98	0.98	Matrix	0.97	2.36
M-25	9.34	0.94	-	-	26.90	0.99	0.57	23.16	1.00	-0.06	0.89	0.89	0.89	0.89	Peppas	1.50	3.18
M-26	10.56	0.80	-0.29	0.98	31.19	0.98	0.64	24.96	0.94	-0.06	0.95	0.95	0.95	0.95	Matrix	0.92	1.93
M-27	12.07	1.00	-	-	28.77	0.93	1.08	10.66	1.00	-0.09	0.91	0.91	0.91	0.91	Peppas	2.03	3.17
M-28	10.13	1.00	-	-	25.13	0.90	1.20	6.86	1.00	-0.07	0.88	0.88	0.88	0.88	Peppas	2.77	4.18
M-29	7.39	1.00	-0.13	0.97	20.31	0.92	1.32	3.92	0.99	-0.04	0.99	0.99	0.99	0.99	Zero order	3.52	5.40
M-30	6.22	0.99	-0.10	0.98	16.98	0.91	1.46	2.46	0.99	-0.03	0.99	0.99	0.99	0.99	Peppas	4.30	6.52
M-31	5.87	0.99	-0.09	0.98	16.00	0.90	1.16	4.01	1.00	-0.03	0.98	0.98	0.98	0.98	Peppas	4.60	6.98
M-32	5.23	0.99	-0.07	0.97	14.16	0.89	1.37	2.31	0.99	-0.02	0.98	0.98	0.98	0.98	Peppas	5.25	-
M-33	463.45	1.00	-	-	231.72	1.00	-	-	-	-6.17	1.00	1.00	1.00	1.00	Zero order	0.06	0.09
M-34	491.64	1.00	-	-	245.82	1.00	-	-	-	-6.45	1.00	1.00	1.00	1.00	Zero order	0.05	0.08
M-35	461.28	1.00	-	-	230.64	1.00	-	-	-	-6.14	1.00	1.00	1.00	1.00	Zero order	0.06	0.09

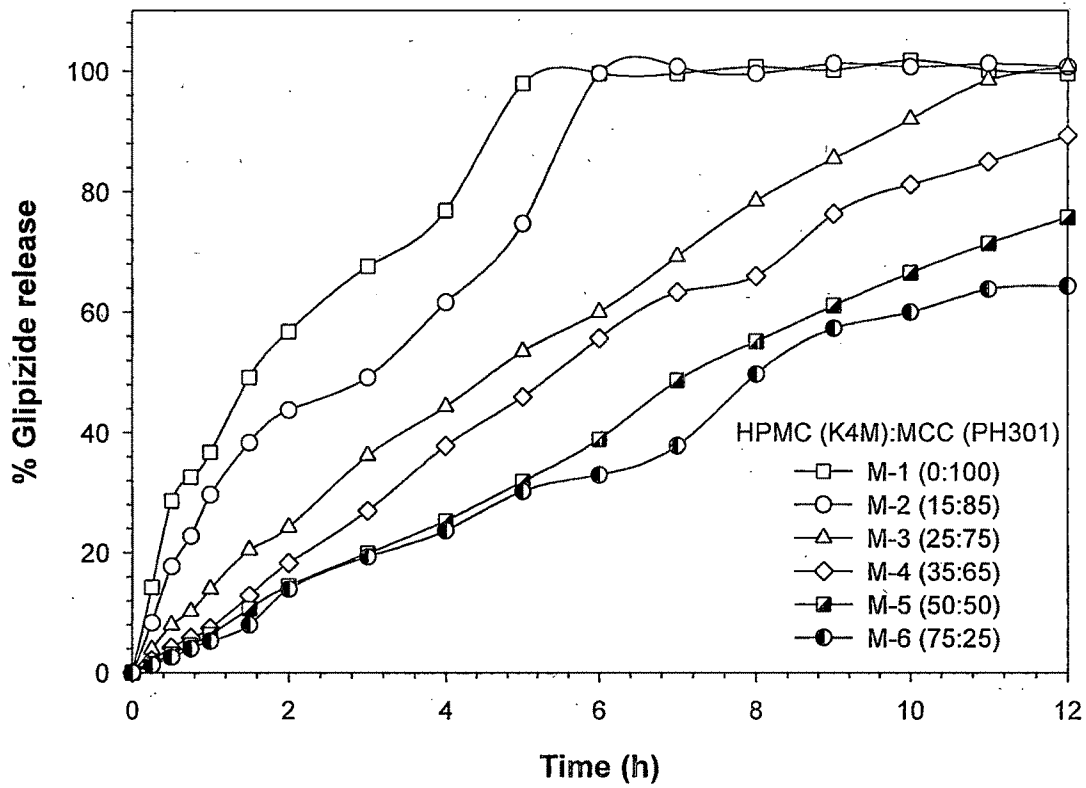


Figure 6.1. Effects of HPMC K4M : MCC PH301 ratio on glipizide release profile.

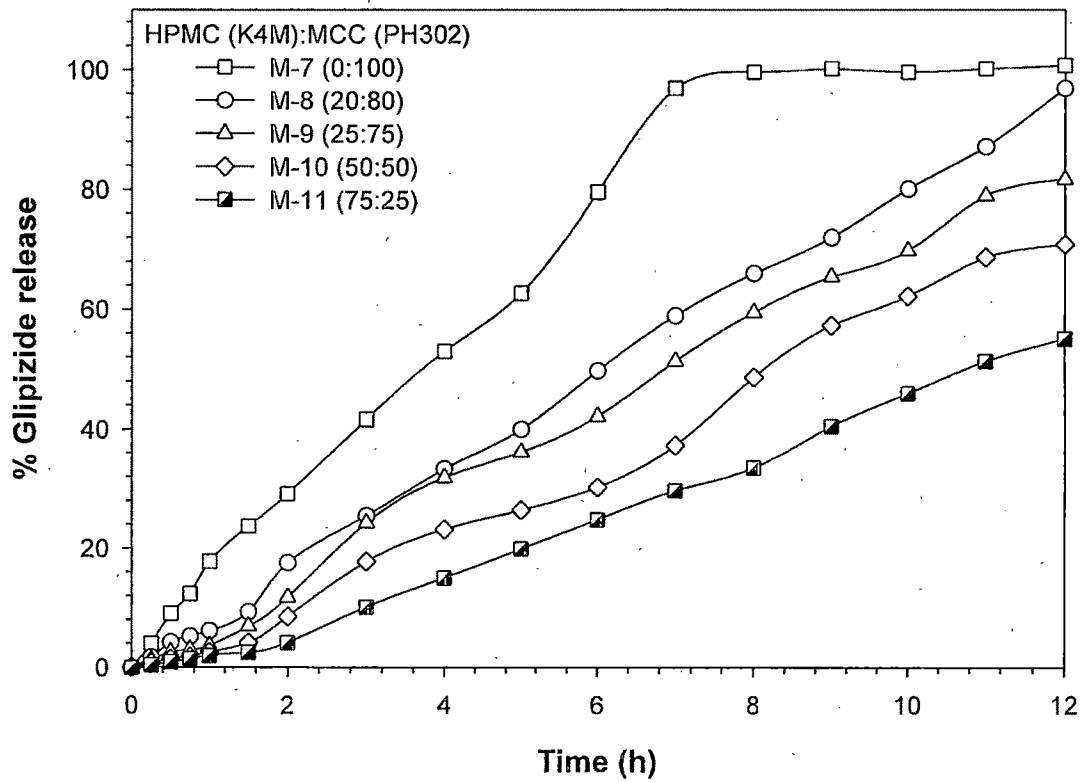


Figure 6.2. Effects of HPMC K4M : MCC PH302 ratio on glipizide release profile.

amount of water bound to HPMC is related to both the substitution and the polymer molecular weight. Within the gel layer, there obviously exists a moisture gradient from the outside surface in contact with liquid to the inner dry core. Water appears to exist in at least three distinct states within a hydrated gel of pure polymer (McCrystal et al., 1997). Upon complete polymer hydration at the outer surface, chain disentanglement begins to occur, i.e., erosion of the matrix. The rate of erosion is related to molecular weight over a wide range by an inverse power law. In addition, erosion rate is affected by the composition and ionic strength of electrolytes in the liquid medium and, by the composition and level of drugs and other additives within the matrix. Viscosity of HPMC solutions is the result of hydration of polymer chains, primarily through H-bonding of the oxygen atoms in the numerous ether linkages, causing them to extend and form relatively open random coils. A given hydrated random coil is further H-bonded to additional water molecules, entrapping water molecules within, and may be entangled with other random coils. All of these factors contribute to larger effective size and increased frictional resistance to flow.

Each MCC microfibril is composed of two areas, (a) the paracrystalline region, an amorphous flexible mass of cellulose chains, and (b) the crystalline region, which is composed of tight bundles of microfibrils in a rigid linear arrangement. Drying the crystalline bundles results in aggregates of very porous particles. This porosity allows the particles to absorb large amounts of water or oil onto the surface.

Matrix tablets prepared by direct compression of HPMC K4M with MCC PH 301 (M-1 to M-6) and with MCC PH 302 (M-7 to M-11) in different combinations. Their release profiles are depicted in Figure 6.1 and Figure 6.2, respectively. In both the cases, a faster release was observed with only MCC tablets (100% was achieved within 5-7 hr) and a quick disintegration was also noted. Behavior of this matrix was sensitive to its hydration, even if it cannot dissolve because of its partially microcrystalline structure. Hard compacts of microcrystalline cellulose disintegrate rapidly due to the rapid passage of water into the compact and the instantaneous rupture of hydrogen bonds (Shangraw, 1989). When MCC tablets were in contact with the dissolution medium, it penetrated between the MCC granules and into the amorphous areas, hence a local swelling occurred. Water was "trapped" in MCC as a result of adsorption and capillary effects. This process has been described as the molecular sponge model (Lustig-Gustafsson et al., 1999). Then, the crystalline framework burst and MCC fragmented into smaller particles (Kleinebudde, 1997). Drug release was controlled by diffusion through the particles followed by dissolution at the particles surface. The MCC tablets were completely eroded at the end of the dissolution test. The mean particle size of Avicel PH-301 and PH-302 were 50 and 100 μm , respectively.

Hence, the specific surface area of Avicel PH-301 is significantly higher than that of the PH-302, which allowed greater amount of dissolution medium to enter the matrix. This difference is responsible for the higher rate of hydration followed by increased burst (and hence higher release with MCC PH-301). At higher concentrations, apparently, the small particles get physically trapped between the deformed microcrystalline cellulose particles, which delays wetting and dissolution, which can be easily overcome by adding portions of water-soluble direct-compression excipients (Shangraw, 1989). Release profiles of all batches were fitted to different release kinetics models and their results has been summarized in Table 6.1. As can be seen for M-1 to M-11, the release profile followed Higuchi model's profile when only MCC PH301 was used, while changed to Korsmeyer-Peppas' power law equation upon addition of HPMC as a matrix former. Further, from the release exponent (n) of Peppas model, it can be observed that, drug release mechanism changed from anomalous to super case-II transport with increase in HPMC content (M-1 to M-11) and viscosity (M-12 to M-14).

With inclusion of the gel forming polymer, HPMC, the burst and completed disintegration of tablet can be controlled. The relative increase in HPMC content, a decrease in the glipizide release was observed. Moreover, as shown in Figure 6.3, as the HPMC viscosity increases, glipizide release decreased significantly. The drug release rate increased in the order HPMC K100LV > K4M > K15M > K100M. One possible explanation for differences in performance of the various HPMC substitution types may be the mobility of water within the gel layer, which is lower within the Methocel K4M Premium containing matrix, leading to greater diffusional resistance to water. This directly reduces the diffusion of drug out of the matrix and indirectly affects the state of hydration within the gel, thus affecting that component of drug release due to erosion of the dosage form. The kinetics of gel growth is also very similar for all substitution types of HPMC; the observed apparent differences in swelling behavior are attributed to differential expansion of the glassy core (Rajabi-Siahboomi et al., 1994). Increasing viscosity yields slower drug release as a stronger more viscous gel layer is formed, providing a greater barrier to diffusion and slower attrition of the tablet. Release kinetic study showed that zero order release profile can be achieved with use of HPMC K100LV due to its low viscosity (Table 6.1, M-18 to M-21).

With increasing HPMC concentration and/or macro-molecular weight, the degree of entanglement of the polymer chains increases. Thus, the mobility of the macromolecules in the fully swollen systems decreases. According to the free volume theory of diffusion, the probability for a diffusing molecule to jump from one cavity into another, hence, decreases (Fan and Sing, 1989). This leads to decreased drug diffusion coefficients and decreased drug release rates with

increasing HPMC level or molecular weights. Figure 6.3 represents the effects of different HPMC grade (molecular weight) on the glipizide cumulative release from HPMC : MCC PH301 (25:75) matrices. Thus, HPMC was found to be dominating excipient controlling the release rate of glipizide in matrix tablets. The effect of the compression force in terms of tablet hardness is shown in Figure 6.4. At higher compression force, the interparticulate gap reduces, which hinders the entry of the dissolution medium and thereby, reduces the drug diffusion through the matrix. It ultimately resulted in decreased glipizide release at higher compression force. Different grades of HPMC can be combined to finely tailor the release profiles. At the same polymer level, shifting from K100LV to K4M grade (Figure 6.3), the time for complete drug release changed from 6 to 12 h. However, with the proper selection of combination of different viscosity grade of HPMC, an intermediate drug release profiles can also be achieved as shown in Figure 6.5.

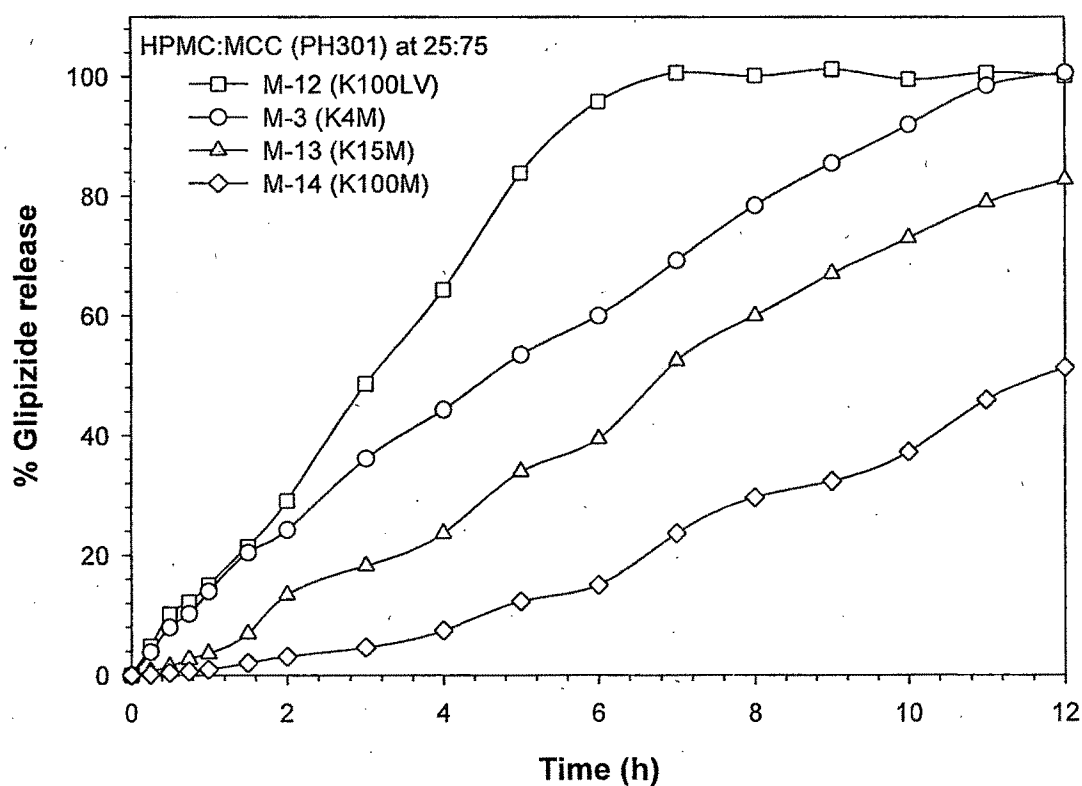


Figure 6.3. Effects of HPMC grades on glipizide release profiles from HPMC : MCC PH301 matrices at 25:75 ratio.

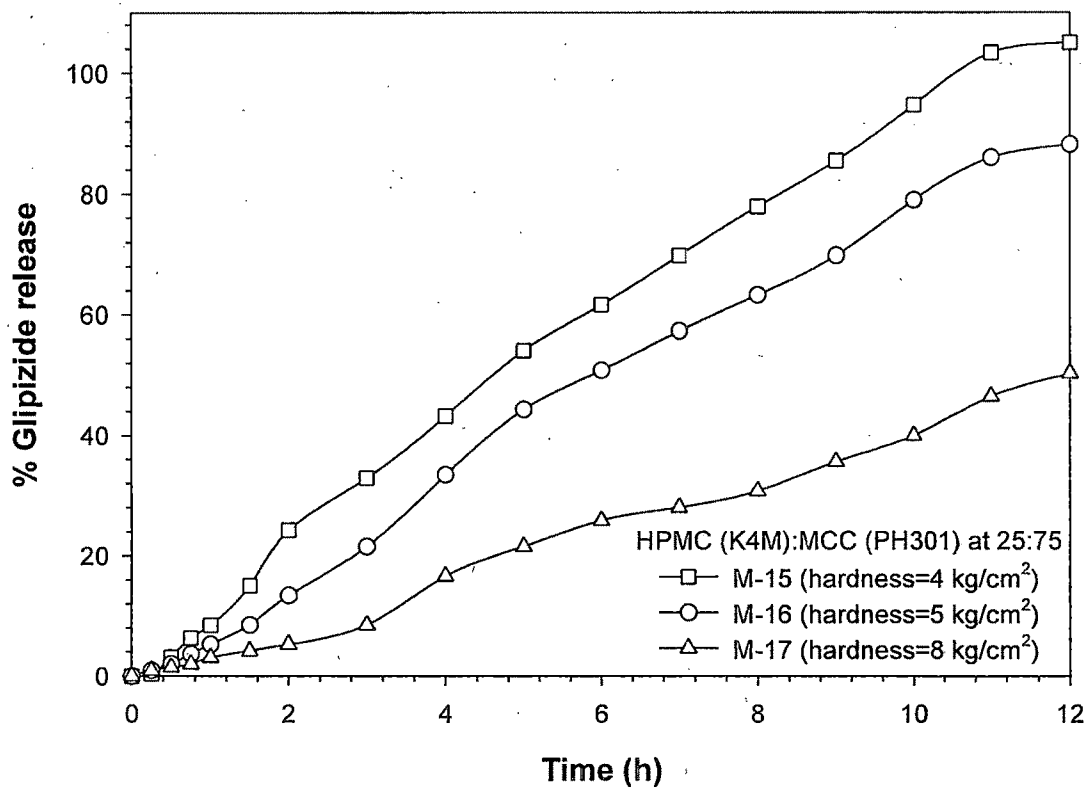


Figure 6.4. Effects of hardness on glipizide release profile from HPMC K4M : MCC PH301 matrices at 25:75 ratio.

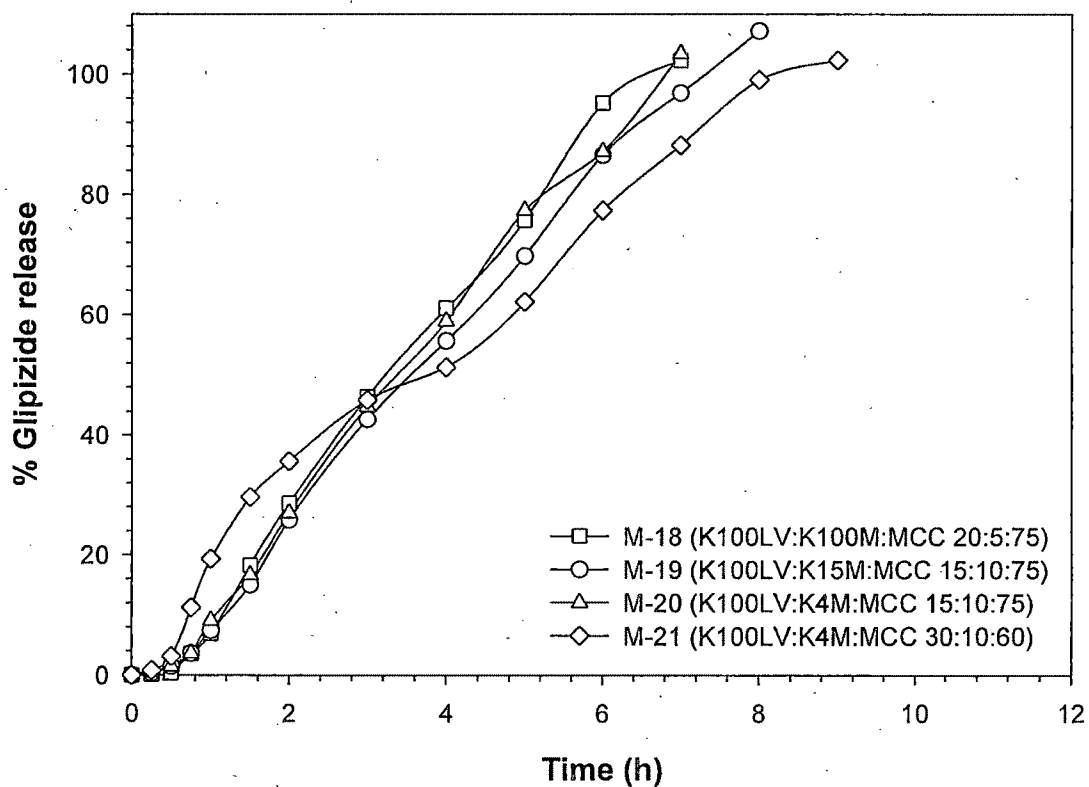


Figure 6.5. Effects of different HPMC grade combinations on glipizide release profile.

Starch 1500 consists of intact starch grains and ruptured starch grains that have been partially hydrolyzed and subsequently agglomerated, composed of two polymers, amylose and amylopectin which are tightly bound in a specific spherocrystalline structure (Shangraw, 1989). Through partial pregelatinization, the bond between portions of the two polymers is broken, and results in partial solubility, increased particle size, improved flow properties and compactability. Each amylopectin molecule contains up to two million glucose residues in a compact structure. The molecules are oriented radially in the starch granule, with the consequent formation of concentric regions of alternating amorphous and crystalline structure. The higher the amylose content (constitute non-branched linear chain, crystalline region), the lower is the swelling power and the smaller is the gel strength for the same starch concentration. The amylopectin (highly branched amorphous region) absorbs water and cause swelling.

Starch can act as a hydrogel former as well as a super-disintegrant (due to swelling) depending on its composition in the tablet. The glipizide dissolution data of batches M-22 to M-26 (Figure 6.6) shows the effect of starch on the drug release profiles of HPMC-MCC matrices. When starch is less than MCC, swelling of starch is not significant to cause burst and HPMC forms a strong elastic hydrogel before starch swells, which release the drug continuously. However, when starch is more than MCC in the matrices, super-disintegration power of starch particles present on the tablet surface accounts for the higher drug release well before the tight hydrogel develop. Initial burst effect with higher starch may be explained by following. Starch is insoluble in water and insoluble solids may produce non-uniformity of the polymeric membranes around the drug, causing the imperfections in the membranes, leading to quick release of drug from the tablets. Another most probable reason for the enhancement in the release rates of the drug could be that starch is water-swellaable, and its this property might rupture the polymeric membrane, causing a tremendous increase in the release rate. Nevertheless, after the initial phase, starch gives synergistic effect with HPMC by forming more elastic hydrogel to control the release of drug by diffusion. Release profiles were fitted to different release kinetics models and results are shown in Table 6.1. With incorporation of Starch 1500 into HPMC-MCC matrices (M-22 to M-26), glipizide release profile changed from super case-II type to non-Fickian (anomalous) transport mechanism. For the tablets prepared with HPMC and starch (M-28 to M-32), there was a synergistic effect on viscosity of the resultant hydrogel was observed and gives higher values of n indicating super case-II transport mechanism.

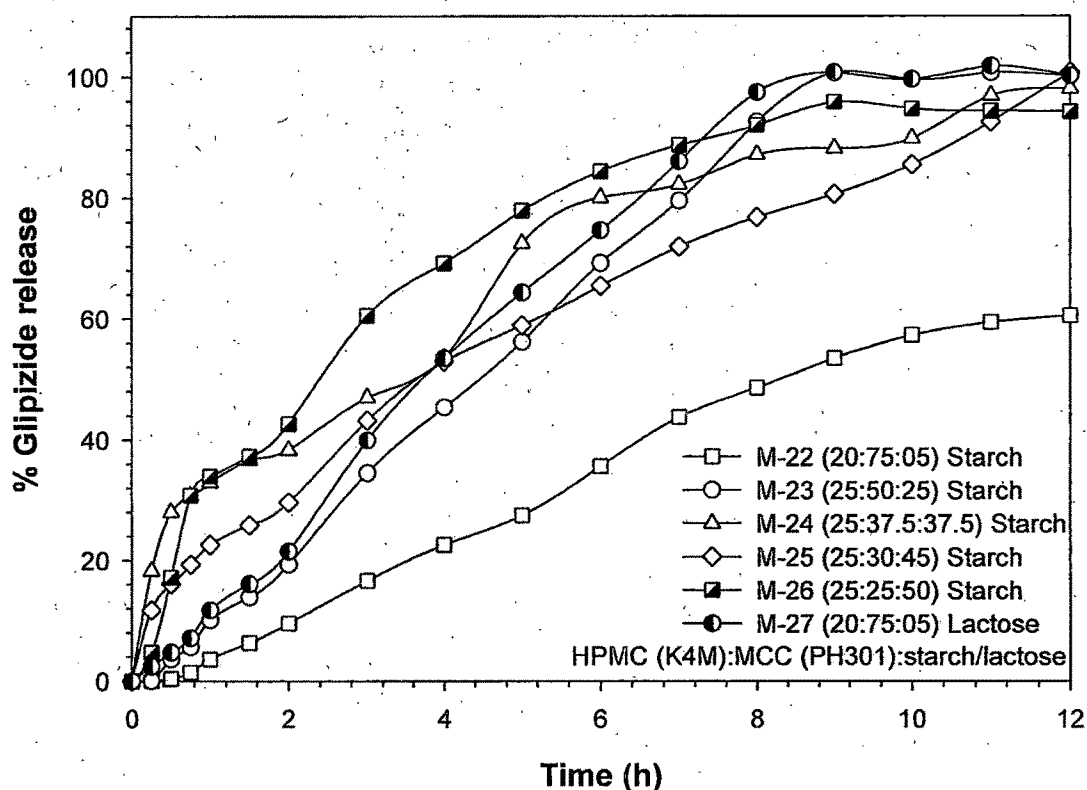


Figure 6.6. Effects of HPMC K4M : MCC PH301:starch/lactose ratio on glipizide release profile.

An important factor for the modified release of these matrix formulations is the ability of the hydrophilic polymer to readily hydrate and form a gel. The spherogranular morphology, and partially pregelatinized nature of Starch 1500 produces an ordered adhesive mixture of drug and excipient in the premix and hence, enhanced particle to particle homogeneity, due to its inherent moisture content (~10%). The highly polar water molecules allow for the formation of hydrogen bonds between the drug and excipient molecules. It is speculated that during the premixing of the active and Starch 1500, a form of granulation takes place as a result of the change in free energy (Ahmed and Shah).

The effect of adding water-soluble (lactose) fillers to matrix tablets containing glipizide, MCC and HPMC (M-27) on the resulting drug release kinetics is shown in Figure 6.6. Clearly, the release rate increased when adding the lactose and can be explained by decreasing the relative HPMC amounts and, thus, the less tight hydrogel structures upon swelling. The increase in release rate with lactose was higher than that of MCC. These findings concurred with the results of previous studies which reported that added lactose into the gel-forming matrix can create osmotic forces that may break up the membranous barrier, resulting in higher release rates of drugs (Lapidus and Lordi, 1966; Alderman, 1984; Ford et al., 1987a; Khan and Zhu, 1998; Vlachou et al., 2000; Nokhodchi et al., 2002).

The effect of varying the blend ratio on drug release from HPMC K4M / starch 1500 combinations (M-28 to M-32) is illustrated in Figure 6.7. When starch 1500[®] (partially pregelatinized maize starch) used as hydrogel former, drug release was significantly decreased compared to formulations containing MCC or lactose (see Figure 6.6). Due to its partially pregelatinized nature, starch 1500 also aids in controlling the release rate of the glipizide by changing the tensile strength of the gel layer. Thus, the effect seen with starch 1500 is not just a spatial effect due to the presence of any filler, but it actively contributes to the dissolution kinetics (Levina and Rajabi-Siahboomi, 2004). The presence of 25-75% starch in the systems leads to weakening of the strong elastic characteristic of HPMC gel structure. The comparatively weak intra-molecular links facilitate both the dissolution media penetration and the acceleration of the macromolecular relaxation, which results in a higher hydration rate of the mixed matrices. Hence, probably due to the weaker gel structure, the degree of drug release is being gradually enhanced with the increase of the pregelatinized starch fraction hydrogels (Cunningham, 2000). Replacing a portion of the HPMC with Starch 1500 can lower the overall cost of the formulation.

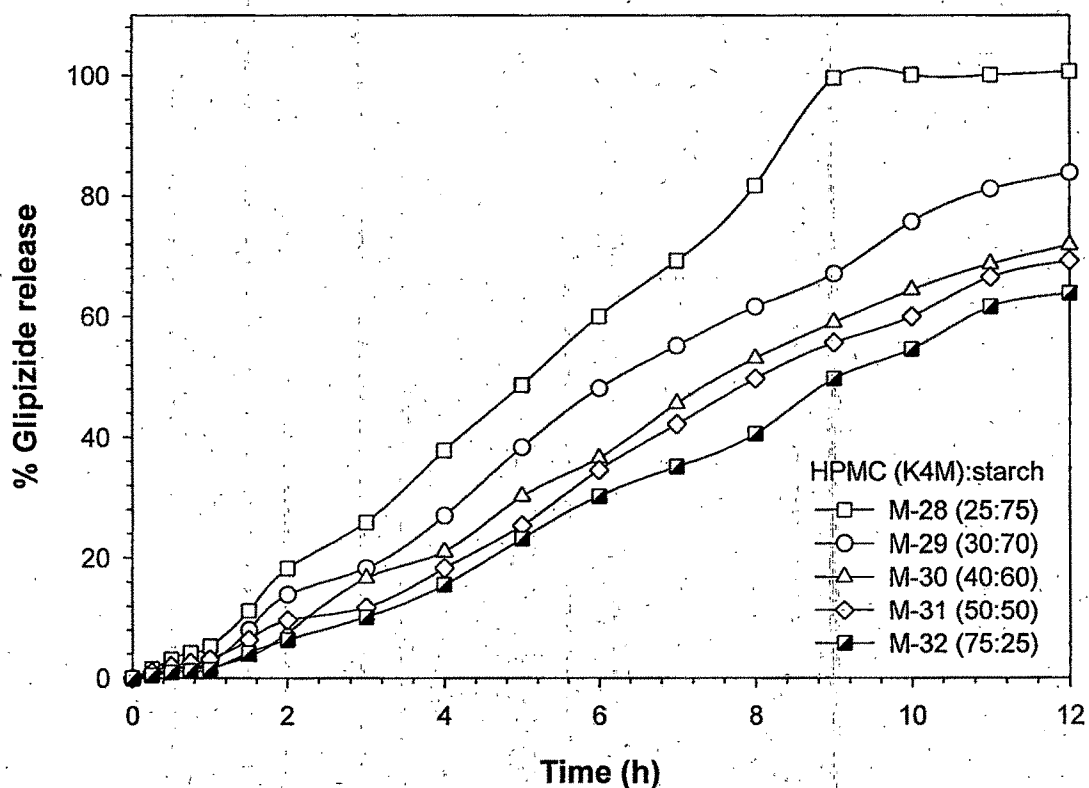


Figure 6.7. Effect of HPMC K4M : starch 1500 ratio on glipizide release profile.

The gel forming ability of starch was also checked in the presence of MCC (M-33 to M-35). Only starch 1500 has lower compressibility index (as compared to MCC alone), and the blend was difficult to compress, resulted in tablets (M-33) with hardness of 3 kg/cm² only even at the maximum compression pressure. In subsequent batches, as the proportion of the MCC increases, the compressibility index increase and resulted in tablets of 4 and 6 kg/cm² for M-34 and M-35, respectively. Hence, MCC-Starch matrices showed fast disintegration and complete drug release within 15 min (data not shown). The reason can be explained by the inability of starch to form a quick gel like HPMC. Moreover, at higher concentration if starch forms a gel, the tensile strength of gel is too less and can get dissolve easily. MCC also helps in releasing the drug due to its crystalline and hydrophobic nature. Both these lead to complete drug release within very short time.

6.1.1.1. 3² Full factorial Experimental Design

All HPMC-MCC matrices (M-1 to M-21) were checked for suitability to fit into constraint response variables (Q_i) and only M-3 (HPMC K4M:MCC PH 301=25:75) resulted in satisfactory release profile, hence was studied further using 3² full factorial experimental design with two formulation variables (MCC:HPMC ratio) shown 'Experimental Work' section. The formulation variables (in coded values) and measured responses of model formulations (A-1 to A-9) of glipizide sustained-release matrix tablets are shown in Table 6.2.

Table 6.2. The measured responses of model formulations of glipizide sustained-release matrix tablets studied by 3² full factorial design.*

Batch No.	Factor		Q ₂	Q ₄	Q ₆	Q ₈	Q ₁₀	Q ₁₂	MDT ₅₀	MDT ₆₀
	A	B								
A-1	-1	-1	37.70	53.90	76.30	90.70	101.00	101.00	1.82	3.01
A-2	-1	0	24.60	47.40	66.50	79.70	92.30	99.70	2.09	3.55
A-3	-1	1	19.80	43.10	58.40	70.70	85.30	93.60	2.40	4.14
A-4	0	-1	31.60	58.40	81.65	98.80	104.30	104.30	1.61	2.72
A-5	0	0	26.60	51.70	72.60	86.40	98.30	106.20	1.87	3.15
A-6	0	1	23.00	47.60	65.50	78.20	92.00	101.00	2.11	3.59
A-7	1	-1	103.39	103.39	103.39	103.39	103.39	103.39	0.15	0.24
A-8	1	0	106.80	106.80	106.80	106.80	106.80	106.80	0.22	0.37
A-9	1	1	51.60	82.40	105.56	105.56	105.56	105.56	0.69	1.53

* The responses in the bold figures are within the defined constraints.

'In vitro' glipizide release profile for above batches is shown in Figure 6.8. Two batches (A-2 and A-6) from above model formulations were found to fit the constraint range of Q_(t).

For MCC:HPMC tablets, the drug release was almost steady throughout the dissolution study and 100% release was achieved within 12 h. It is well known that water adsorption enhances the molecular mobility of hydrophilic pharmaceutical solids, explaining the enhanced chemical reactivity of these materials in the presence of water (Byrn et al., 2001). At high level of HPMC, the burst effect decreased and drug released at later stage was incomplete ($Q_{(12)} < 90\%$). With increased compaction force (hence tablet hardness), the powder bed densifies to a greater extent and eliminates more of the air from the powder bed and voids in individual particles. The increased densification process results in a tablet with greater mechanical strength, lower porosity and higher tortuosity (Crowley et al., 2004). Thus, release rate of glipizide decreased with increase in tablet hardness.

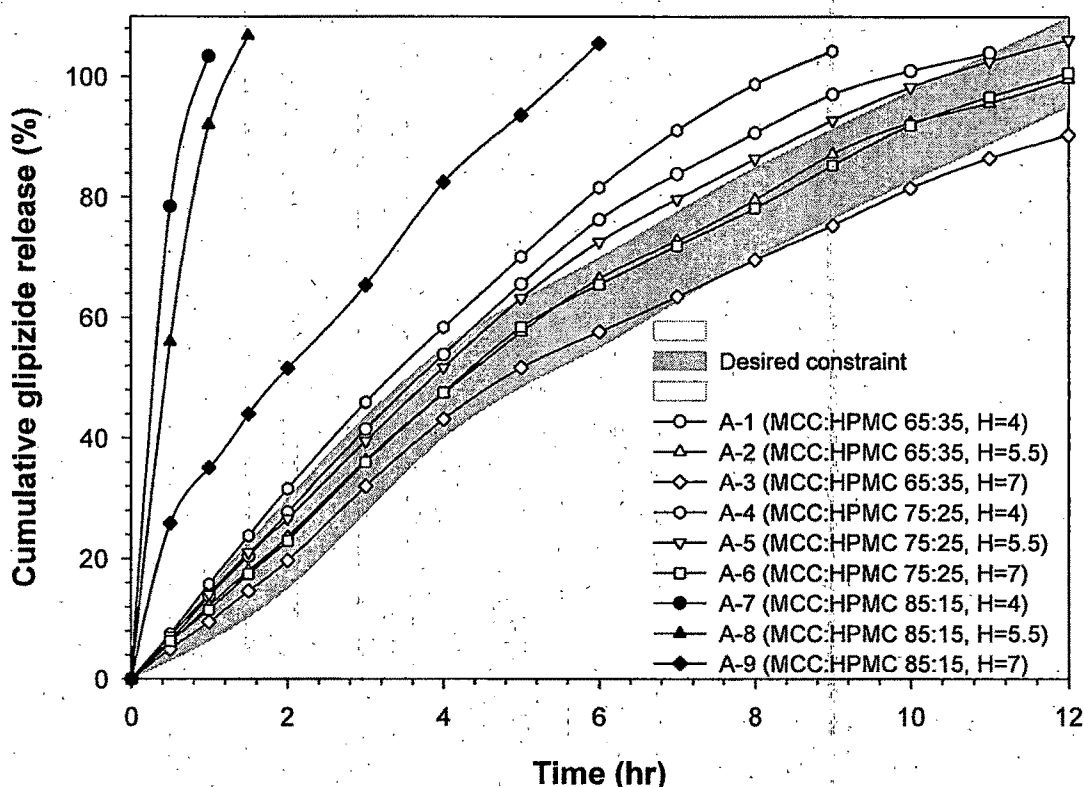


Figure 6.8. In vitro dissolution profile for A-1 to A-9 studied by 3^2 full factorial design.

During contact between HPMC matrix and dissolution medium or water, it undergoes rapid hydration and macromolecular chain relaxation (Colombo, 1993; Colombo et al., 1999) to form a viscous gelatinous layer at the surface of the tablet around a dry-like core (Rajabi-Siahboomi et al., 1992). This hydrated viscous layer controls water penetration into the central dry core of the tablet and prevents disintegration. Failure to form a uniform and coherent gel layer may cause immediate drug release. Growth of this gel layer occurs as water

permeates through it to hydrate the polymer particles that are immediately beneath it. Concomitantly the outer layers become fully hydrated and dissolve. Water continues to penetrate towards the core of the tablet causing hydration of deeper parts of the granules and maintained constant drug release until all the tablet has dissolved (Siepmann et al., 1999). Not only the diffusion path length but also the resistance to diffusion increased with time and the rate of drug release progressively decreased (Higuchi, 1963). Drug diffusion occurred at the core-gel interface then through gel layer (Nokhodchi et al., 1997) and it was expected due to the higher affinity of this excipient for water and higher mobility of the matrix protons (Chambin et al., 2004). It is generally assumed that water soluble drugs are released primarily through diffusion through the gel layer and that poorly water soluble drugs are primarily released through erosion of the gel layer. It is the relative contribution from each process that is controlled by the solubility of a drug (Ford et al., 1987b).

The contour plots of $Q_{(x\%)}$ illustrating the simultaneous effect of the formulation factors on individual response variable are represented in Figure 6.9 (a-f). The superimposed response surfaces (Figure 6.10) and contour plots (Figure 6.11) illustrate the optimized region. The results showed that the amount HPMC in formulation was a key factor in controlling the drug release rate, thus indicating that the burst effect of formulation can be reduced by increasing the amount of HPMC.

The values of the release exponent (n) and the kinetic constant (K) were derived from different release models for glipizide release from the matrix tablets and are presented in Table 6.3. The drug release data show a good fit to the Korsmeyer-Peppas' power law model which can further be confirmed by comparing the values of the correlation coefficient (r) with those of other models. The values of release exponent (n) determined for the various matrix tablets studied ranged from 0.58 to 0.94 (except A-7) suggesting the probable release by anomalous (non-Fickian) diffusion. The K_k values ranged from 10.22 to 103.39 where high K_k value may suggest a burst drug release from the matrix which was observed with the formulation A-7.

Finally, the release profile of the optimized formulations (A-2 and A-6) and that of the commercial formulation (Glytop[®] 10 SR) are shown in the Figure 6.12. They were compared using pair wise approach of similarity factor (f_2) and the value was found to be 73.29 and 72.53 for A-2 and A-6, respectively, which suggests that both the formulations are similar to the marketed formulation.

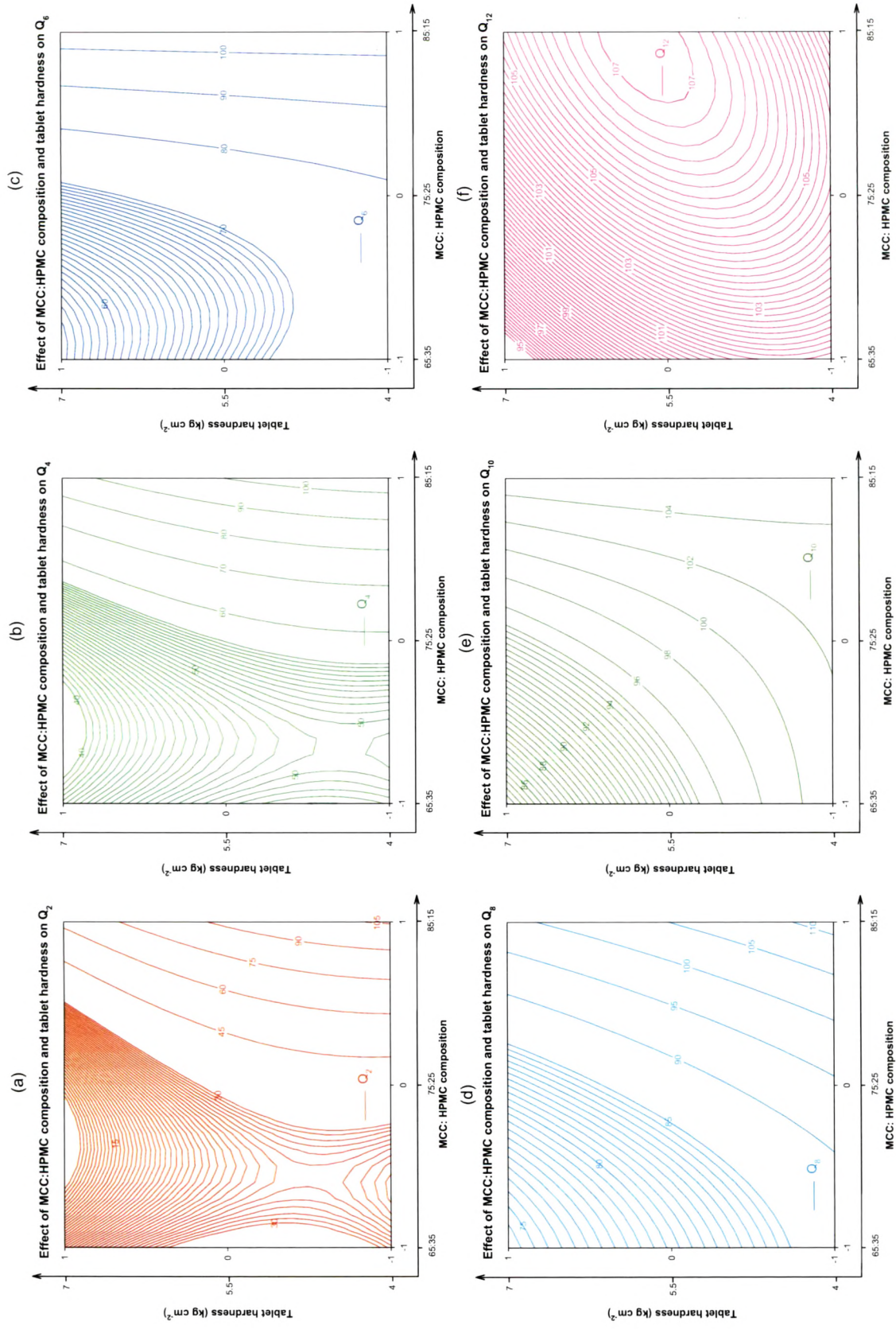


Figure 6.9. Contour plots of (a) Q_2 , (b) Q_4 , (c) Q_6 , (d) Q_8 , (e) Q_{10} and (f) Q_{12} as a function of MCC: HPMC composition and tablet hardness.

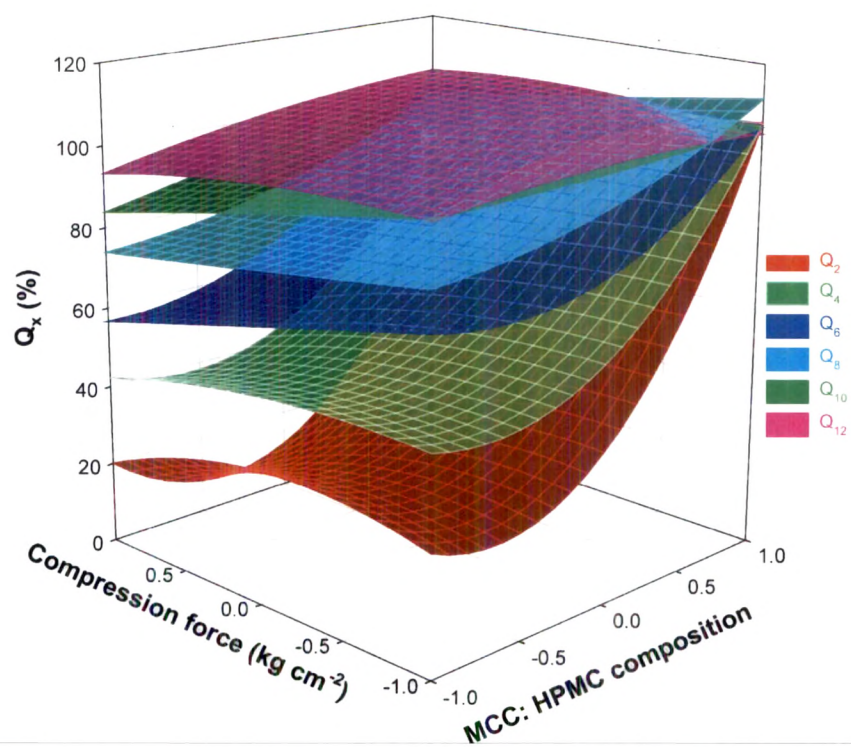


Figure 6.10. Superimposed response surfaces of Q_x as a function of variables studied.

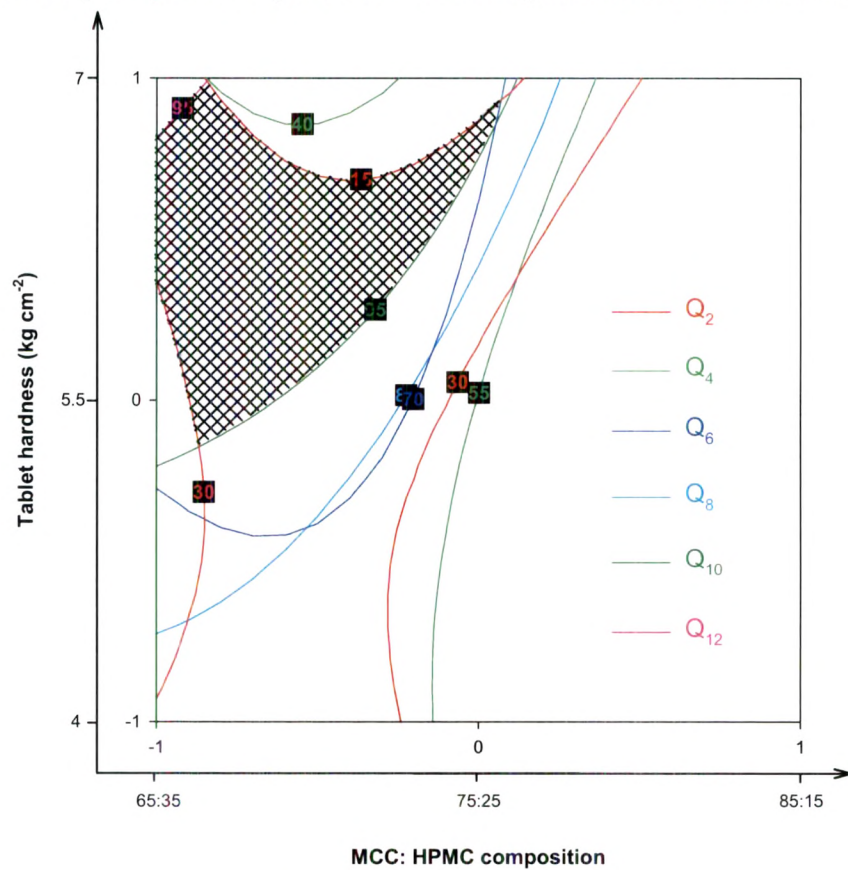


Figure 6.11. Superimposed contour plots of Q_x along with optimized crossed region.

Table 6.3. Comparison of the characteristics of different kinetic models used to fit the matrix tablets dissolution data.

Batch No. *	Release model								
	Zero-order		Higuchi matrix		Korsmeyer-Peppas			Hixson-Crowell	
	K_0	t_0	K_H	t_H	n	K_k	t_k	K_s	t_s
A-1	10.95	0.976	29.85	0.976	0.91	13.84	0.994	-0.09	0.915
A-2	9.47	0.978	26.94	0.965	0.89	12.52	0.996	-0.06	0.978
A-3	8.64	0.987	24.46	0.958	0.94	10.22	0.996	-0.05	0.993
A-4	12.86	0.988	31.52	0.958	0.91	15.75	0.997	-0.10	0.898
A-5	10.19	0.973	29.08	0.970	0.85	14.50	0.996	-0.09	0.909
A-6	9.44	0.981	26.83	0.964	0.89	12.37	0.996	-0.06	0.912
A-7	114.11	0.949	105.93	0.998	0.40	103.39	1.000	-1.22	0.970
A-8	80.06	0.957	87.47	0.996	0.60	86.81	0.989	-0.80	0.945
A-9	19.73	0.940	40.28	0.991	0.58	36.12	0.996	-0.16	0.885

* The results of optimized batches are shown in the bold figures.

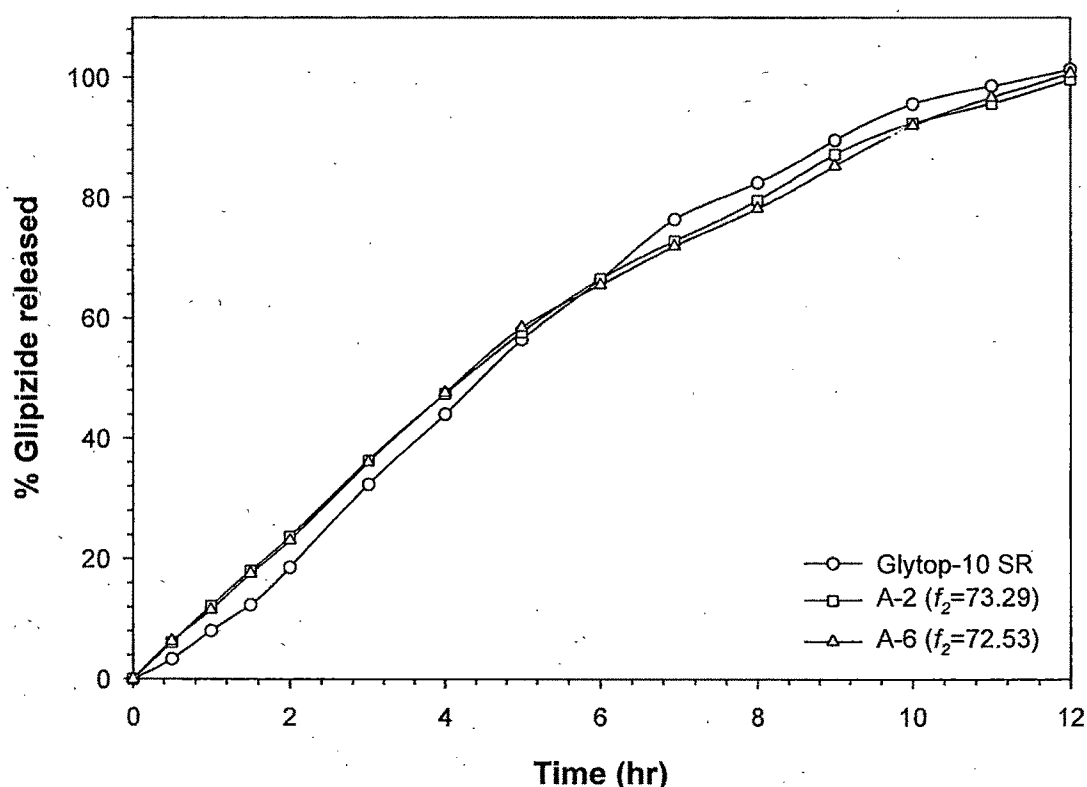


Figure 6.12. Dissolution profile comparison of Glytop® 10 SR, A-2, and A-6.

6.1.2. CHARACTERIZATION OF OPTIMIZED FORMULATIONS

Based on the in vitro glipizide release profile for M-1 to M-35, two batches (M-3 and M-25) were found to be the batches falling within the constraints. Hence, they were characterized further for release mechanism by Kopcha model (Kopcha et al., 1991), swelling study, and SEM study before and after dissolution at different time interval.

6.1.2.1. Release Mechanism by Kopcha Model

The drug release mechanism from these hydrogels is a diffusion-controlled one. It is determined by the structural characteristics of the gel layer (structural organization, diffusion capability, gel strength), and by the processes of both polymer swelling and gel layer erosion (Herman and Remon, 1989). The results obtained from the Kopcha model parameters for M-3 and M-25 formulations at different time intervals are shown in Figure 6.13.

Initially A/B was <1 and express the predominance of surface erosion relative to drug diffusion inside the matrices for M-3 (HPMC K4M : MCC PH301 at 25:75). During this initial phase, HPMC is in process of preparing the viscous gel layer and drug release is mainly controlled by erosion of the surface MCC particles. The viscous gel layer of HPMC is very thin and hence more dissolution medium can penetrate towards the core area and create channels which are responsible for initial release. However, term A increases in the course of time as diffusion of glipizide from viscous gel layer appears. Within the gel layer, there obviously exist a moisture gradient from the outside surface in contact with liquid to the inner dry core. The self-diffusion coefficient at given position within HPMC gel is significantly and consistently lower. This implies that the mobility of water within the gel layer is lower, leading to greater diffusional resistant to water. This directly reduces the diffusion of drug out of the matrix and indirectly affects the state of hydration within the gel.

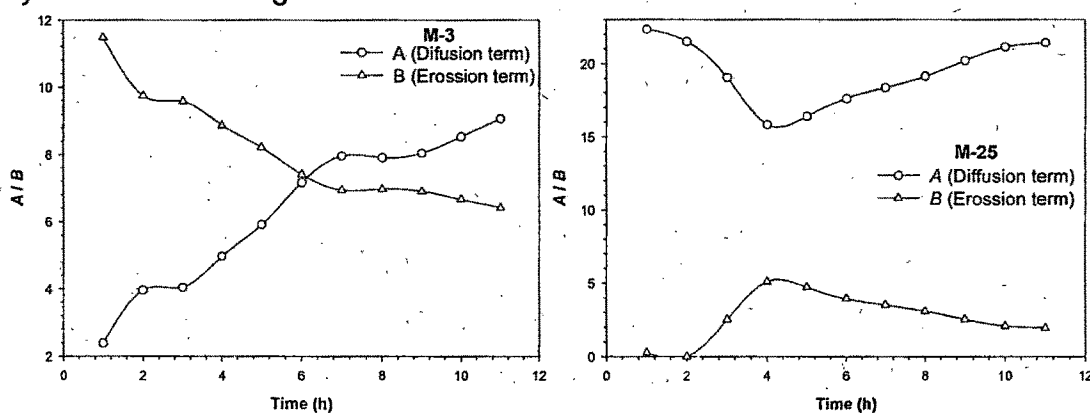


Figure 6.13. Kopcha model parameters (A and B) versus time profile for M-3 and M-25 formulations, respectively.

M-25 (HPMC K4M : MCC PH301 : Starch 1500 at 25:30:45) contained majority proportion of Starch 1500 which is hydrophilic and quickly hydrate along with HPMC to form a strong hydrogel (Figure 6.13). Thus, diffusion was the predominant than the erosion. Slight decrease in diffusion was observed up to 4 hr, due to MCC content. However, this effect was not significant and diffusion was the predominant through out the dissolution profile. This further confirms the

hypothesis that starch can form a strong hydrogel with non-ionic HPMC, as discussed earlier.

6.1.2.2. Swelling Study

The swelling study results for M-3 (HPMC K4M : MCC PH301 at 25:75) are graphically presented in Figure 6.14. As can be seen, the water uptake was significantly high for initial 3 h and remained almost constant through out the study. Similarly, the axial and radial expansion were also maximum at 3 h and declined at very slow rate (due to surface erosion). This can also be seen from the photographs of tablets at different time interval at the top of the Figure 6.14. Initially during 3 h, the dissolution medium penetrated up to the core of the HPMC matrix tablet and might have prepared the viscous hydrogel which is sufficient to retard glipizide diffusion. Though, complete drug was released at 12 h by diffusion, the hydrogel was so strong to maintain its integrity. After 24 h, the outer most gel layer was fully hydrated and chain disentanglement begun, i.e. erosion of the matrix.

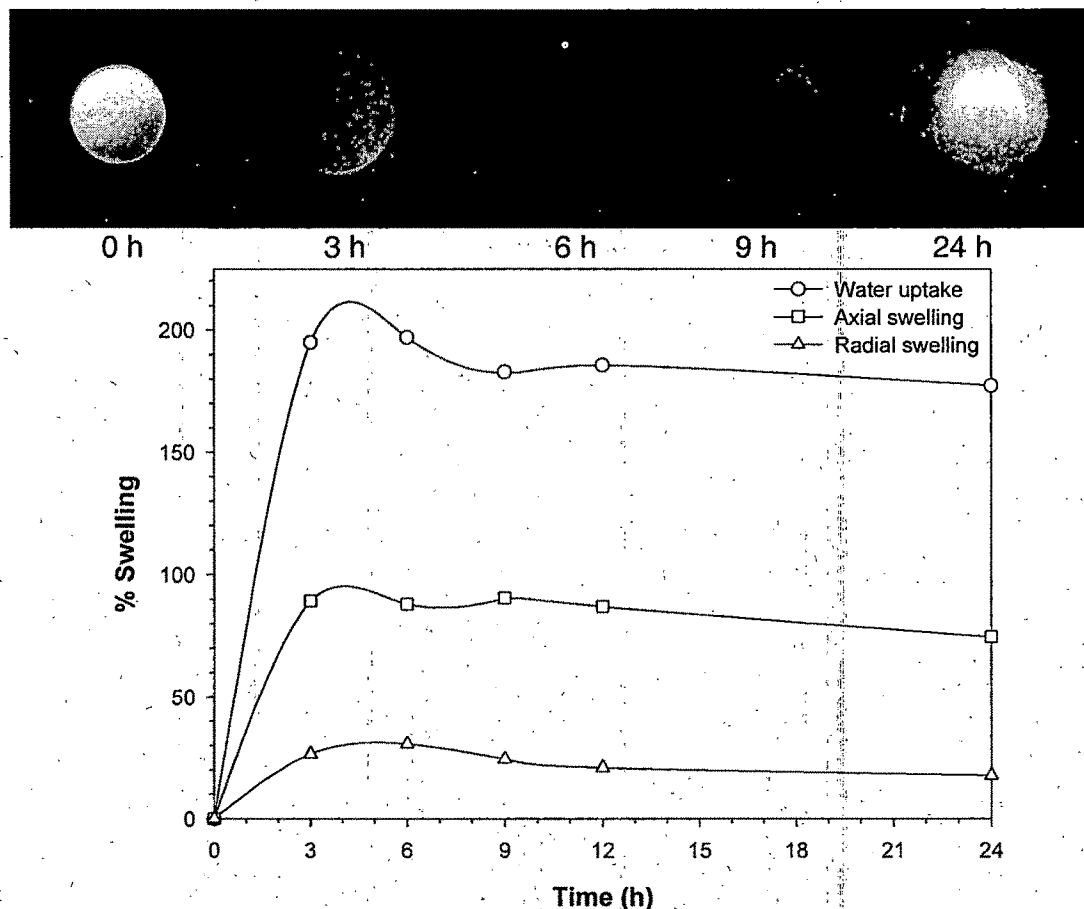


Figure 6.14. Percent water uptake, axial, and radial swelling results for M-3 formulation (HPMC K4M : MCC PH301 at 25:75).

6.1.2.3. SEM Study

Figure 6.15 (a-e) depicts the changes in the HPMC:MCC tablet (M-3) surface structure as the dissolution progresses. Tablet surface was slightly rough before

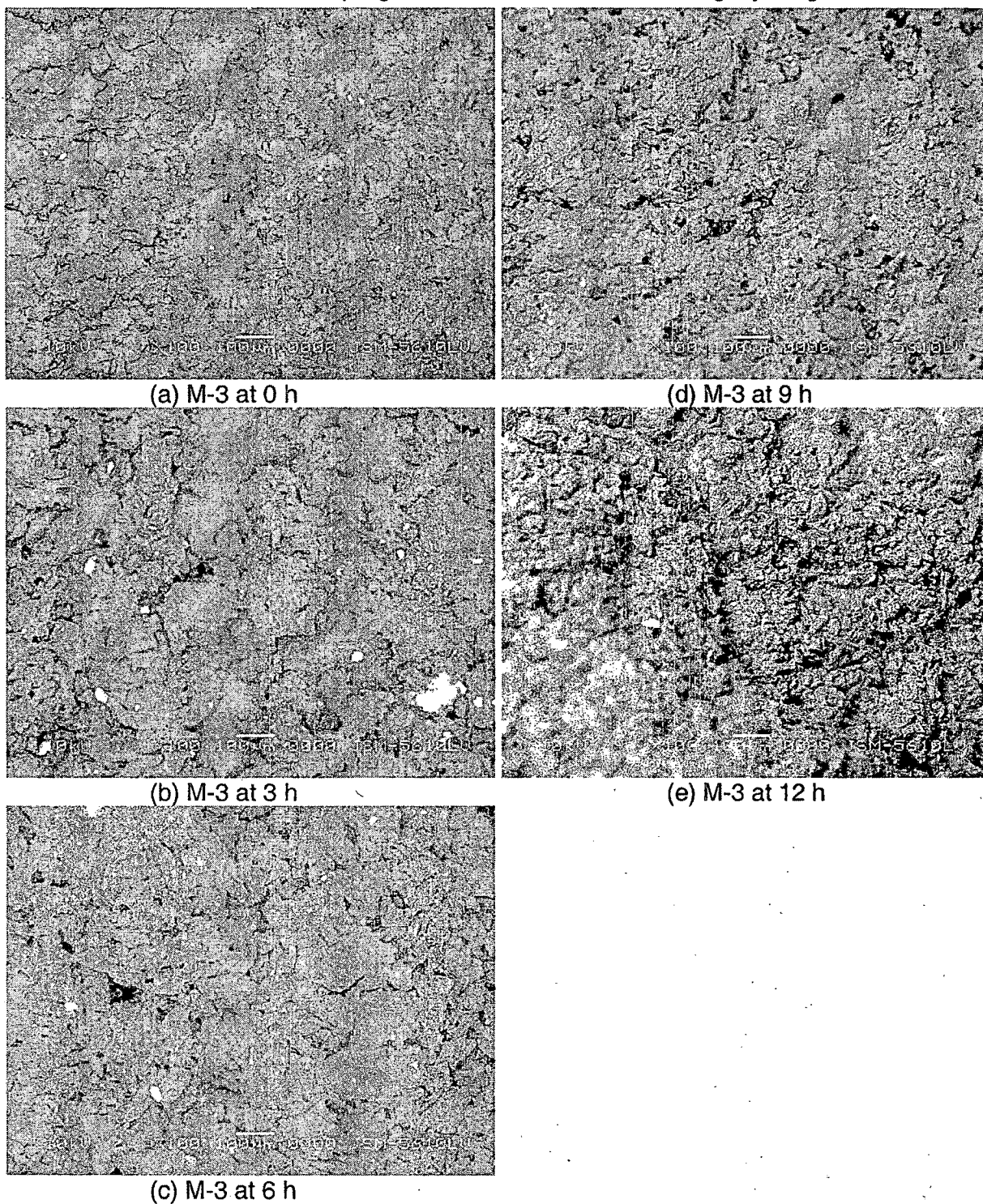
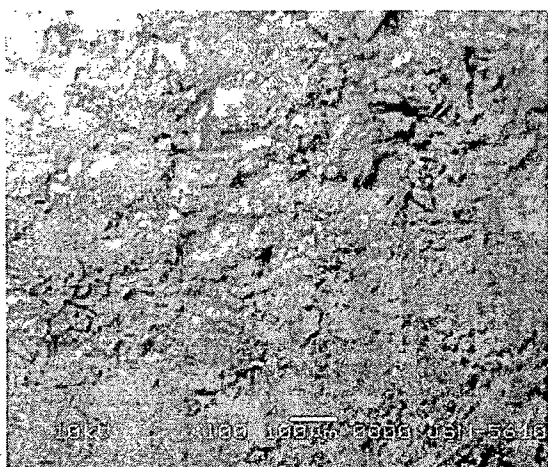
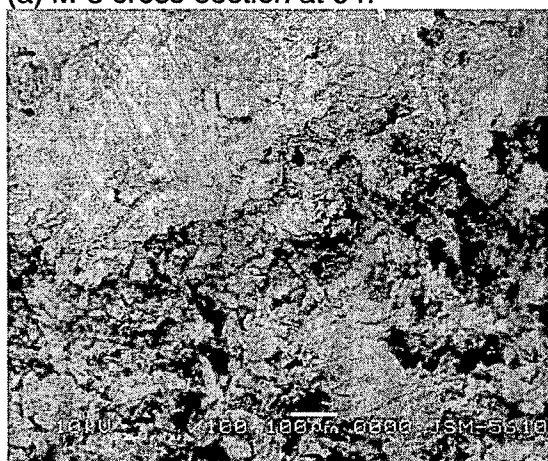


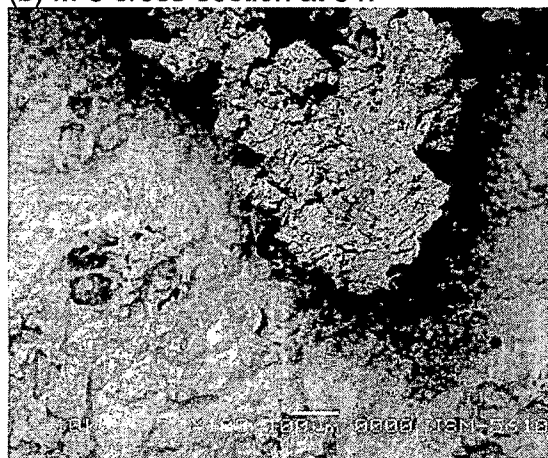
Figure 6.15. SEM photographs of M-3 tablet surface after dissolution at different time points.



(a) M-3 cross-section at 0 h



(b) M-3 cross-section at 6 h



(c) M-3 cross-section at 12 h

Figure 6.16. (a-c) SEM photographs of HPMC-MCC (optimized batch M-3) tablet cross-section after dissolution at different time points.

dissolution (0 h) and as the dissolution proceeds, surfaces becomes rubbery due to quick hydrogel forming nature of HPMC, drug starts to diffuse out of the tablet core and results in pore formation on the tablet surface. Further, the tightness of the surface particles weakens with dissolution. Whereas Figure 6.16 (a-c) are the cross-section of the HPMC:MCC tablet at 0, 6, and 12 h, respectively which further confirms the observations made above.

Figure 6.17 (a-e) depicts the changes in the M-25 (HPMC K4M :MCC PH301 :Starch 1500 at 25:30:45) surface structure after 0, 3, 6, 9, 12 h dissolution study. The phenomenal of formation of viscous gel of starch in presence of HPMC can be seen from the figure. This further confirms the contribution of excipient on release profile discussed earlier. In comparison to M-3, surface of and M-25, was more viscous elastic gel type in nature.

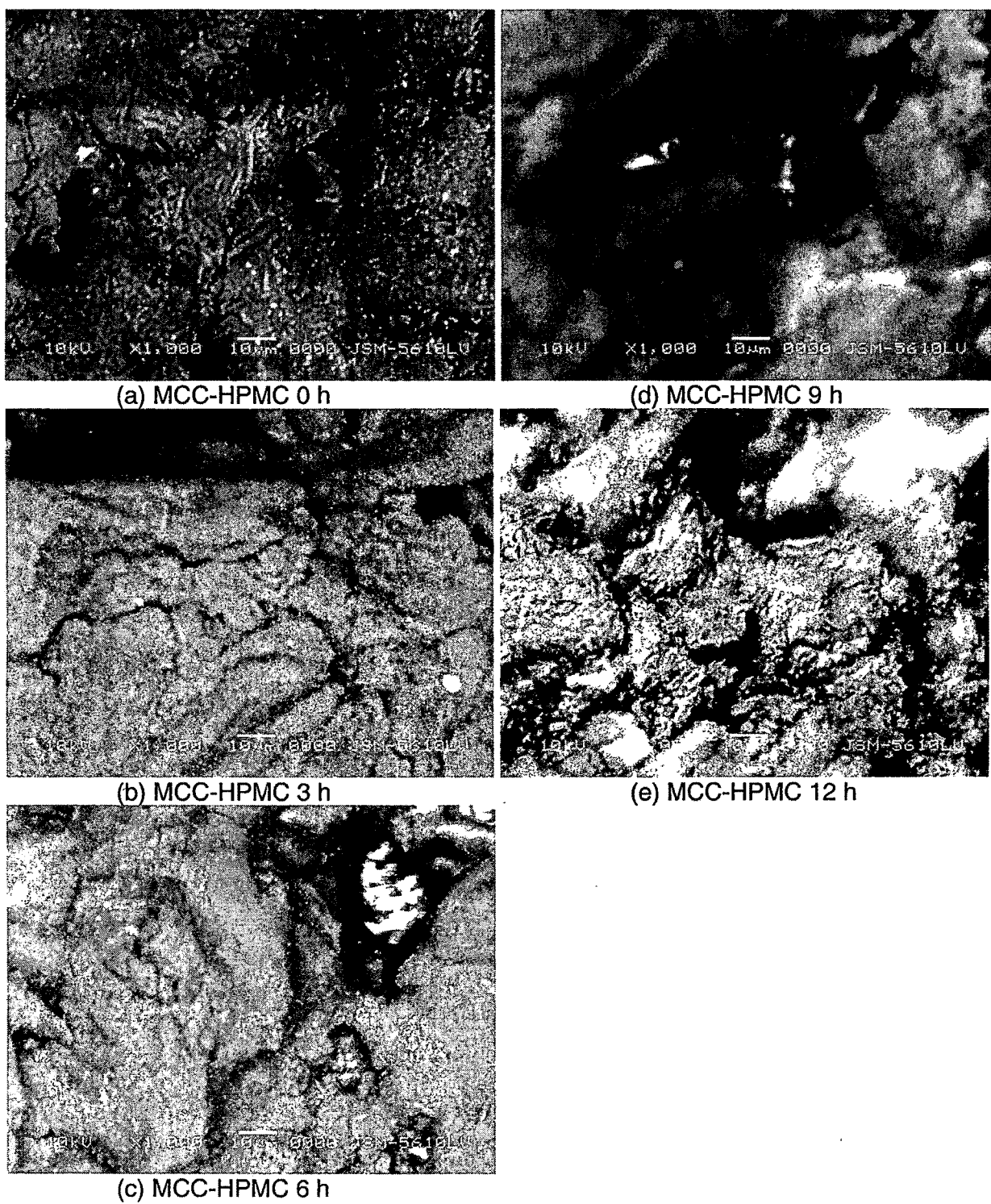


Figure 6.17. SEM photographs of M-25 (HPMC K4M : MCC PH301 : Starch 1500 at 25:30:45) tablet surface after dissolution at different time points.

6.2. MCC-Alginate & MCC-Glyceryl Behenate Matrices

In this study, MCC-sodium alginate matrices were studied without and with sodium and/or calcium salts to tune the glipizide release.

6.2.1. IN VITRO DISSOLUTION & RELEASE KINETIC STUDIES

Figure 6.18 depicts the effects of dibasic calcium phosphate (DCP) and di-sodium hydrogen phosphate (DHP) on drug release profiles of different MCC-alginate matrices (M-36 to M-43). On dissolving alginates in water, the molecules hydrate and the solution gains viscosity. The dissolved molecules are not completely flexible; rotation around the glycosidic linkages in the G-block regions is somewhat hindered, resulting in a stiffening of the chain. Solutions of stiff macromolecules are highly viscous. After gelation, the water molecules are physically entrapped by the alginate matrix, but are still free to migrate. The water holding capacity of the gel is due to capillary forces. Complete drug release from the matrices was achieved within 2 h except for M-39. The glipizide release data indicate that the presence of divalent cation extend the duration of drug release

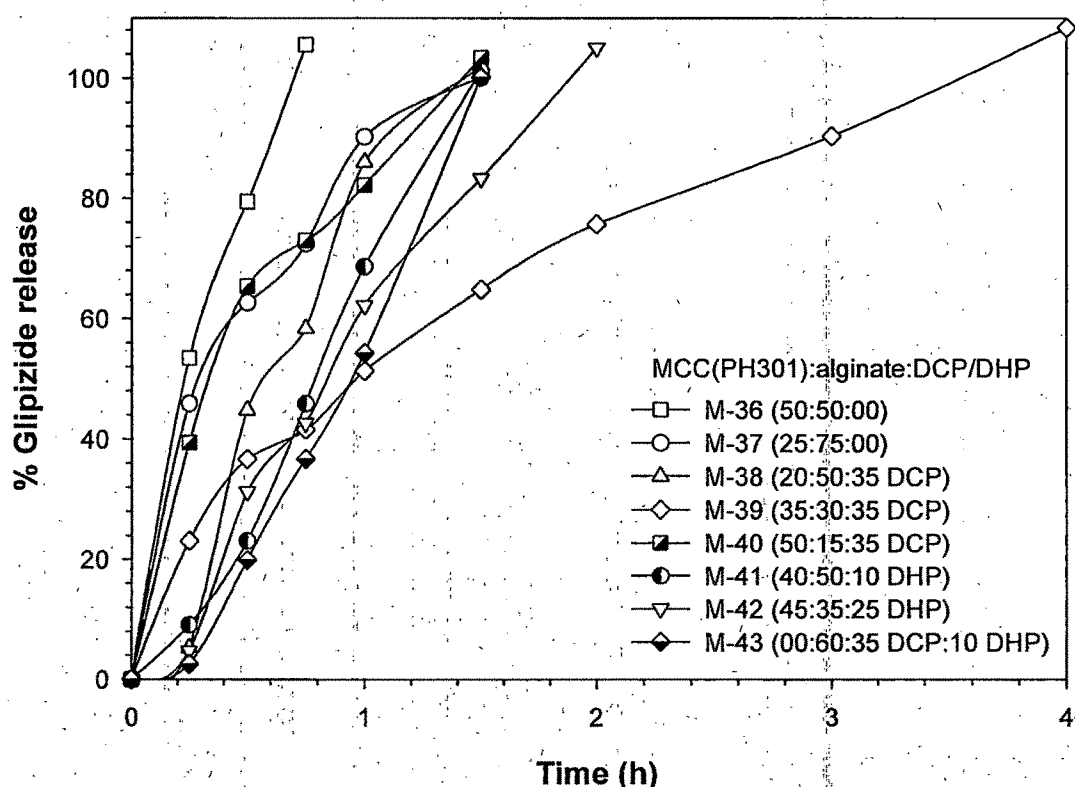


Figure 6.18. Effects of dibasic calcium phosphate and di-sodium hydrogen phosphate on the glipizide release from MCC-alginate matrices.

as compared to that of matrices without any cation (M-36 & M-37). This is due to the ability of the alginates to form an insoluble gel with cations, which act as a barrier for the penetration of the dissolution media into the matrices and for the diffusion of the drug from the matrices. Moreover, the amount of MCC as an insoluble carrier also plays significant contribution in release profiles. When, the proportion of alginate and salt is approximately equal, the formulation shows longer dissolution duration (see release profiles of M-39 and M-42) as compared to other proportions. Güngör, S. et al has also seen similar observation in their studies (Güngör et al., 2003). Functional properties of the polymer can be further investigated in order to achieve a desired release kinetics for the desired duration period.

The anionic Protonal LF 120M can form a highly viscous gel with cationic chitosan, and the glipizide release was significantly retarded as compared to alginate-inorganic salt mediated ionotropic gels (compare the release profiles of M-39 and M-42 with M-46 and M-47). Only about 30-45% glipizide was released by first order release mechanism within 12 hr with the formulations containing chitosan (M-46 and M-47, Figure 6.19, Table 6.4).

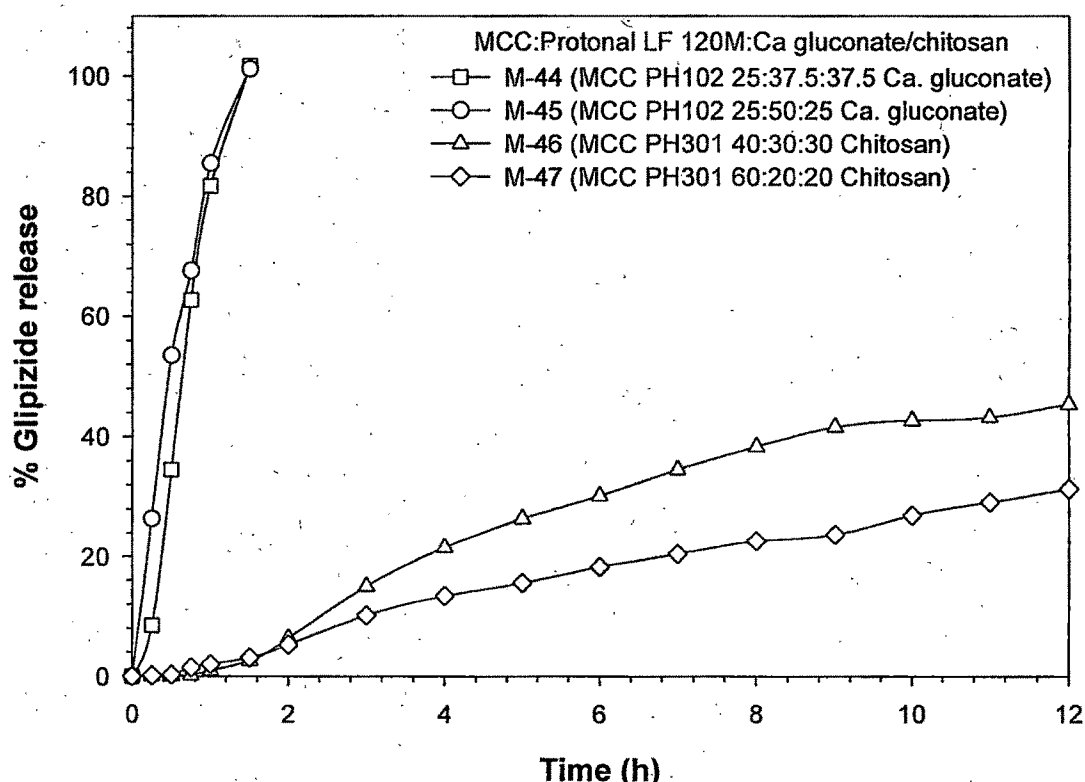


Figure 6.19. Effects of calcium gluconate and chitosan on the glipizide release from MCC-alginate matrices.

Table 6.4. An overview of the comparative characteristics of different drug release kinetic models, best fit model, MDT50 and MDT80 for batches M-36 to M-51.

Batch No	Release model											Best fit model	MDT ₅₀	MDT ₈₀	
	Zero-order	First-Order	Higuchi matrix	Korsmeyer-Peppas	Hixson-Crowell	Zero-order	First-Order	Higuchi matrix	Korsmeyer-Peppas	Hixson-Crowell	Zero-order				
	K_0	K_1	K_H	K_k	K_s	f_0	f_1	f_H	f_k	f_s	r_0	r_1	r_H	r_k	r_s
M-36	139.76	0.96	-	106.82	0.96	0.57	108.85	0.86	-1.40	0.85	Matrix	0.12	0.26		
M-37	83.07	0.85	-	87.00	0.99	0.46	86.70	0.98	-0.67	0.97	Matrix	0.14	0.30		
M-38	74.23	0.97	-	73.90	0.92	1.63	78.39	0.93	-0.64	0.90	Zero order	0.37	0.53		
M-39	32.25	0.88	-	52.99	1.00	0.55	50.96	1.00	-0.28	0.91	Peppas	0.36	0.81		
M-40	81.13	0.88	-	84.53	1.00	0.52	84.89	0.99	-0.70	0.92	Matrix	0.16	0.31		
M-41	65.17	0.99	-	63.33	0.88	1.39	63.32	1.00	-0.57	0.84	Peppas	0.48	0.66		
M-42	54.90	0.99	-	62.37	0.93	1.41	52.35	0.95	-0.48	0.87	Zero order	0.41	0.70		
M-43	56.39	0.95	-	53.52	0.82	1.97	52.44	0.98	-0.48	0.80	Peppas	0.60	0.82		
M-44	72.92	0.98	-	72.34	0.92	1.41	75.46	0.97	-0.63	0.89	Zero order	0.39	0.54		
M-45	77.91	0.95	-	79.77	0.98	0.75	81.68	0.99	-0.65	0.93	Peppas	0.23	0.41		
M-46	4.33	0.98	-0.06	12.04	0.93	1.91	0.78	0.97	-0.02	0.99	1st order	-	-		
M-47	2.74	0.99	-0.03	7.63	0.94	1.40	1.38	0.98	-0.01	1.00	1st order	-	-		
M-48											No tablets				
M-49											No tablets				
M-50											No tablets				
M-51											No tablets				

Moreover, MCC PH 301 was also combined with the glyceryl behenate and the effects of these auxiliary excipients on glipizide release characteristics were studied. Batch M-48 is discussed in the next section with other guar gum matrices. Glyceryl behenate was waxy in nature and matrices were tried to prepare by hot-melt granulation technique. HPMC or MCC were added to the melted glyceryl behenate and mixed thoroughly, allowed to cool at room temperature. This mixture was sieved; lubricant/glidants were added and compressed to form compact mass. In this case, the powder showed poor flow and compression characteristics, acceptable hardness was not achieved within the full compression scale, majority of the tablets resulted in capping as well as cracks on the surface. Hence, these batches were not studied further. Release exponent and regression coefficient for different release kinetics models are summarized in Table 6.4.

6.3. EC- HPMC, Guar Gum & Xanthan gum Matrices

Ethylcellulose (EC), a hydrophobic polymer, is an ether cellulose derivative and is used to control drug release (Klinger et al., 1990; Katikaneni et al., 1995; Rekhi and Jambhekar, 1995; Pollock and Sheskey, 1996). Natural polysaccharide such as xanthan gum and guar gum matrices were also tried.

6.3.1. IN VITRO DISSOLUTION & RELEASE KINETIC STUDIES

'In vitro' release profile for matrix tablets (M-52 to M-61) prepared with EC and HPMC K4M, K15M, and K100M are shown graphically in Figure 6.20, Figure 6.21, and Figure 6.22, respectively. EC-HPMC tablets exhibited a much slower release during 0–4 h. The dissolution rate was the slowest because of low water affinity of the EC. Callahan et al observed that EC absorbs very little water from humid air or during immersion (Callahan et al., 1982; Velazquez de la et al., 2001). This may be the reason for maintaining the integrity of tablets at the end of the dissolution study. This suggests that water and glipizide diffused through the tablets without any important damage to the matrix structure and similar results were observed by Neau (Neau et al., 1999). As the relative composition of EC

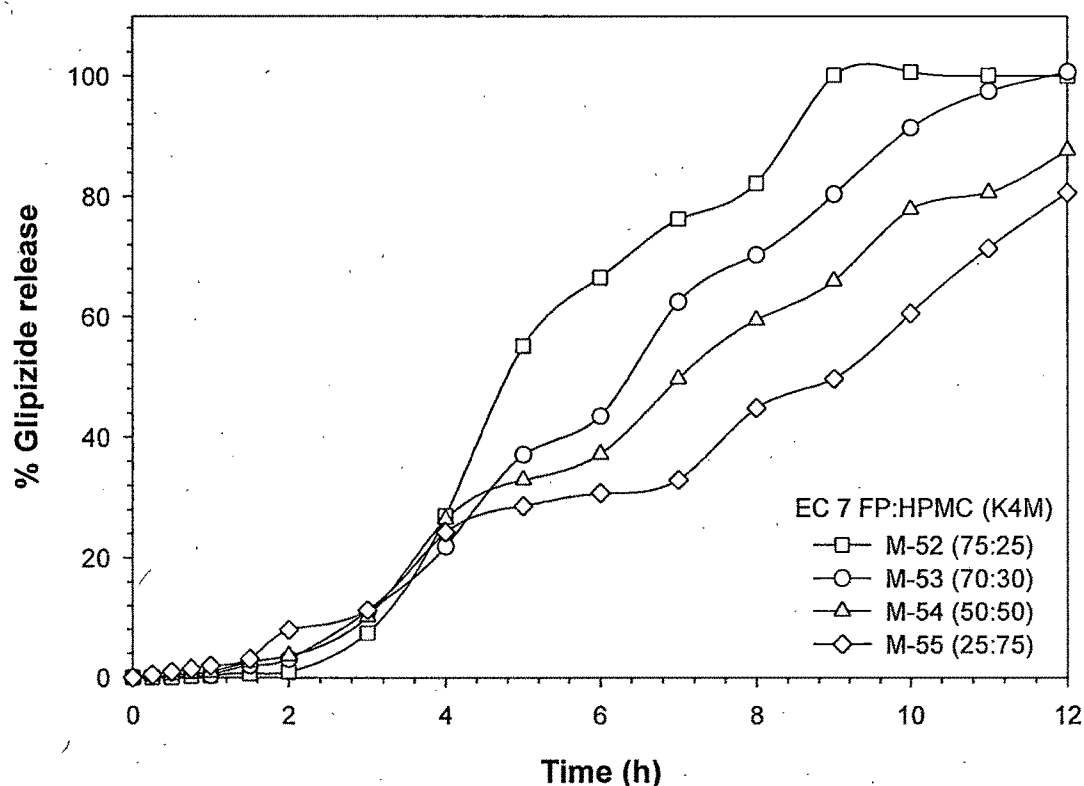


Figure 6.20. Effects of EC 7 FP : HPMC K4M ratio on the glipizide release profile.

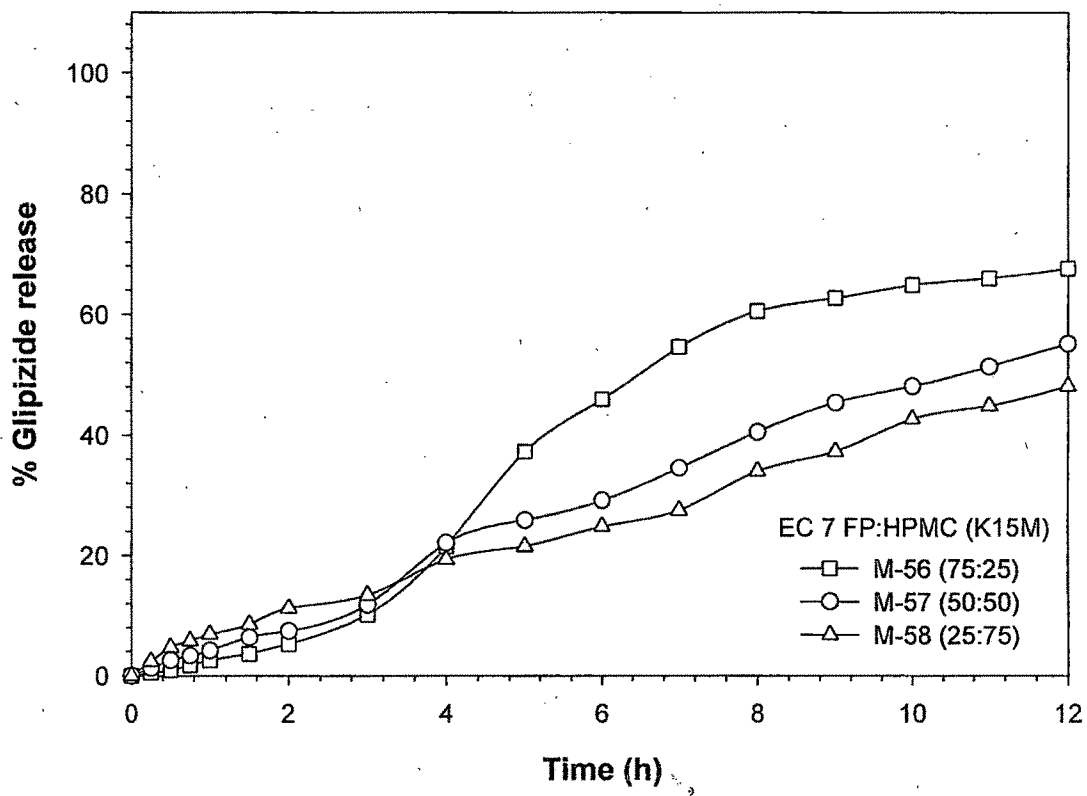


Figure 6.21. Effects of EC 7 FP : HPMC K15M ratio on the glipizide release profile.

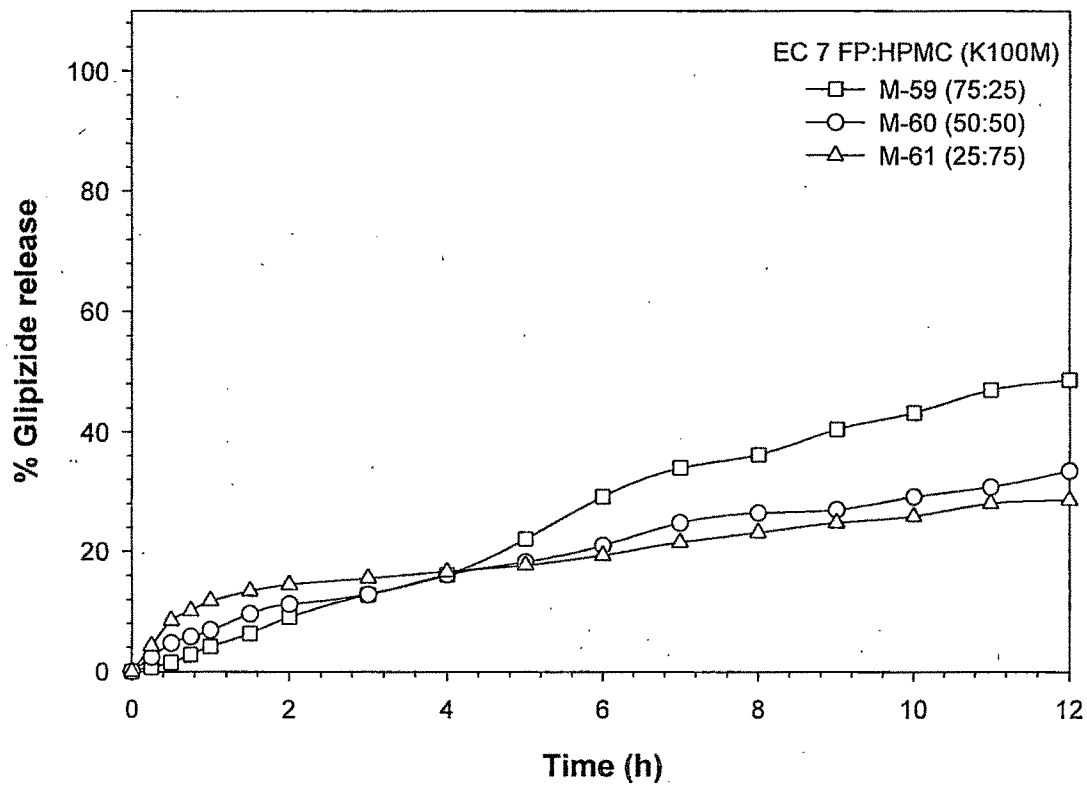


Figure 6.22. Effects of EC 7 FP : HPMC K100M ratio on the glipizide release profile.

increased in the tablet, it retards the penetration of dissolution medium by providing more hydrophobic environment and thus cause delay in release of drug from the tablet. The physicochemical properties of the EC do not seem to affect the release profile significantly after 4 h. The glipizide diffusion was expected to take place through a porous network created by glipizide already dissolved within the matrix together with the initial voids in the matrix, and filled by liquid medium (Kulvanich et al., 2002). After 4 hr, glipizide release decreased with increase in HPMC content and viscosity/molecular weight. The drug release rate decreased in the rank order HPMC K4M>K15M>K100M as observed and discussed in HPMC-MCC matrices. Thus, HPMC was found to be dominating excipient controlling the release rate of glipizide in matrix tablets.

SEM photograph of EC-HPMC (group I, J-2) tablet surface (3 and 6 h) and tablet cross-section (6 h) after dissolution are shown in Figure 6.23 (a-c). It is obvious from the figure that there was no considerable change in the tablet surface even

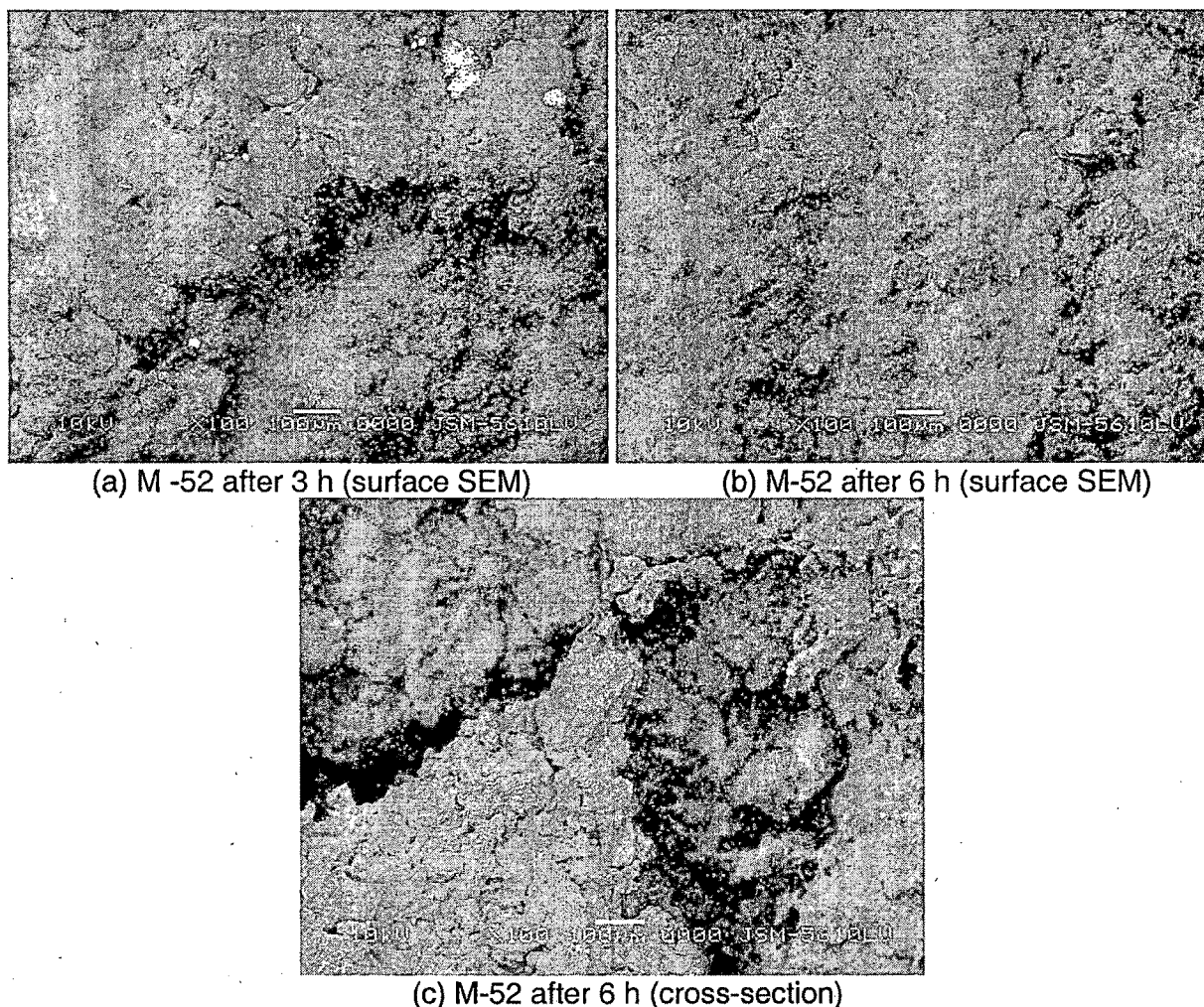


Figure 6.23. SEM photograph of M-52 (EC-HPMC) tablet surface (a, b) and tablet cross-section (c) after dissolution at different time points.

after 6 h. This may be due to hydrophobic nature of EC which does not allow the dissolution medium to wet the tablet surface and dissolve the drug easily. The cross-section after 6 h showed a dried gel layer (due to HPMC) which controlled the release. However, the matrix did not showed much pores or channel indicting that the EC matrix structure was intact.

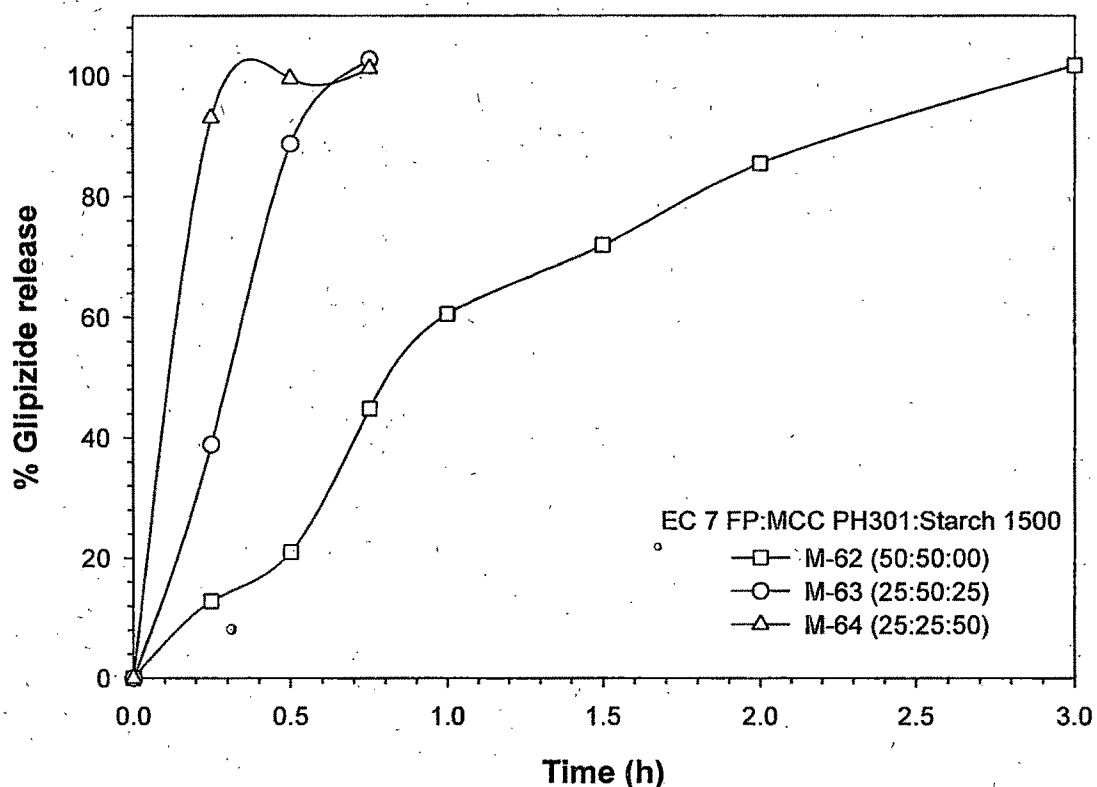


Figure 6.24. Effects of EC 7 FP : MCC PH301: Starch 1500 ratio on the glipizide release profile.

As shown in Figure 6.24 both the co-excipients (MCC and Starch) used in this investigation exhibited substantial enhancement in the drug release rates from the tablets. The EC-MCC system can sustain the drug release up to 3 h, but as starch is added, the matrix resulted in complete drug release within 0.7 h. The faster release rates observed with microcrystalline cellulose and starch might be due to its inherent disintegrant properties as discussed earlier in HPMCC-MCC matrices and HPMC-starch matrices section. Similar findings have also been reported by other researchers where microcrystalline cellulose (Chilamkurti et al., 1983; Cameron and McGinity, 1987) and starch (Michailova et al., 2001) used as co-excipient caused an increase in the release rates of drugs.

It was not possible to obtain tablets for the formulation composition of M-65 to M-67. The tablet powder mixtures were with poor carr's index value (below 5%) and it was difficult to compress it into matrix form. Even at maximum compression force, the guar gum containing mixture resulted in hardness of 2 kg/cm². Such a low hardness was not suitable for the handling of formulation and matrices were broken easily. These batches were discontinued for further study.

Xanthan exhibits pseudoplasticity (shear-reversible property) in aqueous solutions. This characteristic solution property of the xanthan gum can be explained on the basis of its helical structure. A xanthan solution in presence of salts like sodium or potassium chloride can maintain its ordered structure and viscosity. Increase in xanthan gum viscosity is due to the unwinding of the ordered conformation such as helix into a random coil with a consequent increase in resultant shape and size of the molecules. The presence of anionic side chains on the xanthan gum molecules enhances hydration and makes xanthan gum soluble in cold water. In addition, the form and the rigidity of the macromolecules determine the rheology of the solutions. Nine xanthan gum based formulations were screened to select those characterized by a minimal burst effect and a slow release of glipizide over 12 h (shown in Figure 6.25 and

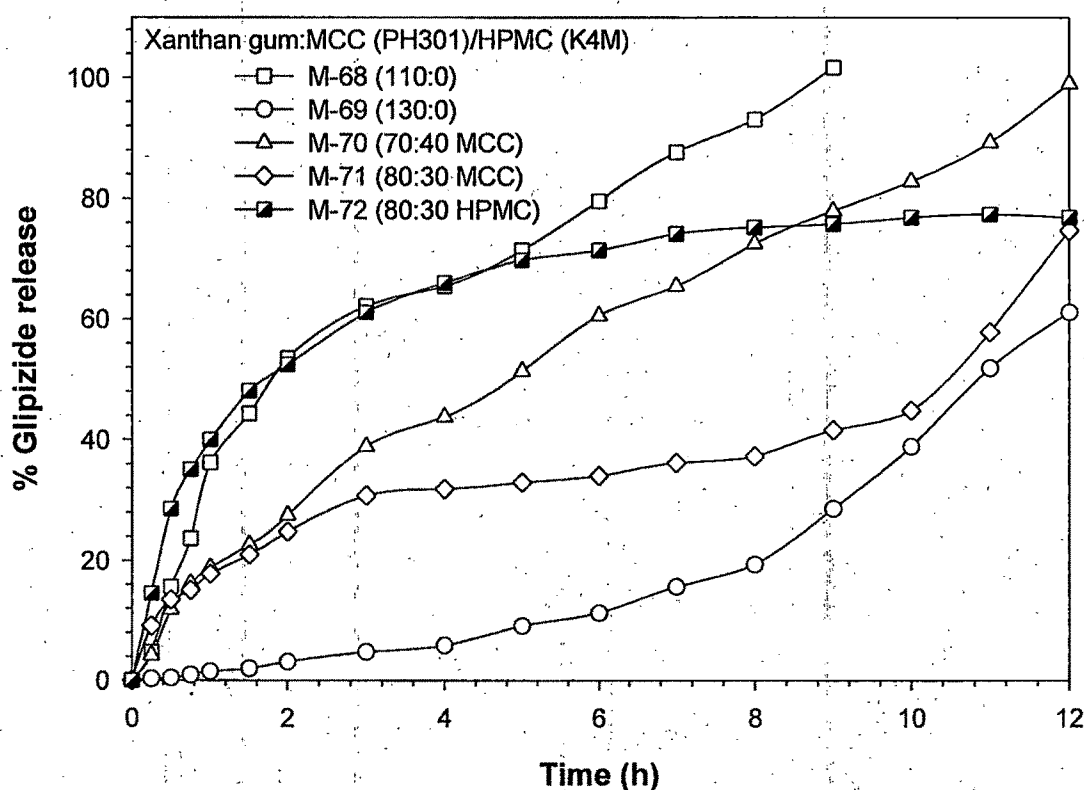


Figure 6.25. Effects of MCC PH301 and HPMC K4M on glipizide release profiles from xanthan gum matrices.

Figure 6.26). At a fixed glipizide dose, the total content of hydrophilic natural xanthan gum show a dramatic change in their dissolution profile as shown in Figure 6.25 (M-68 and M-69).

At lower xanthan gum level, rapid swelling of matrices with less tight hydrogel structure resulted in higher initial drug release followed by completion within 9 h. Conversely at the higher xanthan gum level, the hydrated gel layer became highly viscous and due to tight network formation, the initial drug release was diminished and drug diffuses slowly continuously for more than 12 h. This difference in release profiles can be explained on the basis of a change in the integrity of the matrix at different polymer concentration. Moreover, the decreased drug release rate in the order of increasing proportion of xanthan gum can be reasoned that as the amount of xanthan gum in the matrix increased, there would be a greater degree of hydration with simultaneous swelling. This would result in a corresponding lengthening of the drug diffusion pathway and reduction in drug release rate. It seems that, there is some threshold level for xanthan gum, within which the slight difference in its concentration can result in statistically significant different drug release profiles. Xanthan can produce much more viscous gel as compared to HPMC and similar findings were reported by other researchers also. (Dhopeswarkar and Zatz, 1993).

Partial replacement of xanthan gum by MCC PH301 caused increase in drug release and (M-70 and M-71 as compared to M-69) and linearization of the release profile (M-70). During dissolution, xanthan gum absorbs water, swells, and becomes a hydrated gel. At the same time, MCC PH301, having disintegration properties as discussed earlier, promoted the disintegration and erosion of the matrices, which resulted in higher drug release. Batch M-70 gave the glipizide release within the defined constraints and was considered optimized for further study. When HPMC K4M was added to xanthan gum matrix (M-72), it swells considerably immediately and release the glipizide from the channels created by dissolution medium penetration. However, as time elapse, xanthan and HPMC showed synergetic gelling ability and produce such an extremely visco-elastic gel that only 75% of glipizide released within 12 h.

As shown in Figure 6.26, the combination of two different excipients with xanthan gum (M-73 to M-76) gave more linear release profiles as compared to above matrices of xanthan gum only or with single excipient (M-68 to M-72). This may be due to the alteration in the thickness, porosity and gel structure of more complex peripheral hydrated layer through which drug diffuses out. Inclusion of MCC PH301, starch 1500, and lactose resulted in intermediate drug release rate as compared to M-68 and M-69. Hence, apart from providing acceptable flow and compression properties to the formulation, these auxiliary excipients contributed significantly in controlling the drug release without burst effect or lag phase (very

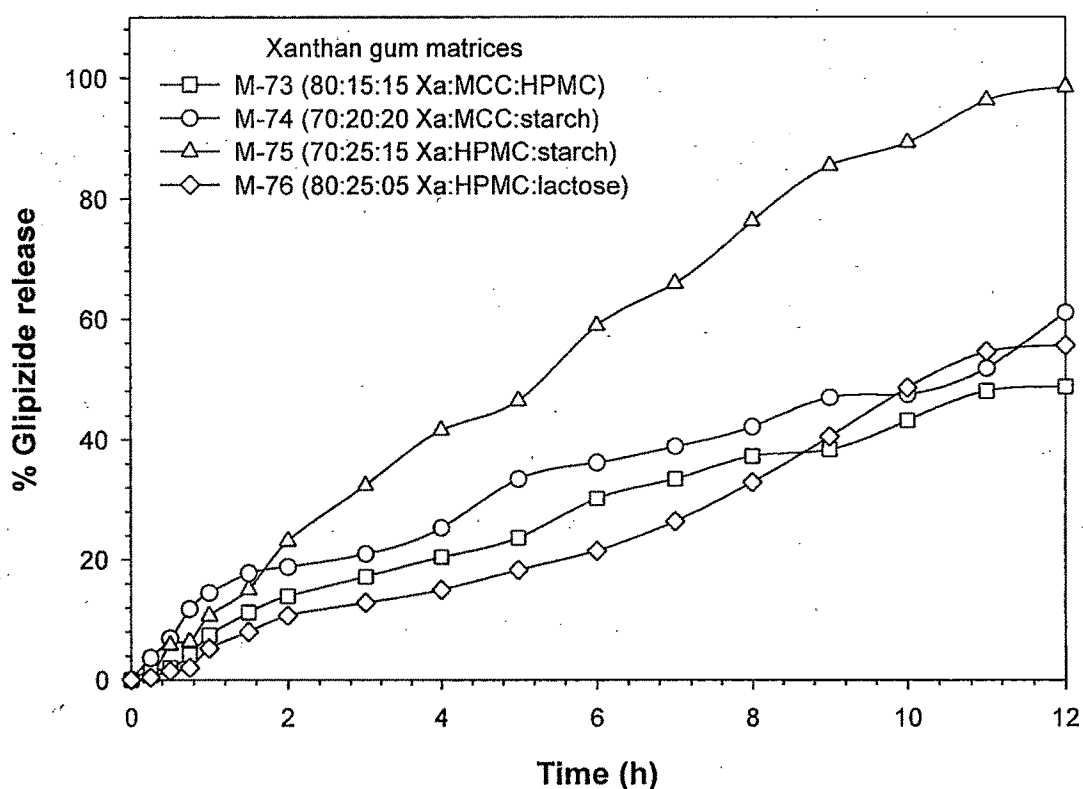


Figure 6.26. Effects of co-excipients on the glipizide release from xanthan gum matrices.

negligible initial drug release). Glipizide release of matrix M-75 containing xanthan, HPMC and starch fits within the constraint limits and was selected as an optimized batch.

With EC-HPMC matrices, as the molecular weight/viscosity and composition of HPMC in matrix tablet increases, the release profile changes from super case-II transport to Fickian diffusion mechanism (M-52 to M-61, Table 6.5). Tablets prepared with only xanthan gum follows Higuchi's square root of time equation when in low concentration, while follows Korsmeyer-Peppas' power law equation (M-68 and M-69). Matrices of xanthan with either MCC or HPMC releases drug by Korsmeyer-Peppas' equation at all studied combinations (M-70 to M-72). M-75 (xanthan-HPMC-starch) formulation comply with zero order release mechanism as depicted in Table 6.5.

Table 6.5. An overview of the comparative characteristics of different drug release kinetic models, best fit model, MDT₅₀ and MDT₈₀ for batches M-52 to M-76.

Batch No	Release model											Best fit model	MDT ₅₀	MDT ₈₀
	Zero-order K ₀	First-Order K ₁	f ₁	Higuchi matrix K _H	f _H	Korsmeyer-Peppas K _k	n	f _k	Hixson-Crowell K _s	f _s	f _s			
M-52	10.07	0.95	-	22.72	0.82	2.59	0.44	0.99	-0.07	0.83	Peppas	3.74	4.57	
M-53	8.41	0.98	-	22.52	0.87	-	-	-	-0.06	0.87	Zero order	4.14	5.39	
M-54	7.15	0.99	0.94	19.26	0.88	1.76	1.40	0.99	-0.04	0.96	Peppas	4.28	5.94	
M-55	5.94	0.98	0.92	16.01	0.88	1.40	2.49	0.99	-0.03	0.95	Peppas	4.87	6.96	
M-56	6.46	0.98	0.98	17.72	0.90	1.42	2.64	0.99	-0.03	0.98	Peppas	4.30	-	
M-57	4.81	1.00	0.99	13.29	0.93	1.01	4.61	1.00	-0.02	1.00	Zero order	5.10	-	
M-58	4.16	0.99	0.99	11.66	0.95	0.75	6.84	1.00	-0.02	1.00	Peppas	5.85	-	
M-59	4.36	1.00	1.00	12.08	0.94	1.09	3.71	1.00	-0.02	1.00	Peppas	5.64	-	
M-60	3.11	0.95	0.97	8.91	0.99	0.64	6.74	1.00	-0.01	0.97	Peppas	-	-	
M-61	2.85	0.72	0.81	8.44	0.98	0.41	10.12	0.98	-0.01	0.78	Matrix	-	-	
M-62	40.41	0.94	-	56.22	0.96	0.88	47.33	0.97	-0.33	0.93	Peppas	0.47	0.76	
M-63	154.16	0.99	-	116.99	0.97	0.96	152.89	0.98	-1.56	0.92	Zero order	0.16	0.24	
M-64	176.31	0.77	-	140.49	0.95	0.13	111.22	0.98	-1.88	0.99	Peppas	0.06	0.09	
M-65, M-66, M-67	No tablets													
M-68	13.17	0.88	-	33.20	0.99	0.72	24.56	0.95	-0.09	0.90	Matrix	0.80	1.93	
M-69	3.64	0.91	0.86	9.45	0.77	1.39	1.25	0.99	-0.01	0.88	Peppas	7.73	9.41	
M-70	5.53	0.86	0.88	16.02	0.94	0.45	17.29	0.97	-0.02	0.89	Peppas	3.78	6.65	
M-71	8.84	0.97	0.86	25.19	0.98	0.72	16.47	0.99	-0.05	0.96	Peppas	1.90	3.78	
M-72	8.92	-	0.77	27.18	0.90	0.37	35.68	0.95	-0.04	0.65	Peppas	0.57	-	
M-73	4.46	0.99	1.00	12.57	0.96	0.91	5.71	0.99	-0.02	0.99	1st order	-	-	
M-74	5.29	0.95	0.98	15.15	0.98	0.64	11.54	0.99	-0.02	0.98	Peppas	3.98	-	
M-75	9.05	0.99	0.92	25.30	0.95	1.17	7.14	0.96	-0.05	0.98	Zero order	2.43	4.07	
M-76	4.48	0.99	0.97	12.24	0.90	1.16	3.24	0.98	-0.02	0.97	Zero order	5.87	-	

6.3.2. CHARACTERIZATION OF OPTIMIZED FORMULATIONS

From the release profiles of EC-HPMC, EC-MCC, and xanthan gum matrices, M-70 and M-75 were selected as the optimized formulations as they fit all the release constrains. Both formulations were studied further for release mechanism by Kopcha model (Kopcha et al., 1991), swelling study, and SEM.

6.3.2.1. Release Mechanism by Kopcha Model

Matrix tablets M-70 (xanthan : MCC PH301 at 70:40) showed predominance of erosion relative to diffusion for initial 2 h. This was contributed by the presence of water insoluble MCC. However, xanthan gum prepared strong gel and the diffusion takes over erosion term after 2 h and was maintained through out the release profile. For the M-75 formulation (xanthan : HPMC K4M:Starch 1500 at 70:25:15) showed matrix erosion as major release mechanism. However, the diffusion term increase up to 5 h and become steady after that, it was less significant than erosion.

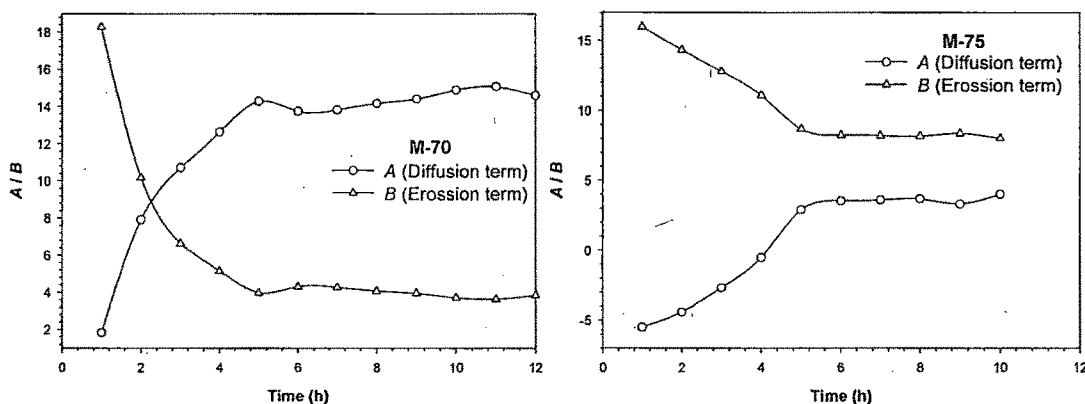


Figure 6.27. Kopcha model parameters A (diffusion term) and B (erosion term) as a function of time for M-70 and M-75 formulations.

6.3.2.2. Swelling Study

Results of water uptake, axial and radial expansion for M-70 (xanthan : MCC PH301 at 70:40) are enumerated in Figure 6.28 and the photographs at different time intervals are also presented. It is evident that water uptake was continuously rising through out the study. Same is the case with radial and axial swelling. This supports the observation of Kopcha model that the diffusion was predominant. The terminal water uptake and radial/axial swelling was less steep because the diffusional path length, hence distance to be traveled for dissolution media to

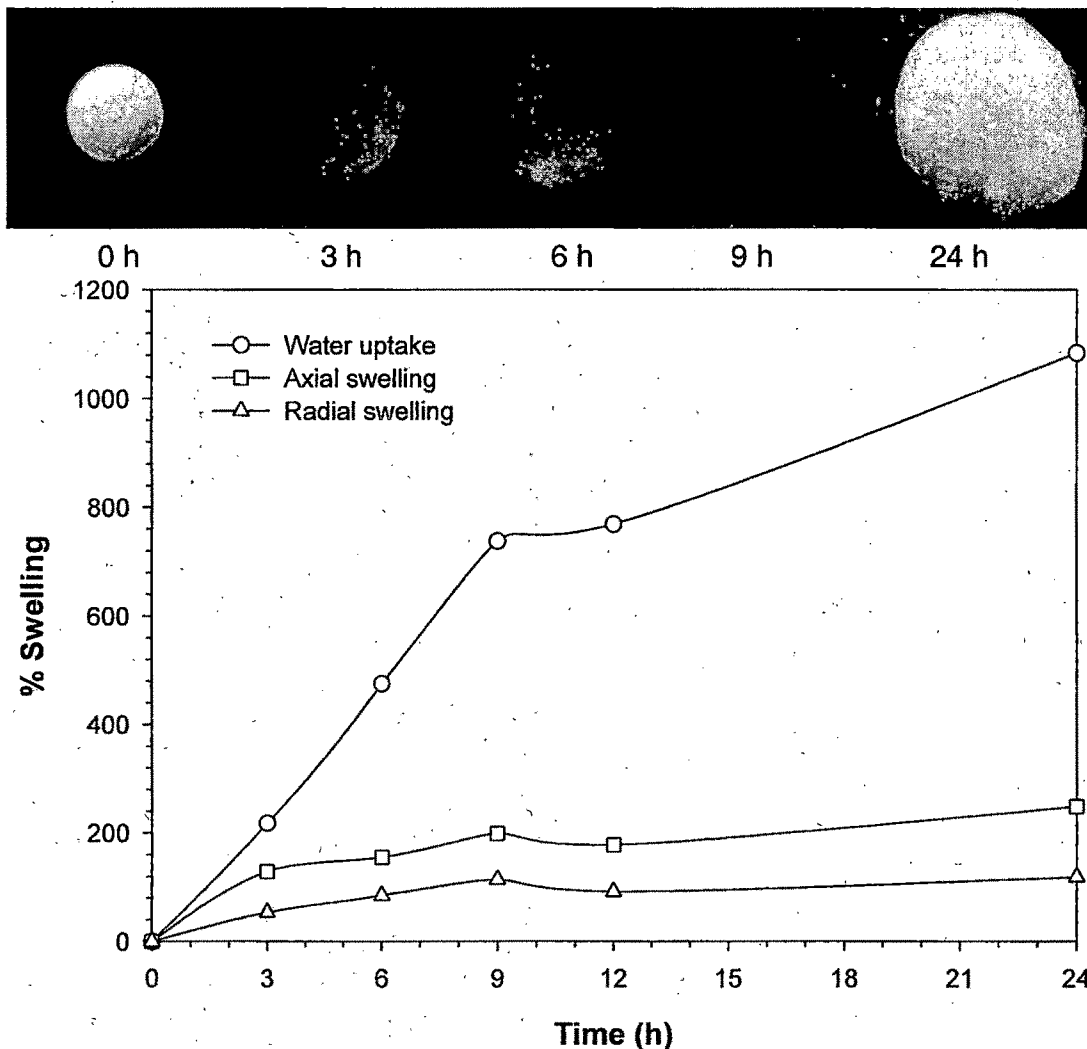


Figure 6.28. Percent water uptake, axial, and radial swelling results for M-70 formulation (xanthan : MCC PH301 at 70:40).

reach the dry core increases with time. Hence, the drug release profile fits into the Korsmeyer-Peppas power law equation.

Figure 6.29 summarizes the results of water uptake, axial and radial expansion for M-75 (xanthan : HPMC K4M : Starch 1500 at 70:25:15). Though water uptake was continuously increasing with time similar to M-70, the radial and axial expansion was almost constant after 6 h. This suggests the role of erosion to maintain constant diffusional path length because of proper synchronization between erosion and diffusion. This ultimately releases the drug by zero order. Over hydration of the outer most gel layer and its erosion can be seen in the last photograph.

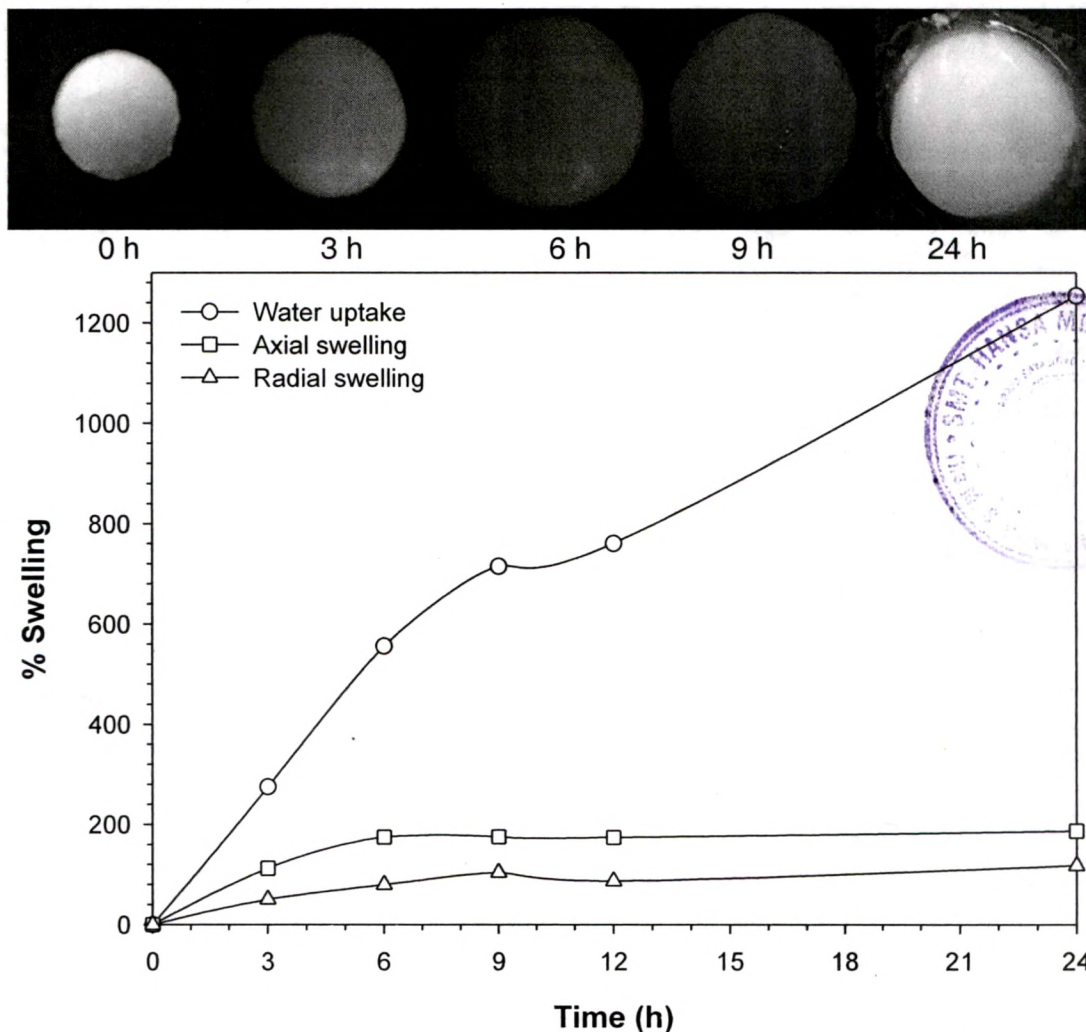


Figure 6.29. Percent water uptake, axial, and radial swelling results for M-75 formulation (xanthan : HPMC K4M : Starch 1500 at 70:25:15).

6.3.2.3. SEM Study

Surface structure of M-70 after 12 h dissolution was studied by SEM analysis and shown in Figure 6.30. From the above discussion, it is evident that the release was due to diffusion of drug and hence the opening of the channels can be seen in the form of pores on the surfaces (shown by arrows). The higher magnification photographs shows viscous gel like rubbery structure.

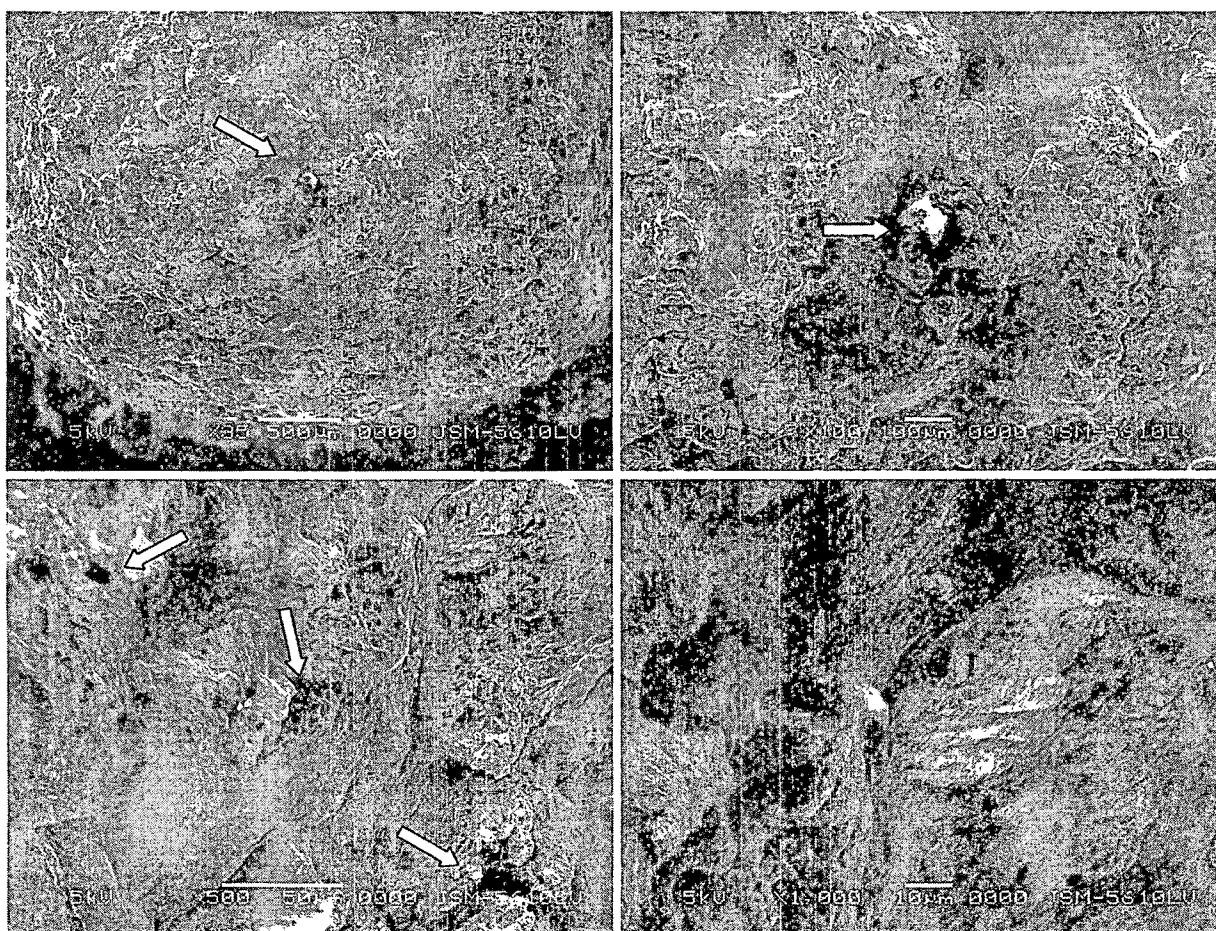


Figure 6.30. Scanning electron micrograph of M-70 after 12 h dissolution at different magnifications (pores created due to diffusion are shown by arrows).

Scanning electron micrograph of M-75 surfaces after 12 h dissolution are presented in Figure 6.31. The micrographs further verify the hypothesis of surface erosion as discussed above in Kopcha model and swelling study. None of the micrograph showed any pores nor any viscous gel like structure. Instead, the eroded surfaces were observed.

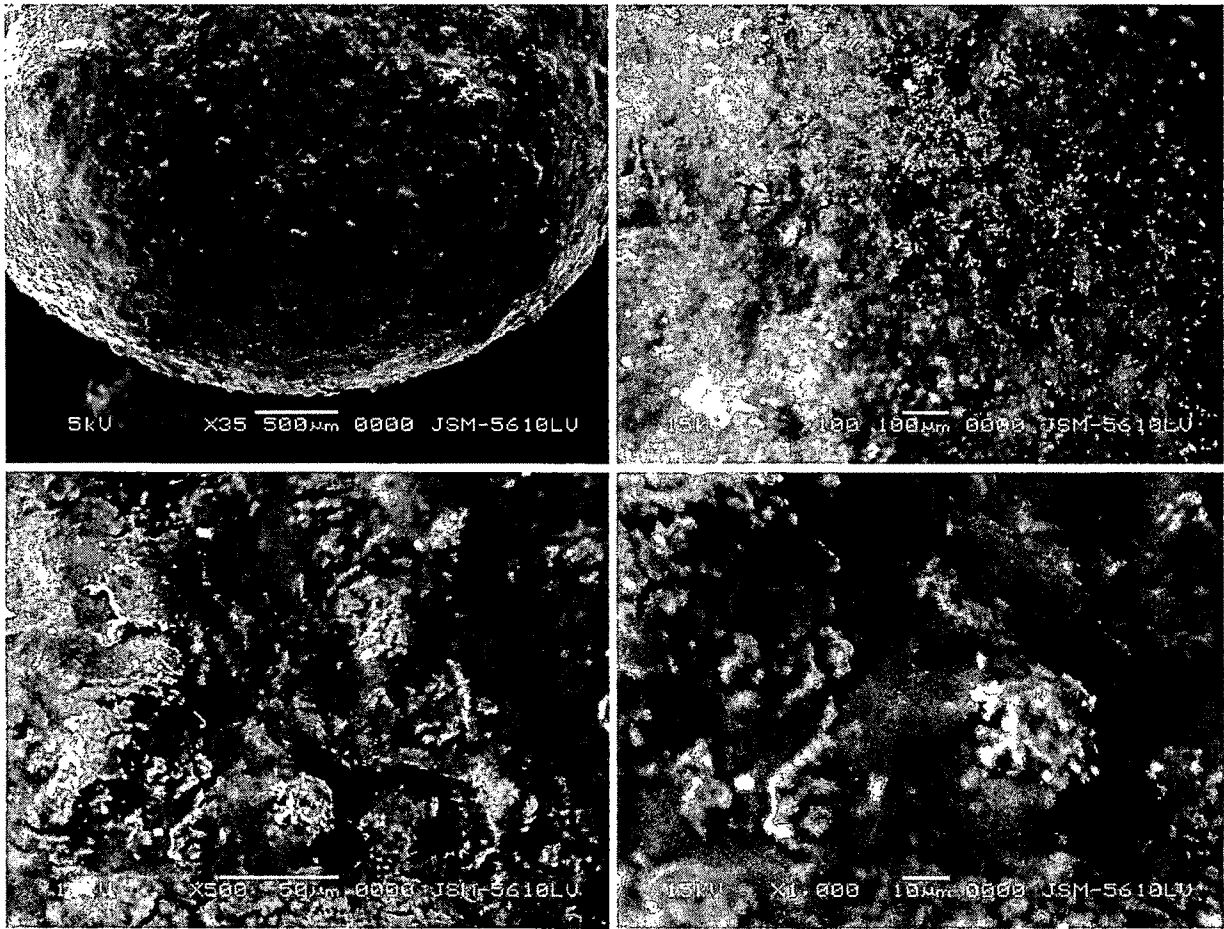


Figure 6.31. Scanning electron micrograph of M-75 after 12 h dissolution at different magnifications.

6.4. Carbopol Matrices

Matrices of different grade carbopol polymers with other co-polymers or excipients were prepared to study and understand the effects of matrix composition on their in vitro release kinetics.

6.4.1. IN-VITRO DISSOLUTION & RELEASE KINETIC STUDIES

Generally, in the dry state, the drug is trapped in a glassy core of carbopol matrix system. As the external surface of carbopol matrices hydrated, it also forms a gelatinous layer, which is significantly different structurally from the other traditional matrix tablet. The hydrogels are not entangled chains of polymer, but discrete microgels made up of many polymer particles, in which the drug is dispersed. The crosslink network enables the entrapment of drugs in the hydrogel domains. Since these hydrogels are not water soluble, they do not dissolve, and erosion in the manner of linear polymers does not occur. But, when the hydrogel is fully hydrated, osmotic pressure from within works to break up the structure, essentially by sloughing off discrete pieces of the hydrogel. As the thermodynamic activity or chemical potential increases, the gel layer around the tablet core actually acts almost like a rate-controlling membrane, resulting in linear release of the drug. Because of this structure, drug dissolution rates are affected by subtle changes in hydration rate and swelling of the individual polymer hydrogels, which are dependent on the molecular structure of the polymers, including crosslink density, chain entanglement, and crystallinity of the polymer matrix. Upon exposure to water, the polymer chains start gyrating and the radius of gyration becomes bigger and bigger. Macroscopically, this phenomenon manifests as swelling and the magnitude and rate of swelling is dependent on the pH of the dissolution medium. The channels, which form between the polymer hydrogels, are influenced by the concentration of the polymer, as well as the degree of swelling. Increasing the amount of polymer will decrease the size of the channels, as does an increase in swelling degree (Hosmani, 2006). All of these factors affected glipizide release profiles significantly and discussed below. All the carbopol resins, when first dispersed in water; they are tightly knotted together via hydrogen bonding, thus limiting its thickening capability until the resins are partially neutralized. This neutralization ionizes the carbopol polymer, generating negative charges along the polymer backbone. Repulsions of these like negative charges cause the molecule to uncoil into an extended structure. However, to achieve the highest possible performance with the polymer, the molecule must be completely uncoiled. This

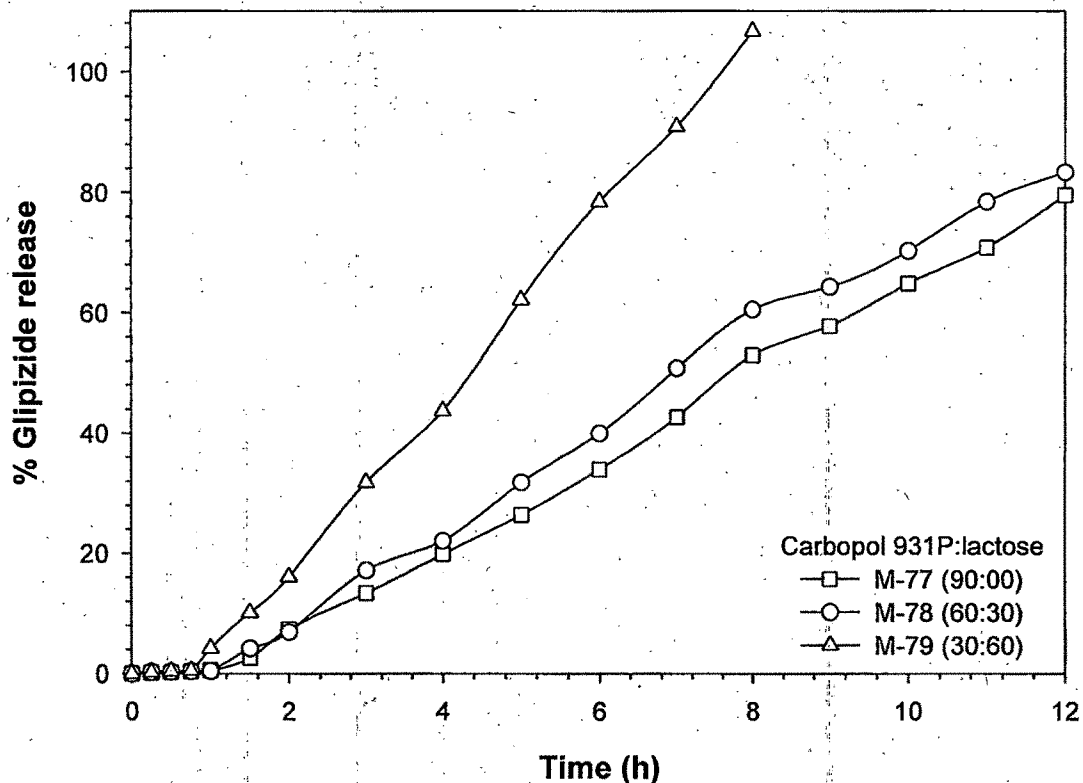


Figure 6.32. Effects of Carbopol 931P : lactose ratio on the glipizide release profile.

reaction is rapid and gives instantaneous thickening and swelling (Noveon Bulletin, 2002b).

The glipizide release influenced by the change in Carbopol 931P and lactose ratio is depicted in Figure 6.32. Rate of hydration of carbopol matrices are highest because of its strong hydrophilic nature. Thus, when this matrix come in contact of dissolution medium, it rapidly hydrate and form a strong elastic gel which restrict the entry of medium towards the glassy core, hence almost negligible release during first hour. Directly compressible lactose was included as diluent for its high aqueous solubility which increases the rate and amount of water imbibition to peripheral layer (Nandita and Sudip, 2004). Lactose increases the rate of swelling of polymers, which in turn forms a gelled matrix to control the release linearly. As lactose is water soluble, it easily dissolves in dissolution media and hence higher lactose concentration provides more channels for the drug to diffuse out of the hydrated gel layer resulting in higher release rate. The dissolution data of all the batches (M-77 to M-97) were fitted to different drug release modalities and an overview of the comparative kinetic constants, regression coefficients, best fit model, MDT₅₀ and MDT₈₀ values are summarized in Table 6.6. Matrices composed of Carbopol 931P : lactose followed zero-order drug release kinetics due to highly water soluble characteristic of lactose.

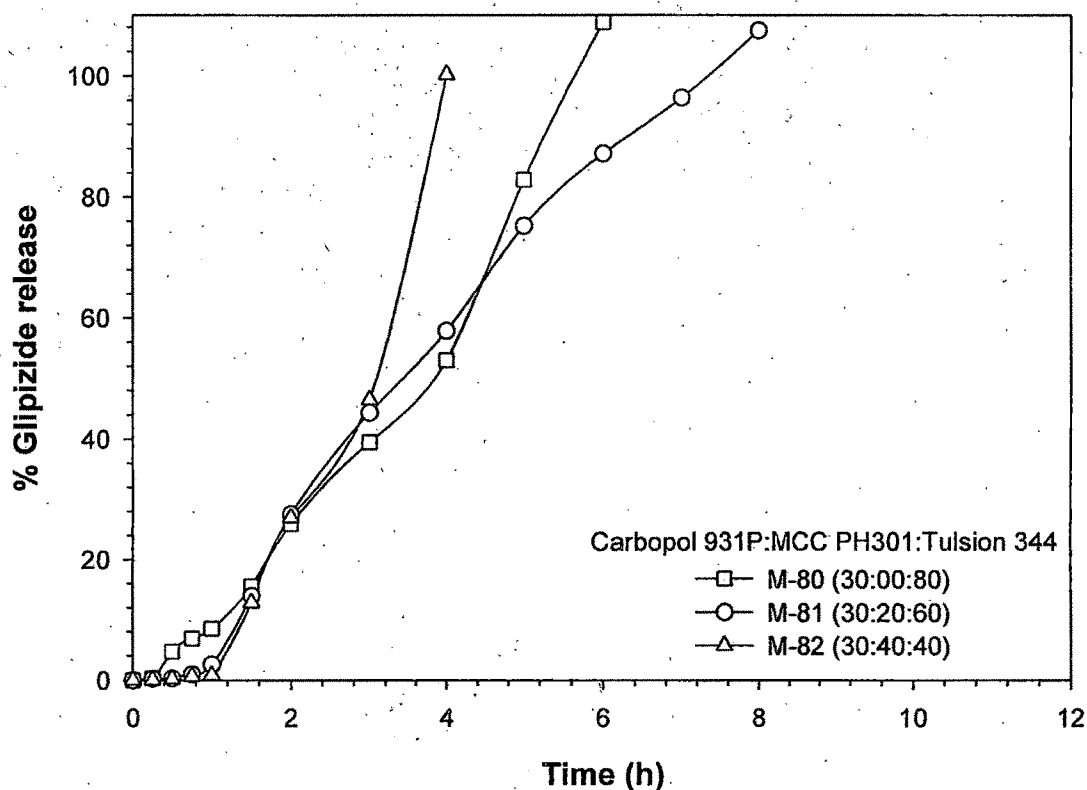


Figure 6.33. Effects of Carbopol 931P : MCC PH301 : Tulsion 344 ratio on the glipizide release profile.

Tulsion-344 is ion exchange resin containing sulfonic (anionic) functional group. At pH 6.8 of dissolution medium, carbopol is also anionic. Thus it was tried to check whether the anionic ion exchange resin can give synergistic effect on swelling and hence viscosity of carbopol by providing negative charge to the matrix. However, as can be seen in Figure 6.33, there was no significant contribution of ion-exchange resin on the release profile of glipizide from carbopol matrices.

Figure 6.34 enumerates the effects of Carbopol 931P : MCC PH 301 ratio on glipizide release profiles. It is obvious from the figure that at higher carbopol levels (M-83), the release profile can be divided in three segments, the initial burst effect (0-1h), almost steady phase (1-8 h) and last rapid release phase (8-12 h). This can be explained as follow: As the pKa of the carbopol polymer is 6.0 ± 0.5 , at dissolution medium pH of 6.8, higher swelling occurs because of maximum dissolution medium penetration. This result in porous gel due to channels created by medium penetration and through which glipizide diffuses faster and easily during initial burst. On the other hand, in the presence of nearly neutral pH, the hydroxyl group of the dissolution media combines with the carboxylic group of the polymer via hydrogen bond and this result in thickening of the gel layer. This mechanism is time dependent and can take from few minutes

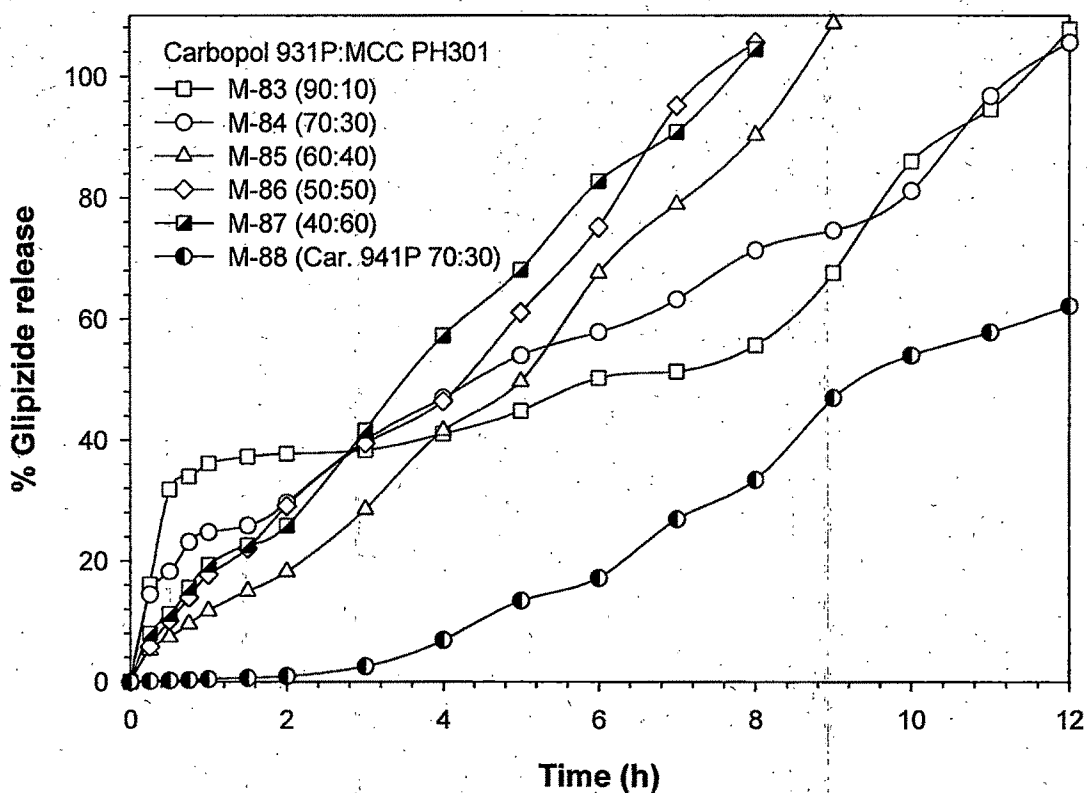


Figure 6.34. Effect of Carbopol 931P : MCC PH301 ratio on the glipizide release profile.

to several hour to attain maximum thickening (Noveon Bulletin, 2002a). Hence, once the viscous gel layer develops in the presence of dissolution medium, it retards the glipizide release significantly (approximately 20 % drug release in 1-8 h). Lastly when the hydrogel is fully hydrated, as discussed earlier, due to osmotic pressure developed within the matrix play role to break up the gel structure by sloughing off discrete pieces of the hydrogel until complete erosion, and thereby higher drug release during 8-12 h. When carbopol content is higher (M-83 and M-84), matrix followed Higuchi's square-root of time and Korsmeyer-Peppas release kinetics, respectively (shown in Table 6.6).

This tri-phasic release behavior is gradually decreased and more linearization of release profile is observed as the MCC PH301 content increased. This ultimately changes the best fit release model from Higuchi or Korsmeyer to first order as shown in Table 6.6. The decreased initial burst can be reasoned that the presence of insoluble MCC PH 301 hinders the penetration of dissolution medium and thereby swelling also, which ultimately changes the gel integrity and decreased release rate. During the middle phase, the insoluble and disintegrant nature of MCC PH301 caused linear increase in release rate. In addition, this continuous erosion of the outermost gel layer and drug release, osmotic pressure developed was much lower and hence terminal glipizide release was also controlled in linear fashion (M-84 to M-87, Figure 6.34). From this group, M-84

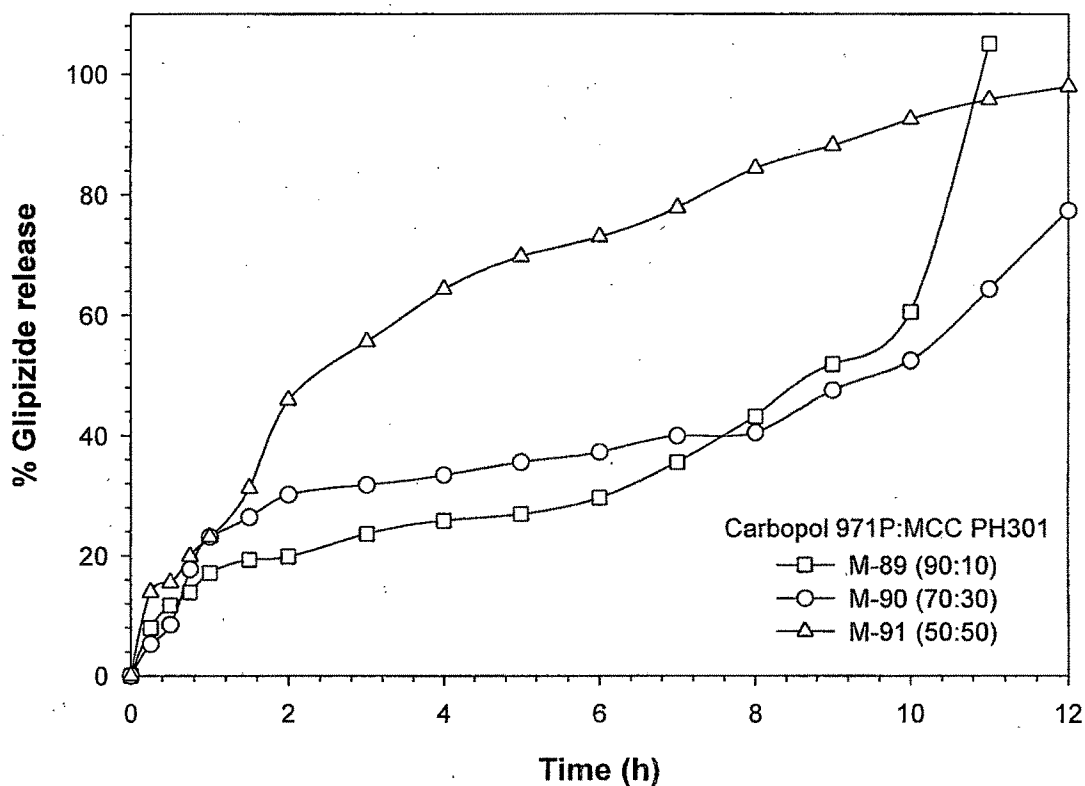


Figure 6.35. Effect of Carbopol 971P : MCC PH301 ratio on the glipizide release profile.

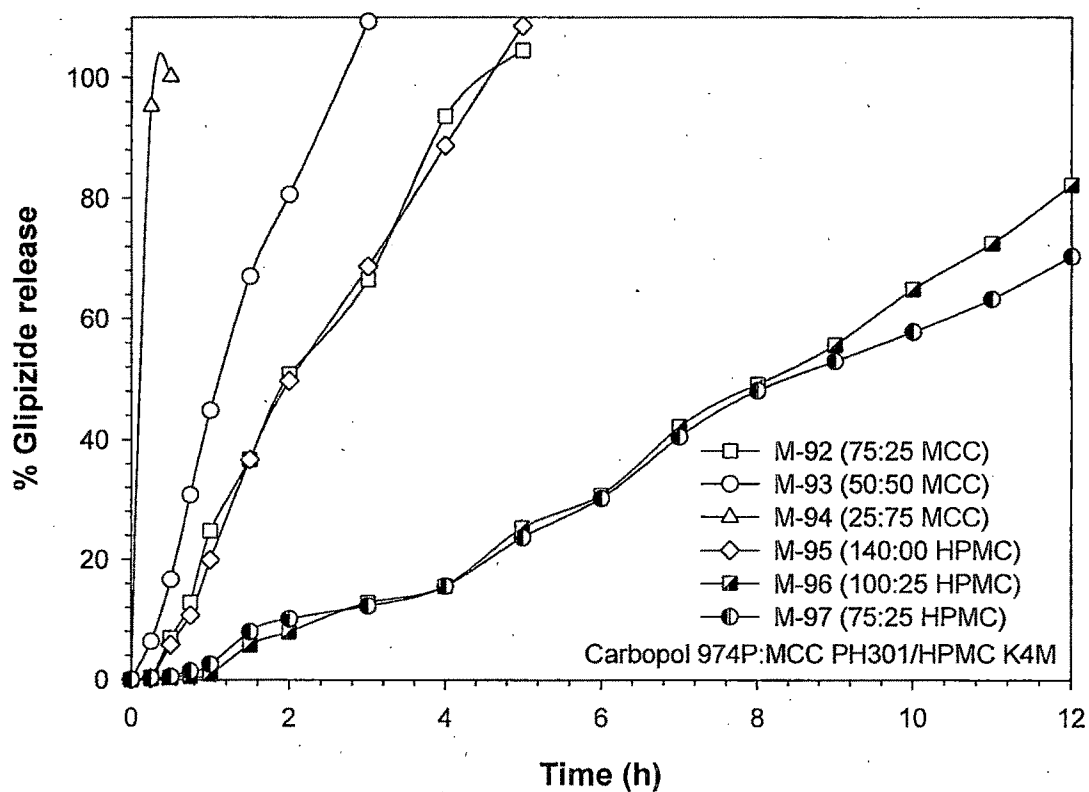


Figure 6.36. Effects of Carbopol 974P : MCC PH301/HPMC K4M ratio on the glipizide release profile.

batch fitted the glipizide release at all time points of the desired constraint, and considered as an optimized. This batch follows Korsmeyer-Peppas power law equation with the n value of 0.5, indicating the drug release by fickian diffusion mechanism. Decrease drug release with Carbopol 941P observed was due to difference in cross-link density of the polymer (M-88). The pattern of glipizide release profiles from the Carbopol 971P : MCC PH301 matrices (Figure 6.35, M-89 to M-91) are identical to that of the Carbopol 931P : MCC PH301 matrices and can be explained same as above. The glipizide release data fits into Peppas and Higuchi models. The only difference is the overall suppression of drug release rate, and can be reasoned for the increase in the viscosity of the Carbopol 971P. The matrices prepared with Carbopol 974P : MCC PH301 at different ratios (M-92 to M-94) resulted in rubbery type structure, and tablets were not broken at maximum scale of the hardness tester ($>10-12 \text{ kg/cm}^2$). At the higher force of hardness tester, tablets developed cracks but not broken into discrete fragments. The glipizide release from the Carbopol 974P : MCC PH301 matrices (Figure 6.36, M-92 to M-94) became faster as the MCC PH301 proportion in the matrix increases. At the lowest level of MCC PH301, glipizide release was sustained up to 5 h. As seen from the Table 6.6, as the carbopol content increases in the matrix, best fit model shifts from first order to Korsmeyer-Peppas model with diffusion mediated drug release mechanism.

Only Carbopol 974P containing matrix, M-95, gave almost identical release profile to that of M-92. Matrix tablets completely prepared with Carbopol 974P could not reduce the drug release rate further. Hence, HPMC K4M was included in the next two batches (M-96 and M-97). Inclusion of HPMC K4M synergistically increases the viscosity of the hydrogel and resulted in significant decrease in glipizide release with almost negligible glipizide release within first hour of dissolution. This is because of the inherent quick gelling power of the HPMC K4M. It should be noticed that with same HPMC level, the change in carbopol quantity resulted in almost similar glipizide release. This indicate that there exists some threshold level for carbopol quantity beyond which further increase in carbopol fraction just increases the matrix weight and do not actively change the active drug release. This can be further confirmed by comparing the release data of M-92 and M-95. The drug release data fitting into the different release kinetic models revealed that formulation M-95 to M-97 fits into zero-order and Peppas models with supercase - II transport release mechanism ($n > 1$) as depicted in Table 6.6.

Table 6.6. An overview of the comparative characteristics of different drug release kinetic models, best fit model, MDT₅₀ and MDT₈₀ for batches M-77 to M-97.

Batch No	Release model										Best fit model	MDT ₅₀	MDT ₈₀	
	Zero-order	First-Order	Higuchi matrix	Korsmeyer-Peppas	Hixson-Crowell									
	K_0	f_0	K_1	f_1	K_H	f_H	n	K_k	f_k	K_s	f_s			
M-77	6.28	0.99	-0.10	0.95	16.94	0.88	1.88	1.03	0.99	-0.03	0.97	Zero order	4.61	6.62
M-78	6.96	0.99	-0.12	0.96	18.87	0.90	1.80	1.33	0.97	-0.03	0.98	Zero order	4.12	5.95
M-79	12.52	0.99	-	-	27.08	0.87	1.99	2.47	0.97	-0.10	0.82	Zero order	2.57	3.55
M-80	15.81	0.98	-	-	29.14	0.85	1.59	7.33	0.97	-0.13	0.79	Zero order	2.03	2.92
M-81	14.00	0.99	-	-	30.79	0.90	2.03	2.79	0.97	-0.11	0.87	Zero order	2.00	2.91
M-82	18.55	0.90	-	-	25.86	0.72	2.92	2.03	0.98	-0.16	0.76	Peppas	2.00	2.53
M-83	8.61	0.81	-	-	24.97	0.91	0.35	31.42	0.91	-0.06	0.76	Matrix	1.39	4.09
M-84	9.05	0.94	-	-	25.94	0.98	0.50	24.90	0.99	-0.06	0.83	Peppas	1.57	3.66
M-85	11.41	0.99	-	-	26.82	0.90	0.88	12.94	0.99	-0.09	0.79	Zero order	2.48	3.78
M-86	10.80	0.85	-	-	27.10	0.95	0.42	29.98	0.97	-0.07	0.76	Peppas	1.12	3.26
M-87	13.46	0.99	-	-	30.43	0.95	0.77	19.31	0.99	-0.10	0.85	Zero order	1.69	2.81
M-88	4.61	0.95	-0.06	0.92	12.08	0.81	1.86	0.58	0.98	-0.02	0.93	Peppas	6.50	-
M-89	6.71	0.89	-	-	17.84	0.84	0.52	15.35	0.94	-0.05	0.63	Peppas	3.99	6.22
M-90	6.07	0.86	-0.09	0.90	17.60	0.95	0.55	16.18	0.95	-0.03	0.91	Peppas	3.12	6.08
M-91	10.59	0.88	-0.25	0.99	29.59	0.99	0.57	26.32	0.99	-0.06	0.99	Matrix	1.05	2.34
M-92	22.21	0.99	-	-	38.55	0.92	1.65	12.83	0.94	-0.19	0.89	Zero order	1.09	1.74
M-93	38.99	0.99	-	-	52.44	0.93	1.16	37.53	0.99	-0.35	0.88	Zero order	0.63	0.95
M-94	236.43	0.86	-	-	157.92	0.97	0.07	105.27	1.00	-2.29	1.00	Peppas	0.06	0.09
M-95	22.53	1.00	-	-	38.72	0.90	1.82	10.76	0.94	-0.19	0.86	Zero order	1.15	1.77
M-96	6.22	0.99	-0.10	0.93	16.71	0.88	1.70	1.47	0.99	-0.03	0.96	Peppas	4.79	6.76
M-97	5.66	0.99	-0.08	0.97	15.39	0.90	1.45	2.30	0.99	-0.02	0.98	Zero order	4.82	7.13

6.4.2. CHARACTERIZATION OF OPTIMIZED FORMULATIONS

In the group of all carbopol matrices (M-77 to M97), batch M-84 (Carbopol 931P : MCC PH301 at 70:30) was the optimized batch and was studied further for thorough understanding and confirmation of the drug release kinetics as follow.

6.4.2.1. Release Mechanism by Kopcha Model

As discussed in vitro dissolution section, Carbopol 931P can hydrate quickly due to anionic nature; the dissolution media penetrate easily and dissolve the drug. This dissolved drug diffusion is the key mechanism for drug release kinetics. Results of Kopcha model analysis for M-84 are enumerated in Figure 6.37. It is seen from the figure that diffusion term is much higher than the erosion term, and confirms that the predominance of diffusion mechanism responsible for the drug release. The swelling of this matrix in dissolution medium was almost similar to that of batch M-70 (xanthan gum : MCC PH301). At end of the swelling study, the swollen tablet maintains its integrity and this supports the negligible erosional term as suggested by Kopcha model analysis. Moreover, Kopcha model results

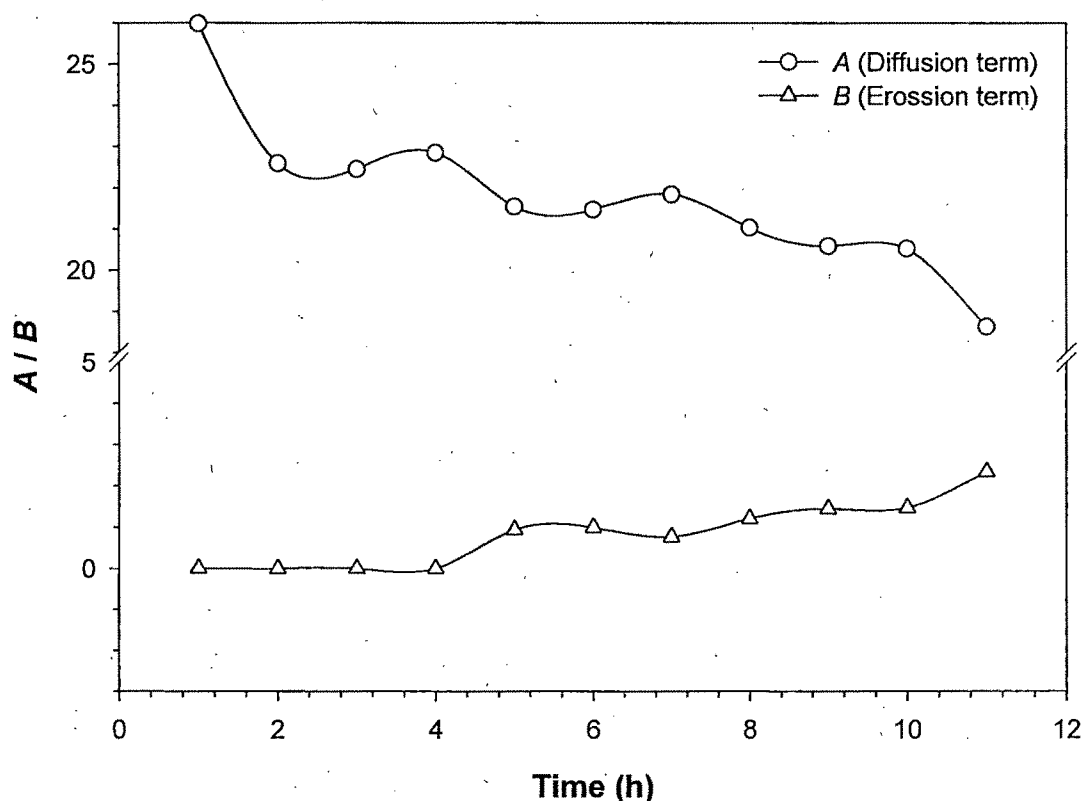


Figure 6.37. Kopcha model parameters A (diffusion term) and B (erosion term) as a function of time for M-84.

show the decrease in rate of diffusion as the time passes. This can be explained on the basis that as the volume of swollen matrix increases, the diffusional pathlength increases, and drug takes more time to travel it and appear in the dissolution medium.

6.4.2.2. SEM Study

The scanning electron micrographs of the matrix surface after 12 h dissolution at different magnification are shown in Figure 6.38. The pores created by opening of the channels through which drug has diffused out are seen clearly and indicated by arrows in the figure. This adds one more confirmation for the predominance of diffusion as a major mechanism for drug release. Moreover, the glassy matrix core converted into a rubbery visco-elastic gel like structure is also obvious. The lower magnification SEM photograph show the integrity (without erosion) of the swollen hydrogel at the end of the dissolution study.

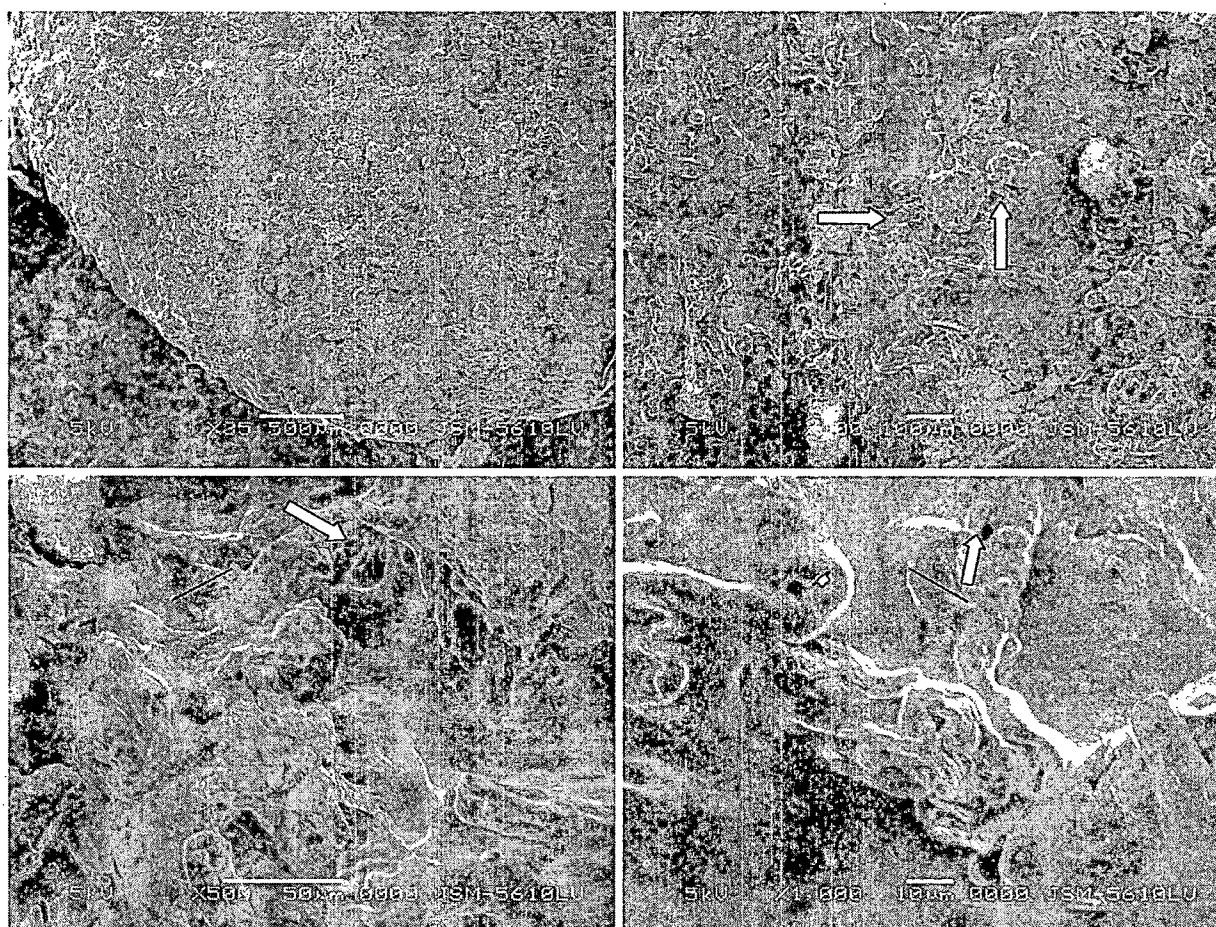


Figure 6.38. Scanning electron micrograph of M-84 after 12 h dissolution at different magnifications (pores created due to diffusion are shown by arrows).

6.5. Carrageenan Matrices

The gelling ability of different types of carrageenans was applied to sustain the drug release from the directly compressed matrices alone or in combination with other co-excipients or release rate modifiers and outlined below.

6.5.1. IN VITRO DISSOLUTION & RELEASE KINETIC STUDIES

The key element to drug release from swellable matrices is the use of polymers that will undergo transition from the glassy to the rubbery state, which is characterized by a gel like layer, upon hydration by water. This transition should occur fairly rapidly so that the drug has to pass through the viscous gel layer before it is released (Nerurkar et al., 2005). The rate at which the drug is released from the swellable hydrophilic matrices is determined by combination of one or more processes such as hydration of the polymer that leads to swelling, diffusion of the drug through the hydrated polymer, drug dissolution and polymer erosion simultaneously.

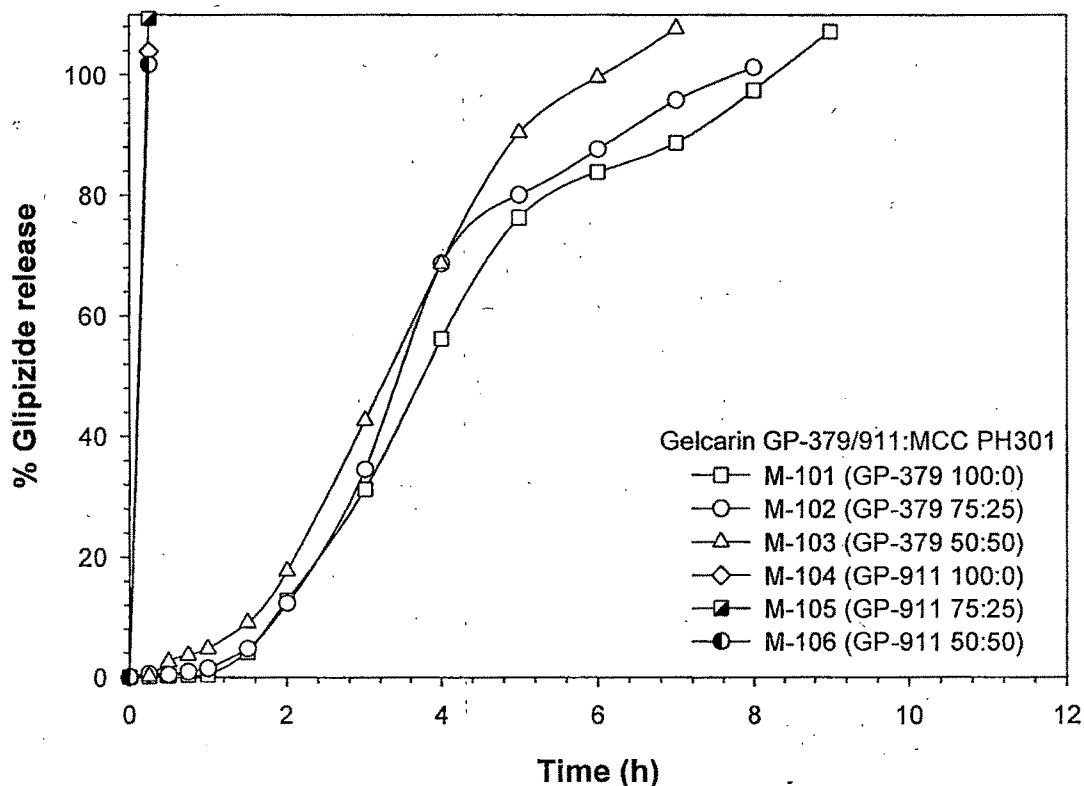


Figure 6.39. Effects of Gelcarin type and Gelcarin : MCC PH301 ratio on the glipizide release profiles.

Different carrageenan types were checked for their performance to sustain the glipizide release from directly compressible matrices. The batches M-98 to M-100 were prepared with κ -carrageenan (S. D. Fine Chem) but all the prepared powder mixture characteristics were beyond the limits for good compressibility and flow properties (data not shown). The matrices tried to prepare and resulted in hardness of less than 2.5 kg/cm², some of them also resulted in excessive capping and not included in further study.

Figure 6.39 depicts the effects of Gelcarin GP-379 and Gelcarin GP-911 on the glipizide matrices prepared with Gelcarin and MCC PH301. The premature disintegration and complete release within 20 min for matrices containing Gelcarin 911 (κ -carrageenan, M-104 to M-106, Figure 6.39) was due to very rapid hydration of the gelling polymer particles in the dissolution media to form gel layer which is rigid and brittle. It was not able to maintain its integrity on rapid and excessive hydration. Moreover, in presence of water insoluble MCC PH 301, the isolated pockets of gelcarin aggregates could have assisted the disintegration of the tablets due to localized wetting and the formation of a discontinuous gel layer (Wan et al., 1993). This consequently led them to behave as disintegrants rather than as release retarding polymers. Similar observation have been supported by other researchers (Nerurkar et al., 2005).

At the same time, Gelcarin GP-379 (ι -carrageenan) containing matrices (Figure 6.39, M-101 to M-103) forms elastic and cohesive gels upon hydration, that can maintain its network in the presence of MCC PH301 also and sustained glipizide release up to 7-9 h depending on the gelcarin : MCC ratio. Hence, Gelcarin GP-379 was further studied with other polymers and cations. Results of dissolution curve fitting into different drug release models, kinetic constants, MDT₅₀ and MDT₈₀ have been summarized in Table 6.7. The in vitro dissolution profiles of matrix with only Gelcarin GP-379 fits into zero order kinetics. The addition of MCC PH102 changes the release profile from zero order to Korsmeyer-Peppas type (M-101 to M-103). The drug release from these matrices is mainly by super case II transport mechanism ($n > 1$) as shown in Table 6.7.

Presence of HPMC gave synergistic effect on the viscosity of the Gelcarin GP-379 gel formed, and its effects can be seen on the release profiles of M-107 to M-109 (Figure 6.40). M-107 and M-108 batches maintained the linear drug release up to 11 h, but Gelcarin GP-379 : MCC PH301 at 80:30 ratio (M-109) produced extremely viscous hydrogel that allowed only about 10% glipizide to be released within 12 h. Since the sulfated groups containing carrageenans are anionic in nature, they have a tendency to interact with nonionic HPMC, resulting in an increase in the gel viscosity. Nerurkar et al has also reported similar observations

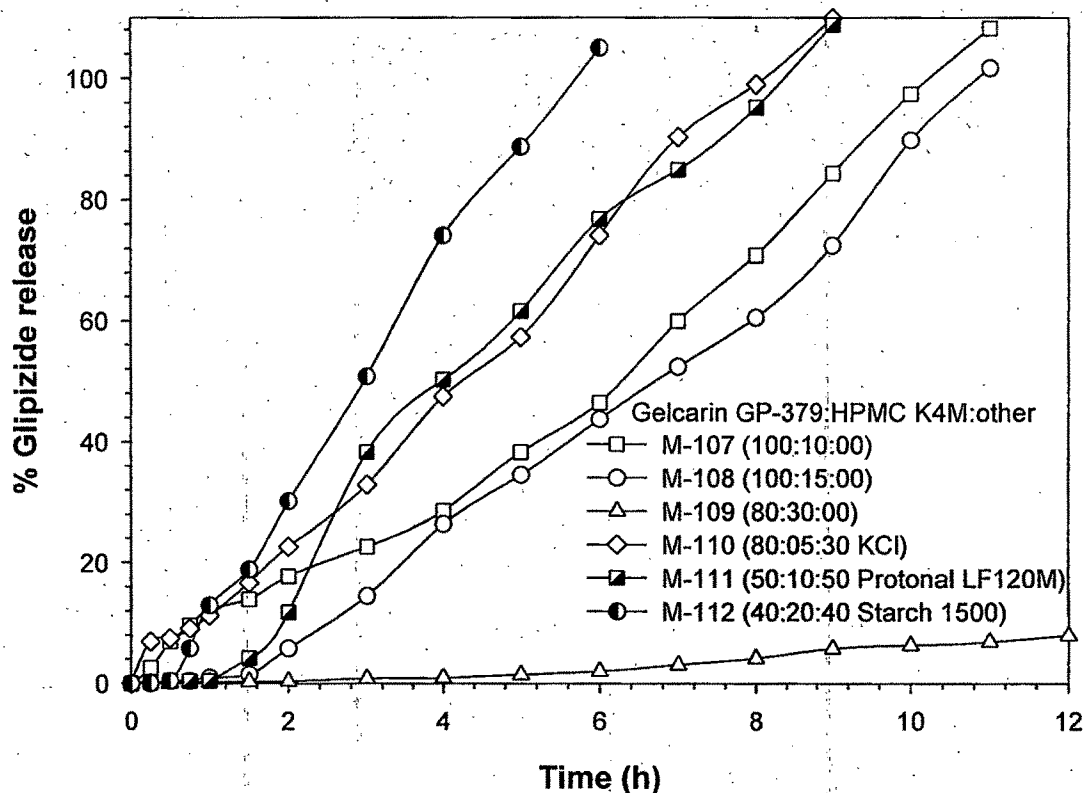


Figure 6.40. Effects of KCl, Protanal LF 120M and Starch 1500 on the glipizide release profiles from the Gelcarine GP-379 : HPMC K4M matrices.

(Nerurkar et al., 2005). Moreover, ionic interactions between anionic sodium carboxy methyl cellulose and HPMC as well as Carbopol and HPMC have also reported by other scientists (Rao et al., 2001; Samani et al., 2003). The ability of Gelcarin to form hydrogen bonds with the hydroxyl groups of HPMC led to a synergistic effect on gel viscosity that could better control the release of active drug by its resistance to erosion.

The effects of Protanal LF 120M, Starch 1500, and inorganic salt KCl on the Gelcarin GP-379: HPMC K4M matrices behavior was investigated and the results are depicted in Figure 6.40 (M-110 to M-112). All of them had a beneficial effect on the viscosity of the matrices and thereby contributed on the glipizide release. M-110 gave initial high release due to good aqueous solubility of KCl, while in M-111 batch Protanal LF 120M promoted the quick gelling of HPMC by ionic interaction. This led to rapid entry of water molecules into hydrated layer before glipizide started to diffuse out from the gel; hence, lag phase was observed during first hour, later on drug released continuously. Addition of starch (M-112) showed its disintegration effect as discussed earlier and gave comparatively rapid release (complete drug release within 6 h). Except M-109, best fit model for in vitro drug release of this group matrices was zero-order (Table 6.7).

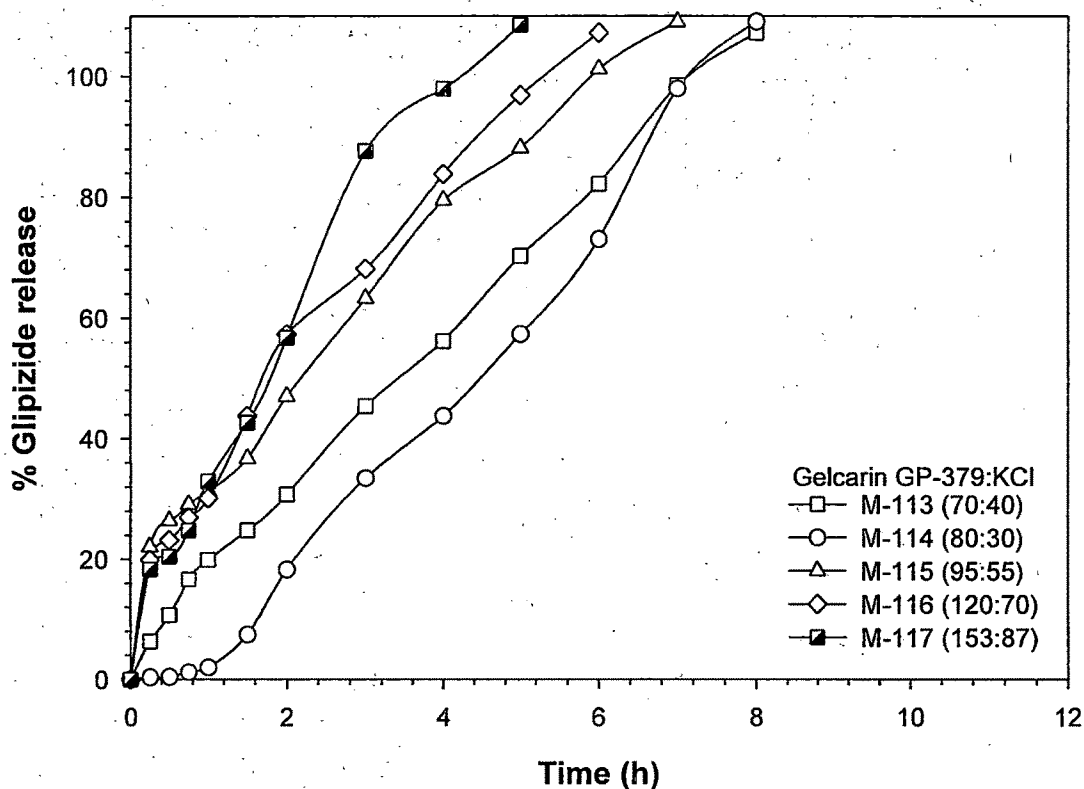


Figure 6.41. Effects of Gelcarin GP-379 : KCl ratio on the glipizide release profiles.

The complete glipizide release was observed within 5-8 h, at the different ratios of Gelcarin GP-379 : KCl studied as shown in Figure 6.41 (M-113 to M-117). Gelcarin-379 : KCl ratio at 70:40 (M-113), glipizide release was linear and followed zero-order kinetics (Table 6.7), but increase in gelcarin content produce more viscous gel and hence, increase the resistance for drug diffusion, which led to slow initial release. At fixed Gelcarin GP-379 : KCl ratio (same as M-133), as the total polymer blend was increased, glipizide release rate was also increased. This can be explained that on contact with dissolution media, as water start to penetrate into the matrix to form the gel, water dissolves KCl and creates channels from which drug can easily diffuse out. Moreover, apart from gelcarin GP-379 : KCl gelation, the dissolved KCl within the gel layer changes its viscosity, porosity, gel structure, tensile strength also. This later effect is more pronounced as compared to gelcarin GP-379 : KCl gelation, which resulted in higher drug release and hence, lower MDT_{50} and MDT_{80} values (M-115 to M-117) at higher matrix loading. Thus, in all cases, type and level of carrageenan present in the matrix is a main drug release governing factor. In vitro dissolution data of M-114 to M-117 fits into Higuchi or Korsmeyer-Peppas model. Depending on the n value, glipizide release from these matrices varies from super case II transport mechanism ($n > 1$) to anomalous type ($0.5 < n < 1$) as shown in Table 6.7.

Table 6.7. An overview of the comparative characteristics of different drug release kinetic models, MDT₅₀ and MDT₈₀ for batches M-98 to M-117.

Batch No	Release model											Best fit model		
	Zero-order k_0	f_0	First-Order K_1	t_1	Higuchi matrix K_H	f_H	Korsmeyer-Peppas n	K_k	t_k	Hixson-Crowell K_s	t_s			
M-98	No tablet													
M-99	No tablet													
M-100	No tablet													
M-101	12.50	0.98	-	-	29.14	0.88	2.27	1.31	0.97	-0.10	0.88	Zero order	2.59	3.29
M-102	13.61	0.97	-	-	29.66	0.87	1.91	2.74	0.97	-0.10	0.90	Peppas	2.47	3.05
M-103	15.82	0.98	-	-	31.88	0.86	1.83	4.61	0.98	-0.14	0.89	Peppas	2.17	2.81
M-104	415.73	1.00	-	-	207.87	1.00	-	-	-	-5.36	1.00	Zero order	0.06	0.10
M-105	437.42	1.00	-	-	218.71	1.00	-	-	-	-5.82	1.00	Zero order	0.06	0.09
M-106	407.06	1.00	-	-	203.53	1.00	-	-	-	-5.04	1.00	Zero order	0.07	0.10
M-107	9.12	0.99	-	-	23.83	0.90	0.90	10.39	0.99	-0.07	0.81	Zero order	3.16	4.78
M-108	8.09	0.98	-	-	20.62	0.86	-	-	-	-0.06	0.79	Zero order	3.99	5.59
M-109	0.56	0.95	-0.01	0.95	1.49	0.82	1.34	0.22	0.98	0.00	0.95	Peppas	-	-
M-110	12.24	1.00	-	-	28.98	0.92	0.88	14.20	0.98	-0.10	0.86	Zero order	2.17	3.38
M-111	11.98	0.99	-	-	27.84	0.88	2.18	1.45	0.97	-0.09	0.85	Zero order	2.51	3.51
M-112	17.30	0.99	-	-	32.33	0.88	2.38	3.50	0.94	-0.14	0.85	Zero order	1.73	2.44
M-113	13.96	1.00	-	-	31.60	0.95	0.81	19.16	1.00	-0.11	0.87	Zero order	1.54	2.70
M-114	12.94	0.98	-	-	27.79	0.85	1.90	2.77	0.99	-0.11	0.81	Peppas	2.55	3.64
M-115	14.18	0.85	-	-	35.89	0.99	0.49	36.12	0.98	-0.11	0.96	Matrix	0.78	1.65
M-116	20.34	0.94	-	-	40.81	0.99	0.58	36.14	0.98	-0.17	0.91	Matrix	0.72	1.46
M-117	25.05	0.97	-	-	44.87	0.96	0.68	36.09	0.98	-0.22	0.92	Peppas	0.74	1.31

6.6. Eudragit Matrices

Eudragit L100 and Eudragit S100 were included in the direct compression sustained release matrices to check their performance alone or in combination of other co-excipients and inorganic salts. Moreover, their role in the drug release mechanism was also studied by Kopcha model analysis, swelling study and SEM analysis.

6.6.1. IN VITRO DISSOLUTION & RELEASE KINETIC STUDIES

Eudragit L100 is a methacrylic acid-methacrylate copolymer with a free carboxyl to ester groups of approximately 1:1. While Eudragit S100 is an anionic copolymer of methacrylic acid and methyl methacrylate at a ratio 1:2 between the free carboxyl and the methyl ester groups. This difference makes Eudragit L100 hydrophilic and Eudragit S100 hydrophobic. The difference in the drug release profiles of these polymer containing matrices is based on this carboxyl :ester group ratio.

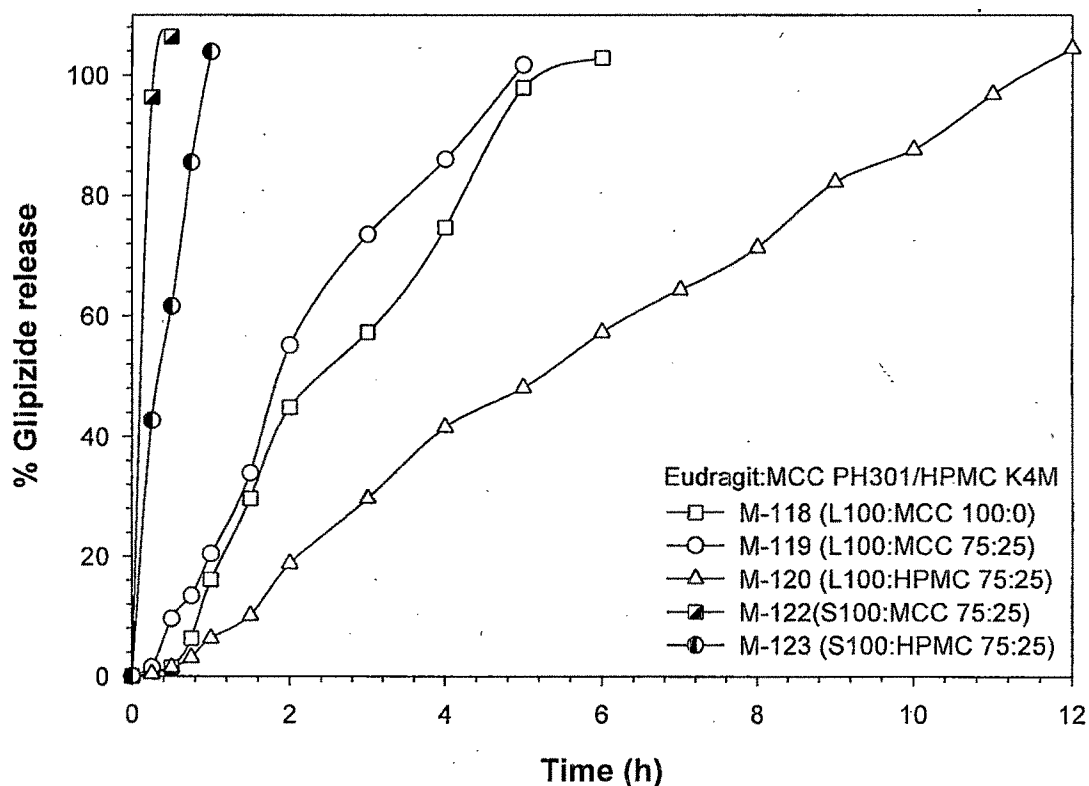


Figure 6.42. Effects of eudragit types and HPMC K4M or MCC PH 301 on the glipizide release profiles.

In vitro dissolution profiles for the matrices containing both type of eudragit alone and with MCC PH301 and HPMC K4M are depicted in Figure 6.42 (M-118 to M-123). Eudragit L100 due to its hydrophilic nature allows dissolution media penetration into the matrix to cause swelling and prepare hydrogel. Only Eudragit L100 matrix can sustain the drug release up to 5.5 h (M-118). Eudragit L100 also contributes significantly in drug release by polymer particle erosion, which is characterized by erosion of partially swollen polymer particles. Unlike the classical eroding tablets, which dissolve completely during the dissolution test, a turbid solution or suspension is formed during the drug release study of tablets showing polymer particle erosion. Lindner et al. and Zuleger et al have also noticed this special type of polymer particle erosion controlled drug delivery with Tylose, a methyl hydroxyl ethyl cellulose (Lindner and Lippold, 1995; Zuleger and Lippold, 2001). Addition of MCC PH301 (M-119) causes slight increase in the overall drug release rate and results in lower MDT_{50} and MDT_{80} as compared to that of only Eudragit L100 matrices. The increased release rate is due to swellable insoluble particles of MCC which promote disintegration. The Eudragit L100 : HPMC K4M matrix (M-120) can successfully sustain the drug release over 12 h (Figure 6.42). HPMC and eudragit both are hydrophilic in nature and absorbs aqueous media readily, causes swelling of the polymer and controls the drug release linearly by forming hydrogel. In contrast to HPMC-MCC matrices (drug release is combination of diffusion and erosion), this matrices releases drug solely by eudragit polymer particle erosion. Visual observation of the dissolution process showed the insoluble particles suspended in the dissolution media. The kinetic constants for different models with the regression coefficients are summarized in Table 6.8 and the best fit model for the release profile for these three batches (M-118 to M-120, Table 6.8) was zero order. Batch M-120 was found to be optimized one as it passes dissolution constraints at all time points and studied further for characterization of swelling behavior. Eudragit S100 has poor compressibility (I_c value below 4) and the batch containing this polymer alone (M-121) was difficult to compress, resulted in tablets with hardness of less than 3 kg/cm^2 at maximum compression force (hence no dissolution data for this batch). The presence of MCC PH301 or HPMC K4M improved the powder mixture characteristics and matrices with acceptable hardness could be produced. Both the batches (M-122 and M-123) completed the dissolution study within 1 h and not satisfied their ability to sustain the drug release as shown in Figure 6.42. Similar findings have been reported by Colo et al. (Colo et al., 2002). Further the eudragit L100 was combined with other excipients such as lactose, Starch 1500, Protonal LAF 120M and chitosan to investigate whether any combination of these polymer-excipient can control the drug release or not.

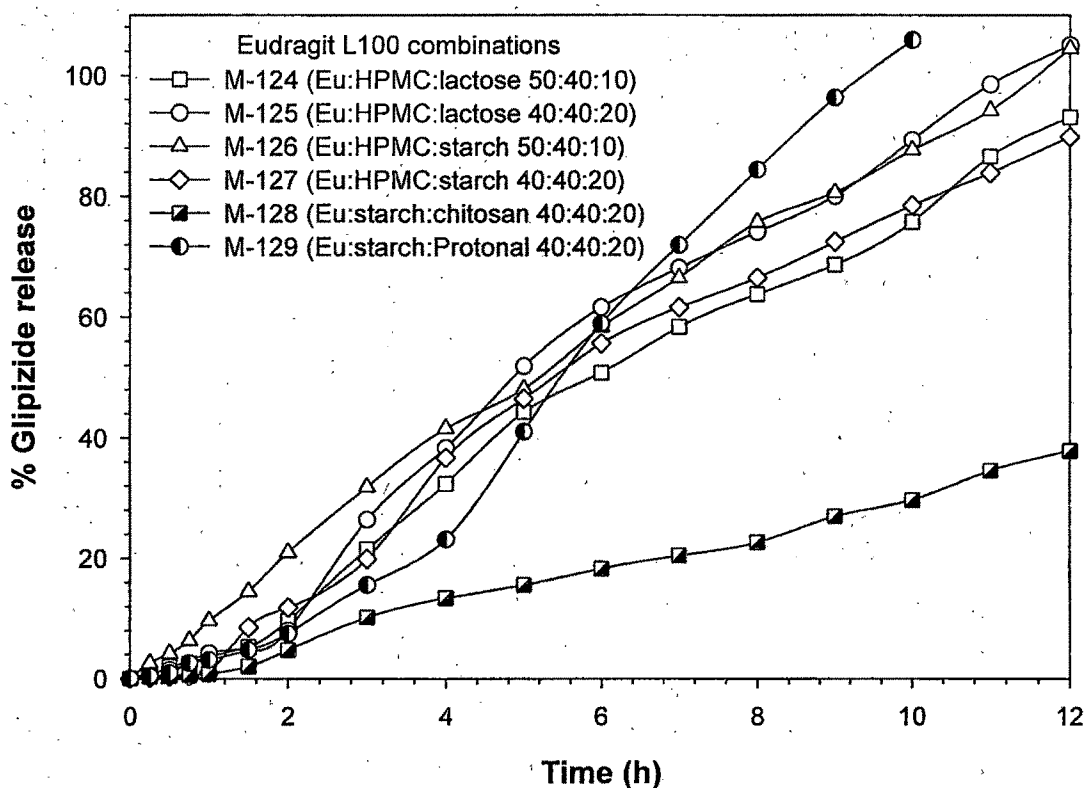


Figure 6.43. Effects of different polymeric combinations with eudragit L100 on the glipizide release profiles.

Different Eudragit L100 combinations were compressed into the matrices and their cumulative dissolution profiles are shown in Figure 6.43 (M-124 to M-129). Inclusion of water soluble lactose, promoted the entry of dissolution media into matrix by forming channels and thus with increase in lactose caused increase in drug release by zero order (M-124 and M-125, Table 6.8). As can be seen from the release patterns, the addition of the starch (M-126) raised the initial glipizide release and fitted the complete release profile within constraints, hence selected as optimized. It follows Korsmeyer-Peppas release kinetics with non-Fickian (anomalous) release mechanism as shown in Table 6.8. The eudragit, carboxylic group containing polymer, reacted with cationic chitosan (M-128) to provide highly viscous matrix structure, which hinders polymer particle erosion of the eudragit molecules and ultimately released hardly about 40% of the active drug within 12 h. In contrast to this, when chitosan was replaced by negatively charged Protional LF 120M (M-129), complete drug was released within 10 h. This can be reasoned that repulsion of the like charges of carboxylic groups of eudragit and alginate, which moves apart each other, generally known as swelling. Therefore, because of rapid hydration, more dissolution media enters the matrix to cause over-hydration and promoted eudragit particle erosion, and thereby increased drug release.

Table 6.8. An overview of the comparative characteristics of different drug release kinetic models, best fit model, MDT₅₀ and MDT₈₀ for batches M-118 to M-129.

Batch No	Release model										Best fit model	MDT ₅₀	MDT ₈₀	
	Zero-order	First-Order	Higuchi matrix	Korsmeyer-Peppas	Hixson-Crowell									
K_0	f_0	K_1	f_1	K_H	f_H	η	K_k	f_k	K_s	f_s				
M-118	18.42	0.99	-	-	35.10	0.91	1.58	9.38	0.97	-0.15	0.90	Zero order	1.33	2.11
M-119	21.86	0.99	-	-	38.12	0.92	1.32	16.86	0.97	-0.17	0.89	Zero order	1.09	1.64
M-120	8.97	1.00	-	-	24.83	0.93	1.38	4.60	0.99	-0.06	0.86	Zero order	2.65	4.31
M-121	No tablet													
M-122	263.32	0.92	-	-	173.98	0.99	0.27	140.64	1.00	-3.01	1.00	Peppas	0.06	0.10
M-123	111.76	0.98	-	-	97.16	0.99	0.65	101.94	1.00	-1.00	0.88	Peppas	0.15	0.29
M-124	7.84	0.99	-0.16	0.94	21.52	0.92	1.38	3.73	0.99	-0.04	0.97	Zero order	3.28	5.13
M-125	9.06	0.99	-	-	24.91	0.92	1.36	4.33	0.99	-0.07	0.87	Zero order	2.96	4.37
M-126	9.03	1.00	-	-	25.17	0.95	0.99	9.52	1.00	-0.06	0.86	Peppas	2.46	4.11
M-127	7.98	0.99	-0.15	0.97	22.01	0.92	1.86	1.56	0.97	-0.04	0.99	Zero order	3.14	4.85
M-128	3.03	0.99	-0.04	0.99	8.31	0.91	1.39	1.37	0.98	-0.01	0.99	Zero order	-	-
M-129	10.13	0.97	-	-	24.42	0.85	1.57	3.05	1.00	-0.08	0.80	Peppas	3.66	4.72

6.6.2. CHARACTERIZATION OF OPTIMIZED FORMULATIONS

In the group of all eudragit matrices (M-118 to M-129), batches M-120 (Eudragit L100 : HPMC K4M at 75:25) and M-126 (Eudragit L100 : HPMC K4M : Starch 1500 at 50:40:10) were the optimized batches and were studied further for thorough understanding of drug release kinetics by Kopcha model, swelling study, and SEM analysis.

6.6.2.1. Release Mechanism by Kopcha Model

Both the matrix tablets (M-120 and M-126) showed similar drug release mechanism according to Kopcha Model Figure 6.44). It showed that there was a predominance of erosion through out the release profile. Initially up to 3 h, the erosion term increased as Eudragit L100 swells continuously. However, after this period, HPMC forms hydrogel and slow down the erosion. Consequently, marginal rise in diffusion term was also observed in the terminal phase due to diffusion through HPMC hydrogel. However, the magnitude of diffusion was far less than the erosion. This observation further supports the polymer particle erosion theory of Eudragit L100 matrices.

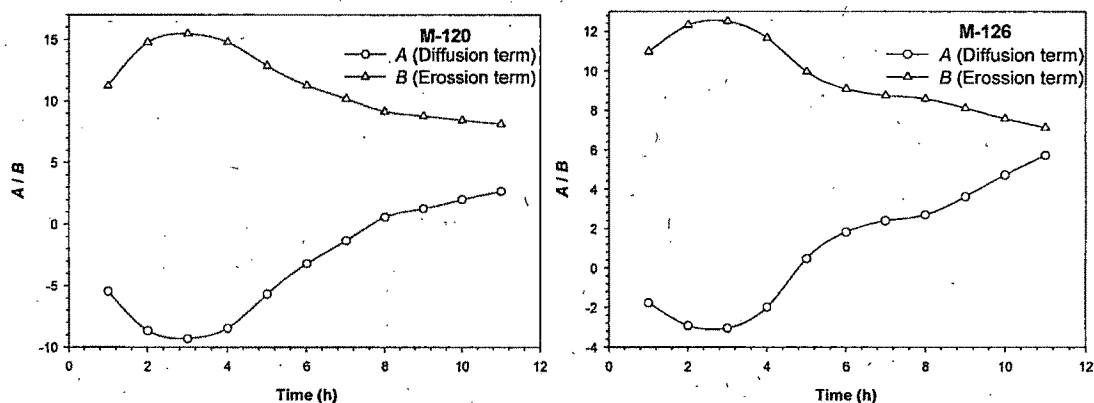


Figure 6.44. Kopcha model parameters A (diffusion term) and B (erosion term) as a function of time for M-120 and M-126 formulations.

6.6.2.2. Swelling Study

Results of water uptake, axial and radial expansion for M-120 and M-126 are depicted in Figure 6.45 and Figure 6.46, respectively. Water uptake and axial as well as radial expansion for M-120 was highest at 3 h. All three parameters declined continuously after 3 h. These observations are in accordance to the Kopcha model results. The HPMC hydrogel formed in this case was not

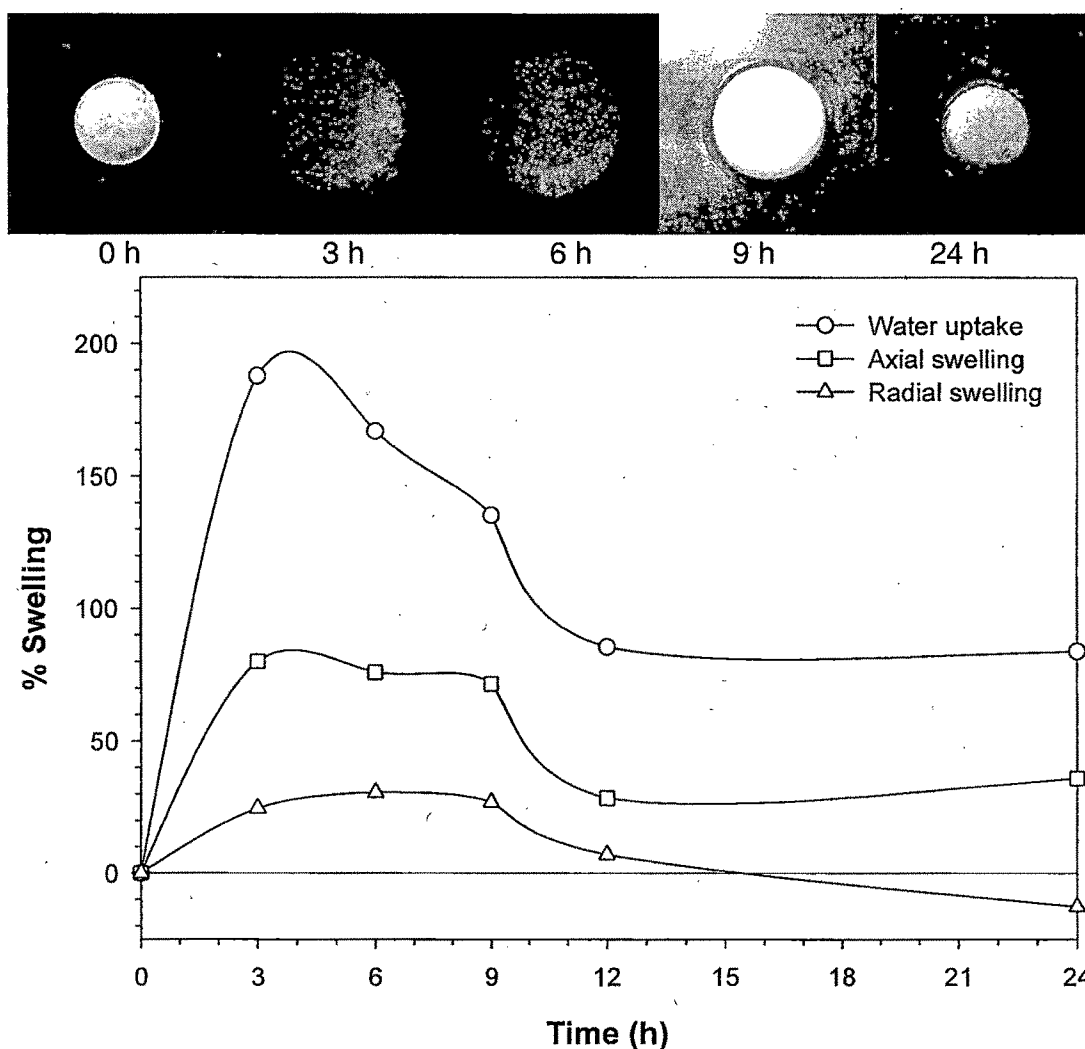


Figure 6.45. Percent water uptake, axial, and radial swelling results for M-120 formulation (Eudragit L100 : HPMC K4M at 75:25).

sufficiently elastic to hold the eroded particles within the hydrogel. Hence, the eroded polymer particles were suspended in the dissolution medium during in vitro dissolution study. This phenomenon was responsible for gradual reduction in matrix size as can be seen in the photographs shown at the top of Figure 6.45.

For the matrix tablet M-126 containing Eudragit L100 along with HPMC K4M and Starch 1500, comparatively more elastic hydrogel was formed because of the synergistic interaction of starch and HPMC (discussed earlier). However, this hydrogel is not strong enough to restrict the erosion completely but it reduces the magnitude of erosion slightly. The outer most layer of this hydrogel has a capacity to imbibe large amount of water and can suspend the eroded polymer particles before released into dissolution medium (the last photograph at the top of Figure 6.46). Erosion phenomena can be predicted from the decrease in radial swelling. The continues rise in axial swelling and water uptake can be explained

by more elastic hydrogel formation at the surface. Near to end of release profile, diffusion contribution of drug release increased and become almost equal to erosion due to the hydrogel formation.

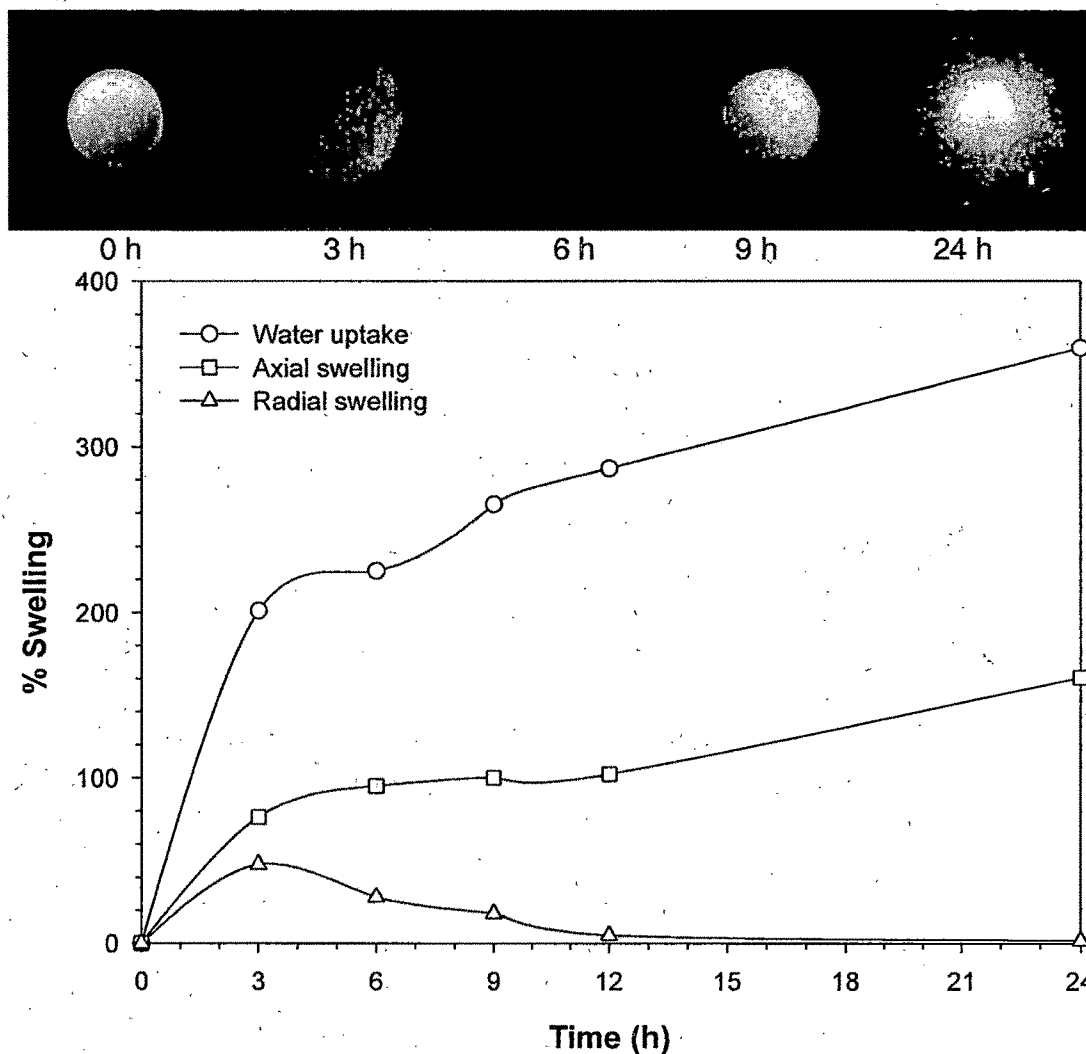


Figure 6.46. Percent water uptake, axial, and radial swelling results for M-126 formulation (Eudragit L100 : HPMC K4M : Starch 1500 at 50:40:10).

6.6.2.3. SEM Study

Surface morphology of M-120 at different magnification after 12 h dissolution is shown in Figure 6.47. From the above discussion, it is evident that the release was due to erosion of Eudragit matrix and eroded (rough) surfaces can be seen clearly in the micrographs.

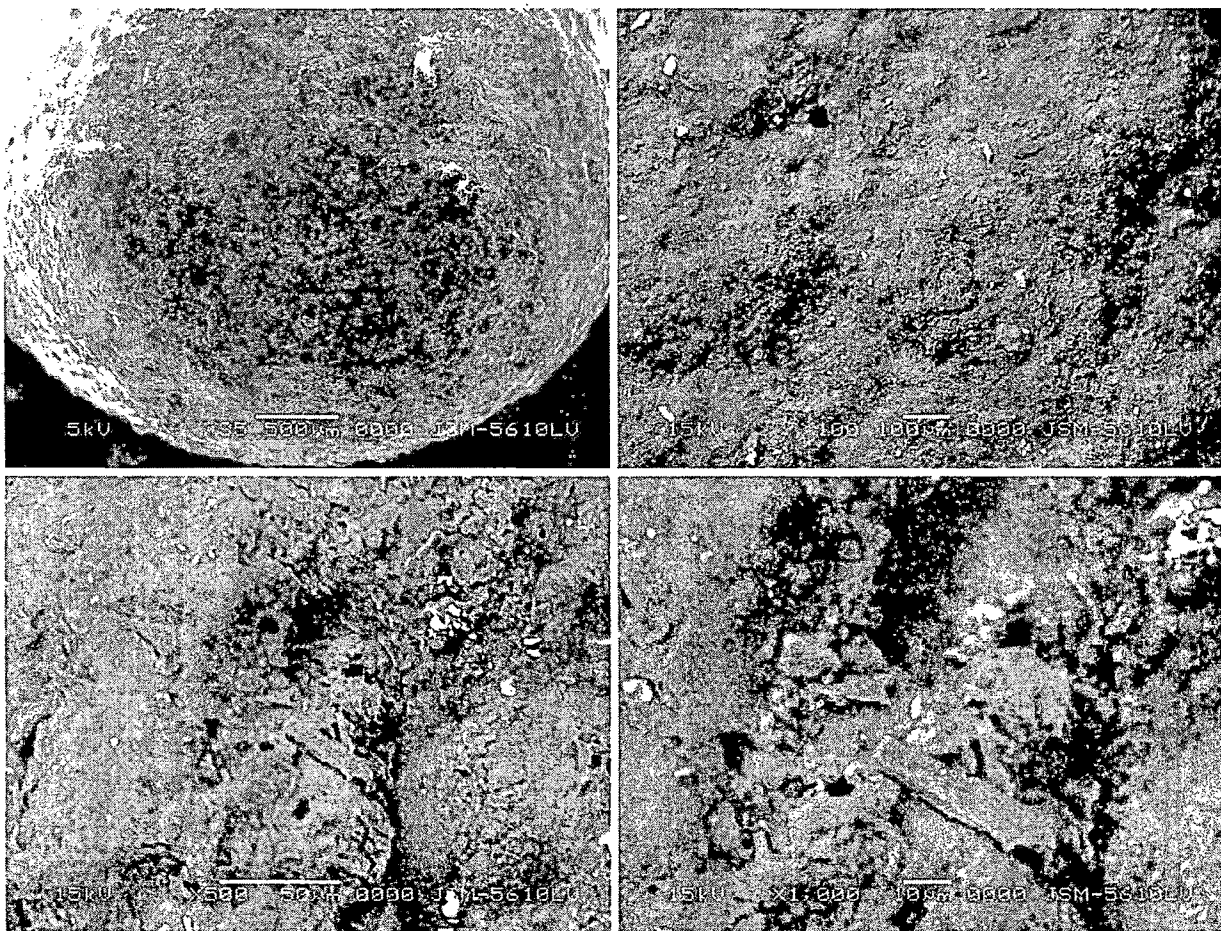


Figure 6.47. Scanning electron micrograph of M-120 after 12 h dissolution at different magnifications.

Scanning electron micrographs for surface characteristics of M-126 at different magnification after 12 h dissolution are displayed in Figure 6.48. As can be seen from micrographs, the surfaces of M-126 batch was smoother than M-120 batch. As discussed earlier, formation of more elastic hydrogel and almost equal magnitude of erosion and diffusion at the end of 12 h dissolution, might be responsible for slightly smooth surfaces.

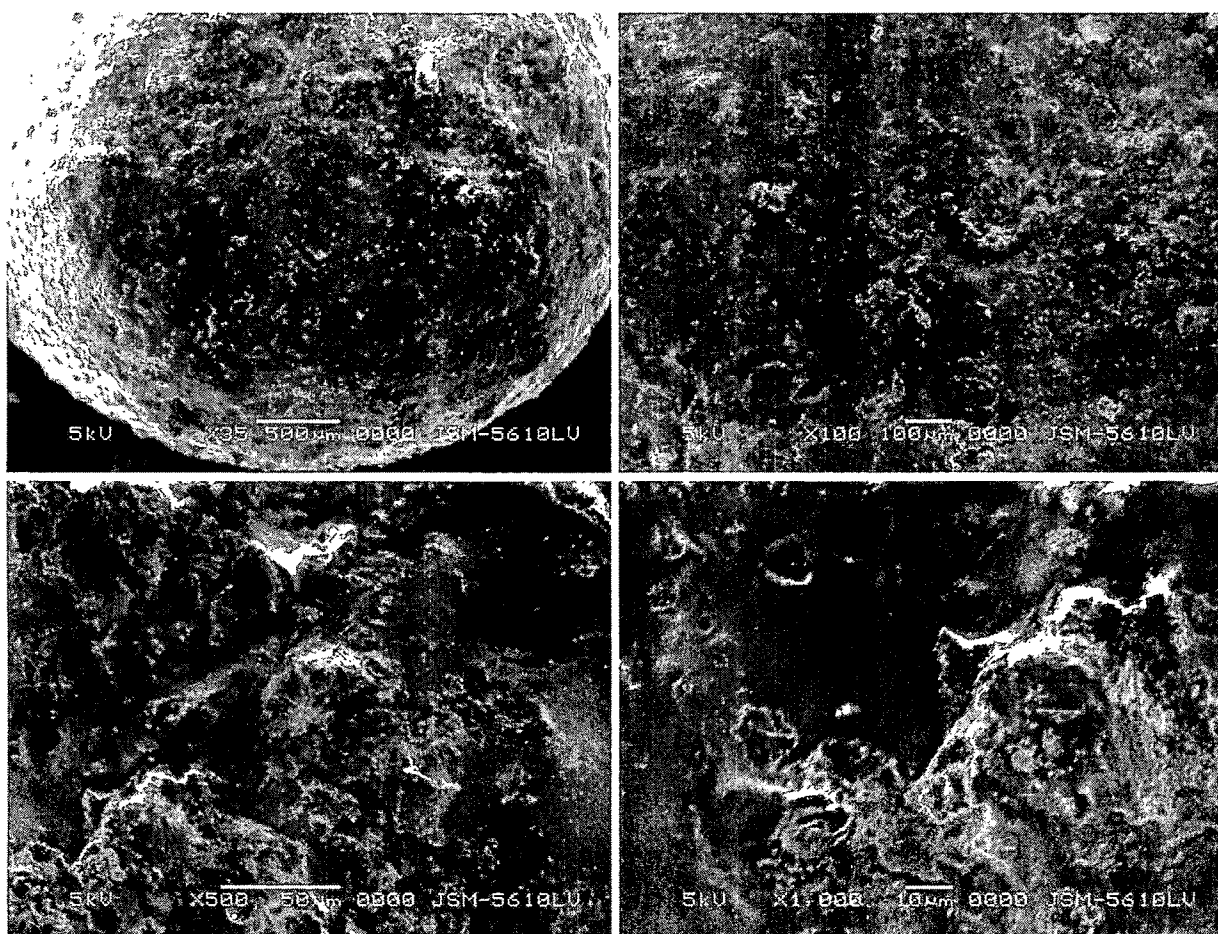


Figure 6.48. Scanning electron micrograph of M-126 after 12 h dissolution at different magnifications.

6.7. Sodium Alginate Matrices

Generally, in the presence of aqueous medium, alginate molecules hydrate. The dissolved molecules are not completely flexible, rotation around the glycosidic linkages in the G-block regions is somewhat hindered, resulting in a stiffening of the chain. In addition, this solution of stiff macromolecules is highly viscous because of the physical gel formed by hydrogen bonding (Handbook of Pharmaceutical Excipients, 1986).

Batch M-130 was prepared with the sodium alginate : Carbopol 931P at 50:50 ratio, but due to the poor compressibility of the sodium alginate powder (S.D. Fine Chem), compression of tablet powder mixture yielded no tablets. Matrices of sodium alginate (S. D. Fine chem.) and disodium hydrogen phosphate (DHP) with carbopol and HPMC K4M were prepared to check whether any combination can synergistically increase the viscosity of the gel upon hydration or not. The release profiles are shown in the Figure 6.49 (M-131 to M-135). It is obvious from the release data for M-131 that the pattern of release profile is similar to that of M-83 (Carbopol 931P:MCC PH301). It indicated the Carbopol 931P played a significant role in controlling the glipizide release may be due to its higher proportion as compared to sodium alginate. When sodium alginate content is increased with inclusion of DHP (M-132), all the glipizide was released within 4 h. This can be attributed to the good solubility of DHP, which easily dissolves in aqueous medium and leaves the matrix by forming channels through which glipizide can easily diffuse out. Moreover, sodium alginate changes the structural properties of negatively charged carbopol gel by providing free carboxylic groups, that causes repulsion between both negative charges and resulted in more swelling of gel. This loose gel structure has tendency to get dissolve/erode rapidly in continuously rotating dissolution medium, and gave complete drug release within 4 h.

Matrix system containing sodium alginate : HPMC K4M at 75:25 ratio (M-133), resulted in complete drug release before 2 h, while reverse ratio (M-134) sustained the glipizide release up to 6 h. This indicated that the presence of sodium alginate significantly changes the hydrogel structure, viscosity, and tensile strength of the HPMC K4M. Alginate swelling causes rapid hydration of the matrix system, increases the porosity of the matrix due to excess water penetration and crosses the disentanglement concentration of the polymer, above which the hydrogel starts to erode easily and results in higher drug release rate. With the same HPMC K4M level, the drug release for M-135 was extended up to 3 h as compared to that of M-133. This may be the result of gelation of alginate in the presence of cations to produce more viscous gel, which hinders

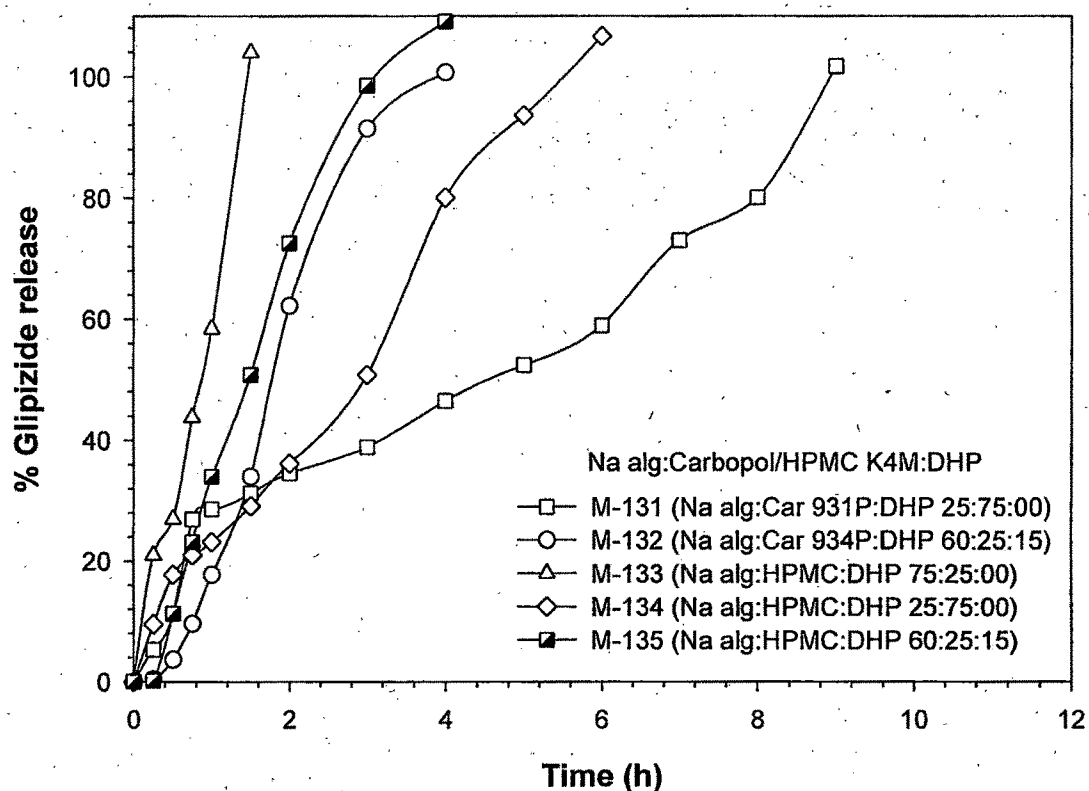


Figure 6.49. Effects of sodium alginate : carbopol/HPMC K4M : DHP ratio on the glipizide release profiles.

the drug release. Except from batch M-131, all other bathes from M-132-to M-135 follows zero order release.

The Protonal LF 120M was combined with HPMC K4M to study the ability of the matrix system to sustain the drug release. As shown in Figure 6.50 (M-136 to M-138), the presence of HPMC K4M quantity showed no significant difference in their release profiles. This ensures the dominant role of Protonal LF 120M on the glipizide release. All three bathes followed zero order release kinetics (Table 6.9). Alginates contain various proportions of mannuronate and guluronate monomers. To form a gel, alginates must contain a sufficient level of guluronate monomers in a block to react with divalent calcium cation, Ca^{2+} . Regions of the guluronate monomers in one alginate molecule can be linked to a similar regions in another alginate molecule by means of calcium or other cations. The divalent calcium cation, Ca^{2+} , fits into the guluronate block structure. This binds the alginate polymers together by forming junction zones, resulting in gelation of the solution. Therefore, to add to the understanding of the formulation possibilities, a system containing a poly anionic polymer (Protonal LF 120 M) and cationic polymer or inorganic ionic salt (chitosan, calcium gluconate, or dibasic calcium phosphate (DCP)) mixtures have been assessed in terms of their ability to produce matrix tablets and their drug release performance is depicted in Figure 6.51 (M-139 to

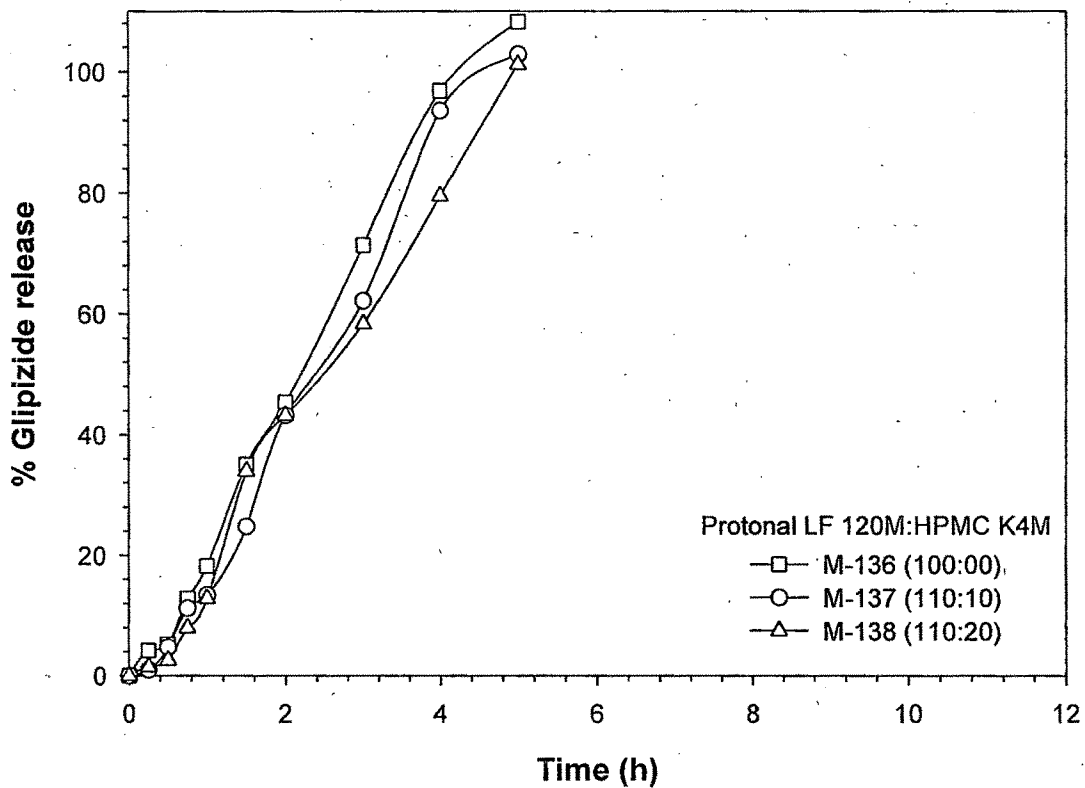


Figure 6.50. Effects of the Protanal LF 120M : HPMC K4M ratio on the glipizide release profiles.

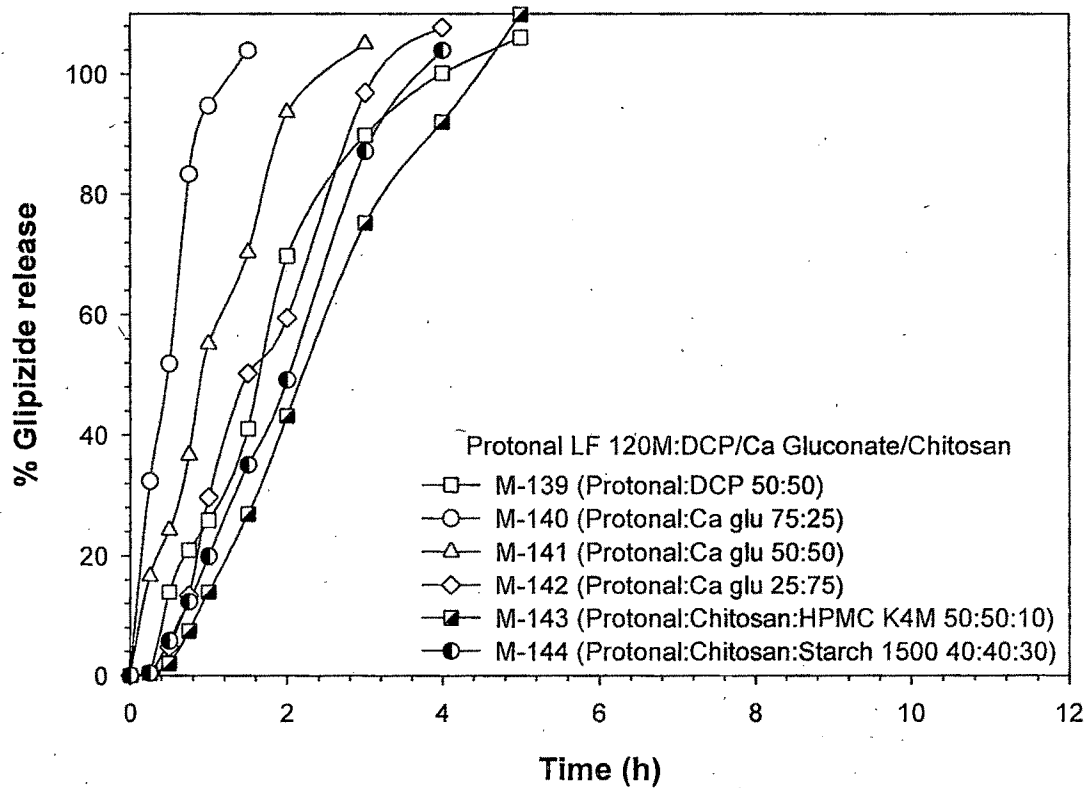


Figure 6.51. Effects of Protanal LF 120M : DCP/calcium gluconate/chitosan ratio on the glipizide release profiles.

Table 6.9. An overview of the comparative characteristics of different drug release kinetic models, best fit model, MDT50 and MDT80 for batches M-130 to M-144.

Batch No	Release model										Best fit model	MDT ₅₀	MDT ₈₀	
	Zero-order	First-Order	Higuchi matrix	Korsmeyer-Peppas	Hixson-Crowell									
	K_0	t_0	K_1	t_1	K_H	t_H	n	K_k	t_k	K_s	t_s			
M-130														
M-131	10.96	0.94	-	-	27.01	0.96	0.67	20.45	0.96	-0.08	0.79	Matrix	1.51	3.34
M-132	26.55	0.98	-	-	39.86	0.86	1.99	11.92	0.97	-0.22	0.91	Zero order	1.17	1.52
M-133	64.44	0.99	-	-	63.28	0.90	0.89	61.31	0.97	-0.60	0.81	Zero order	0.41	0.66
M-134	18.56	0.99	-	-	36.01	0.94	0.75	25.41	0.99	-0.15	0.87	Zero order	1.25	2.08
M-135	30.85	0.99	-	-	47.80	0.92	-	-	-	-0.29	0.92	Zero order	0.82	1.20
M-136	22.68	0.99	-	-	38.99	0.90	1.20	18.09	0.99	-0.20	0.89	Zero order	1.18	1.77
M-137	21.05	0.99	-	-	35.74	0.88	1.52	12.12	0.99	-0.18	0.88	Zero order	1.38	2.00
M-138	19.91	0.99	-	-	33.98	0.89	1.50	11.59	0.98	-0.16	0.85	Zero order	1.32	2.06
M-139	24.95	0.97	-	-	44.23	0.93	1.58	16.48	0.90	-0.24	0.95	Zero order	0.94	1.32
M-140	84.16	0.92	-	-	86.76	0.98	0.70	88.41	0.98	-0.75	0.96	Matrix	0.21	0.36
M-141	59.89	0.97	-	-	69.89	0.98	0.74	66.55	1.00	-0.52	0.92	Peppas	0.48	0.79
M-142	28.90	0.98	-	-	44.01	0.89	-	-	-	-0.26	0.91	Zero order	0.95	1.38
M-143	22.20	0.99	-	-	37.56	0.87	1.88	8.88	0.98	-0.19	0.87	Zero order	1.37	1.86
M-144	25.97	0.99	-	-	38.93	0.87	1.88	13.08	0.96	-0.23	0.87	Zero order	1.16	1.63

M-144). As seen from the figure, it is clear that both the calcium salts and chitosan caused gelation of alginate and prolonged the glipizide release depending on the alginate to salt/chitosan ratio used. However, none of the system could extend the drug release more than 5 h, it can be expected that the increase in polymer loading of the matrix can sustain the drug release further. For, M-140 to M-142, as the calcium gluconate concentration increases, the release profile changes from matrix to Korsmeyer-Peppas to zero order release kinetics. Preformulation batches with chitosan (M-143 and M-144) followed zero order release pattern Table 6.9.

6.8. Stability Studies

All the optimized batches were subjected to accelerated stability study ($40 \pm 2^\circ\text{C} / 75 \pm 5\% \text{RH}$) according to ICH guidelines. 6 month accelerated data for the optimized formulations showed negligible change over time for the parameters like appearance, weight variation, thickness, hardness, and drug content. The similarity factor (f_2) was calculated by a comparison of the dissolution profile at

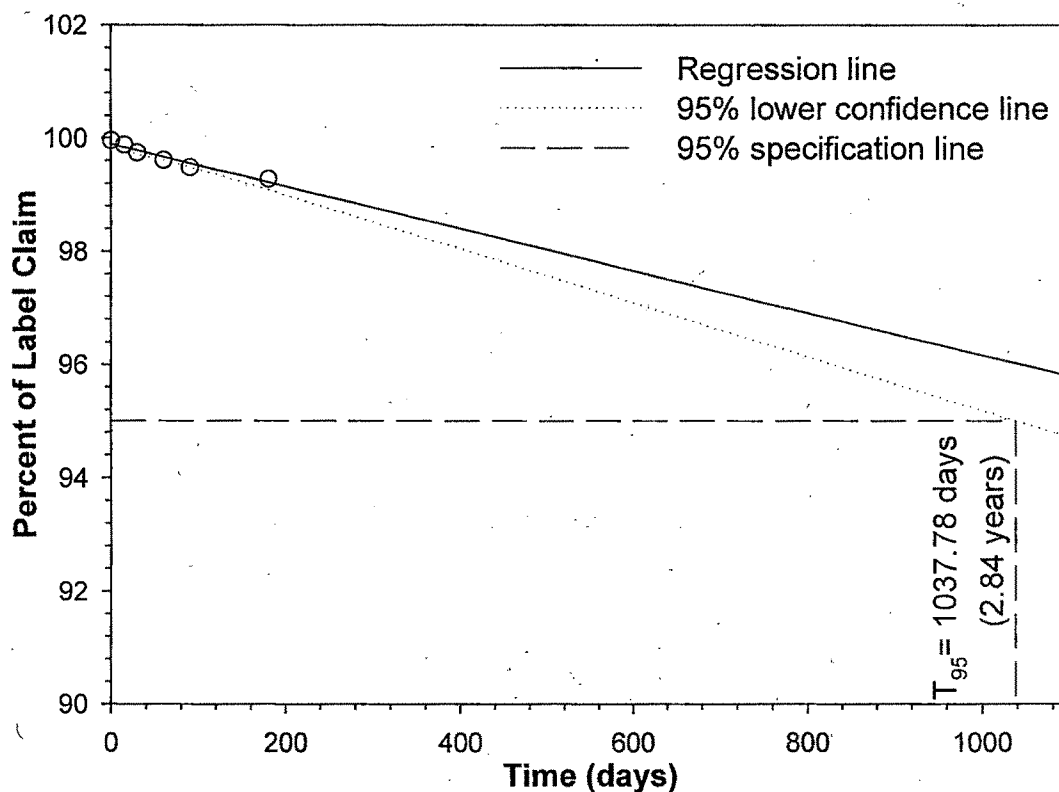


Figure 6.52. Extrapolation of accelerated stability study for determination of shelf-life for M-3 formulation.

each time points with the control at the initial condition. The f_2 factors obtained ranged from 84 to 96, with a 2 to 7% average difference, and the formulations were found to be stable. Evaluation of shelf-life was carried out as per the ICH Q1E Step4 (Evaluation of Stability Data) guidelines for the drug substances intended for room temperature storage. Long-term and accelerated stability data showed little change over time, so the shelf-life up to twice the length of available long-term data can be proposed. Extrapolation of the shelf-life beyond the length of available long-term data can be proposed. For this, an approach for analyzing the data on a quantitative attribute that is expected to change with time is to determine the time at which the 95% one-sided confidence limit for the mean curve intersects the acceptance criterion (not more than 5% change in assay from its initial value) can be accepted. The accelerated stability data of the developed formulations were linearly extrapolated (zero-order kinetics) to calculate the shelf-life. Shelf-life for M-3, M-25, M-70, M-75, M-84, M-120, and M-126 were found to be 2.84, 2.91, 2.69, 2.78, 2.59, 2.97, and 3.12 years, respectively. The linear extrapolation of accelerated stability data for M-3 formulation is shown in Figure 6.52. »

6.9. References

- AHMED, H. and SHAH, N., Formulation of low dose medicines-theory and practice. *American Pharmaceutical Review* 3 (3).
- ALDERMAN, D. A., **1984**. Review of cellulose ethers in hydrophilic matrices for oral controlled-release formulations. *International Journal of Pharmaceutical Technology* 5 (1), 1-9.
- BYRN, S. R., XU, W. and NEWMAN, A. W., **2001**. Chemical reactivity in solid-state pharmaceuticals: formulation implications. *Adv. Drug. Deliv. Rev.* 48, 115-136.
- CALLAHAN, J. C., CLEARY, G. W. and ELEFANT, M., **1982**. Equilibrium moisture content of pharmaceutical excipients. *Drug Dev. Ind. Pharm.* 8 (3), 355-369.
- CAMERON, C. G. and MCGINITY, J. W., **1987**. Controlled-release theophyllin through line tablets containing acrylic resins III: Influence of filler excipients. *Drug Dev. Ind. Pharm.* 13 (2), 303-318.
- CHAMBIN, O., CHAMPION, D., DEBRAY, C., ROCHAT-GONTHIER, M. H., MESTE, M. L. and POURCELOT, Y., **2004**. Effects of different cellulose derivatives on drug release mechanism studied at a preformulation stage. *J. Controll. Rel.* 95, 101-108.
- CHILAMKURTI, R. N., RHODES, C. T. and SCHWARTZ, J. B., **1982**. Some studies on compression properties of tablet matrices using a computerized instrumented press. *Drug Dev. Ind. Pharm.* 8, 63-86.
- CHILAMKURTI, R. N., SCHWARTZ, J. B. and RHODES, C. T., **1983**. Effect of addition of soluble and insoluble drugs on the disintegration of microcrystalline cellulose and

- dicalcium phosphate dihydrate. *Pharmaceutica Acta Helvetica* 58 (9-10), 251-255.
- COLO, G. D., FALCHI, S. and ZAMBITO, Y., **2002**. In vitro evaluation of a system for pH-controlled peroral delivery of metformin. *J. Controlled Rel.* 80, 119-128.
- COLOMBO, P., **1993**. Swelling-controlled release in hydrogel matrices for oral route. *Adv. Drug. Deliv. Rev.* 11, 37-57.
- COLOMBO, P., BETTINI, R. and PEPPAS, N. A., **1999**. Observation of swelling process and diffusion front position during swelling in hydroxypropyl methyl cellulose (HPMC) matrices containing a soluble drug. *J. Controll. Rel.* 61, 83-91.
- CROWLEY, M. M., SCHROEDER, B., FREDERSDORF, A., OBARA, S., TALARICO, M., KUCERA, S. and MCGINITY, J. W., **2004**. Physicochemical properties and mechanism of drug release from ethyl cellulose matrix tablets prepared by direct compression and hot-melt extrusion. *Int. J. Pharm.* 269, 509-522.
- CUNNINGHAM, C. R., **2000**. Starch contrasts - Knowing the differences among pregelatinized starches will produce desired formulation release rates, Starch contrasts - Knowing the differences among pregelatinized starches will produce desired formulation release rates, Excipient Focus, Colorcon Asia Pacific Pte Ltd (http://ebro.colorcon.com/pfq_starch.pdf), Singapor.
- DAHL, T. C., CALDERWOOD, T. and BORMETH, A., **1990**. Influence of physicochemical properties of hydroxypropyl methylcellulose on naproxen release from sustained release matrix tablets. *J. Controlled Rel.* 14, 1-10.
- DHOPEHWARKAR, V. and ZATZ, J. L., **1993**. Evaluation of xanthan gum in the preparation of sustained release matrix tablets. *Drug Dev. Ind. Pharm.* 19, 999-1017.
- ENÉZIAN, G. M., **1972**. Direct compression of tablets using microcrystalline cellulose [in French]. *Pharm. Acta Helv.* 47, 321-363.
- FAN, L. T. and SING, S. K., **1989**. *Controlled Release: A Quantitative Treatment*, Springer, Berlin.
- FORD, J. L., RUBINSTEIN, M. H. and MCCAUL, F., **1987a**. Importance of drug type, tablet shape and added diluents on drug release kinetics from HPMC tablets. *Int. J. Pharm.* 40 (1), 223-234.
- FORD, J. L., RUBINSTEIN, M. H., MCCAUL, F., HOGAN, J. E. and EDGAR, P. J., **1987b**. Importance of drug type, tablet shape and added diluents on drug release kinetics from hydroxypropylmethylcellulose matrix tablets. *Int. J. Pharm.* 40, 223-234.
- GÜNGÖR, S., YILDIZ, A., ÖZSOY, Y., CEVHER, E. and ARAMAN, A., **2003**. Investigations on mefenamic acid sustained release tablets with water-insoluble gel. *Il Farmaco* 58, 397-401.
- Handbook of Pharmaceutical Excipients, **1986**. American Pharmaceutical Association / Pharmaceutical Society of Great Britain, Washington DC, pp. 41-42.
- HERMAN, J. and REMON, J. P., **1989**. Modified starches as hydrophilic matrices for controlled oral delivery. II. In vitro drug release evaluation of thermally modified starches. *Int. J. Pharm.* 56, 65-70.

- HIGUCHI, T., **1963**. Mechanism of sustained-action medication. Theoretical analysis of rate of release of solid drugs dispersed in solid matrices. *J. Pharm. Sci.* 52, 1145-1149.
- HOGAN, J. E., **1989**. Hydroxypropylmethylcellulose sustained release technology. *Drug Dev. Ind. Pharm.* 15, 975-999.
- HOSMANI, A. H., **2006**. Carbopol and its pharmaceutical significance: A review, Carbopol and its pharmaceutical significance: A review.
- KATIKANENI, P., UPADRASHTA, S. M., NEAU, S. H. and MITRA, A. K., **1995**. Ethyl cellulose matrix controlled-release tablets of a water-soluble drug. *Int. J. Pharm.* 123, 119-125.
- KHAN, G. M. and ZHU, J. B., **1998**. Ibuprofen release kinetics from controlled-release tablets granulated with aqueous polymeric dispersion of ethylcellulose II: Influence of several parameters and coexcipients. *J. Controlled Rel.* 56, 127-134.
- KLEINEBUDDE, P., **1997**. The crystallite-gel-model for microcrystalline cellulose in wet-granulation, extrusion, and spheronization. *Pharm. Res.* 14, 804-809.
- KLINGER, G. H., GHALLI, E. S., PORTER, S. C. and SCHWARTZ, J. B., **1990**. Formulation of controlled release matrices by granulation with a polymer dispersion. *Drug Dev. Ind. Pharm.* 16 (9), 1473-1490.
- KOPCHA, M., LORDI, N. and TOJO, K. J., **1991**. Evaluation of release from selected thermosoftening vehicles. *J. Pharm. Pharmacol.* 43, 382-387.
- KULVANICH, P., LEESAWAT, P. and PATOMCHAIWIWAT, V., **2002**. Release characteristics of the matrices prepared from co-spray-dried powders of theophylline and ethylcellulose. *Drug Dev. Ind. Pharm.* 28, 729-739.
- LAMBERSON, R. F. and RAYNOR, G. E., **1976**. Tableting properties of microcrystalline cellulose. *Manuf. Chem. Aerosol News* 47 (6), 55-61.
- LAPIDUS, H. and LORDI, N. G., **1966**. Some factors affecting the release of water-soluble drugs from a compressed hydrophilic matrix. *J. Pharm. Sci.* 55 (8), 840-843.
- LERK, C. F. and BOLHUIS, G. K., **1973**. Comparative evaluation of excipients for direct compression I. *Pharm. Weekbl.* 108, 469-481.
- LERK, C. F., BOLHUIS, G. K. and DE BOER, A. H., **1974**. Comparative evaluation of excipients for direct compression II. *Pharm. Weekbl.* 109, 945-955.
- LERK, C. F., BOLHUIS, G. K. and DE BOER, A. H., **1979**. Effect of microcrystalline cellulose on liquid penetration in and disintegration of directly compressed tablets. *J. Pharm. Sci.* 68, 205-211.
- LEVINA, M. and RAJABI-SIAHBOOMI, A. R., **2004**. The influence of excipients on drug release from hydroxypropyl methylcellulose matrices. *J. Pharm. Sci.* 93 (11), 2746-2754.
- LINDNER, W. D. and LIPPOLD, B. C., **1995**. Drug release from hydrocolloid embeddings with high or low susceptibility to hydrodynamic stress. *Pharmaceutical Research* 12, 1781-1785.
- LUSTIG-GUSTAFSSON, C., JOHAL, H. K., PODCZECK, F. and NEWTON, J. M., **1999**. The influence of water content and drug solubility on the formulation of pellets by extrusion and spheronisation. *Eur. J. Pharm. Sci.* 8, 147-152.

- MCCRYSTAL, C. B., FORD, J. L. and RAJABI-SIAHBOOMI, A. R., **1997**. A study on the interaction of water and cellulose ethers using differential scanning calorimetry. *Thermochimica Acta* 294, 91-98.
- MICHAILOVA, V., TITEVA, S., KOTSILKOVA, R., KRUSTEVA, E. and MINKOV, E., **2001**. Influence of hydrogel structure on the processes of water penetration and drug release from mixed hydroxypropylmethyl cellulose/thermally pregelatinized waxy maize starch hydrophilic matrices. *Int. J. Pharm.* 222, 7-17.
- NANDITA, G. D. and SUDIP, K. D., **2004**. Development of mucoadhesive dosage forms of buprenorphine for sublingual drug delivery. *Drug Delivery* 11, 89-95.
- NEAU, S. H., HOWARD, M. A., CLAUDIUS, J. S. and HOWARD, D. R., **1999**. The effect of the aqueous solubility of xanthine derivatives on the release mechanism from ethylcellulose matrix tablets. *Int. J. Pharm.* 179, 97-105.
- NERURKAR, J., JUN, H. W., PRICE, J. C. and PARK, M. O., **2005**. Controlled-release matrix tablets of ibuprofen using cellulose ethers and carrageenans: effect of formulation factors on dissolution rates. *Eur. J. Pharm. Biopharm.* 61, 56-68.
- NOKHODCHI, A., FORD, J. L. and RUBINSTEIN, M. H., **1997**. Studies on the interaction between water and (hydroxypropyl)methylcellulose. *J. Pharm. Sci.* 86, 608-615.
- NOKHODCHI, A., NOROUZI-SANI, S., SIAHI-SHADBAD, M. R. and LOTFIPOOR, M., **2002**. The effect of various surfactants on the release rate of propranolol hydrochloride from hydroxypropylmethylcellulose (HPMC)-Eudragit matrix. *Eur. J. Pharm. Sci.* 54, 349-356.
- NOVEON BULLETIN, **2002a**. Pharmaceutical Polymers - Product and Regulatory Guide, Pharmaceutical Polymers - Product and Regulatory Guide, B F Goodrich Company, Noveon - The Specialty Chemicals Innovator, Cleveland, OH, Bulletin - 2.
- NOVEON BULLETIN, **2002b**. Noveon, Inc. Polymers in Semisolid Products, Noveon, Inc. Polymers in Semisolid Products, B F Goodrich Company, Noveon - The SPecialty Chemicals Innovator, Cleveland, OH, Bulletin - 8.
- POLLOCK, D. and SHESKEY, P., **1996**. Micronized ethylcellulose: opportunities in direct-compression controlled-release tablets. *Pharmaceutical Technology* 20 (9), 120-130.
- RAJABI-SIAHBOOMI, A. R., BOWTELL, R. W., MANSFIELD, P., HENDERSON, A., DAVIES, M. C. and MELIA, C. D., **1994**. Structure and behavior in hydrophilic matrix sustained-release dosage forms: 2. NMR-imaging studies of dimensional changes in the gel layer and core of HPMC tablets undergoing hydration. *J. Controlled Rel.* 31, 121-128.
- RAJABI-SIAHBOOMI, A. R., MELIA, C. D., DAVIES, M. C., BOWTELL, R. W., MCJURY, M., SHARP, J. C. and MANSFIELD, P., **1992**. Imaging the internal structure of the gel layer in hydrophilic matrix systems by NMR microscopy. *J. Pharm. Pharmacol.* 44, 1062.
- RAO, Y. M., VENI, J. K. and JAYASAGAR, G., **2001**. Formulation and evaluation of diclofenac sodium using hydrophilic matrices. *Drug Dev. Ind. Pharm.* 27 (8), 759-766.

- REKHI, G. S. and JAMBHEKAR, S. S., **1995**. Ethylcellulose-a polymer review. *Drug Dev. Ind. Pharm.* 21, 61-77.
- SAMANI, S. M., MONTASERI, H. and KAZEMI, A., **2003**. The effect of polymer blends on release profiles of diclofenac sodium from matrices. *Eur. J. Pharm. Biopharm.* 55, 351-355.
- SHAH, A. C., BRITTEN, N. J., OLANOFF, L. S. and BADALAMENTI, J. N., **1989**. Gel-matrix systems exhibiting bimodal controlled release for oral delivery. *J. Controlled Rel.* 9, 169-175.
- SHANGRAW, R. F., **1989**. Compressed tablets by Direct Compression. in: LIEBERMAN, H. A., LACHMAN, L. and SCHWARTZ, J. B. (Eds.), *Pharmaceutical Dosage Forms: Tablets*, 2nd Ed., Vol. 1, Marcel Dekker, Inc., New York and Basel, pp. 195-246.
- SIEPMANN, J., PODUAL, K., SRIWONGJANYA, M., PEPPAS, N. A. and BODMEIER, R., **1999**. A new model describing the swelling and drug release kinetics from hydroxypropyl methylcellulose tablets. *J. Pharm. Sci.* 88, 65-72.
- VELAZQUEZ DE LA, C. G., TORRES, J. and MARTIN-POLO, M., **2001**. Temperature effects on the moisture sorption isotherms for methylcellulose and ethylcellulose films. *J. Food. Engin.* 48, 91-94.
- VLACHOU, M., HANI, N., EFENTAKIS, M., TARANTILI, P. A. and ANDREOPOULOS, A. G., **2000**. Polymers for use in controlled release system: the effect of surfactants on their swelling properties. *J. Biomater. Appl.* 15, 65-77.
- WAN, L. S. C., HENG, P. W. S. and WONG, L. F., **1993**. Relationship between swelling and drug release in a hydrophilic matrix. *Drug Dev. Ind. Pharm.* 19 (10), 1201-1210.
- WILSON, H. C. and CUFF, G. W., **1989**. Sustained release of isomazole from matrix tablets administered to dogs. *J. Pharm. Sci.* 78, 582-584.
- ZULEGER, S. and LIPPOLD, B. C., **2001**. Polymer particle erosion controlling drug release. I. Factors influencing drug release and characterization of the release mechanism. *Int. J. Pharm.* 217, 139-152.

7. NATEGLINIDE MATRICES

Based on the previous experience of unique properties of different polymers and excipients investigated and their role in the cumulative drug release kinetics, following few systems were tried to develop sustained release matrices of nateglinide. All nateglinide formulations contain 180 mg of nateglinide, 2 mg of aerosil, and 4 mg of magnesium stearate.

7.1. HPMC-MCC-Starch Matrices

Both the HPMC K4M and MCC PH301 possess the direct compression properties. As we have seen earlier, the mixture of these two polymers resulted in a unique matrix system that can sustain the drug release via combined mechanism of diffusion and erosion depending on the polymer ratio used. The hydrophilic matrix tablets of high dose drug – nateglinide were tried by varying the HPMC K4M to MCC PH301 ratios and also drug to total polymer ratio. The formulation was optimized to target the continuous drug delivery up to 12 h, with minimum polymer levels and without any risk of burst effect or lag phase due to low or high polymer loading in the matrices.

7.1.1. IN VITRO DISSOLUTION & RELEASE KINETIC STUDIES

The influence of the different HPMC grades on the cumulative nateglinide release from HPMC : MCC PH301 (25:75) hydrophilic sustained release matrices is represented in Figure 7.1 (J-1 to J-8). The drug release phenomenon can be explained as discussed earlier in glipizide matrices. In each grade, for a fixed polymer level, the viscosity of the particular polymer selected governs the performance of the matrix by affecting the diffusional and mechanical characteristics of the gel. Briefly, the drug release rate decreased in the rank order K4M>K15M>K100M due to their increasing molecular weight and ability to produce more viscous gel barrier that increases the resistance for the drug to diffuse out of the matrix. Normal grade HPMC (#40 sieve) differs from the controlled release HPMC CR grade (#100 sieve) in their particle size only and influences the polymer performance of hydrophilic matrix systems. The smaller particle size have more surface area relative to equivalent weights of fractions with larger particle size, that provides for better polymer-water contact, thus increasing the overall rate at which complete polymer hydration and gelation occurs. This leads to the more effective formation of the protective gel barrier so

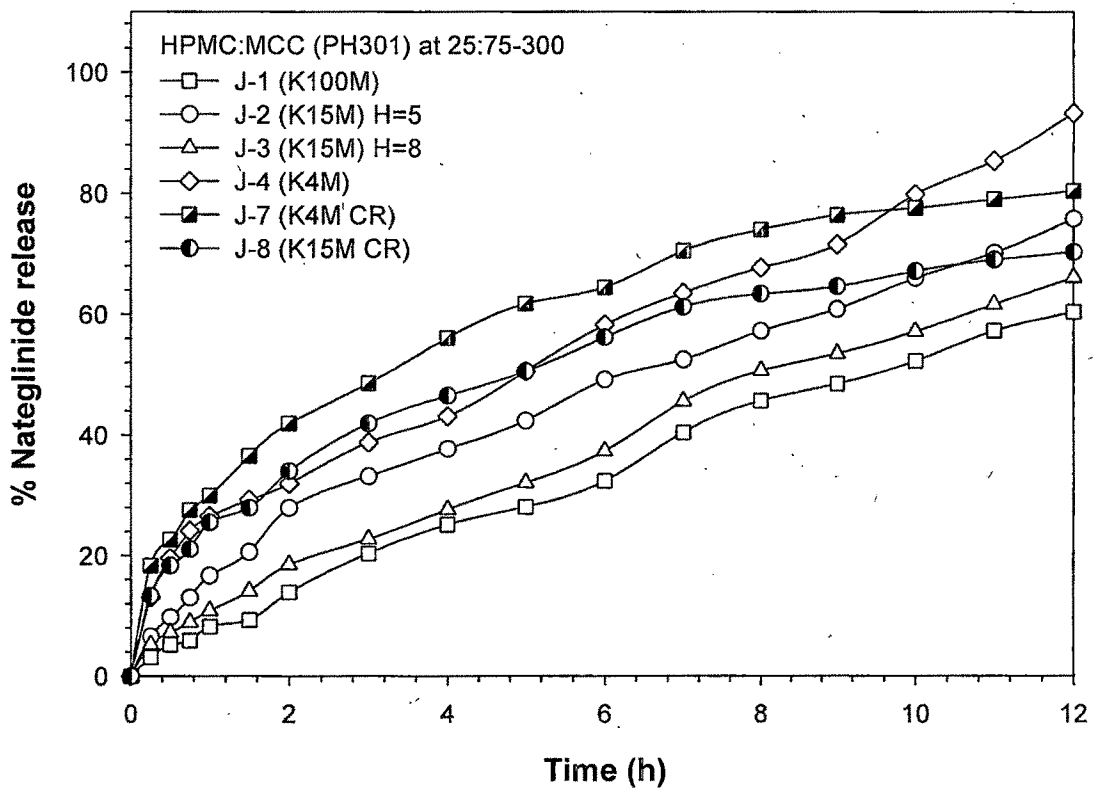


Figure 7.1. Influence of different HPMC grades on cumulative nateglinide release from HPMC : MCC PH301 matrices.

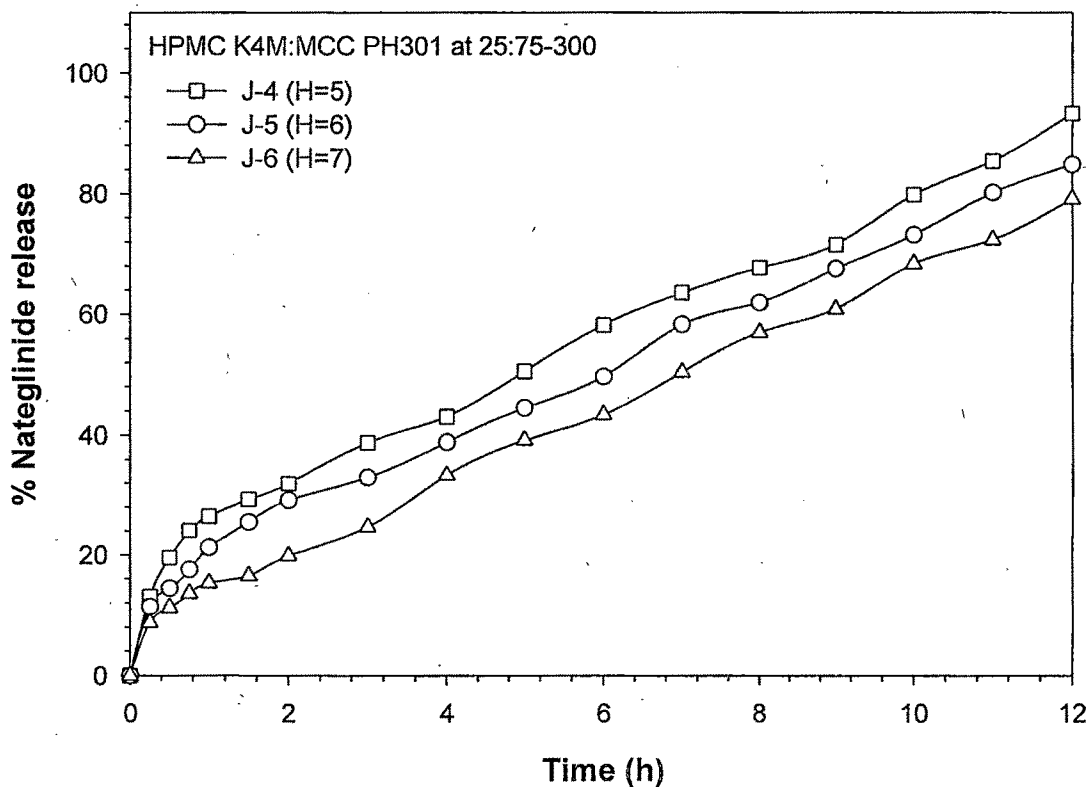


Figure 7.2. Influence of hardness on the nateglinide release from the HPMC K4M : MCC PH301 matrices.

critical to the performance of hydrophilic matrix tablets. From the Figure 7.1, it can be seen that controlled release grade HPMC CR swells immediately upon hydration, the water penetrates the matrix, dissolves nateglinide and starts to diffuse out, which results in initial high drug release. Nevertheless, once the gel gains enough viscosity, it becomes too much tortuous, and the diffusion path length increases, that significantly decreases the drug release rate (compare the dissolution profiles of J-4 with J-7 and J-2 with J-8) at the end of dissolution study. In contrast to this, normal grade HPMC can maintain the constant drug release rate until the matrix reaches disentanglement concentration and dissolves completely. HPMC K4M normal grade results in similar profile initially, and maintaining constant drug delivery up to 12 h and hence was selected for all further studies. At higher compression force (and thereby higher hardness), drug diffusion is impaired greatly due to decreased porosity of matrix, reduced water penetration and matrix hydration as discussed earlier. The reduction in cumulative drug release from HPMC K4M : MCC PH301 matrices shown in Figure 7.2 can also be explained on this basis. Among the group of J-1 to J-8 batches, Hixson-Crowell was the best fit model for J-1 and J-6, while the rest of batches followed Korsmeyer-Peppas release kinetic model. The drug release was governed by non-fickian anomalous transport mechanism for all batches ($0.5 < n < 1$, Table 7.1).

Moreover, MCC is one of the most compressible direct-compression fillers and has the highest dilution potential. This can be explained by the nature of the microcrystalline particles themselves, which are held together by hydrogen bonds between hydrogen groups on adjacent cellulose molecules and accounts almost exclusively for the strength and cohesiveness of compacts. When compressed, the MCC particles are deformed plastically due to the extremely large number of clean surfaces brought in contact during the plastic deformation and the strength of the hydrogen bonds formed (Shangraw, 1989). It has extremely low coefficient of friction (both static and dynamic) and therefore has no lubricant requirements itself.

If the polymer level is too low, a complete gel layer may not form (Cheong et al., 1992). Because hydrophilic matrix tablets containing HPMC absorb water and swell, the polymer level in the outermost hydrated layers decreases with time. The outermost layer of the matrix eventually becomes diluted to the point where individual chains detach from the matrix and diffuse into the bulk solution. The polymer chains break away from the matrix when the surface concentration passes a critical polymer concentration of macromolecular disentanglement (Harland et al., 1988; Bonderoni et al., 1992; Ju et al., 1995). Effect of slower release for higher polymer levels is due to the longer period of time required to reach the disentanglement concentration at the tablet surface, which in turn

equates to greater resistance to surface erosion. There is a threshold level of retardation of drug-release rate that is achievable, where a further increase in polymer loading does not result in further decrease in drug-release rate. This is because drug release does not result solely from polymer erosion, but also from drug diffusion through the hydrated polymer layers. Thus, polymer loading can also significantly affect the wetting time, hydrogel structure, its integrity, and mechanical strength. Hence, matrices with different drug : polymer ratio at different loading were also prepared and the changes in nateglinide release patterns are depicted in Figure 7.3 (J-9 to J-16).

The decrease in drug release rate from J-9 to J-14 is because of increase in HPMC content, and hence it decreased burst effect. The use of water insoluble microcrystalline cellulose as the tablet excipient also partly contributed to the prevention of the tablet matrix from disintegrating. Each MCC microfibril is composed of two areas: One is the paracrystalline region, an amorphous flexible mass of cellulose chains, and the other is crystalline region, which is composed of tight bundles of microfibrils in a rigid linear arrangement. On contacting water, the amorphous regions swell rapidly due to the rapid passage of water into the compact and the instantaneous rupture of hydrogen bonds (Shangraw, 1989). While the denser crystalline domains prevent the complete dissolution of the

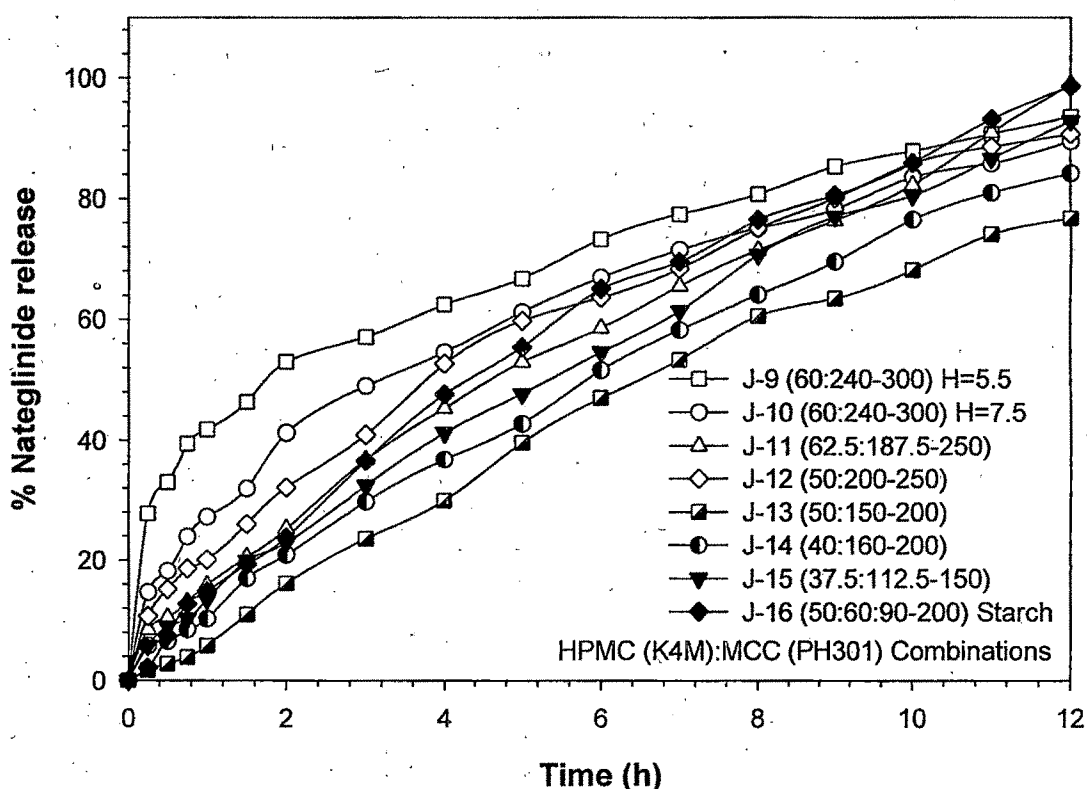


Figure 7.3. Influence of HPMC K4M : MCC PH301 ratio at different polymer loading on nateglinide release profiles.

Table 7.1. Comparison of drug release kinetics of different modalities for the in vitro nateglinide release, best fit model, MDT₅₀ and MDT₈₀ for batches J-1 to J-16.

Batch No	Release model										Best fit model	MDT ₅₀	MDT ₈₀	
	Zero-order	First-Order	Higuchi matrix	Korsmeyer-Peppas	Hixson-Crowell	Zero-order	First-Order	Higuchi matrix	Korsmeyer-Peppas	Hixson-Crowell				
	K_0	r_0	K_1	r_1	K_H	r_H	n	K_k	r_k	K_s	r_s			
J-1	5.37	0.99	-0.07	1.00	15.23	0.96	0.79	8.27	1.00	-0.02	1.00	Hix.Crow.	4.24	-
J-2	6.96	0.95	-0.11	0.99	20.52	0.99	0.62	15.97	1.00	-0.03	0.99	Peppas	2.35	5.11
J-3	6.00	0.98	-0.09	1.00	16.96	0.97	0.69	11.52	1.00	-0.03	1.00	Peppas	3.57	-
J-4	8.47	0.91	-0.17	0.96	24.54	0.99	0.48	25.23	0.99	-0.04	0.98	Peppas	1.60	3.80
J-5	7.70	0.95	-0.14	0.98	22.36	0.99	0.52	20.84	0.99	-0.04	0.99	Peppas	2.11	4.49
J-6	6.92	0.98	-0.12	0.98	20.08	0.97	0.60	15.81	0.99	-0.03	0.99	Hix.Crow.	2.94	5.42
J-7	8.43	0.66	-0.15	0.94	25.53	0.98	0.40	31.19	1.00	-0.04	0.89	Peppas	0.95	2.92
J-8	7.54	0.76	-0.12	0.93	22.04	0.99	0.44	24.77	1.00	-0.03	0.89	Peppas	1.48	-
J-9	9.94	0.39	-0.22	0.96	29.59	0.94	0.32	41.84	1.00	-0.05	0.89	Peppas	0.46	1.99
J-10	9.10	0.83	-0.18	0.99	26.62	1.00	0.48	27.61	1.00	-0.05	0.97	Peppas	1.09	2.89
J-11	8.79	0.98	-0.21	0.86	24.96	0.98	0.68	17.32	1.00	-0.05	0.96	Peppas	1.99	3.88
J-12	9.08	0.92	-0.19	0.99	26.08	0.99	0.58	22.21	1.00	-0.05	0.99	Peppas	1.55	3.30
J-13	6.84	0.99	-0.12	0.99	19.86	0.95	1.04	6.63	1.00	-0.03	1.00	Hix.Crow.	3.24	5.53
J-14	7.74	0.99	-0.14	0.99	22.06	0.97	0.78	12.46	0.99	-0.04	1.00	Hix.Crow.	2.64	4.71
J-15	8.40	0.99	-0.17	0.97	23.81	0.97	0.74	14.45	1.00	-0.04	0.99	Peppas	2.29	4.21
J-16	9.18	0.98	-0.22	0.91	25.88	0.97	0.89	12.47	0.99	-0.05	0.98	Peppas	2.03	3.63

matrix due to its limited interaction with water (Picker, 1999; Durig and Fassihi, 2002). In case of J-15, overall the matrix loading is reduced such an extent that HPMC quantity in the matrix was not sufficient to prepare cohesive gel and therefore, nateglinide suffers less resistance to diffuse through the loose gel formed. This ultimately results in higher drug release as compared to J-14 & J-15. As discussed earlier, Starch 1500 actively contributes in the hydrogel formation with HPMC and results in almost liner drug release for J-16. In this group of matrices, except J-13 and J-14 (which followed Hixson-Crowell model), all other batches best fit into Korsemeyer-Peppas drug release kinetics with non-fickian anomalous transport mechanism (Table 7.1).

7.1.2. CHARACTERIZATION OF OPTIMIZED FORMULATIONS

From J-1 to J-16, in vitro dissolution of batch J-11 and J-16 passes all the constrains defined previously and studied further for their swelling behavior and SEM analysis to confirm the relative contribution of diffusion and/or erosion by Kopcha model.

7.1.2.1. Release Mechanism by Kopcha Model

Overall dissolution profiles of the hydrophilic matrix formulations J-11 (HPMC K4M : MCC PH301 at 62.5:187.5) and J-16 (HPMC K4M : MCC PH301 : Starch 1500 at 50:60:90) were fitted into Kopcha model to understand the proportion of the drug diffused from the matrix or drug released by erosion of the outermost gel layer and results are shown in Figure 7.4. As seen from the figure for J-11, throughout the dissolution study, ratio of $A/B > 1$. It suggests diffusion term is highly predominant in this case. However, the erosion term increases initially up

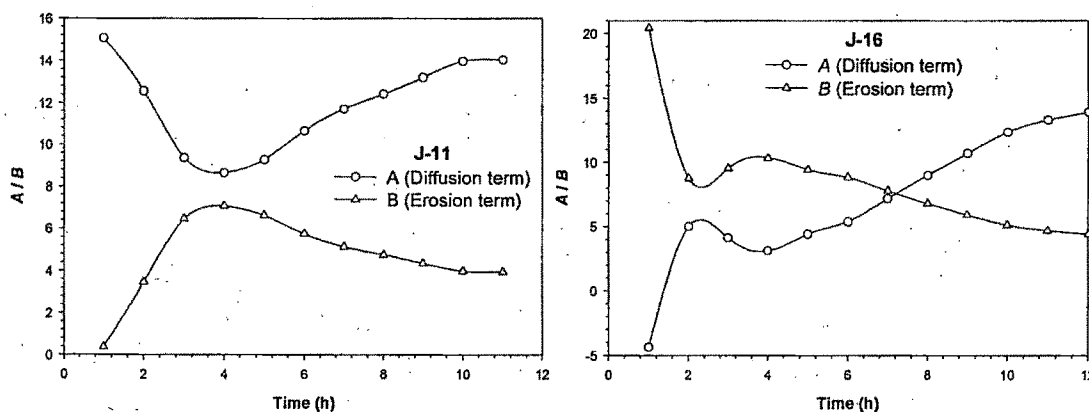


Figure 7.4. Kopcha model parameters (*A* and *B*) versus time profile for J-11 and J-16 formulations, respectively.

to 4 hour, it is not as significant as diffusion. Initially until the water molecules penetrate the matrix core and prepare hydrogel strong enough to control the diffusion of nateglinide, drug is release form the matrix surface easily by erosion due swelling of insoluble MCC PH301. Nevertheless, once hydrogel gains enough viscosity, it controls drug release mainly by diffusion.

In case of J-16, slight lower level of HPMC as compared to J-11 and presence of starch 1500 (because of swelling power of amylose content) as well as insoluble MCC PH301 results in $A/B < 1$ up to 7 hour. Later on HPMC hydrates completely and hydrogel gain enough viscosity to possess control over functionality of MCC and starch, hence nateglinide release mainly by diffusion ($A/B > 1$; Figure 7.4). However, from the figure one can see that the difference in magnitude of the diffusion and erosion terms is almost equal throughout the dissolution study. In short, the drug release in this case is combination of diffusion and erosion where initially erosion prevails slightly and later on diffusion predominates.

7.1.2.2. Swelling Study

The behavior of the gel layer, formed around the hydrophilic matrices after water uptake, is of major importance for the drug release profiles. The structural features of the gel layer are related to the kinetics and mechanism of both water uptake and drug release. Hence, the kinetics of tablet swelling were also investigated and correlated to drug release. The results of water uptake as well as radial and axial swelling for J-16 are enumerated in Figure 7.5. As the matrix comes in contact with water, water starts to penetrate inside, percent water uptake rises with axial and radial swelling of tablet up to 3 hour. This is the time taken by matrix system to get hydrated completely. Simultaneously erosion of surface MCC PH301 and Starch 1500 molecules before HPMC hydrates completely is responsible for initial drug release. The water uptake, axial and radial swelling remains almost constant up to 6 hour. Then radial swelling decreases gradually (which can be seen in the photographs also at the top of the Figure 7.5) but axial swelling still increases until end of the study. This results in minor reduction of water uptake rate. Anisotropic swelling (more swelling in the longitudinal direction than in the radial direction) was seen for HPMC containing nateglinide matrices. Similar phenomena during the swelling of HPMC compacts were observed by Papadimitriou et al. (Papadimitriou et al., 1993; Brabander et al., 2003), who related the axial relaxation of the HPMC compacts to the relief of stress induced during compaction and the unidirectional swelling to the orientation of molecules during compression. This corresponds with continuous increase in drug diffusion in Kopcha model study.

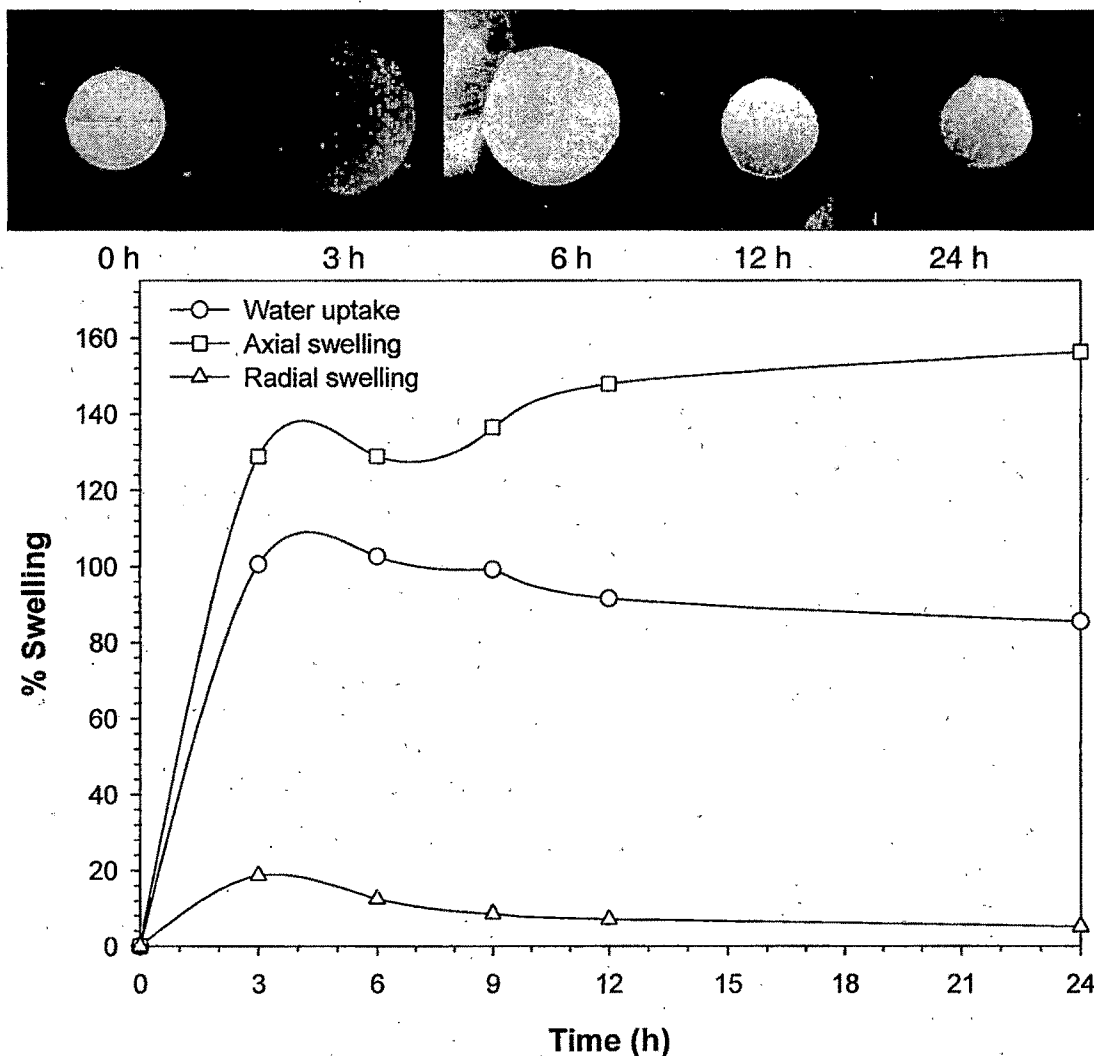


Figure 7.5. Percent water uptake, axial, and radial swelling results for J-16 formulation (HPMC K4M : MCC PH301 : Starch 1500 at 50:60:90).

7.1.2.3. SEM Study

Since the rate of swelling and erosion determines the mechanism and kinetics of drug release, the surface analysis of matrices was carried out at the end of the dissolution study. Figure 7.6 depicts the surface images of J-11 after in vitro dissolution at different time points giving idea about the progress of hydrogel formation. It can be clearly seen that on hydration, the surfaces of the tablets showed the formation of a smoother gel due to the polymer relaxation upon absorption of water. Further, the matrix surface showed smaller pores, which would probably explain the routes for the drugs to travel within the body of the gel layer and finally diffuse out. This supports the results of Kopcha analysis that diffusion of the drug is predominant drug release mechanism for J-11.

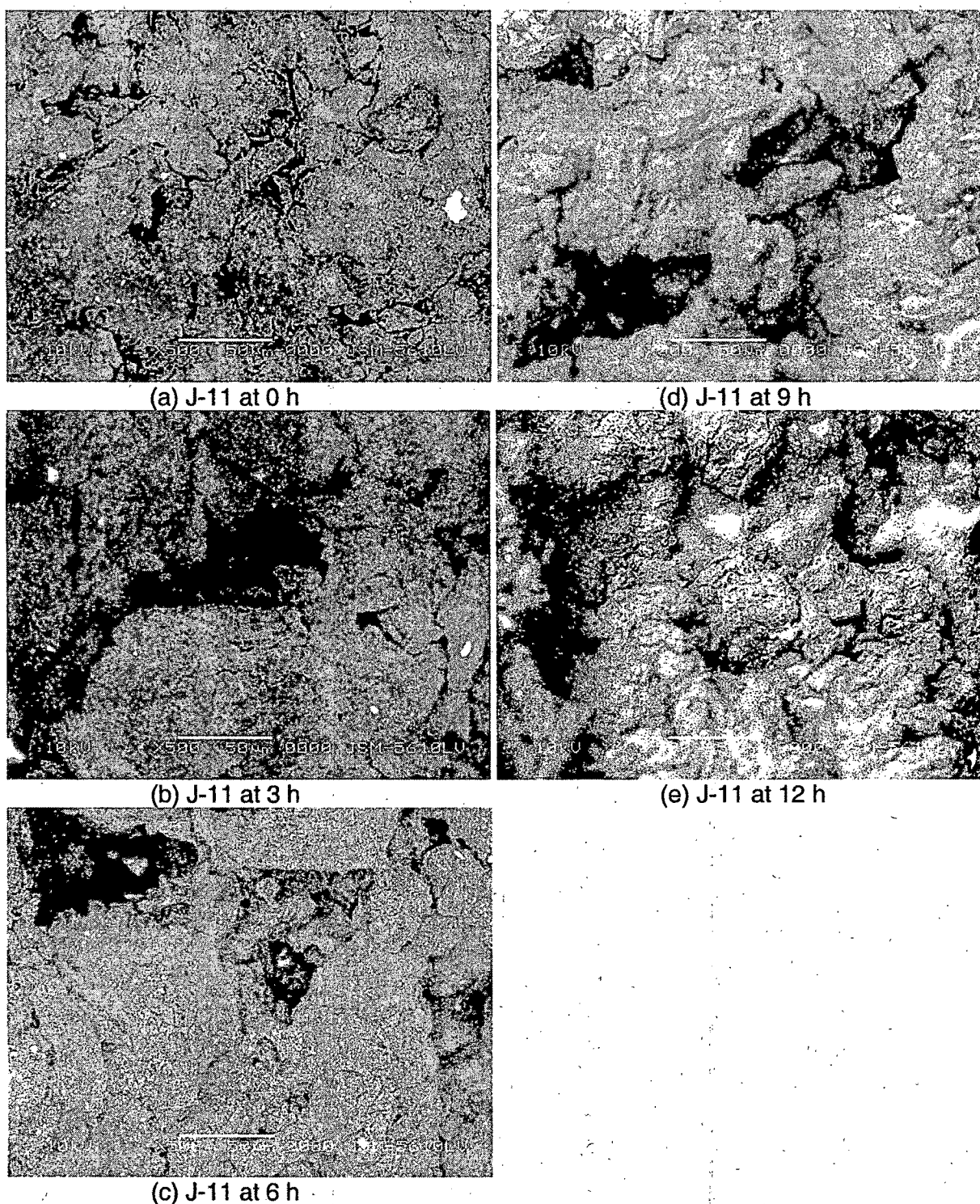


Figure 7.6. SEM photographs of J-11 tablet surface after in vitro dissolution at different time points.

It is clear from the Figure 7.7 (a-c, & f), that the surface morphology is rough initially upto 6 h compared to that after 6 h (Figure 7.7 (d-e)). The micrograph showed that there was a formation of viscous gel after 6 h and controlled the release through diffusion. The mechanism for drug release upto 6 h might be

erosion of matrix tablets. Moreover, the pores on the surface, as visible in Figure 7.7 (c & f), are opening of the channels through which drug has diffused out. The observations are in accordance with the results of swelling study and Kopcha model analysis.

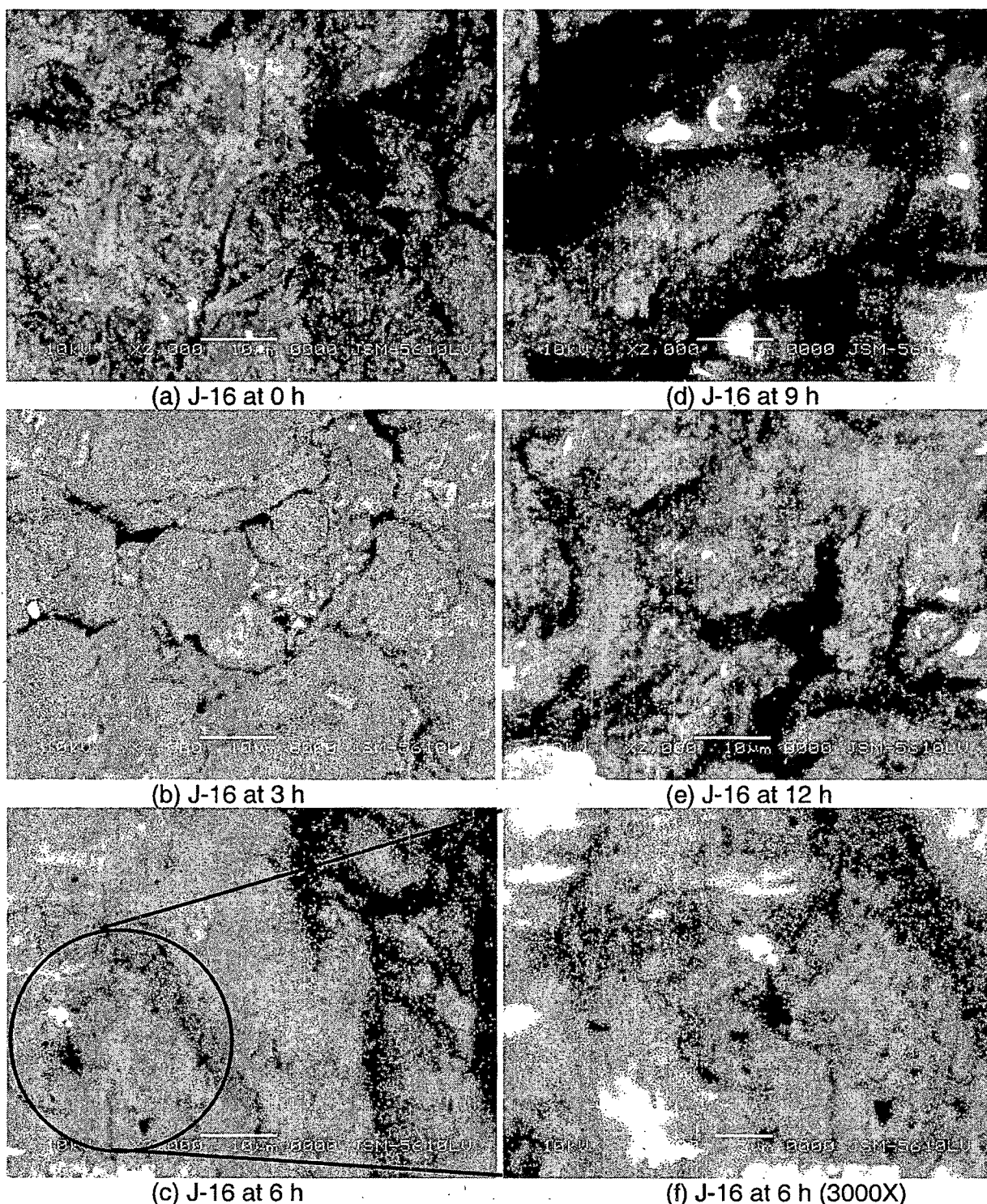


Figure 7.7. SEM photographs of J-16 tablet surface after dissolution at different time points. Micrograph (f) taken after 6 h dissolution showed pores at high magnification.

7.2. Ethyl Cellulose & Carbopol Matrices

Ethylcellulose is hydrophobic in nature and when used with HPMC, it retarded the penetration of the dissolution media into the matrix, that resulted in initial suppression of the drug release rate (as seen in glipizide matrices of EC-HPMC). To overcome this situation, a polymer that can swell upon hydration and thereby improve the initial drug release kinetics is desired. From the results of the different polymer contribution on the drug release discussed in glipizide matrices section, MCC can be expected to fulfill the criteria. Hence, the EC 7FP Premium : MCC PH301 matrices were prepared and their in vitro dissolution results are discussed below.

7.2.1. IN VITRO DISSOLUTION & RELEASE KINETIC STUDIES

In vitro nateglinide release profiles for EC 7FP Premium : MCC PH301 combinations (J-17 to J-20) are enumerated in Figure 7.8. It is obvious from the figure that, as the total polymer content of the matrix decreases (J-17 to J-19), the hydrated layer due to MCC forms less viscous gel, which promotes the

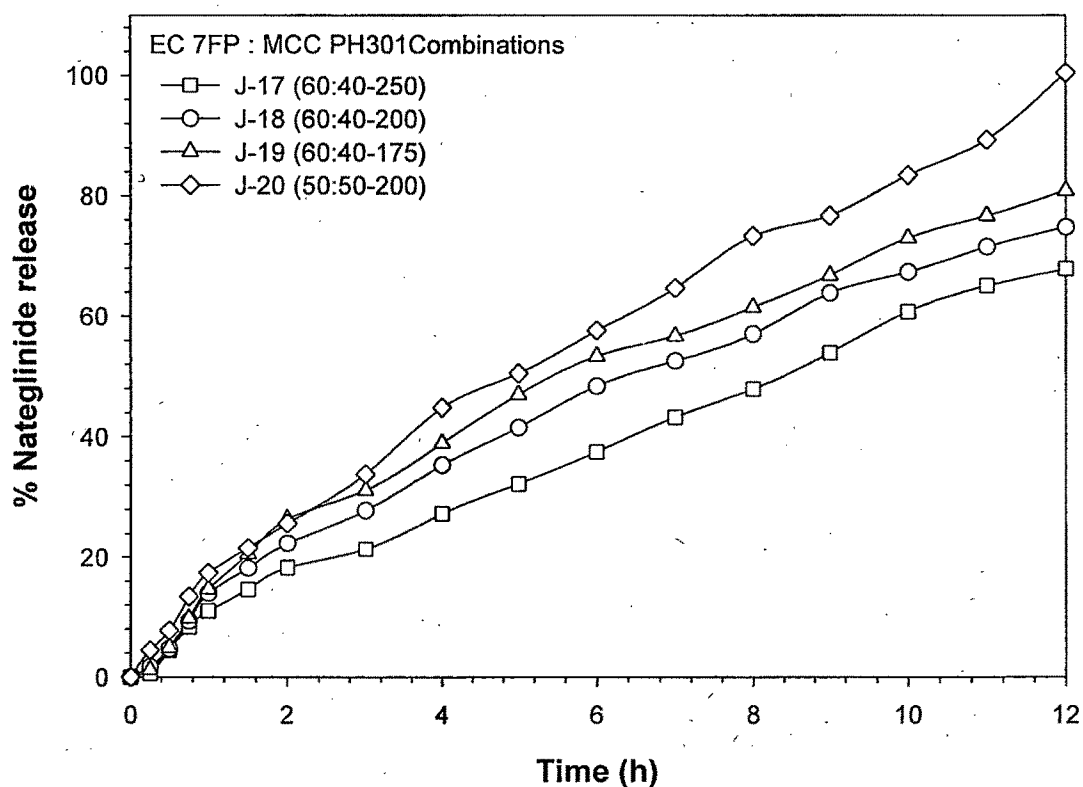


Figure 7.8. Influence of EC 7FP Premium : MCC PH301 ratio at different polymer loading on nateglinide release profiles.

mobility of the water molecules within the gel network of MCC and hence, the dissolved drug can easily diffuse out. This ultimately resulted in lower MDT_{50} and MDT_{80} values, as depicted in Table 7.2. As per the hypothesis applied, inclusion of MCC PH301 in EC 7FP Premium matrices increases the initial drug release, but still none of these three batches showed complete drug release within 12 h. EC is hydrophobic polymer, which restricts the entry of water molecules into the matrix, and thereby controls the swelling and gelling property of MCC. Reducing EC/MCC ratio (J-20) resulted in more hydration and swelling of MCC. This alters the integrity and tortuosity of the hydrogel and promotes the nateglinide diffusion. The drug release profile of this batch was within the limits desired at all time points and considered one of the optimized batch to study the release mechanism in further detail using Kopcha model, swelling study and SEM analysis. The dissolution profiles of J-17 to J-19 best fits in to Hixson-Crowell and first order release kinetic models, while batch J-20 follows Korsmeyer-Peppas release kinetics. All these formulations releases the nateglinide via non-fickian anomalous transport mechanism ($0.5 < n < 1$, as shown in Table 7.2). As the EC/MCC ratio decreases, the drug release kinetic shifts from Hixson-Crowell to Korsmeyer-Peppas model.

The carbopol polymer contains the acrylic acid backbone. The main differences are related to the presence of a comonomer and the cross-link density. Figure 7.9 summarizes the percent nateglinide release as a function of dissolution time for the Carbopol 934P : Eudragit L100 combination formulations. At the same total polymer level, the increase in carbopol content (J-21 and J-22) causes more and more polymer chain gyration with increased radius of the gyration. This resulted in highly swollen hydrogel and increased diffusion path length, which increases the overall mean dissolution time of the system. Moreover, eudragit also contribute significantly in drug release by polymer particle erosion, which is characterized by erosion of partially swollen polymer particles. Unlike the classical eroding tablets, which dissolve completely during the dissolution test, a turbid solution or suspension is formed during the drug release study of tablets showing polymer particle erosion. The visual observation of the dissolution process revealed that J-21 show the lower extent of swelling due to lower carbopol content) and more turbidity in the medium (due to higher eudragit content) as compared to that of the batch J-22. Lindner et al. and Zuleger et al have also noticed this special type of erosion controlled drug delivery with Tylose, a methyl hydroxyl ethyl cellulose (Lindner and Lippold, 1995; Zuleger and Lippold, 2001).

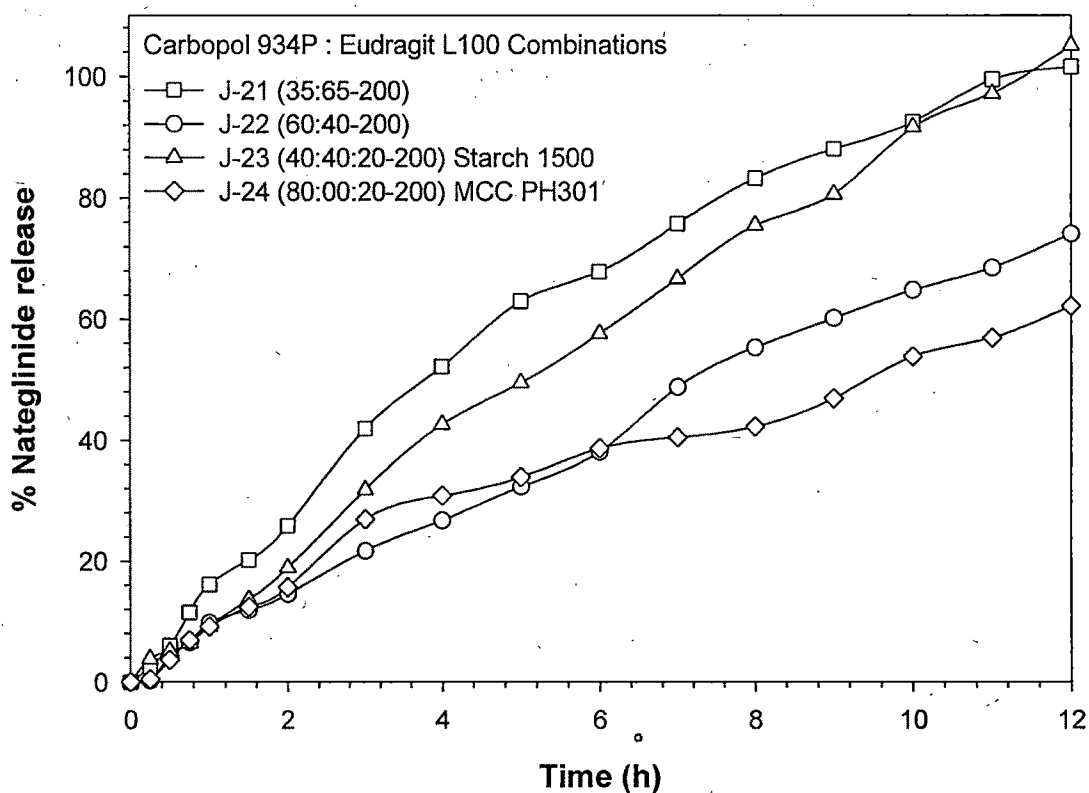


Figure 7.9. Influence of Carbopol 934P : Eudragit L100 : Starch 1500 / MCC PH 301 ratio on nateglinide release profiles.

Partial replacement of Eudragit L100 with Starch 1500 up to certain extent (J-23 as compared to J-21), can also result in almost similar release profile, and also reduces the formulation cost. However, in case of matrices with Carbopol 934P and Starch 1500 (J-24), a polymer-polymer interaction occurs and Starch 1500 gave synergistic effect of drug release retardation (like it actively contributes in the drug release kinetics from HPMC hydrogels). As seen from the in vitro release data for J-24, nateglinide release rate reduces to a considerable extent after 3 h. Moreover, high carbopol content can also slow down the drug release due to its highly cross-linked gel network. From this group of matrices, J-21 and J-23 followed the constraint limits for their dissolution, considered optimized and studied further for thorough understanding and conformation of drug release mechanism. Looking at the results of the drug release kinetics of different modalities (Table 7.2) and formulation composition (J-21 to J-24), the best fit model for dissolution profiles changes from Korsmeyer-Peppas to zero-order to first order. Depending on the value n , these formulations release nateglinide either by non-fickian anomalous or by supercase-II transport mechanism.

Table 7.2. Comparison of drug release kinetics of different modalities for the in vitro nateglinide release, best fit model, MDT₅₀ and MDT₈₀ for batches J-17 to J-24.

Batch No	Release model											MDT ₅₀	MDT ₈₀			
	Zero-order	First-Order	Higuchi matrix	Korsmeyer-Peppas	Hixson-Crowell	Best fit model	K_0	f_0	K_1	n_1	K_H			r_H	η	K_c
J-17	6.03	0.99	-0.09	0.99	17.01	0.96	0.97	6.97	0.96	-0.03	1.00	Hix.Crow.	3.73	-		
J-18	6.83	0.97	-0.11	1.00	20.15	0.98	0.87	9.89	0.98	-0.03	1.00	1st order	2.73	5.32		
J-19	7.50	0.97	-0.13	1.00	21.77	0.98	0.92	9.89	0.97	-0.04	1.00	Hix.Crow.	2.35	4.68		
J-20	8.80	0.98	-	-	24.90	0.97	0.77	14.78	1.00	-0.05	0.87	Peppas	2.06	3.94		
J-21	9.92	0.97	-	-	27.82	0.97	0.91	12.85	0.99	-0.07	0.93	Peppas	1.83	3.22		
J-22	6.49	1.00	-0.11	0.98	18.69	0.95	1.14	5.30	0.94	-0.03	0.99	Zero order	3.67	6.06		
J-23	9.16	1.00	-	-	25.43	0.95	0.94	10.45	1.00	-0.06	0.86	Zero order	2.45	4.10		
J-24	5.52	0.97	-0.08	0.99	15.81	0.97	1.02	6.04	0.95	-0.02	0.99	1st order	3.80	-		



7.2.2. CHARACTERIZATION OF OPTIMIZED FORMULATIONS

From this group of matrices, three optimized batches, namely J-20 (EC 7FP Premium : MCC PH301 at 100:100), J-21 (Carbopol 934P : Eudragit L100 at 70:130) and J-23 (Carbopol 934P : Eudragit L100 : Starch 1500 at 80:80:40) were subjected to further characterization.

7.2.2.1. Release Mechanism by Kopcha Model

Figure 7.10 enumerates the results of Kopcha model analysis for batches J-20, J-21, and J-23, respectively. For J-20 matrix system, hydration of MCC results in formation of hydrogel capable enough to control the drug release mainly by diffusion of the dissolved drug molecules. Initially up to 2 hour, MCC PH301 promotes release of drug by swelling of MCC and creation of channels through which drug diffuses before firm gel is formed. Throughout the dissolution study

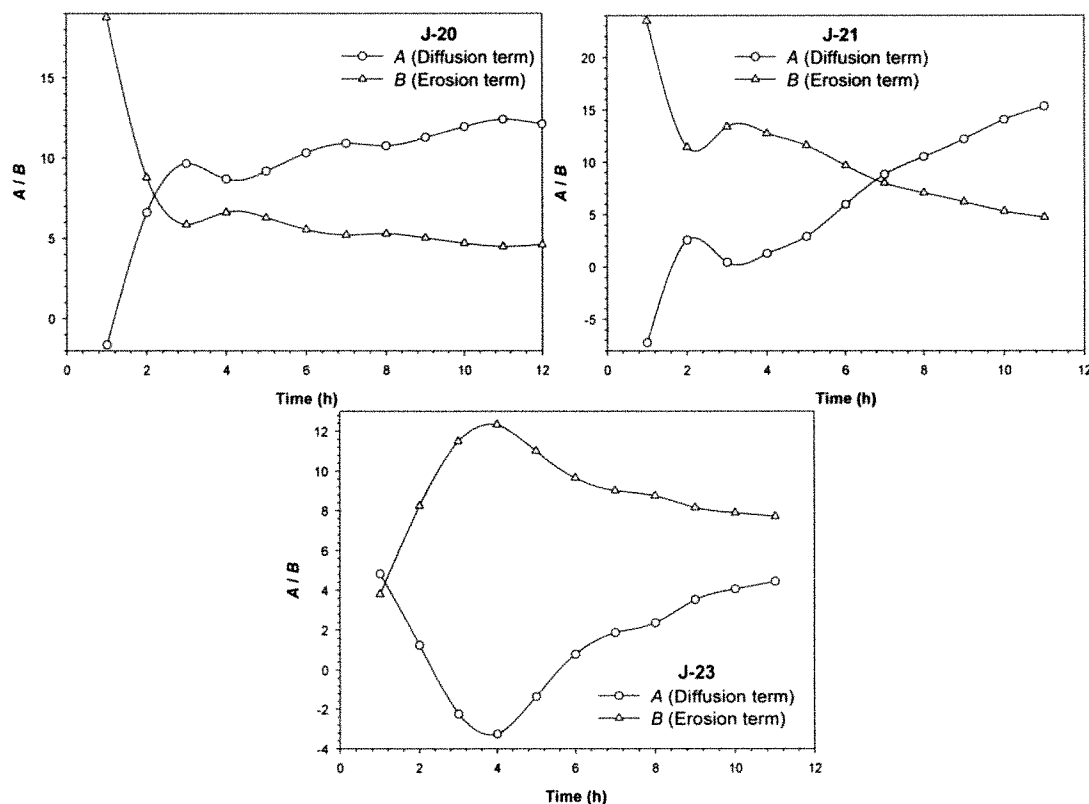


Figure 7.10. Kopcha model parameters (*A* and *B*) versus time profile for J-20 (EC 7FP Premium : MCC PH301 at 100:100), J-21 (Carbopol 934P : Eudragit L100 at 70:130), and J-23 (Carbopol 934P : Eudragit L100 : Starch 1500 at 80:80:40) formulations, respectively.

A/B is greater than unity and indicates that diffusion is the main drug release mechanism from this ethylcellulose matrix. In case of Carbopol 934P : Eudragit L100 containing matrix system J-21, as we have discussed earlier, Eudragit L100 causes nateglinide release by polymer particle erosion (can be seen in Figure 7.10 up to half course of dissolution). The carbopol swells in dissolution media due to repulsion of like negative charges of carbopol molecules and it is time dependent process. Complete hydration of carbopol increases hydrogel viscosity and is mainly responsible for control of drug release by diffusion through the gel during later half course of dissolution. Overall, the drug release is a combination of diffusion and erosion, where initially erosion prevails followed by diffusion predominance.

As seen in Figure 7.10 for J-23, erosion increases during initial 4 hour and then declines gradually with rise in diffusion term. This can be explained on the basis that amylose content of Starch 1500 absorbs water readily and induce swelling of matrix before Carbopol 934P molecules uncoil completely to gain visco-elastic property. Moreover, the Eudragit L100 also supports the drug release by polymer particle erosion.

7.2.2.2. Swelling Study

Since the degree of hydration is one of the factors determining the degree and velocity of drug release from the hydrogel matrices, the relation between the kinetic parameters of water penetration and the viscosity is a characteristic indicator for the gel structure, the degree of swelling and the drug release rate (Michailova et al., 2000). Hence, the kinetics of tablet swelling was also investigated to get insight the drug release mechanism.

The photographs of J-20 matrix system at different time interval of swelling study and the results of water uptake, axial and radial swelling are depicted in Figure 7.11. In contact with dissolution media, MCC gets hydrated, swells, and forms gel that controls diffusion of the drug throughout the dissolution study. Rapid increase in axial and radial swelling with increase in water uptake during initial 3 h indicate hydrogel formation. The swelling remains almost constant up to 9 hour, then radial swelling decreases gradually which can be seen in photographs also. However, the increase in water uptake continues due to increase in axial swelling (anisotropic effect like HPMC based matrices) because of the relaxation of the stress induced during to compression of matrices.

In J-21, carbopol containing matrices, as shown in Figure 7.12, a continuous increase in matrix height and diameter is seen. This is because upon exposure to water, the polymer chains start gyrating and the radius of gyration becomes

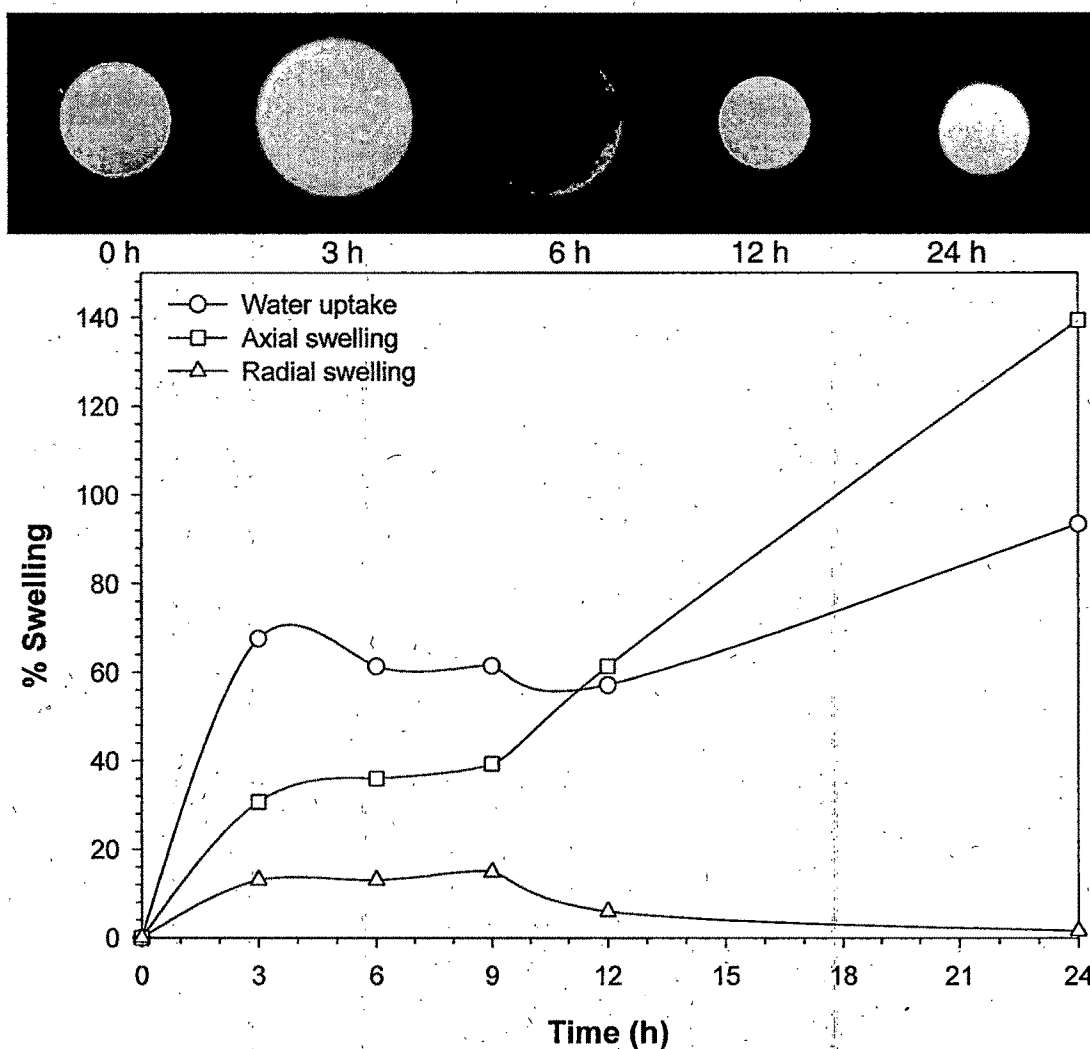


Figure 7.11. Percent water uptake, axial, and radial swelling results for J-20 formulation (EC 7FP Premium : MCC PH301 at 100:100).

bigger and bigger which results in swelling. Dissolution media of pH 6.8 causes neutralization and ionizes the carbopol polymer, generating negative charges along the polymer backbone. Repulsions of these like negative charges cause the molecule to uncoil into an extended structure. This leads to increase in water uptake (around 600 % of its original volume) continuously and can be observed clearly in the photographs of matrices at different time intervals. The dissolution media penetrated in to matrix dissolves nateglinide, and diffuse it out. Initially up to 6 hour, diffusion rate is lower until matrix gets hydrated completely. Then it increases gradually until the dissolution ends. This further supports the results of Kopcha analysis. This confirms the key role of Carbopol 934P as a drug release retardant in hydrophilic matrices.

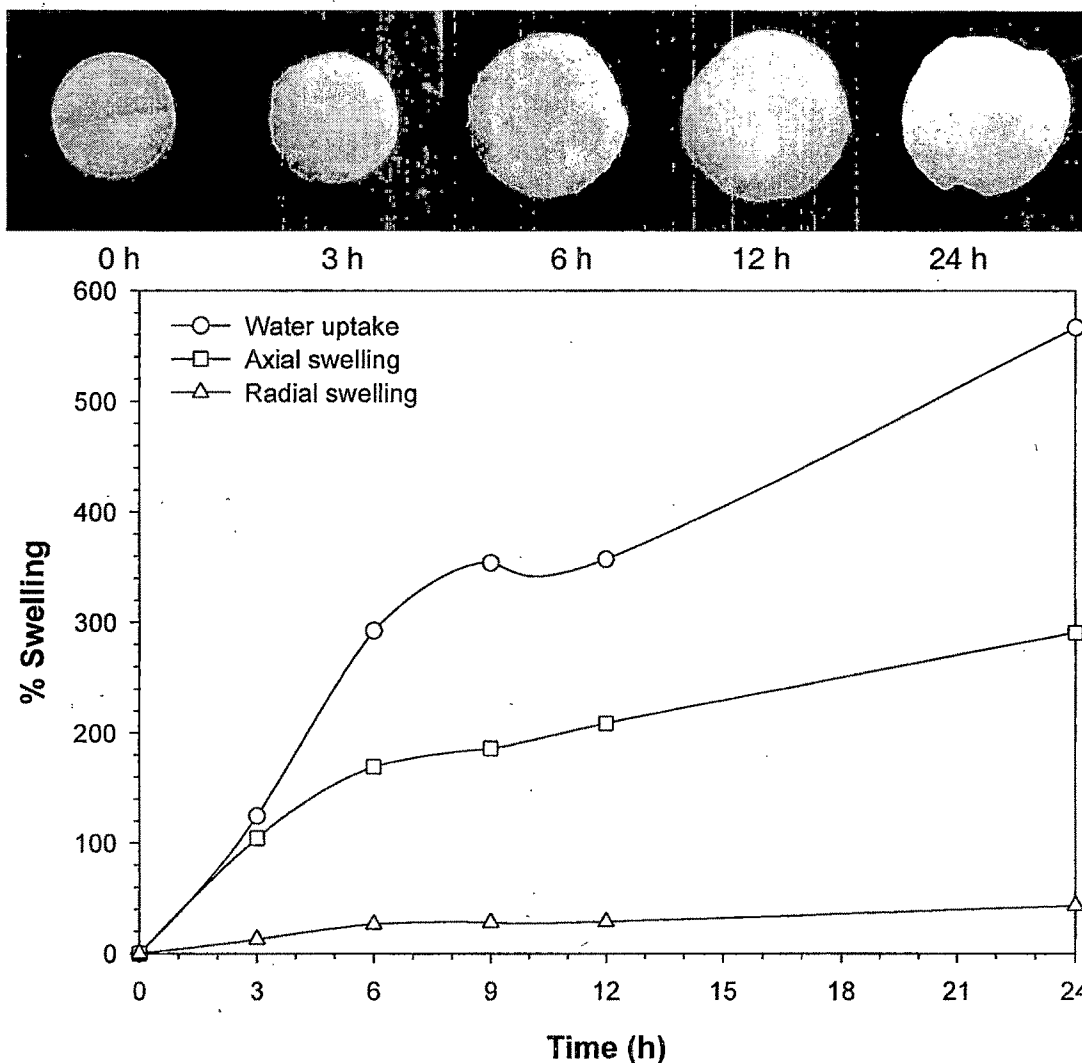


Figure 7.12. Percent water uptake, axial, and radial swelling results for J-21 formulation (Carbopol 934P : Eudragit L100 at 70:130).

The results of swelling study for J-23 are shown in Figure 7.13. The carbopol hydrogel are structurally different from other hydrogels. The hydrogels are not entangled chains of polymer, but discrete microgels made up of many polymer particles, in which the drug is dispersed. Since these microgels are not water soluble, they do not dissolve and erosion in the manner of linear polymers does not occur. But, when the hydrogel is fully hydrated, osmotic pressure from within works to break up the structure, essentially by sloughing off discrete pieces of the hydrogel (Noveon Bulletin, 2002). These fully hydrated discrete pieces can be seen clearly in photographs of 12 hour and 24 hour. The drug release governed by the erosion of this gel are in accordance of the erosion predominance suggested by the Kopcha model analysis.

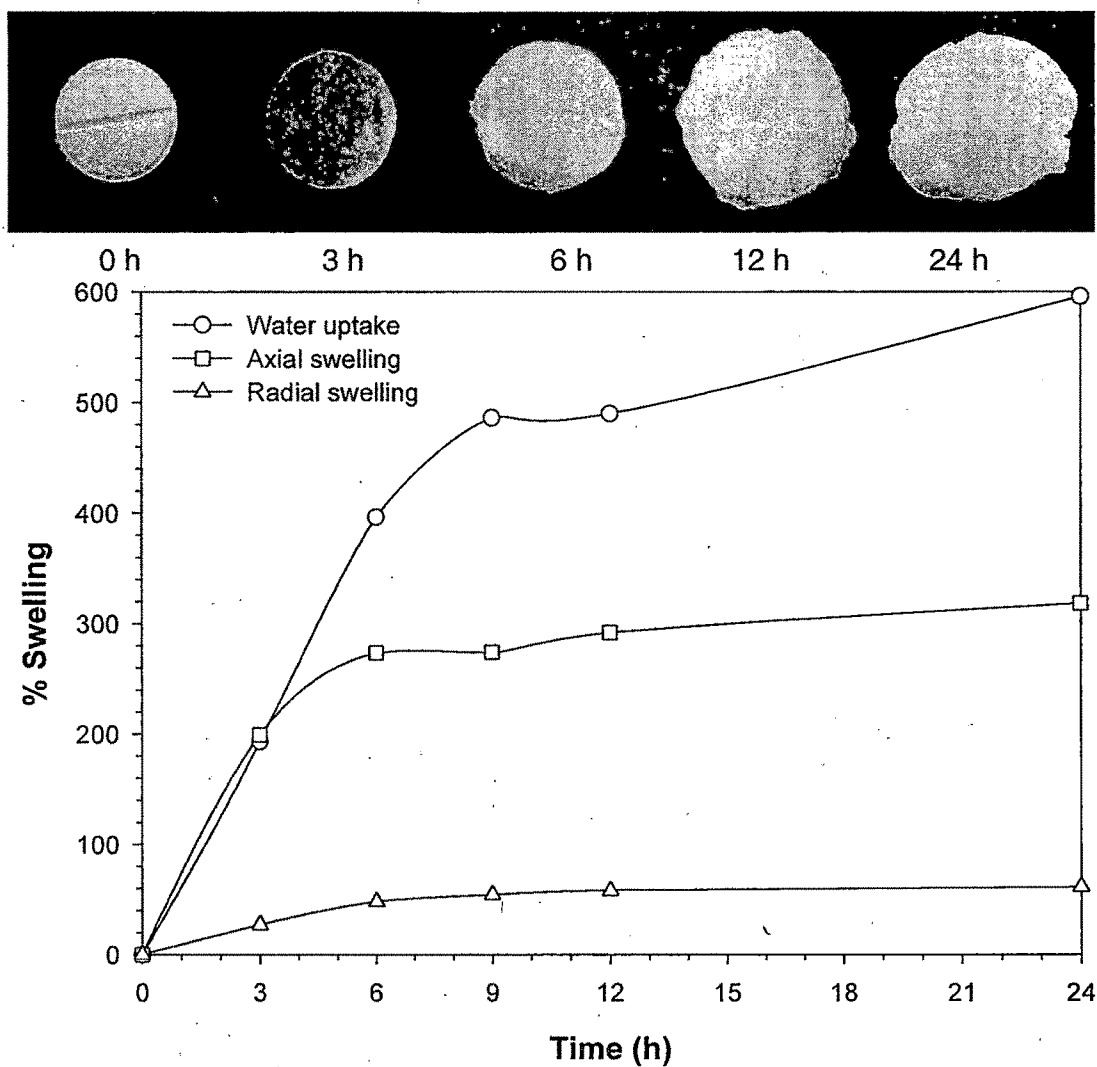


Figure 7.13. Percent water uptake, axial, and radial swelling results for J-23 formulation (Carbopol 934P : Eudragit L100 : Starch 1500 at 80:80:40).

7.2.2.3. SEM Study

Figure 7.14 shows the surface images of the J-20 matrix after 12 hour dissolution at different magnifications. The matrix structure of the EC-MCC tablets were maintained after 12 hour dissolution due to water insoluble EC. However, matrix becomes porous after dissolution because the water swellable MCC created gel through which drug diffused during 12 hour dissolution. Undissolved EC particles are clearly observed in the micrographs shown in Figure 7.14.

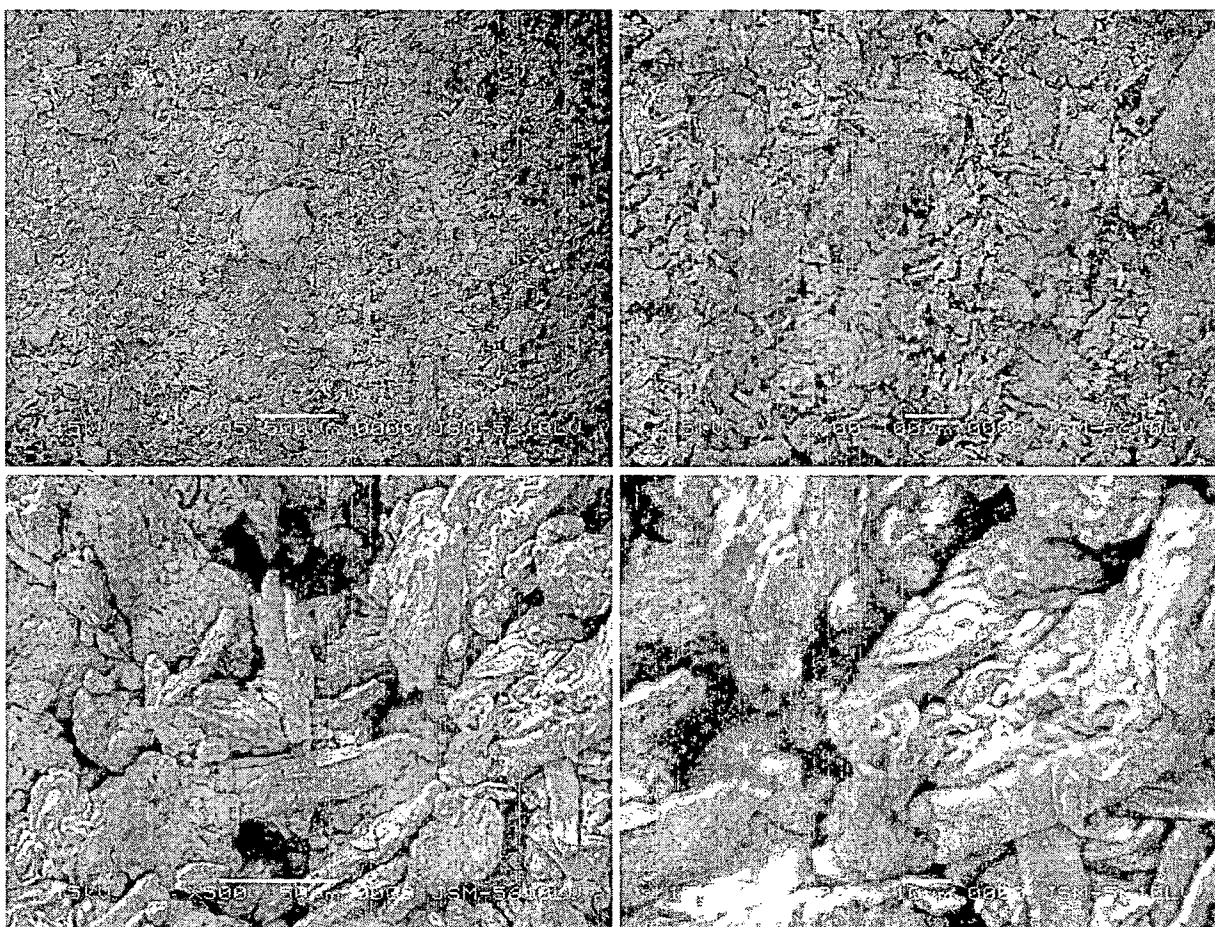


Figure 7.14. Scanning electron micrograph of J-20 after 12 h dissolution at different magnifications.

The surface images of carbopol containing batch J-21 are depicted in Figure 7.15. Carbopol 934P is hydrophilic in nature due to carboxylic groups, it forms very smooth gel (like HPMC) and controls the drug release rate in controlled manner. It absorbs plenty of water and the hydrogel in the form of discrete swollen microgels are seen in the SEM images. When the hydrogel is fully hydrated, osmotic pressure from within works to break up the structure, essentially by sloughing off discrete pieces of the hydrogel. This can be seen clearly in the photographs and SEM images, confirming the diffusion as a major drug release mechanism. Because of its high water uptake the outermost microgel layer becomes almost translucent. Initially carbopol takes time to reach at completely hydrated state and therefore drug release occurs by erosion. During this period also, diffusion is there but not as significant as erosion, but upon complete hydration, carbopol controls the drug release by diffusion mechanism.

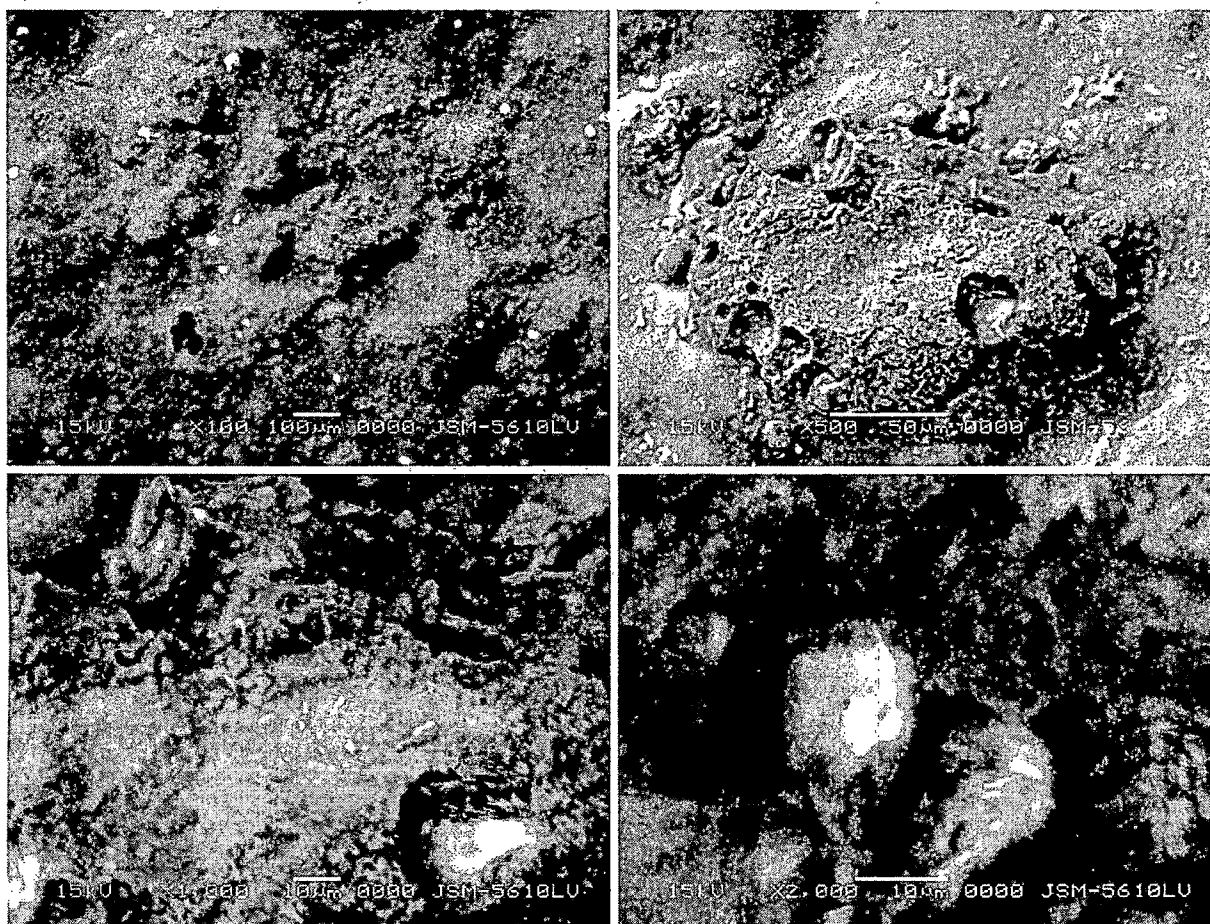


Figure 7.15. Scanning electron micrograph of J-21 after 12 h dissolution at different magnifications.

Figure 7.16 depicts the SEM images of J-23 matrix tablets containing Carbopol 934P, Eudragit L100 and starch 1500. As the external surface of carbopol matrices hydrated, it also forms a gelatinous layer, which is significantly different structurally from the other traditional matrix tablet. Images at lower magnification shows the smooth hydrogel formed due to carbopol. Higher magnification images clearly indicate the eudragit mediated erosion of matrix. This confirms the drug release mechanism of this matrix is mainly erosion mediated as discussed earlier in Kopcha model analysis.

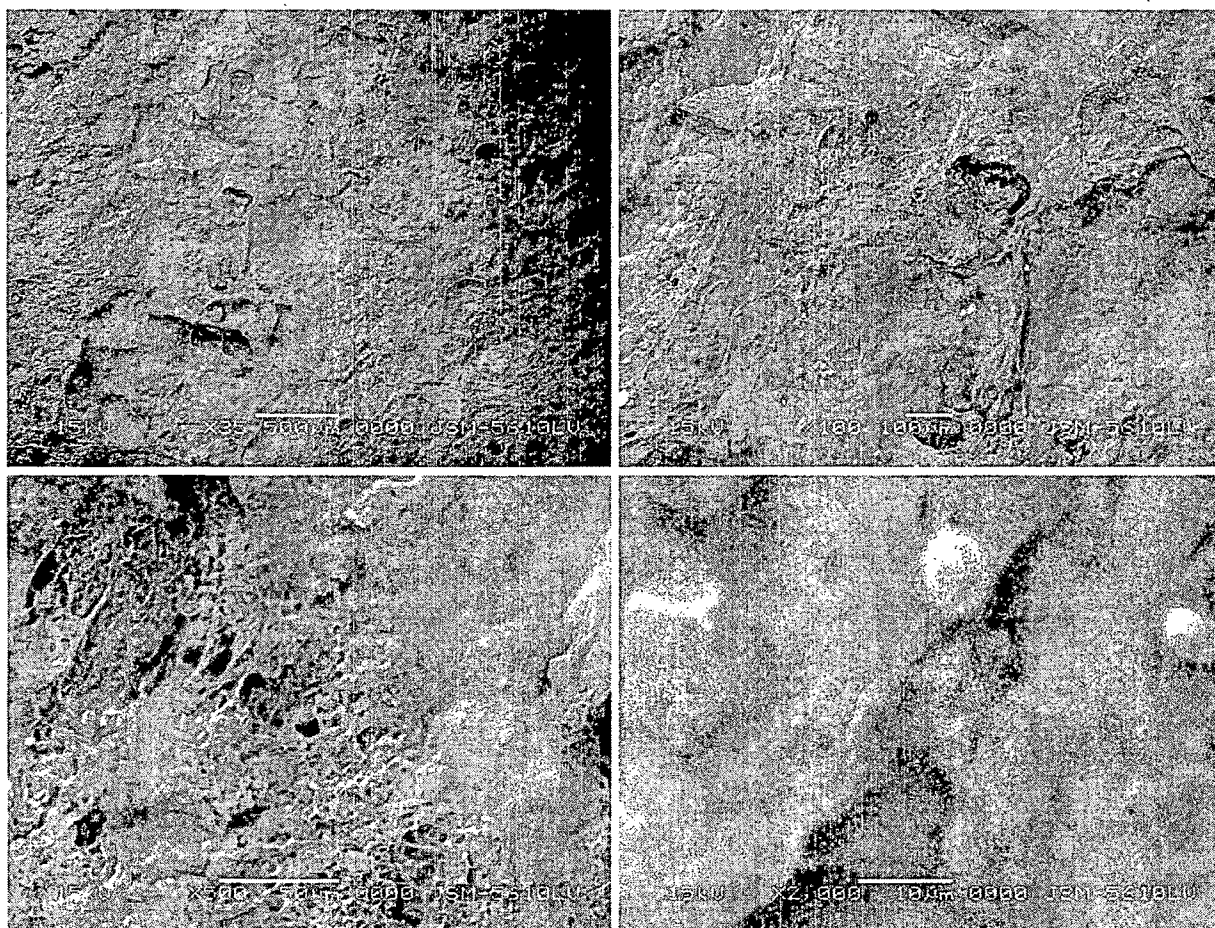


Figure 7.16. Scanning electron micrograph of J-23 after 12 h dissolution at different magnifications.

7.3. Xanthan Gum Matrices

Xanthan gum, a natural gum was used as a main matrix former to retard the nateglinide release. As we have seen earlier in glipizide matrices, that free carboxylic groups of anionic xanthan gum interact with the non-ionic HPMC to produce a firm gel and significantly hinders the drug diffusion. Hence, some water soluble excipients can be added to increase the porosity of the matrix to improve the release rate of active material. Other alternative is the addition of swellable material, which swells upon hydration, increases the distance between the interacting HPMC and xanthan molecules and causes weakening of the gel strength, and thereby promotes the drug release.

7.3.1. IN VITRO DISSOLUTION & RELEASE KINETIC STUDIES

The results of in vitro dissolution study for xanthan gum : HPMC K4M matrices with other excipients – lactose, Starch 1500 and Eudragit L100 are depicted in Figure 7.17 (J-25 to J-29). Lactose, being water soluble easily promoted the nateglinide release through the channels and pores from which it diffuses out.

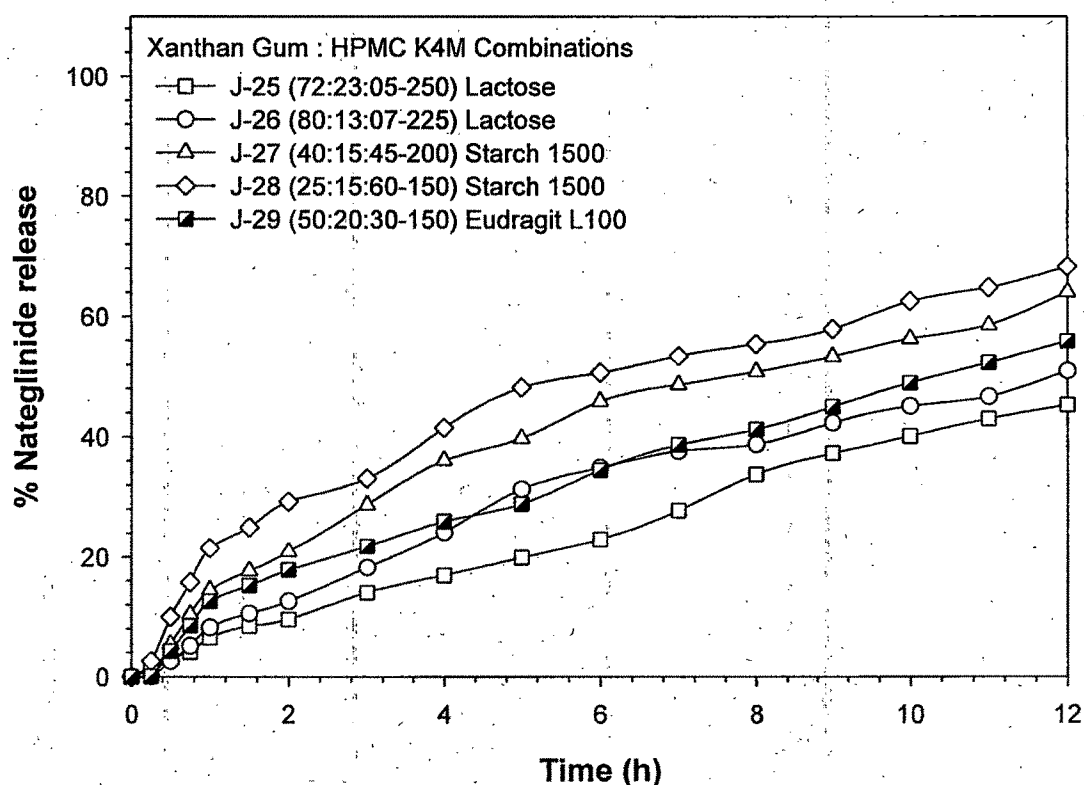


Figure 7.17. Influence of Xanthan gum : HPMC K4M : Lactose / Starch 155 / Eudragit L100 ratio at different polymer loading on nateglinide release profiles.

Starch 1500 played its role due to its inherent swelling power and disintegrant properties while Eudragit L100 increased drug release because of its characteristic polymer particle erosion mechanism. Apart from this, the level of natural gum and HPMC in matrix is also a governing factor for changes in MDT of different matrices. In short, use of all three excipients help in linearization of the dissolution data, though none of them could complete drug release from xanthan : HPMC matrices within 12 h at level they were used. Further changes in the composition of the polymer and excipients can be made to modulate different release rate formulations. Table 7.3 gives comparative idea about the kinetic constants of different drug release modalities. Regression coefficients of different drug release model suggests that addition of lactose (J-25 and J-26) or Eudragit L100 (J-29) into Xanthan gum : HPMC K4M matrices results in Hixson-Crowell or first order kinetics whereas addition of Starch 1500 (J-27 and J-28) gives the release profiles which best fits into Higuchi's square root of time kinetics.

The next group of matrices are based on the combination of xanthan gum with Eudragit L100 with or without other additives. Their release profiles are enumerated in Figure 7.18 (J-30 to J-35). Removal of HPMC from xanthan : HPMC matrices changes the complete dissolution profiles. In xanthan gum : Eudragit L100 combinations, as xanthan can not form protective gel barrier so

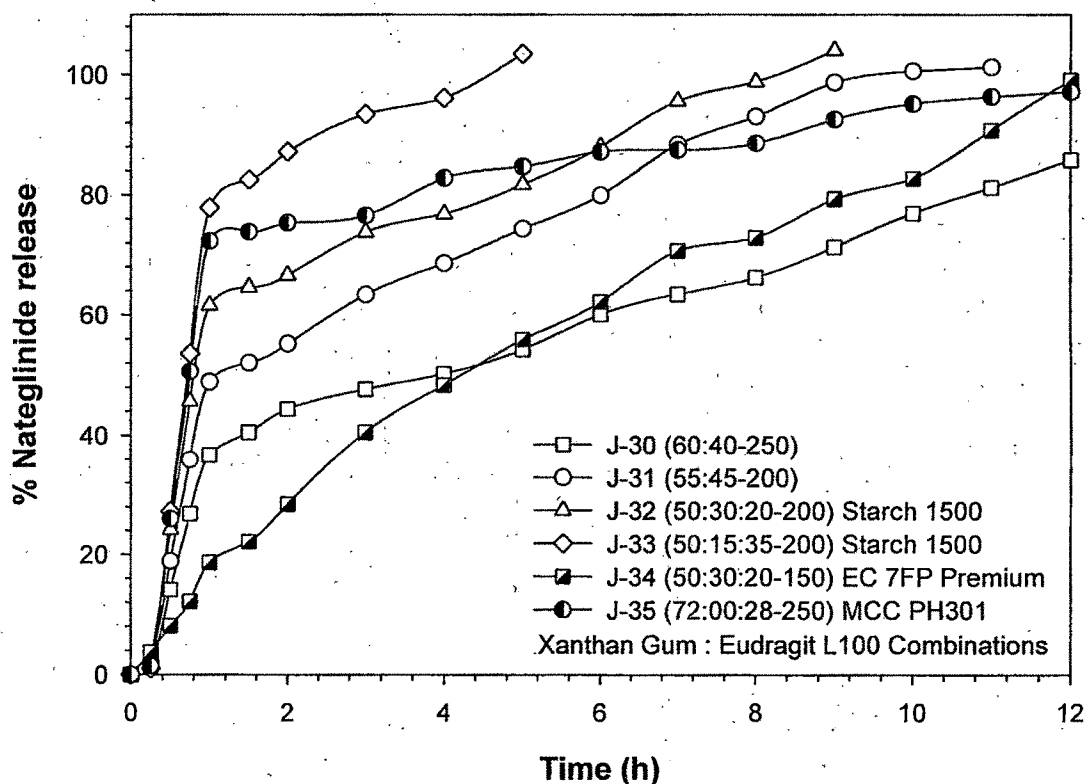


Figure 7.18. Influence of Xanthan gum : Eudragit L100 : Starch 1500 / EC 7FP Premium / MCC PH301 on nateglinide release profiles.

Table 7.3. Comparison of drug release kinetics of different modalities for the in vitro nateglinide release, best fit model, MDT₅₀ and MDT₈₀ for batches J-25 to J-35.

Batch No	Release model										Best fit model	MDT ₅₀	MDT ₈₀	
	Zero-order	First-Order	Higuchi matrix	Koismeyer-Peppas	Hixson-Crowell									
	K_0	f_0	K_1	t_1	K_H	t_H	η	K_k	t_k	K_s	t_s			
J-25	3.93	0.99	-0.05	1.00	11.51	0.95	0.88	5.26	1.00	-0.02	1.00	Hix.Crow.	6.18	-
J-26	4.66	0.97	-0.06	0.99	13.61	0.97	1.23	3.49	0.91	-0.02	0.99	1st order	4.71	-
J-27	6.16	0.94	-0.09	0.98	17.68	0.99	0.95	7.91	0.92	-0.03	0.97	Matrix	2.83	-
J-28	6.90	0.87	-0.10	0.96	19.94	0.99	0.68	14.73	0.95	-0.03	0.94	Matrix	2.05	-
J-29	5.08	0.97	-0.07	0.99	14.70	0.98	1.15	4.59	0.86	-0.02	0.99	1st order	4.21	-
J-30	8.37	0.78	-0.15	0.96	24.84	0.98	0.70	18.15	0.86	-0.04	0.93	Matrix	0.98	3.39
J-31	11.89	0.71	-	-	33.39	0.97	0.69	25.80	0.84	-0.09	0.94	Matrix	0.59	1.67
J-32	14.81	0.53	-	-	37.97	0.93	0.65	32.37	0.81	-0.11	0.91	Matrix	0.50	1.07
J-33	29.01	0.47	-	-	54.49	0.90	1.12	36.76	0.76	-0.23	0.94	Hix.Crow.	0.48	0.62
J-34	9.07	0.96	-0.22	0.87	25.76	0.98	0.79	14.89	0.99	-0.05	0.97	Peppas	1.80	3.55
J-35	11.32	-	-0.32	0.89	34.51	0.79	0.60	31.57	0.73	-0.07	0.70	1st order	0.49	0.78

quickly as HPMC (to retard the drug diffusion), eudragit particle erosion starts immediately upon contact with dissolution medium and resulted in nateglinide burst release with inverse proportion of xanthan level in the matrix system (J-30 to J-32). After about 1 h, xanthan becomes fully hydrated and slow down the drug release promoted by the presence of eudragit, starch, and MCC. Similar to HPMC, ethylcellulose also prepared the tortuous barrier even at least total polymer level (J-34). This heterogeneous gel successfully controlled nateglinide release throughout 12 h within the defined dissolution constraints and selected for further study to confirm the drug release mechanism. As shown in Table 7.3, batches J-30 to J-32 fits into Higuchi's square-root of time model, whereas J-33 and J-35 follows Hixson-Crowell and first order kinetics, respectively. The optimized batch J-34 follows Korsmeyer-Peppas kinetics and releases nateglinide by non-fickian anomalous transport mechanism.

7.3.2. CHARACTERIZATION OF OPTIMIZED FORMULATIONS

Within this group of matrices only J-34 was found to be optimized one and in vitro dissolution data are analyzed by Kopcha model. SEM images were used for better understanding of drug release mechanism.

7.3.2.1. Release Mechanism by Kopcha Model

The relative contribution of diffusional and erosional mechanism of drug release for J-34 (Xanthan gum : Eudragit L100 : EC 7 FP Premium at 75:35:40) is shown in Figure 7.19. Initially until xanthan gum is hydrated fully and forms viscous resistant barrier, the drug release is mainly due to Eudragit L100 mediated polymer particle erosion (diffusion is there but not so significant). At 4 hour diffusion line crosses the erosion line suggesting equal contribution of both the

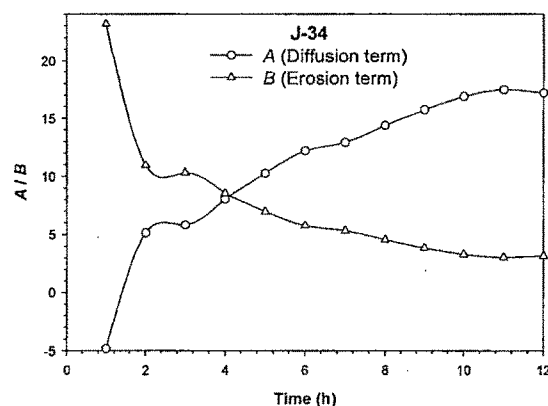


Figure 7.19. Kopcha model parameters (*A* and *B*) versus time profile for J-34 formulation (Xanthan gum : Eudragit L100 : EC 7 FP Premium at 75:35:40).

terms followed by predominance of diffusion term due to hydrogel formed upon complete hydration of xanthan gum. Xanthan gum forms smooth highly viscous hydrogel through which drug can diffuse, and thus it governs the constant drug release rate up to the end of the dissolution study.

7.3.2.2. SEM Study

The matrix surface can give idea about the hydrated gel structure as well as the possibility of drug release mechanism. Scanning electron micrographs of the J-34 after completion of dissolution study are shown in Figure 7.20 at different magnifications. The images shows the viscous hydrogel structure of xanthan gum. Its hydrogel is strong enough to control the polymer particle erosion of Eudragit L100 and hence continuous gel surface is observed in the micrographs. The pores created due to diffusion of nateglinide are clearly seen and confirms the diffusion as a major drug release mechanism from xanthan gum matrices.

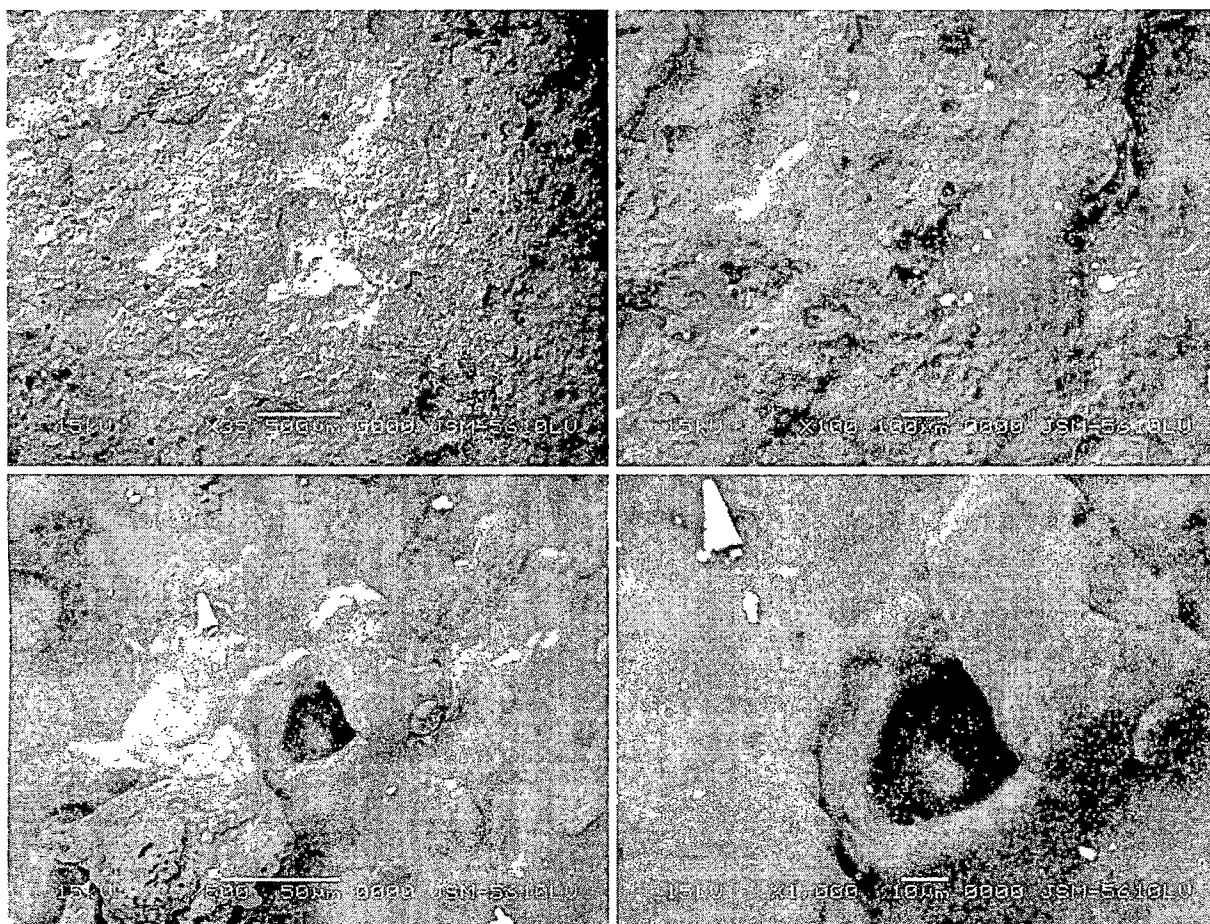


Figure 7.20. Scanning electron micrograph of J-34 after 12 h dissolution at different magnifications.

7.4. Alginate-Chitosan and Eudragit-HPMC Matrices

Protonal LF 120M, anionic sodium alginate forms ionotropic hydrogel in presence of cationic salts or other cationic polymer such as chitosan. Alginate-chitosan combinations were tried to check the ability of combined gel to sustain the nateglinide release.

7.4.1. IN VITRO DISSOLUTION & RELEASE KINETIC STUDIES

Cumulative Nateglinide release from the different combination of Protonal LF 120M : chitosan matrices with the other auxiliary additives – MCC PH301, Starch 1500 and Eudragit L100 are given in Figure 7.21. Looking at the matrices composition and their release profiles, it is obvious that the Protonal LF 120M and chitosan prepare extremely viscous gel. Further, the cations in dissolution medium strengthens it to such an extent that hardly up to 50 % of drug can release even in the presence of swelling or disintegration promoting excipients in the matrices (J-36 to J-38). However, it can be valuable in controlling the active

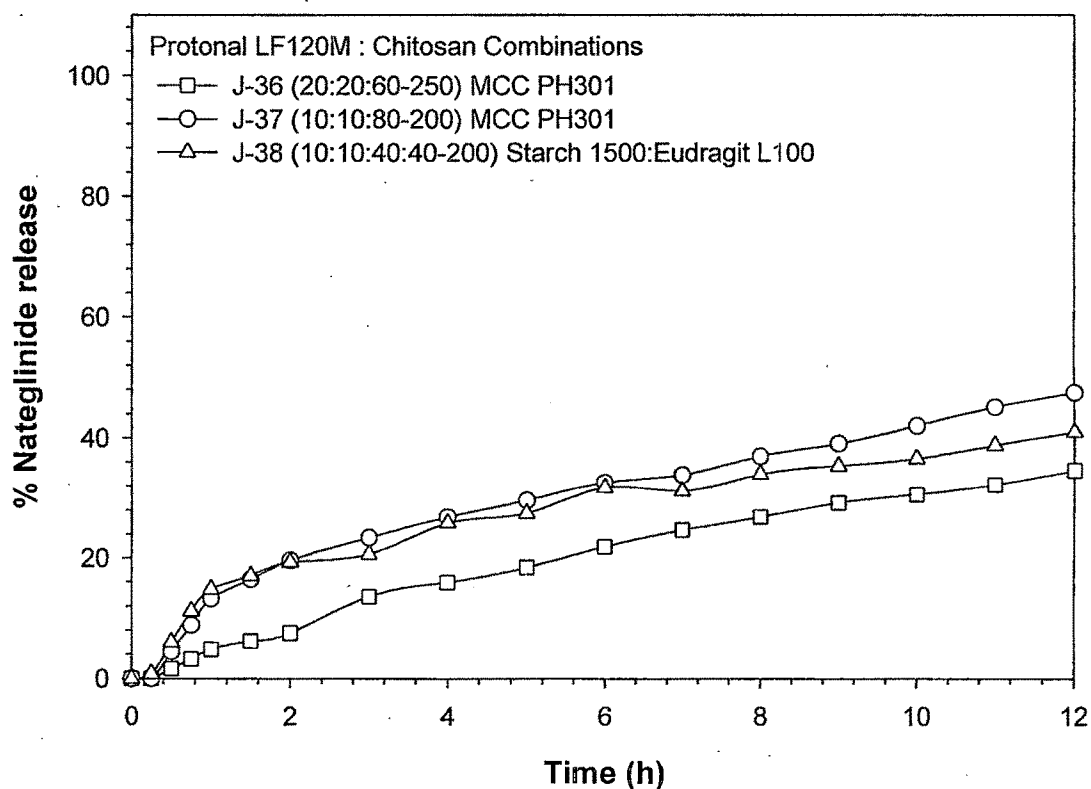


Figure 7.21. Influence of Protonal LF 120M : Chitosan : MCC PH301 / Starch 1500 / Eudragit L100 on nateglinide release profiles.

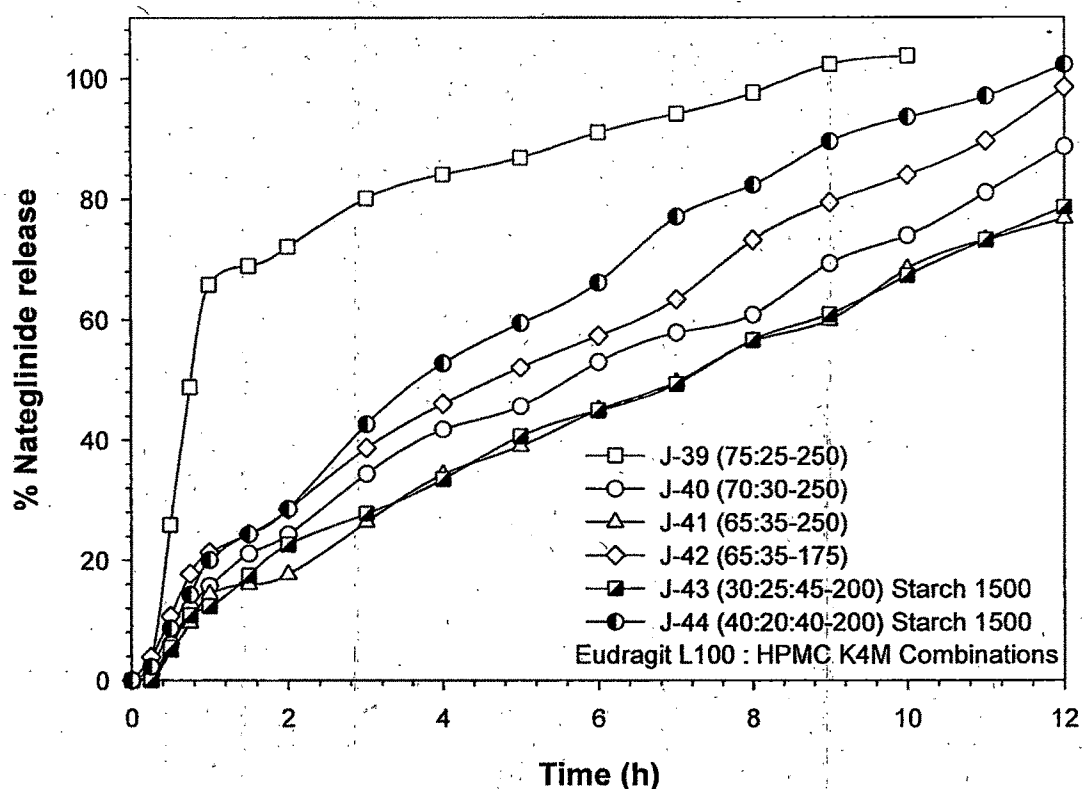


Figure 7.22. Influence of Eudragit L100 : HPMC K4M : Starch 1500 ratio at different polymer loading on nateglinide release profiles.

agent release for longer duration of time for other applications also. Drug release kinetic constants summarized in Table 7.4 suggests Hixson-Crowell as the best fit model for J-36, while Higuchi for J-37 and J-38.

As discussed above in carbopol-eudragit matrices, Eudragit L100 promotes the drug release via polymer particle erosion; its functionality was checked in HPMC based matrices. Nateglinide release profiles for the matrices prepared with HPMC K4M : Eudragit L100 at different polymer ratio and different polymer loading level are depicted in Figure 7.22. At constant total polymer loading, the increase in Eudragit L100 level results in decreased MDT_{50} and MDT_{80} (Table 7.4), indicating higher drug release rate due to higher degree of erosion from the outermost gel layer (see the release profiles for J-39 to J-41). Moreover, at the same polymer ratio, decrease in matrix loading gives overall higher drug release (compare the release profiles for J-41 and L-42) due to lower hydrogel tortuosity at lower matrix former concentration. Overall, higher drug release rate of J-44 as compared to J-43 is responsible for lower HPMC K4M and higher Eudragit L100 content of the formulation. Partial replacement of Starch 1500 in place of Eudragit L100 can make the formulation more economic without significant change in the formulation release kinetics. From this group of matrices (J-36 to J-44), two batches, J-42 and J-44 fits into the predetermined drug release constraints at all

Table 7.4. Comparison of drug release kinetics of different modalities for the in vitro nateglinide release, best fit model, MDT₅₀ and MDT₈₀ for batches J-36 to J-44.

Batch No	Release model											Best fit model	MDT ₅₀	MDT ₈₀
	Zero-order K_0	t_0	First-Order K_1	r_1	Higuchi matrix K_H	r_H	Korsmeyer-Peppas n	K_k	f_k	Hixson-Crowell K_s	r_s			
J-36	3.20	0.98	-0.04	0.99	9.01	0.96	-	-	-	-0.01	0.99	Hix.Crow.	-	-
J-37	4.40	0.91	-0.06	0.96	13.30	0.99	-	-	-	-0.02	0.95	Matrix	4.74	-
J-38	4.10	0.84	-0.05	0.90	12.04	0.99	0.74	8.19	0.89	-0.02	0.88	Matrix	-	-
J-39	15.32	0.23	-	-	39.66	0.90	0.64	34.85	0.80	-0.11	0.90	Matrix	0.48	0.84
J-40	7.83	0.98	-0.14	0.98	22.47	0.98	0.92	10.21	0.96	-0.04	0.99	Hix.Crow.	2.26	4.55
J-41	6.78	0.99	-0.11	0.99	19.79	0.97	-	-	-	-0.03	1.00	Hix.Crow.	3.01	5.51
J-42	8.91	0.97	-0.21	0.89	25.31	0.98	0.72	16.62	0.98	-0.05	0.97	Peppas	1.80	3.75
J-43	6.89	0.98	-0.12	0.99	20.02	0.97	-	-	-	-0.03	0.99	Hix.Crow.	2.88	5.40
J-44	9.93	0.96	-	-	27.94	0.98	0.86	14.45	0.98	-0.07	0.92	Matrix	1.68	3.17

time points and found to be optimized formulations. Drug release mechanism of both these formulations was studied in detail by Kopcha model analysis, swelling study and SEM analysis. As shown in Table 7.4 and Figure 7.22, the decrease in Eudragit L100 / HPMC K4M ratio shifts the drug release profiles from Higuchi's matrix type to Hixson-Crowell kinetics due to more linearization of dissolution curves. In vitro dissolution profiles of the optimized formulations, J-42 and J-44 fits into Korsmeyer-Peppas and Higuchi's square-root of time kinetics, respectively with non-fickian anomalous transport release mechanism ($0.5 < n < 1$, Table 7.4).

7.4.2. CHARACTERIZATION OF OPTIMIZED FORMULATIONS

From J-36 to J-44, in vitro dissolution of batch J-42 and J-44 passes all the constrains defined previously and found to be optimum. Since the rate of swelling and erosion determines the mechanism and kinetics of drug release these formulations were studied further for their swelling behavior and SEM analysis to confirm the relative contribution of diffusion and/or erosion by Kopcha model.

7.4.2.1. Release Mechanism by Kopcha Model

Figure 7.23 represents the results of Kopcha model analysis for J-42 and J-44. In both the case, diffusion increases initially and then takes over the erosion, followed by major drug release due to diffusion. In case of J-42, at the start of hydration process, the surface Eudragit L100 particles shows erosion and slight high drug release. Simultaneously HPMC starts to form hydrogel quickly to retard the drug release and within 2 hour HPMC mediated diffusion becomes higher and governs drug release up to the end of study. While in case of J-44, during 2-4

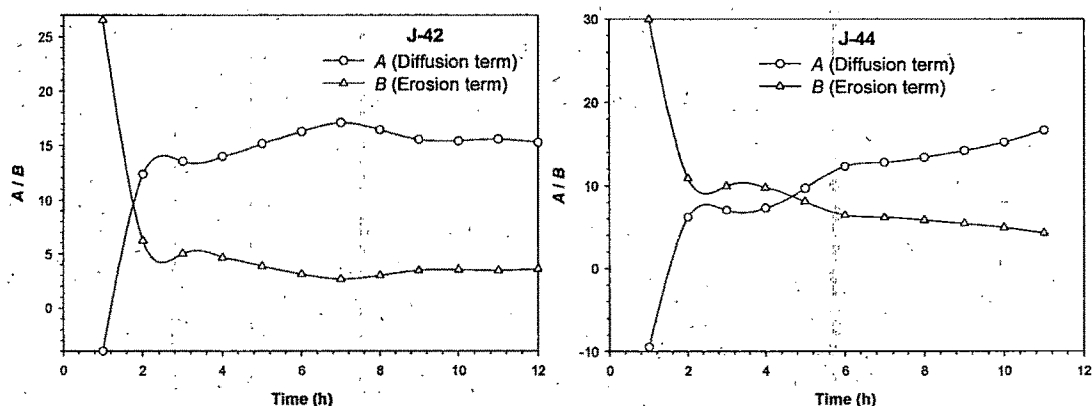


Figure 7.23. Kopcha model parameters (A and B) versus time profile for J-42 (Eudragit L100 : HPMC K4M at 114:61) and J-44 (Eudragit L100 : HPMC K4M : Starch 1500 at 80:40:80) formulations, respectively.

hour diffusion and erosion are almost equally contribute in nateglinide release. Finally, HPMC acts as major drug release retardant. In both the cases, at the end of dissolution study, the erosion term reaches almost zero level and drug release is solely by diffusion of nateglinide through unique HPMC hydrogel.

7.4.2.2. Swelling Study

Figure 7.24 shows the results of the axial and radial swelling as well as water uptake of batch J-42. In this case, all three parameters increase up to 12 hour and then gradually declines and it can be seen in the photographs attached herewith. Upon hydration, HPMC swells and forms hydrogel capable of retarding the drug release at almost constant rate by diffusion.

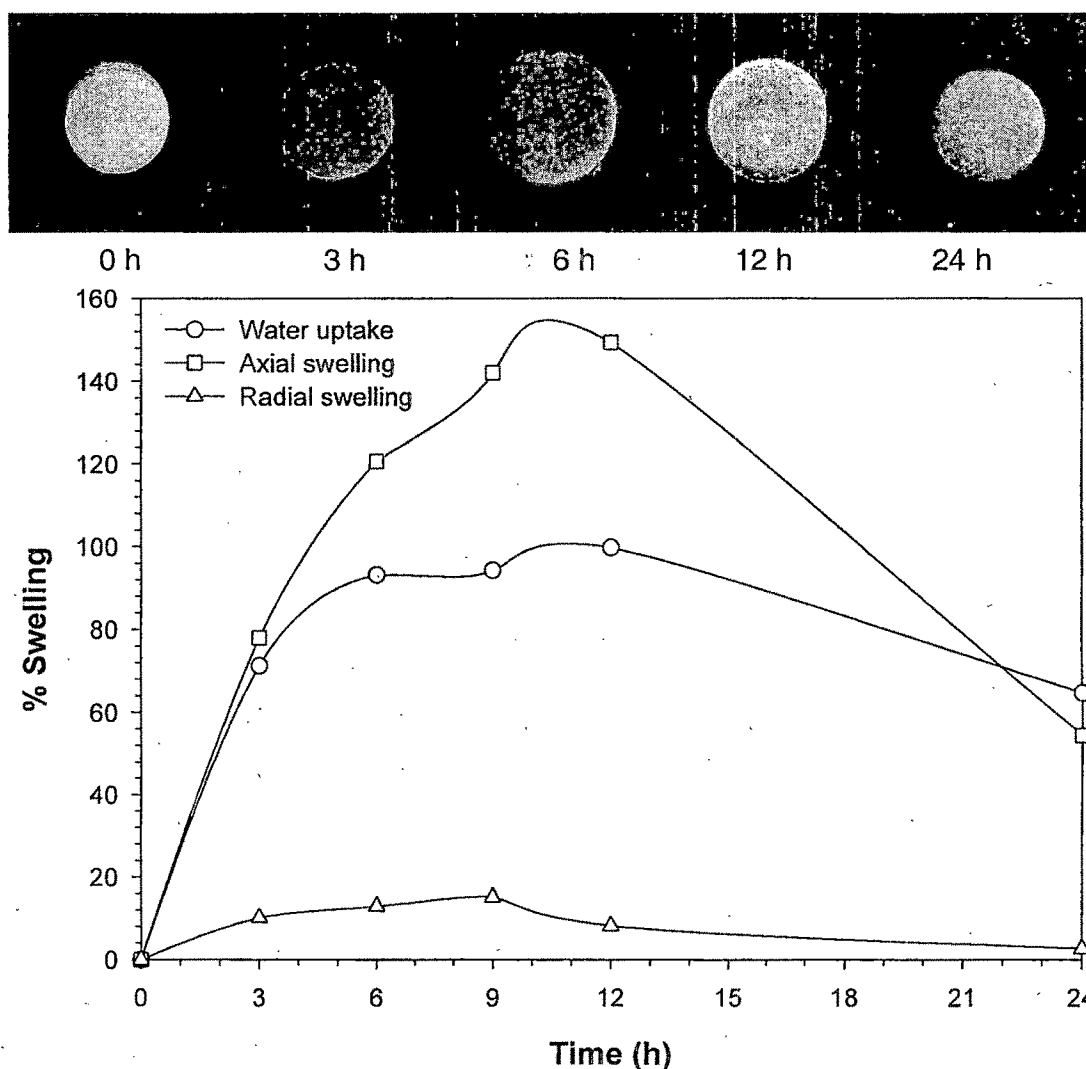


Figure 7.24. Percent water uptake, axial, and radial swelling results for J-42 formulation (Eudragit L100 : HPMC K4M at 114:61).

The swelling study results for batch J-44 are enumerated in Figure 7.25. As seen with other HPMC containing matrices, here also anisotropic swelling was observed. Upon hydration, progressive increase in the size of this hydrated layer results in axial and radial swelling up to 3 hour, followed by decline in radial expansion. However, matrices expand axially and water uptake remains almost constant until the end of study and it can be seen in photographs. As compared to J-20, fast expansion in axial and radial direction may be attributed to the presence of Starch 1500 and its swellable amylose fraction. HPMC gel prevents the polymer particle erosion of Eudragit L100 by forming strong hydrogel.

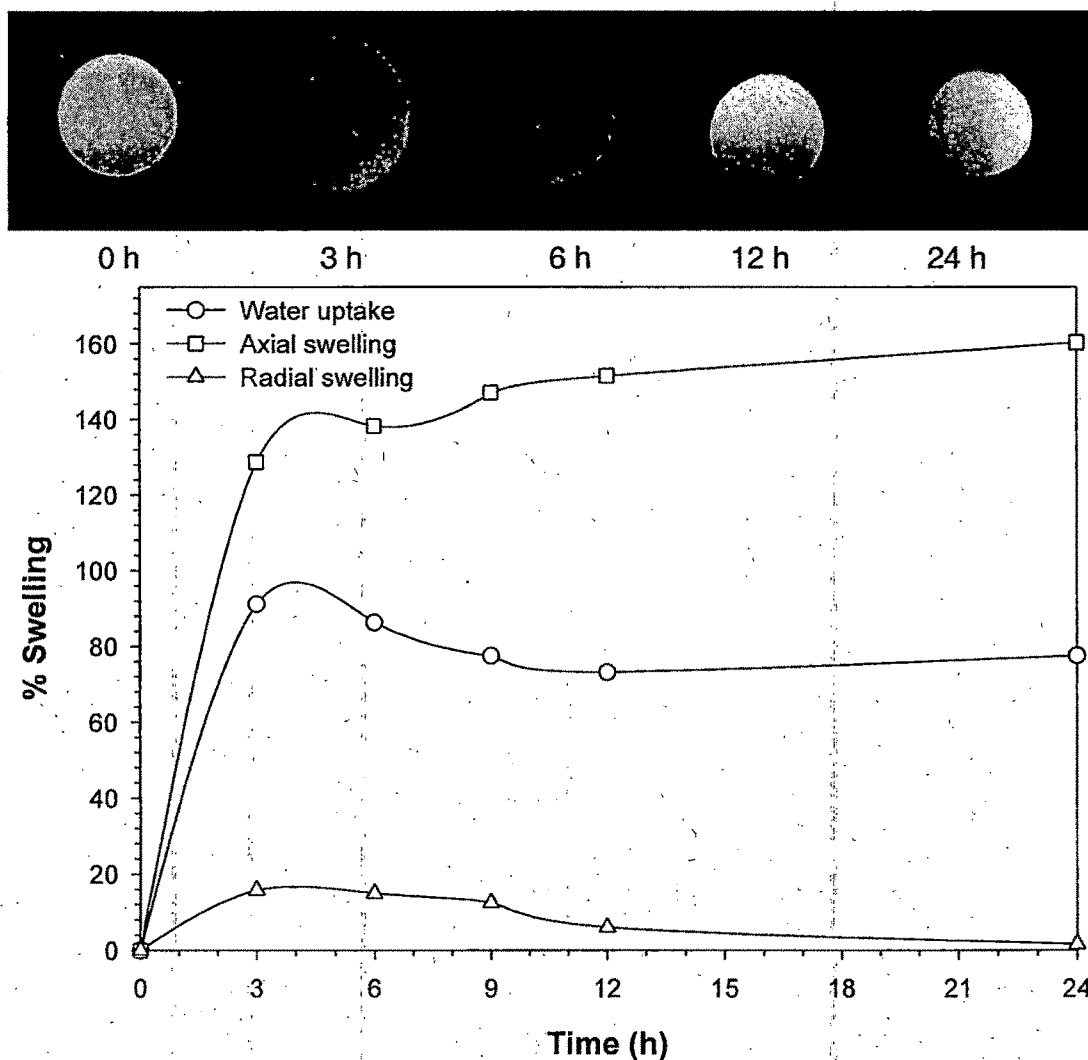


Figure 7.25. Percent water uptake, axial, and radial swelling results for J-44 formulation (Eudragit L100 : HPMC K4M : Starch 1500 at 80:40:80).

7.4.2.3. SEM Study

Figure 7.26 represents the SEM images of batch J-44. The combined HPMC-starch gel results in smooth viscous hydrogel through which drug can diffuse in a controlled manner. As with other HPMC matrices, the pores created by diffusion of drug are seen within the structure of this heterogeneous hydrogel. This is in accordance with the diffusion predominance at the end of dissolution study discussed in Kopcha model parameters analysis.

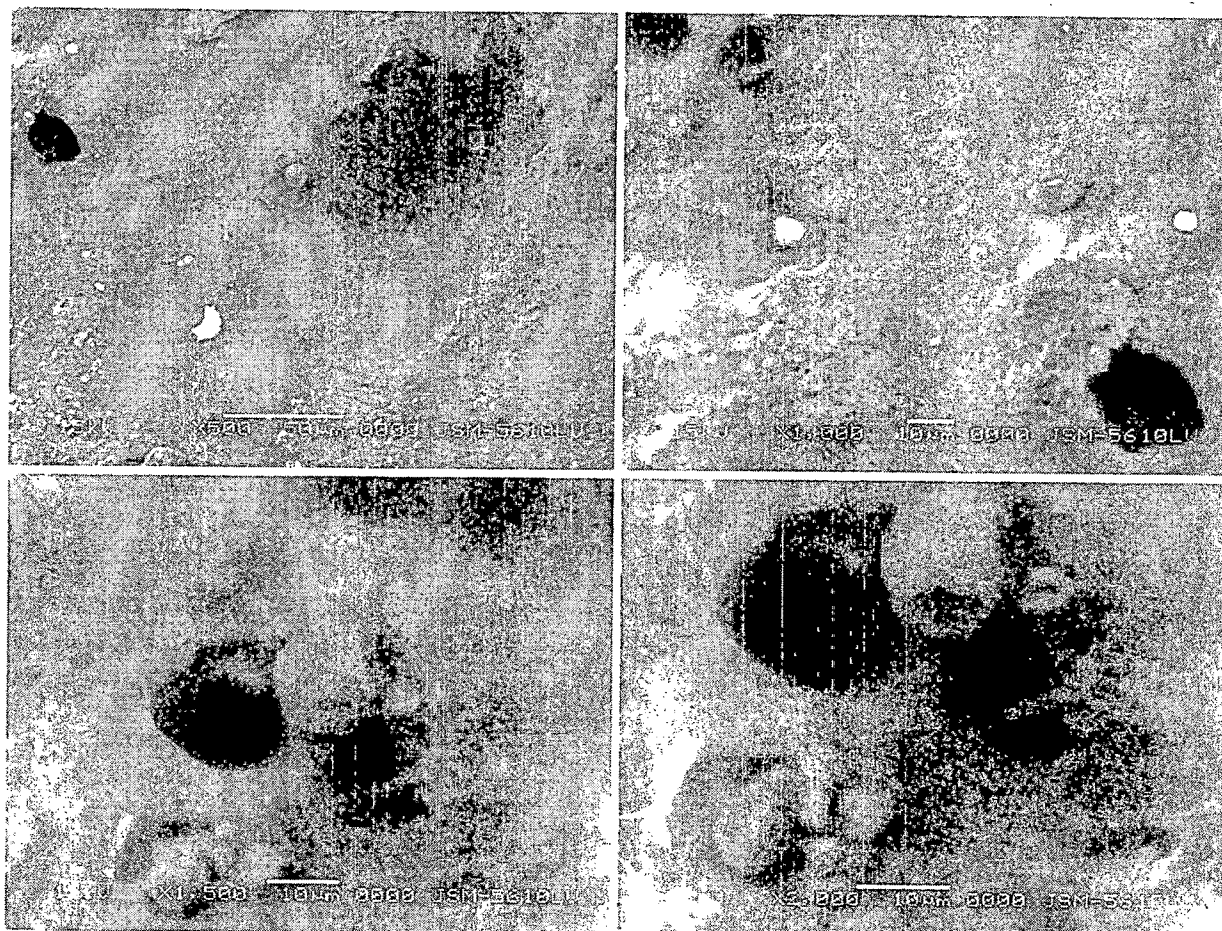


Figure 7.26. Scanning electron micrograph of J-44 after 12 h dissolution at different magnifications.

7.5. Stability Studies

All the optimized batches were subjected to accelerated stability study ($40 \pm 2^\circ\text{C}$ / $75 \pm 5\%$ RH) according to ICH guidelines. The accelerated stability data for all optimized formulations of both drugs showed no change in appearance and negligible variation (within ± 3 SD) over time for the parameters like weight

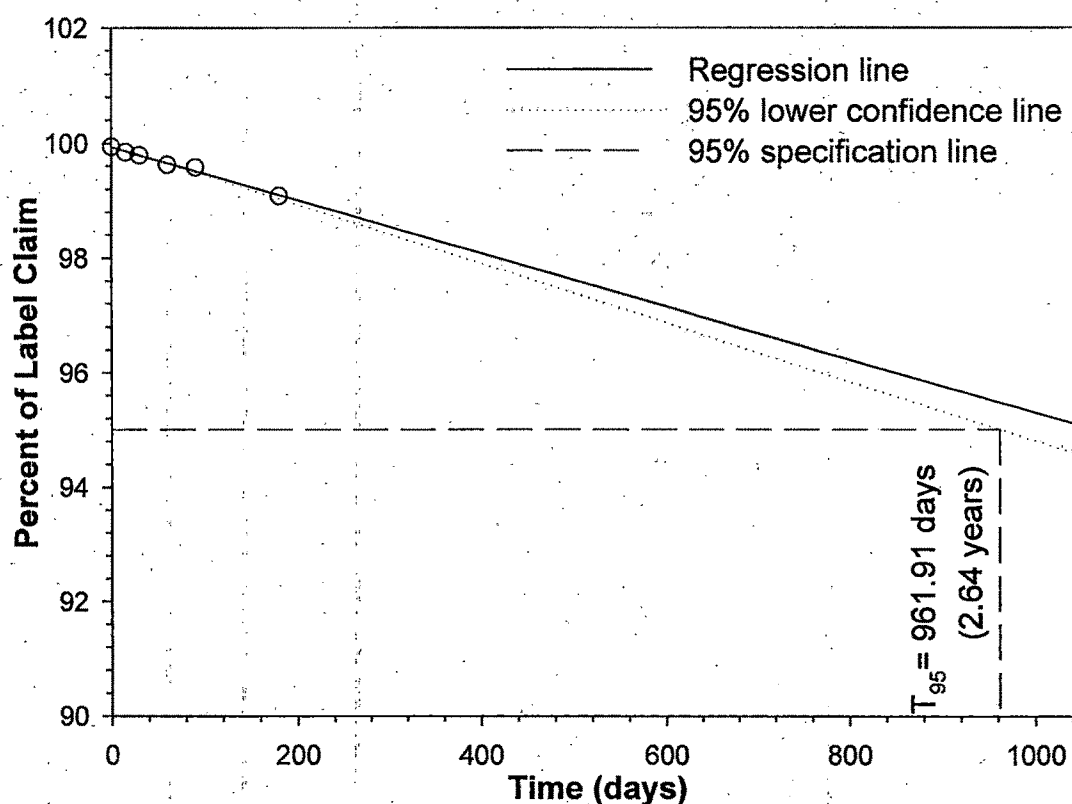


Figure 7.27. Extrapolation of accelerated stability study for determination of shelf-life for J-21 formulation.

variation, thickness, hardness, and drug content. 6 month accelerated data for the optimized formulations showed negligible change over time for the parameters like appearance, weight variation, thickness, hardness, and drug content. The similarity factor (f_2) was calculated by a comparison of the dissolution profile at each time points with the control at the initial condition. The f_2 factors obtained ranged from 82 to 92, with a 2 to 7% average difference, and the formulations were found to be stable. Shelf-life of optimized formulations were calculated by linear (zero-order) extrapolation of the accelerated stability data as discussed under 'Stability Studies' of 'Glipizide Matrices'. Shelf-life for J-11, J-16, J-20, J-21, J-23, J-34, J-42, and J-44 were found to be 2.73, 2.87, 3.06, 2.64, 2.98, 3.17, 2.95, and 3.22 years, respectively. The linear extrapolation of accelerated stability data for J-21 formulation is shown in Figure 7.27.

7.6. References

- BONDERONI, M. C., CARAMELLA, C., SANGALLI, M. E., CONTE, U., HERNANDEZ, R. M. and PEDRAZ, J. L., **1992**. Rheological behaviour of hydrophilic polymers and drug release from erodible matrices. *J. Controlled Rel.* 18, 205-212.
- BRABANDER, D. C., VERVAET, C. and REMON, J. P., **2003**. Development and evaluation of sustained release mini-matrices prepared via hot melt extrusion. *J. Controlled Rel.* 89, 235-247.
- CHEONG, L. W. S., HENG, P. W. S. and WONG, L. F., **1992**. Relationship between polymer viscosity and drug release from a matrix system. *Pharm Research* 9 (11), 1510-1514.
- DURIG, T. and FASSIHI, R., **2002**. Guar-based monolithic matrix systems: effect of ionizable and non-ionizable substances and excipients on gel dynamics and release kinetics. *J. Controlled Rel.* 80, 45-56.
- HARLAND, R. S., GAZZANIGA, A., SANGALLI, M. E., COLOMBO, P. and PEPPAS, N. A., **1988**. Drug/polymer matrix swelling and dissolution. *Pharm Research* 5, 488-494.
- JU, R. T. C., NIXON, P. R. and PATEL, M. V., **1995**. Drug release from hydrophilic matrices 1. New scaling laws for predicting polymer and drug release based on the polymer disentanglement concentration and the diffusion layer. *J. Pharm. Sci.* 84, 1455-1463.
- LINDNER, W. D. and LIPPOLD, B. C., **1995**. Drug release from hydrocolloid embeddings with high or low susceptibility to hydrodynamic stress. *Pharmaceutical Research* 12, 1781-1785.
- MICHAILOVA, V., TITEVA, S., KOTSILKOVA, R., KRUSTEVA, E. and MINKOV, E., **2000**. Water uptake and relaxation processes in mixed unlimited swelling hydrogels. *Int. J. Pharm.* 209, 45-56.
- NOVEON BULLETIN, **2002**. Pharmaceutical Polymers - Product and Regulatory Guide, Pharmaceutical Polymers - Product and Regulatory Guide, B F Goodrich Company, Noveon - The Specialty Chemicals Innovator, Cleveland, OH, Bulletin -2.
- PAPADIMITRIOU, E., BUCKTON, G. and EFENTAKIS, M., **1993**. Probing the mechanisms of swelling of hydroxypropyl methylcellulose matrices. *Int. J. Pharm.* 98, 57-62.
- PICKER, K. M., **1999**. The use of carrageenan in mixture with microcrystalline cellulose and its functionality for making tablets. *Eur. J. Pharm. Biopharm.* 48, 27-36.
- SHANGRAW, R. F., **1989**. Compressed tablets by Direct Compression. in: LIEBERMAN, H. A., LACHMAN, L. and SCHWARTZ, J. B. (Eds.), *Pharmaceutical Dosage Forms: Tablets*, 2nd Ed., Vol. 1, Marcel Dekker, Inc., New York and Basel, pp. 195-246.
- ZULEGER, S. and LIPPOLD, B. C., **2001**. Polymer particle erosion controlling drug release. I. Factors influencing drug release and characterization of the release mechanism. *Int. J. Pharm.* 217, 139-152.

8. IN VIVO STUDY

In vitro – in vivo correlations (IVIVCs) can decrease regulatory burden by decreasing the number of biostudies required in support of a drug product. IVIVC can impart in vivo meaning to the in vitro dissolution test and can be useful as surrogate for bioequivalence. Further, IVIVC can also allow setting of more meaningful dissolution specifications. Both the regulatory agencies and industry sponsors have understood this value of IVIVCs. Therefore, the activity in the area of IVIVC for oral extended release dosage forms has increased in the last 5 years (Uppoor, 2001).

From the list of optimized formulations, selected batches were subjected to in vivo study to establish IVIVC. Pharmacokinetic parameters for glipizide containing matrices M-3 (HPMC K4M : MCC PH301 at 25:75), M-25 (HPMC K4M : MCC PH301 : Starch 1500 at 25:30:45), M-75 (xanthan gum : HPMC K4M : Starch 1500 at 70:25:15), and M-120^o (Eudragit L100 : HPMC K4M at 75:25) were compared with that of the marketed sustained release formulation Glytop[®] 2.5 SR. Similarly, results of in vivo study of nateglinide containing matrices J-11 (HPMC K4M : MCC PH301 at 62.5:187.5) and J-21 (Carbopol 934P : Eudragit L100 at 70:130) were compared with that of marketed immediate release formulations Natelide[®] 60.

8.1. Pharmacokinetic study of M-3 Matrices

As compared to initial IVIVC development and evaluation of predictability using single batch, more additional data may be needed to define the IVIVC's predictability completely. Some combination of three or more formulations with adequate different (e.g. by 10%) release rates is considered optimal (US FDA CDER Guidance for the Industry, 1997). Out of the 9 batches (A-1 to A-9) of HPMC K4M : MCC PH301 system studied using 3² full factorial design, three batches namely A-3, A-6 (\approx M-3), and A-4 exhibited the slow, medium, and fast release profile, respectively. Hence, these three batches were selected for establishment of IVIVC according to US FDA guidelines.

8.1.1. DRUG ABSORPTION STUDY IN RABBITS AND PHARMACOKINETIC ANALYSIS

Based on the in vitro release profiles, following three formulations of HPMC K4M : MCC PH301 combinations studied by 3² full factorial design were selected for establishing IVIVC according to USFDA guidelines (1997a): slow (A-3), medium

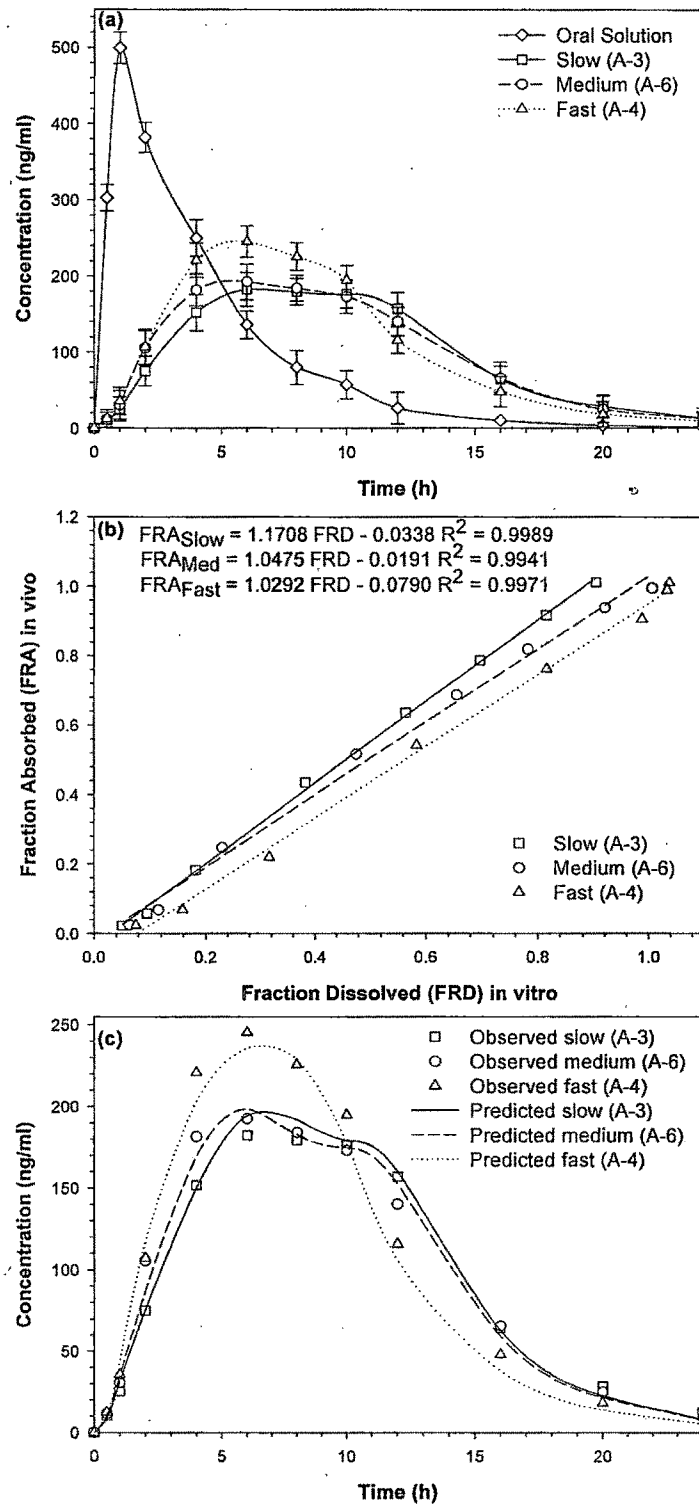


Figure 8.1. (a) Mean plasma glipizide concentration vs. time profile after administration of single dose of oral solution, slow (M-3), medium (M-6), and fast (M-4) release tablet in white albino rabbits. Each value represents the mean ($n=3$) (b) Fraction absorbed (FRA) in vivo vs. fraction dissolved (FRD) in vitro for establishment of IVIVC for slow, medium, and fast release tablet. (c) Comparison of observed and predicted plasma profile of slow, medium, and fast release formulation.

(A-6 which is same as M-3), and fast (A-4) release rate matrix tablets. For pharmacokinetic study, the developed matrix tablets were administered orally to white albino rabbits. The drug plasma concentrations for matrix tablets were monitored for 24 h and that for the oral solution was monitored for 12 h as shown in Figure 8.1 (a). The glipizide plasma profile following oral solution after 12 h was below LoQ and hence the same for 16, 20, and 24 h were extrapolated using $A \cdot e^{-k_e t}$, where A is the intercept of the terminal elimination regression line of the ln(concentration) vs. time profile. The mean glipizide pharmacokinetic parameters for oral solution and matrix tablets are summarized in Table 8.1. The results were calculated from plasma drug concentration data by non-compartmental analysis. The rapid decrease in glipizide concentration after oral solution administration reflects the fast disposition and elimination of the drug. The pharmacokinetic parameters like C_{max} and MRT as well as the plasma concentration–time profiles of glipizide explicitly indicate that all three matrix tablets sustained the absorption of glipizide as compare to oral solution. Though the AUC of glipizide for matrix tablets were comparable with each other, the C_{max} and k_a for A-3 < A-6 < A-4, and MRT for A-3 > A-6 > A-4, which reflect the difference in the release rate kinetics of glipizide between them.

Table 8.1. Observed and predicted pharmacokinetic parameters of glipizide after administration oral solution and sustained release matrix tablets to white albino rabbits.

Formulation	$AUC_{0-\infty}$ (ng·h/ml)			C_{max} (ng/ml)			T_{max} (h)	MRT (h)	k_a (h^{-1})	k_e (h^{-1})
	Observed	Predicted	PE (%)	Observed	Predicted	PE (%)				
Oral sol ⁿ	2287.51	-	-	499.41	-	-	1	4.21	0.59	0.26
A-3 Slow)	2452.29	2456.30	-0.16	182.30	194.41	-6.64	6	9.53	0.31	0.19
A-6 (Med)	2526.04	2449.98	3.01	192.49	198.41	-3.08	6	9.10	0.32	0.19
A-4 (Fast)	2646.86	2463.84	6.91	245.34	235.73	3.92	6	8.37	0.41	0.22

Each value represents the mean of three rabbits.

8.1.2. ESTABLISHMENT OF IVIVC

It is necessary to establish an in vitro test method that can predict the progress of drug release and the absorption of products in vivo (Varshosaz et al., 2000), particularly during the development of an innovative dosage form. In the present study, the in vivo absorption profiles of developed formulations were deconvoluted using Wagner-Nelson method as described above. The possibility of developing a level A IVIVC between the in vitro fraction dissolved (FRD) and the in vivo fraction absorbed (FRA) for matrix tablets was investigated using linear and nonlinear regression. As can be seen from Figure 8.1 (b), a good linear point-to-point relationships were observed for A-3 ($r^2=0.9989$), A-6 ($r^2=0.9941$),

and A-4 ($r^2=0.9971$) formulations with slope approaching to unity, indicating a close correlation between the in vitro release rate with their in vivo absorption.

8.1.3. INTERNAL VALIDATION OF IVIVC

The validity of correlations was assessed by determining how well the IVIVC models could predict the rate and extent of glipizide absorption as characterized by C_{max} and $AUC_{0-\infty}$. The predicted and observed values for these criteria as well as the calculated % prediction error (PE) are listed in the Table 8.1. The predicted C_{max} values were found to be very close to the observed mean values as can be seen by very low prediction errors for the slow (6.64%), medium (3.08%), and fast (3.92%) formulations. Similarly, the PE for observed mean and predicted $AUC_{0-\infty}$ values were 0.16, 3.01, and 6.91% for slow, medium and fast release rate formulations, respectively. The percent PE values were within the acceptable range of FDA guidance of IVIVC. The results of internal predictability is depicted graphically in Figure 8.1 (c), and revealed that the predicted profiles were comparable to the observed profiles for all three formulations. The established IVIVC confirms the efficacy of this in vitro model in simulating in vivo conditions.

8.2. Pharmacokinetic study of Glytop-2.5 SR, M-25, M-75 and M-120 Matrices

Initial IVIVC development and evaluation of predictability using single batch was carried out for Glytop 2.5 SR, M-25, M-75, and M-120 tablets. A group of three white albino rabbits was used for each formulation selected. Figure 8.2 represents (a) Mean plasma glipizide concentration vs. time profile after administration of single dose of oral solution and Glytop 2.5 SR in white albino rabbits including predicted plasma concentrations for Glytop 2.5 SR (b) $\ln(C_p)$ vs. time curves for estimation of K_e and K_a . (c) Fraction dissolved (FRD) in vitro vs. fraction absorbed (FRA) in vivo for establishment of IVIVC for Glytop 2.5 SR. Similar pharmacokinetic details for M-25, M-75, and M-120 are depicted in Figure 8.3; Figure 8.4, and Figure 8.5, respectively. Whereas, comparative results of observed and convolution predicted $AUC_{0-\infty}$ and C_{max} with other pharmacokinetic parameters are enumerated in Table 8.2. The pharmacokinetic parameters, grouped in Table 8.2, were calculated using a non-compartmental approach. The absorption parameters were calculated by the residual method (Bourne, 2002) and C_{max} and t_{max} were estimated directly from the plasma profiles.

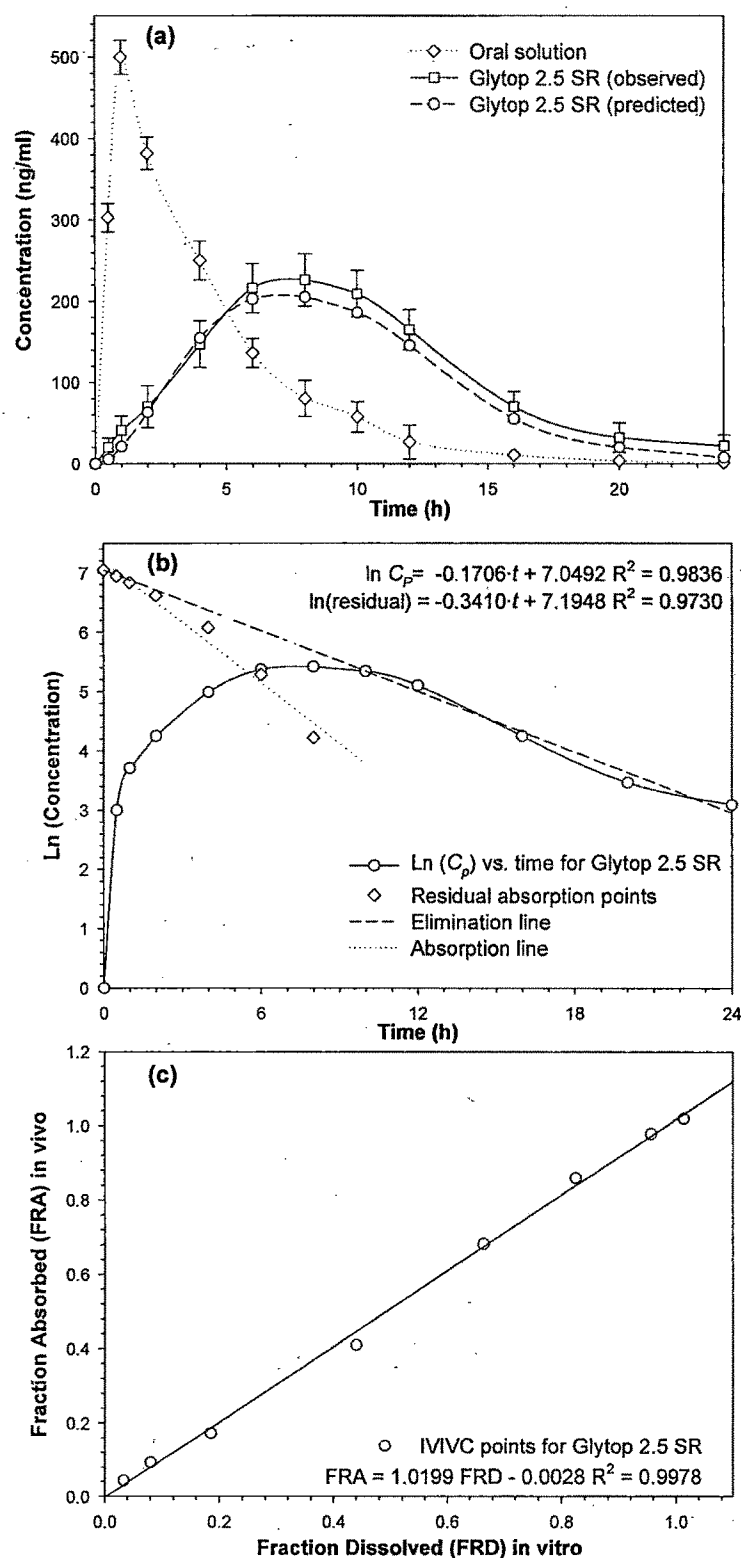


Figure 8.2. (a) Mean plasma glipizide concentration vs. time profile after administration of single dose of oral solution and Glytop-2.5 SR in white albino rabbits including predicted plasma concentrations for Glytop-2.5 SR. (b) Ln (C_p) vs. time curves for estimation of K_e and K_a . (c) Fraction dissolved (FRD) in vitro vs. fraction absorbed (FRA) in vivo for establishment of IVIVC for Glytop-2.5 SR.

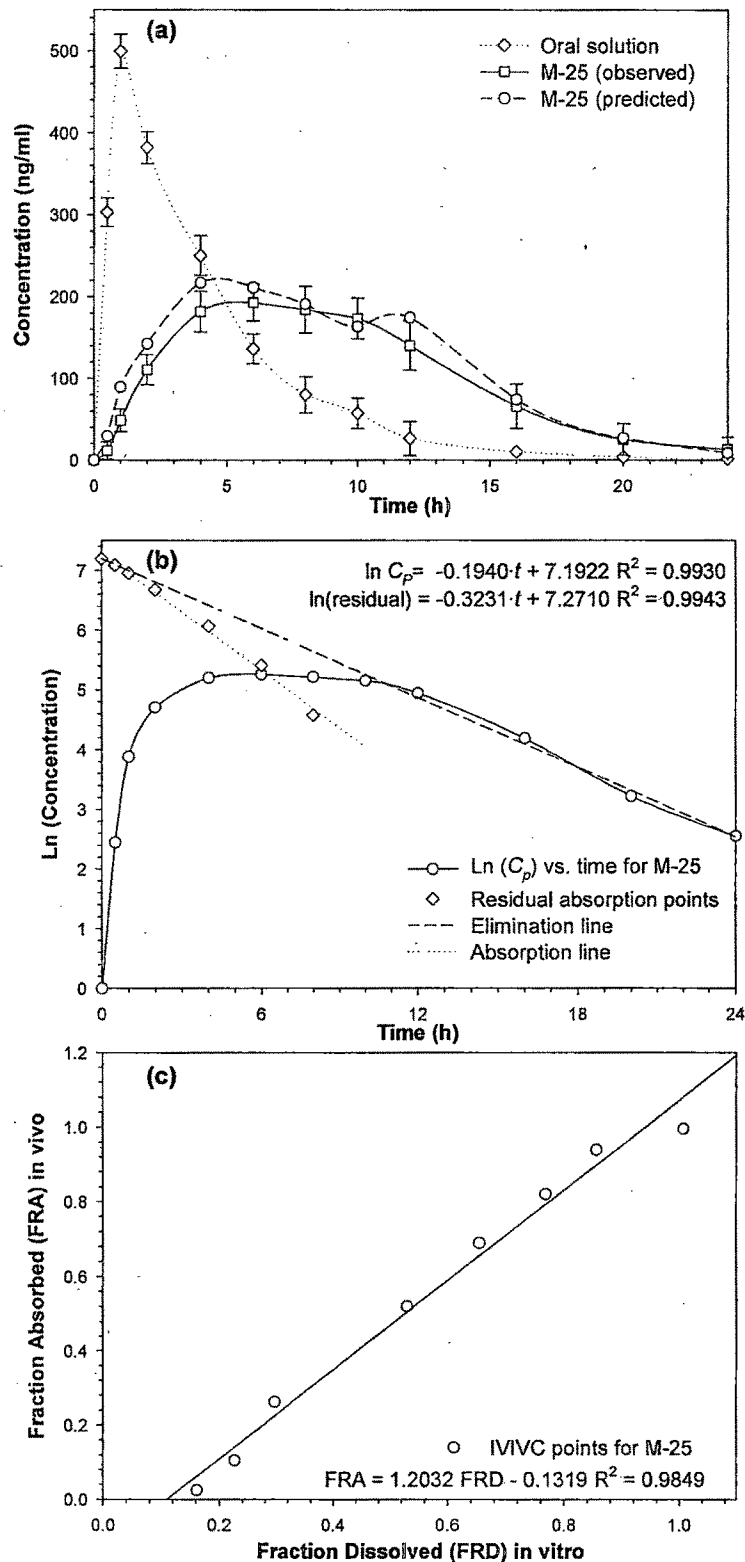


Figure 8.3. (a) Mean plasma glipizide concentration vs. time profile after administration of single dose of oral solution and M-25 in white albino rabbits including predicted plasma concentrations for M-25 (b) $\ln(C_p)$ vs. time curves for estimation of K_e and K_a . (c) Fraction dissolved (FRD) in vitro vs. fraction absorbed (FRA) in vivo for establishment of IVIVC for M-25.

Glipizide plasma concentration vs. time curve after administration of M-25 is shown in Figure 8.3 (a). In vivo absorption profiles were also calculated by means of deconvolution method and obtained fraction absorbed in vivo (FRA) were also compared with their fraction dissolved in vitro (FRD) for each matrix system as shown in Figure 8.3 (c). Good point-to-point relationship was observed for M-25 matrices with regression coefficient of 0.9849. The reliability of the developed IVIVC model was evaluated by using the internal predictability procedure as described in relevant regulatory guidance (US FDA CDER Guidance for the Industry, 1997). According to it, the permissible % prediction error (PE) values for C_{max} and AUC should be less than $\pm 15\%$ for each product and less than 10% for the average. Data from oral solution was used as the impulse function during numerical convolution. As seen from the results, the IVIVC model fulfilled these criteria (Table 8.2) and the result for the internal predictability is depicted graphically in Figure 8.3(c). The established IVIVC was of level A, which confirms the efficacy of this in vitro model in simulating in vivo conditions. This kind of correlation is quite important since it represents a point-to-point relationship between in vitro dissolution and the in vivo input rate of the drug from the dosage form (Cardot and Beyssac, 1993).

The results of pharmacokinetic parameters for M-75 and M-120 are summarized in Table 8.2. All three developed directly compressed sustained release glipizide hydrophilic matrices showed comparable in vitro and in vivo profiles with respect to marketed sustained release formulation. There are negligible variations in T_{max} and MRT of prepared matrices, which could reflect the difference seen between their in vitro release kinetics and confirms that prepared sustained release matrix is able to modify drug release from tablets in vivo also. It can be considered that directly compressed matrices successfully maintained AUC of glipizide, also suggesting that it was absorbed almost completely during transit through the gastrointestinal tract. Results of internal predictability revealed that the predicted profiles were comparable to the observed profiles of the developed and reference formulations.

Table 8.2. Observed and predicted pharmacokinetic parameters of glipizide after administration oral solution, Glytop 2.5 SR tablet (market sample), prepared sustained release matrices M-25, M-75 and M-120 to white albino rabbits.

Formulation	$AUC_{0-\infty}$ (ng·h/ml)			C_{max} (ng/ml)			T_{max} (h)	MRT (h)	k_a (h^{-1})	k_e (h^{-1})
	Observed	Predicted	PE (%)	Observed	Predicted	PE (%)				
Glytop SR	2817.68	2402.23	14.74	226.00	204.91	9.33	8	9.61	0.34	0.17
M-25	2547.12	2847.13	-11.78	192.49	217.08	-12.77	6	9.04	0.32	0.19
M-75	2754.57	2349.81	14.69	191.36	180.83	5.51	6	9.72	0.30	0.16
M-120	2962.15	2582.58	12.81	239.00	194.97	18.42	10	10.03	0.29	0.18

Each value represents the mean of three rabbits.

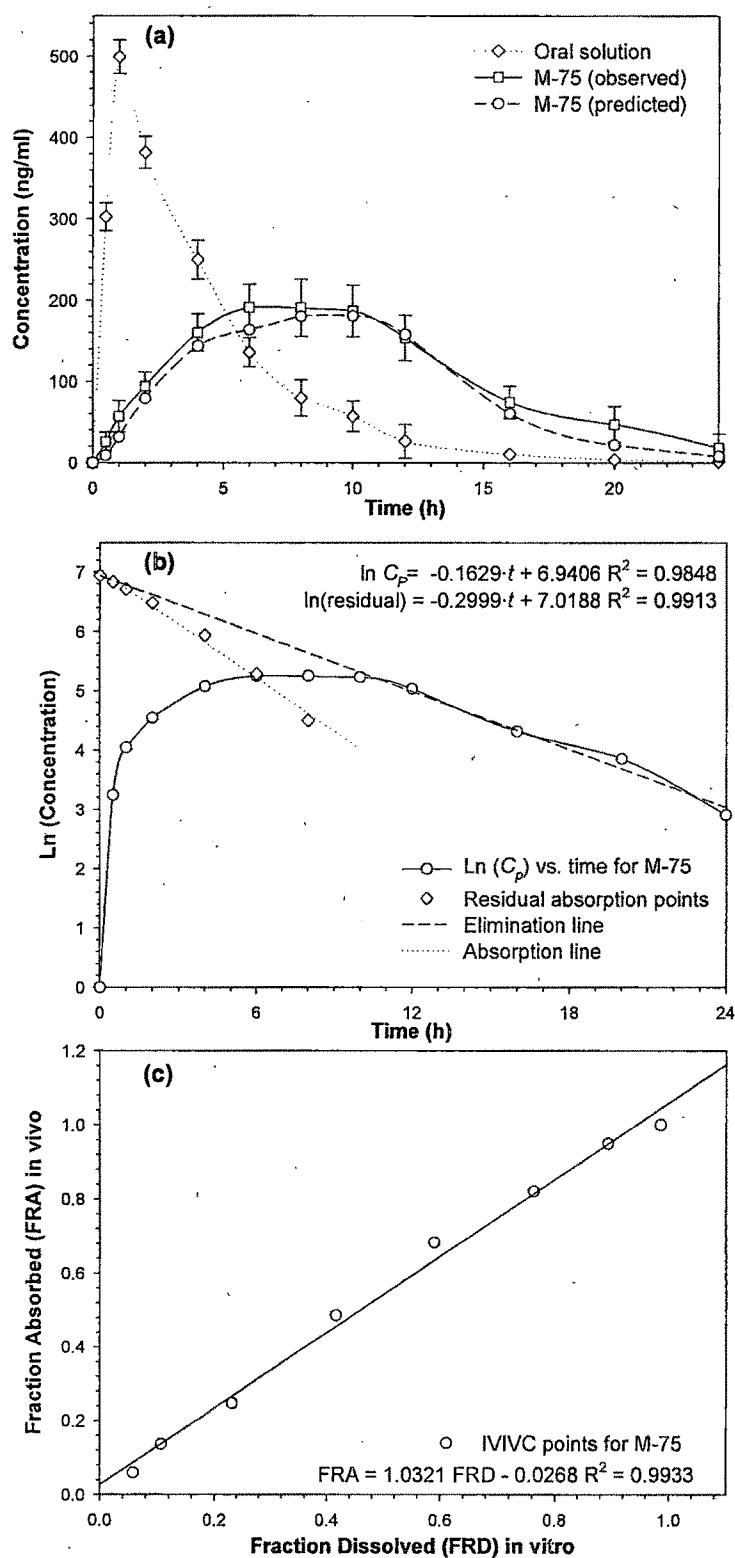


Figure 8.4. (a) Mean plasma glipizide concentration vs. time profile after administration of single dose of oral solution and M-75 in white albino rabbits including predicted plasma concentrations for M-75 (b) $\ln(C_p)$ vs. time curves for estimation of K_e and K_a . (c) Fraction dissolved (FRD) in vitro vs. fraction absorbed (FRA) in vivo for establishment of IVIVC for M-75.

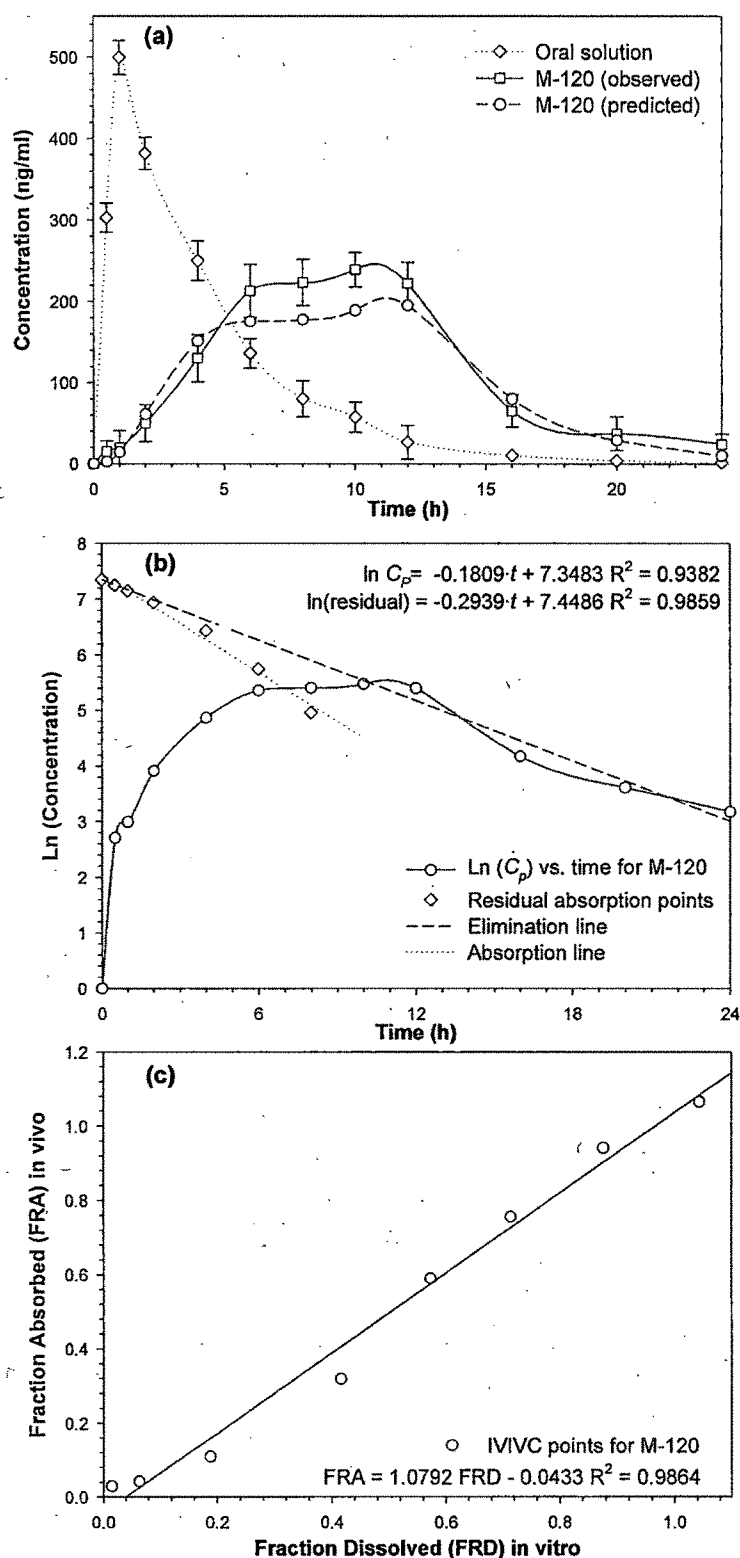


Figure 8.5. (a) Mean plasma glipizide concentration vs. time profile after administration of single dose of oral solution and M-120 in white albino rabbits including predicted plasma concentrations for M-120 (b) $\ln(C_p)$ vs. time curves for estimation of K_e and K_a . (c) Fraction dissolved (FRD) in vitro vs. fraction absorbed (FRA) in vivo for establishment of IVIVC for M-120.

8.3. Pharmacokinetic study of Natelide-60, J-11 and J-21 Matrices

In vivo oral absorption of nateglinide from the two different directly compressed matrices (J-11 and J-21) was evaluated under the fasted condition. Similarly, immediate release marketed preparation Natelide-60 is also included in the study for the comparison of drug release kinetics in vivo.

The mean plasma concentration–time profiles of nateglinide explicitly indicate that both J-11 and J-21 successfully sustained the absorption of nateglinide as shown in Figure 8.6 (a and b) and Figure 8.7 (a and b), respectively. Both matrices significantly delayed T_{max} and prolonged MRT (Table 8.3), compared with immediate release tablets-Natelide 60, indicating that sustained release of nateglinide from directly compressed matrices successfully resulted in the sustained absorption of nateglinide in vivo. The sustained plasma level was due to the constant release pattern of the matrix systems in vivo. The absorption parameters were calculated by method of residuals (Bourne, 2002). The absorption and pharmacokinetic parameters following administration of the marketed nateglinide immediate release (Natelide-60) and developed matrices J-11 and J-21 are summarized in Table 8.3. The In vivo absorption profiles of developed matrices were deconvoluted using Wagner-Nelson model (Bourne, 2002). When fraction released in vitro (FRD) was plotted against fraction in vivo input (FRA) to seek an IVIVC as shown in Figure 8.6 (c) and Figure 8.7 (c), a linear correlation with a slope close to unity and intercept close to zero was obtained ($r^2 > 0.99$), indicating a close correlations for J-11 and J-21, respectively. Further, to assess the predictability and the validity of the correlations, we determined the observed and IVIVC model-predicted C_{max} and AUC values for each formulation (internal validation of IVIVC model). The percent PE ($\pm 15\%$) for both parameters are summarized in Table 8.3 and Figure 8.6 (a) and Figure 8.7 (a). Data from immediate release marketed formulation was used as the impulse function during numerical convolution. Overall, the pharmacokinetic parameters for J-11 and J-21 were almost comparable with each other and can be reasoned that the in vitro dissolution profiles of both batches are close to each other and fits within the constraints selected.

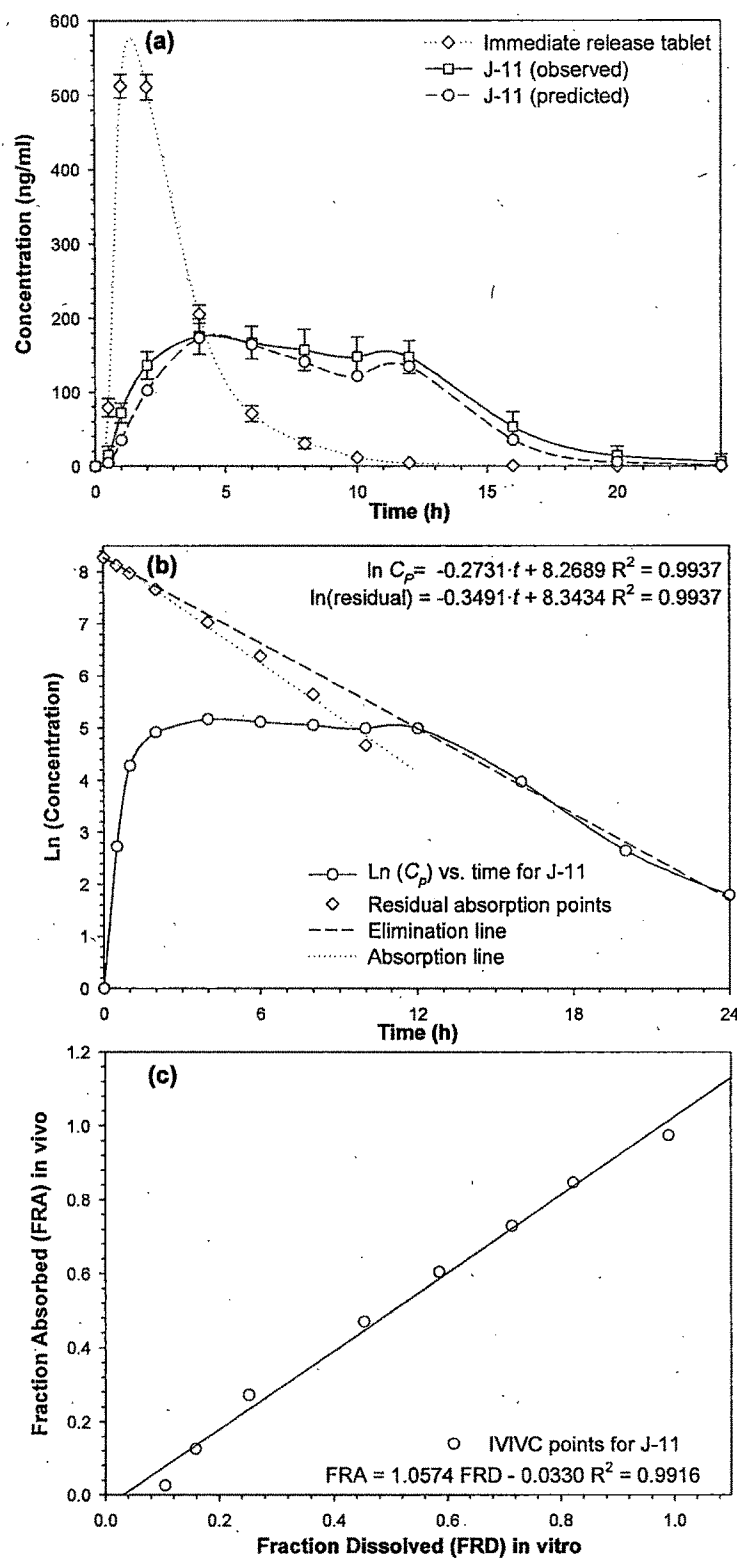


Figure 8.6. (a) Mean plasma nateglinide concentration vs. time profile after administration of single dose of immediate release market formulation and J-11 in white albino rabbits including predicted plasma concentrations for J-11 (b) $\ln(C_p)$ vs. time curves for estimation of K_e and K_a . (c) Fraction dissolved (FRD) in vitro vs. fraction absorbed (FRA) in vivo for establishment of IVIVC for J-11.

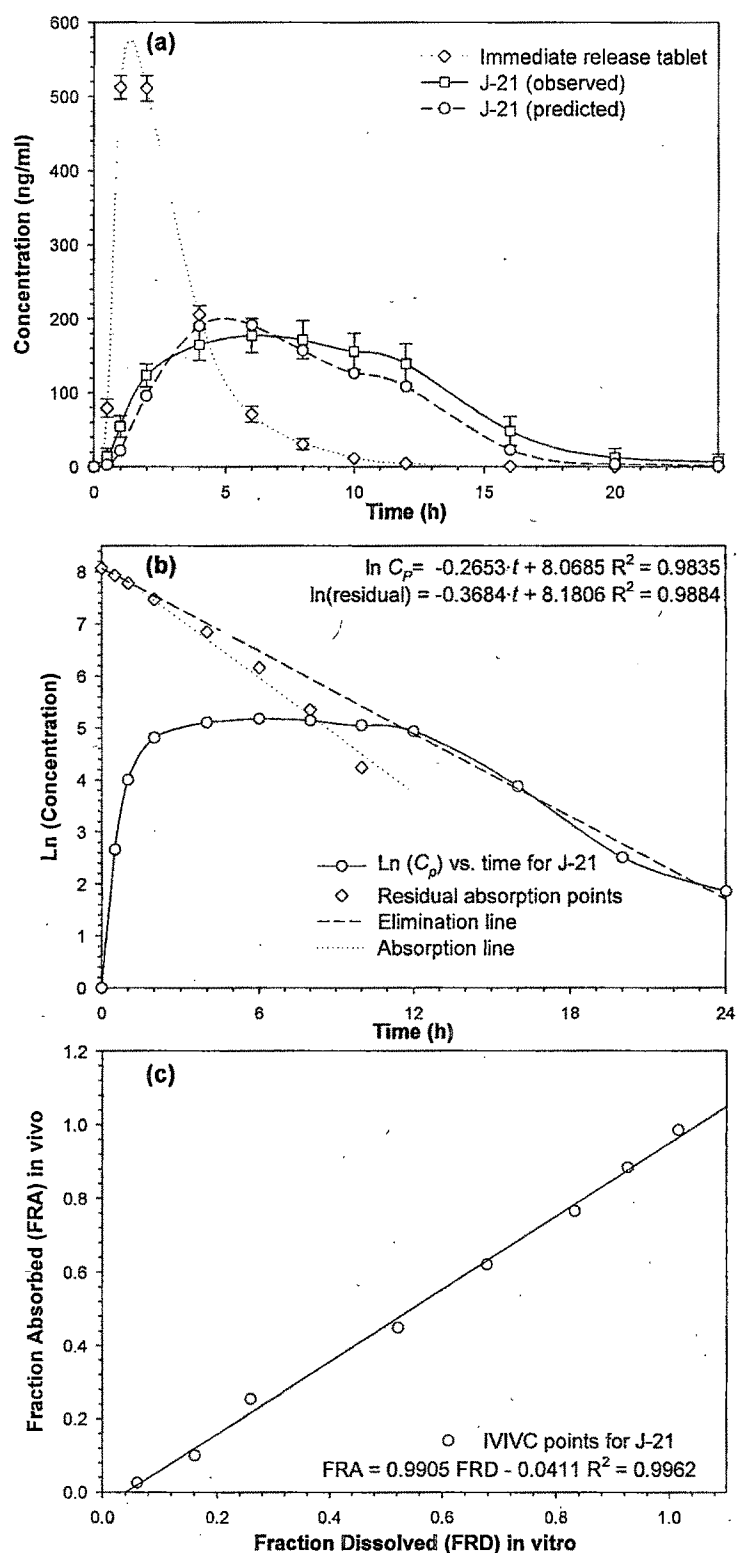


Figure 8.7. (a) Mean plasma nateglinide concentration vs. time profile after administration of single dose of immediate release market formulation and J-21 in white albino rabbits including predicted plasma concentrations for J-21 (b) $\ln(C_p)$ vs. time curves for estimation of K_e and K_a . (c) Fraction dissolved (FRD) in vitro vs. fraction absorbed (FRA) in vivo for establishment of IVIVC for J-21.

Table 8.3. Observed and predicted pharmacokinetic parameters of glipizide after administration oral solution, Glytop 2.5 SR tablet (market sample), prepared sustained release matrices M-25, M-75 and M-120 to white albino rabbits.

Formulation	$AUC_{0-\infty}$ (ng·h/ml)			C_{max} (ng/ml)			T_{max} (h)	MRT (h)	k_a (h^{-1})	k_e (h^{-1})
	Observed	Predicted	PE (%)	Observed	Predicted	PE (%)				
Natelite-60 [®]	1843.71	-	-	512.40	-	-	1	2.91	1.45	0.48
J-11	2307.12	1955.92	15.22	175.66	173.25	1.37	4	8.52	0.35	0.27
J-21	2244.14	2244.14	12.83	185.78	194.54	-4.71	6	8.40	0.37	0.26

Each value represents the mean of three rabbits.

After internal validation of developed IVIVC model, in vitro dissolution method could be considered bioindicative and might be used as a surrogate for bioequivalence studies. An in vitro dissolution test can replace absorption studies during the pre-approval process, to develop a desirable formulation, and to ensure batch-to-batch bioequivalence. It could also be extremely useful in performing possible post-approval changes in the formulation, scale-up or changes in the drug substance or excipient supplier.

8.4. References

- BOURNE, D. W. A., 2002. Pharmacokinetics. in: BANKER, G. S. and RHODES, C. T. (Eds.), *Modern Pharmaceutics, Drugs and the Pharmaceutical Sciences*, 4th Ed., Vol. 121, Marcel Dekker, Inc., New York and Basel, pp. 67-92.
- CARDOT, J. M. and BEYSSAC, E., 1993. In vitro/in vivo correlation: scientific implications and standardization. *European Journal of Drug Metabolism and Pharmacokinetics* 18 (113-120).
- UPPOOR, V. R. S., 2001. Regulatory perspectives on in vitro (dissolution) / in vivo (bioavailability) correlations. *J. Controlled Rel.* 72, 127-132.
- US FDA CDER Guidance for the Industry, 1997. Extended Release Solid Oral Dosage Forms: Development, Evaluation and Application of In Vitro/In Vivo Correlations, US Department of Health, Food and Drug Administration, Centre for Drug Evaluation and Research (CDER), Rockville, MD.
- VARSHOSAZ, J., GHAGHAZI, T., RAISI, A. and FALAMARAZIAN, M., 2000. Biopharmaceutical characterization of oral theophyllin and aminophyllin tablets: Quantitative correlation between dissolution and bioavailability studies. *Eur. J. Pharm. Biopharm.* 50, 301-306.